Fermilab, 02/20/2012

Medical Applications of Radiation Detectors

(“Spin-offs from Particle Physics”)

Stan Majewski, PhD (HEP)

(with contributions from many ☺)

Director, Nuclear Medicine Imaging Instrumentation Program,
Center for Advanced Imaging,
Department of Radiology, West Virginia University, Morgantown, WV

Past life: CERN, Serpukhov, Fermi, UF, Jefferson Lab

Rationale

-Spin-offs from the "big physics" projects are popular and expected by all the "stakeholders", even if not part of the main "mission"

-Scientists involved are to a large extent "normal" people sharing the concerns of the society

-Medical imaging was and is a natural spin-off from the particle physics community via:

-Relevant technical expertise

-Radiation detection instrumentation

-Fast readout electronics and data acquisition systems

-Fast computers

-Computing algorithms, including simulations ("Monte Carlo")

-Special opening is in the dedicated organ specific imagers, where the technology advancements (compact, mobile, offer new opportunities to implement what particle physics is using or developed initially for the main mission.

Imaging Modalities

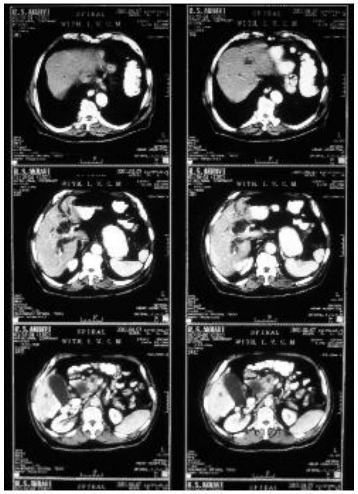

CT

A

Tissue Density, Z

20-50 µm

Ultrasound

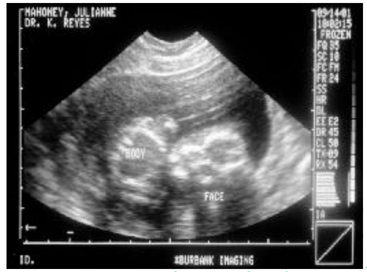

A F

Structure

0.1 mm

Doppler

Optical

(Bioluminescence, fluorescence)

A M

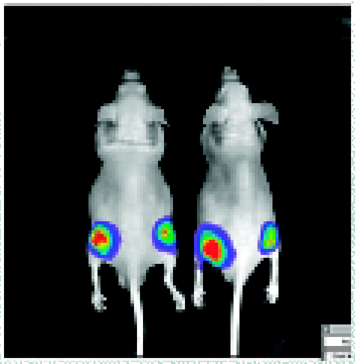

Topography

µm to mm

~10^3 cells

≠ quantitative

MRI

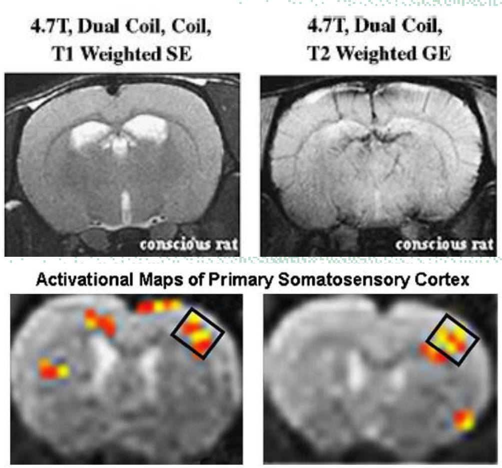

A F M

H Concentration

0.1 mm

BOLD, DCE

β-galactocidase

0.1 µmole H / µmole ^{31}P

PET/SPECT

F M

Radiotracer

~1-2 mm

<10^{-12} mole

= quantitative

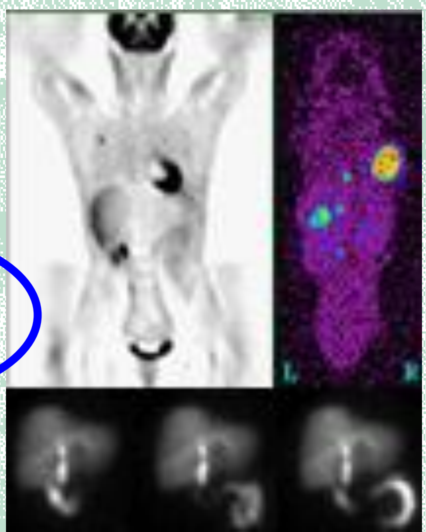

What Modality ?

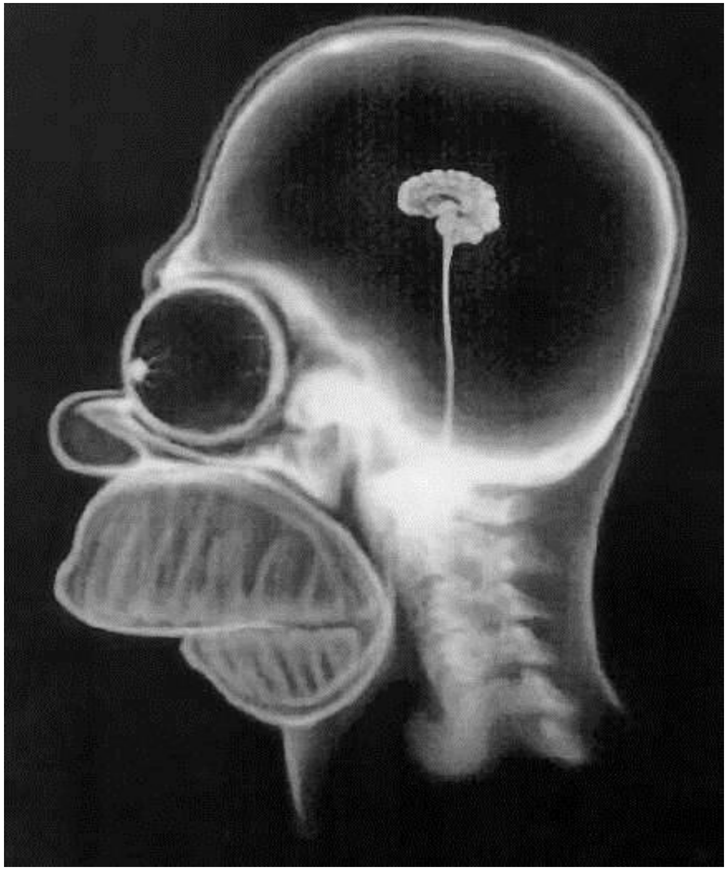

Content of the Talk
(and disclaimers)

-First impulse is to talk only about Nuclear Medicine – an obvious spin off from experimental nuclear physics/high energy physics:

- -Physics concept of PET and SPECT
- -New scintillators
- -New photodetectors (new PMTs, Silicon PMTs)
- -New concepts on improving PET: TOF PET, magnification
- -Organ specific PET imagers: breast, prostate, brain, heart, etc

- Gas detectors
- Solid state detectors (Silicon)
- Multi-modality imagers
- Not discussed: electronics
- Not discussing small animal imagers, only human imagers ☺
- Only brief mention of MRI

2-D / 3-D MRI

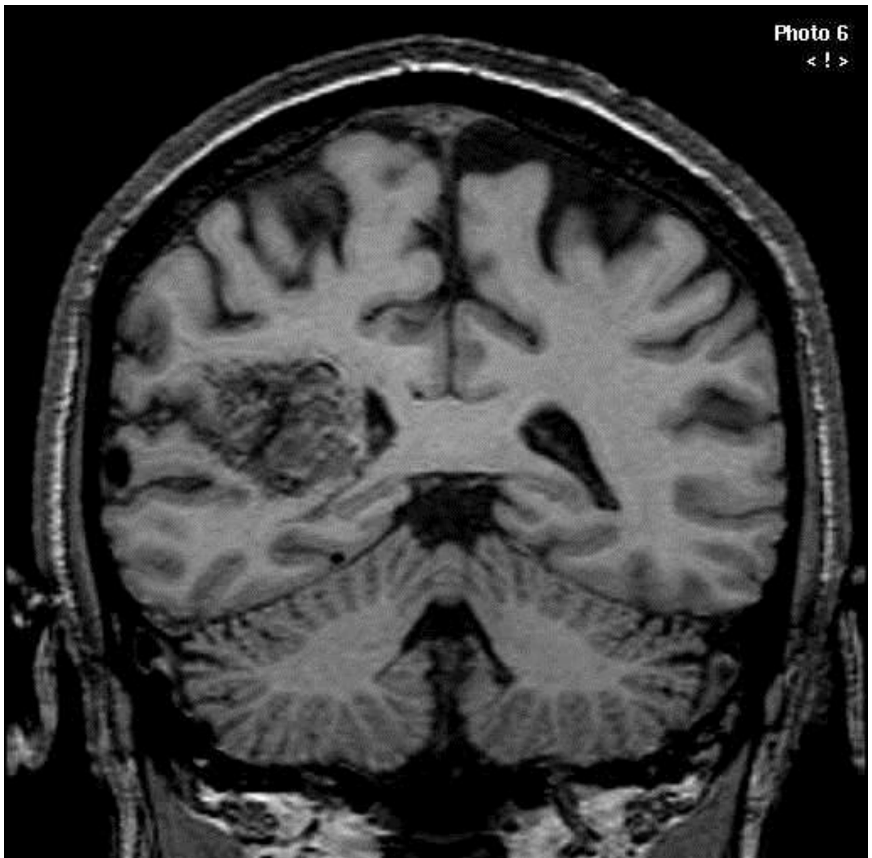

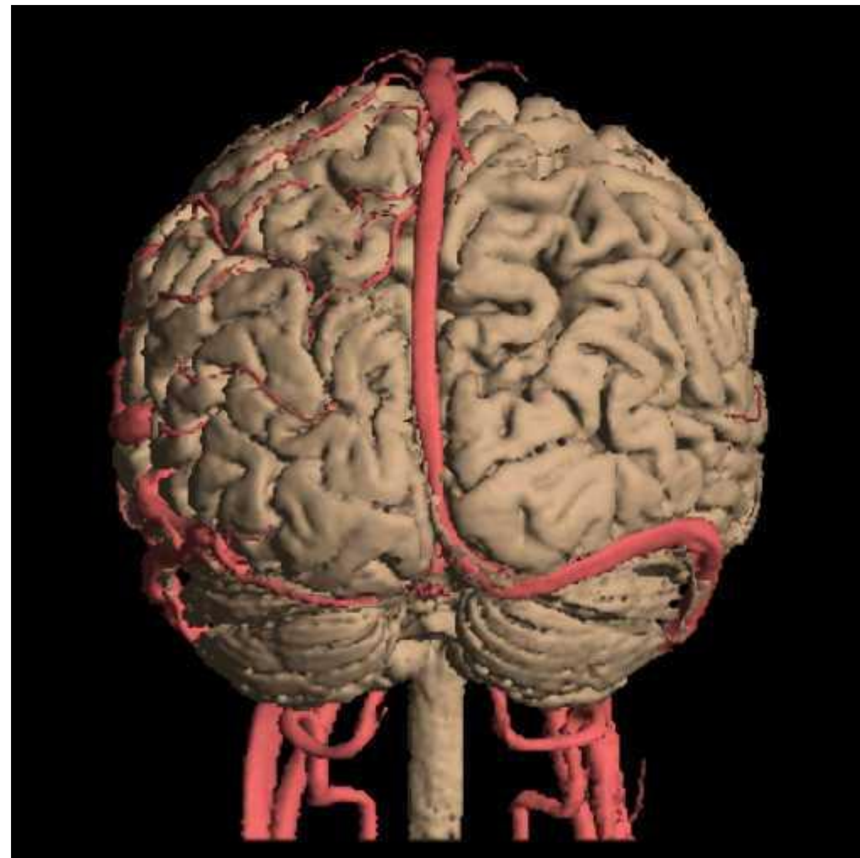

MRA

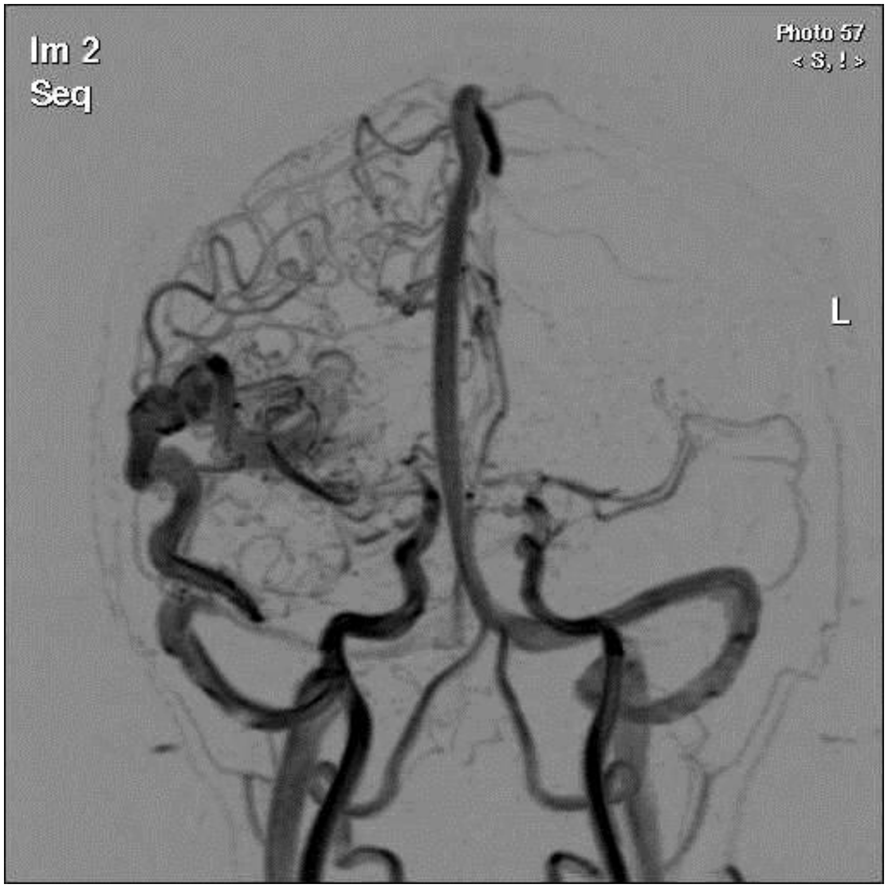

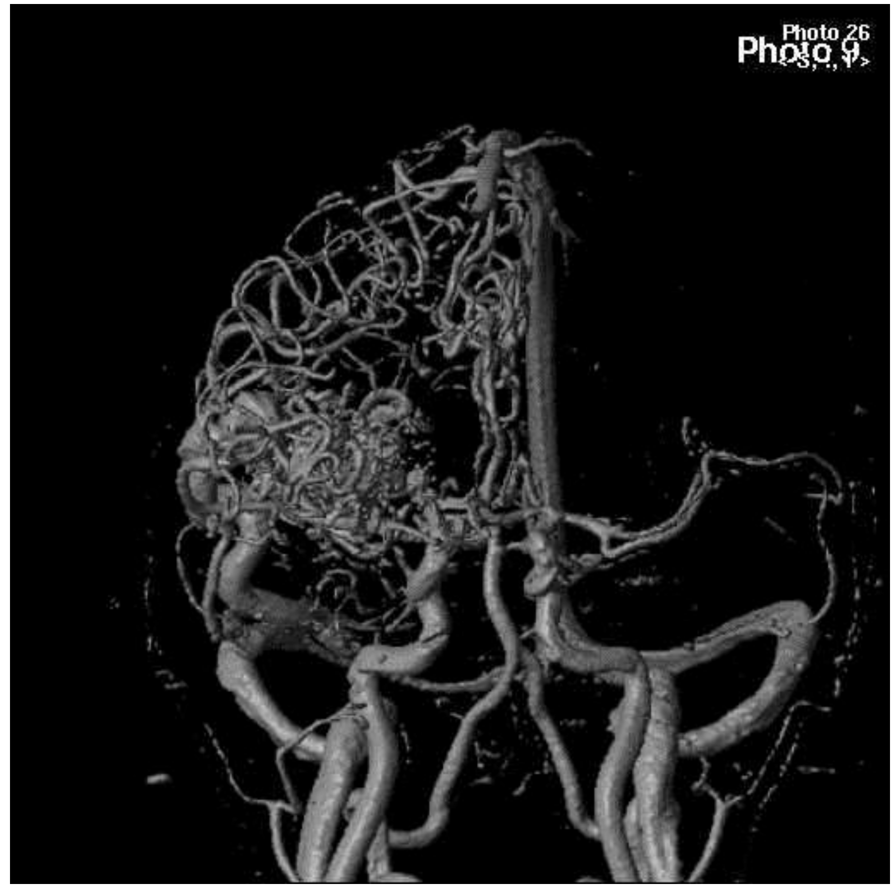

Figure 2. Brain Glucose Metabolic Images Showing Axial Planes at the Level of the Orbitofrontal Cortex

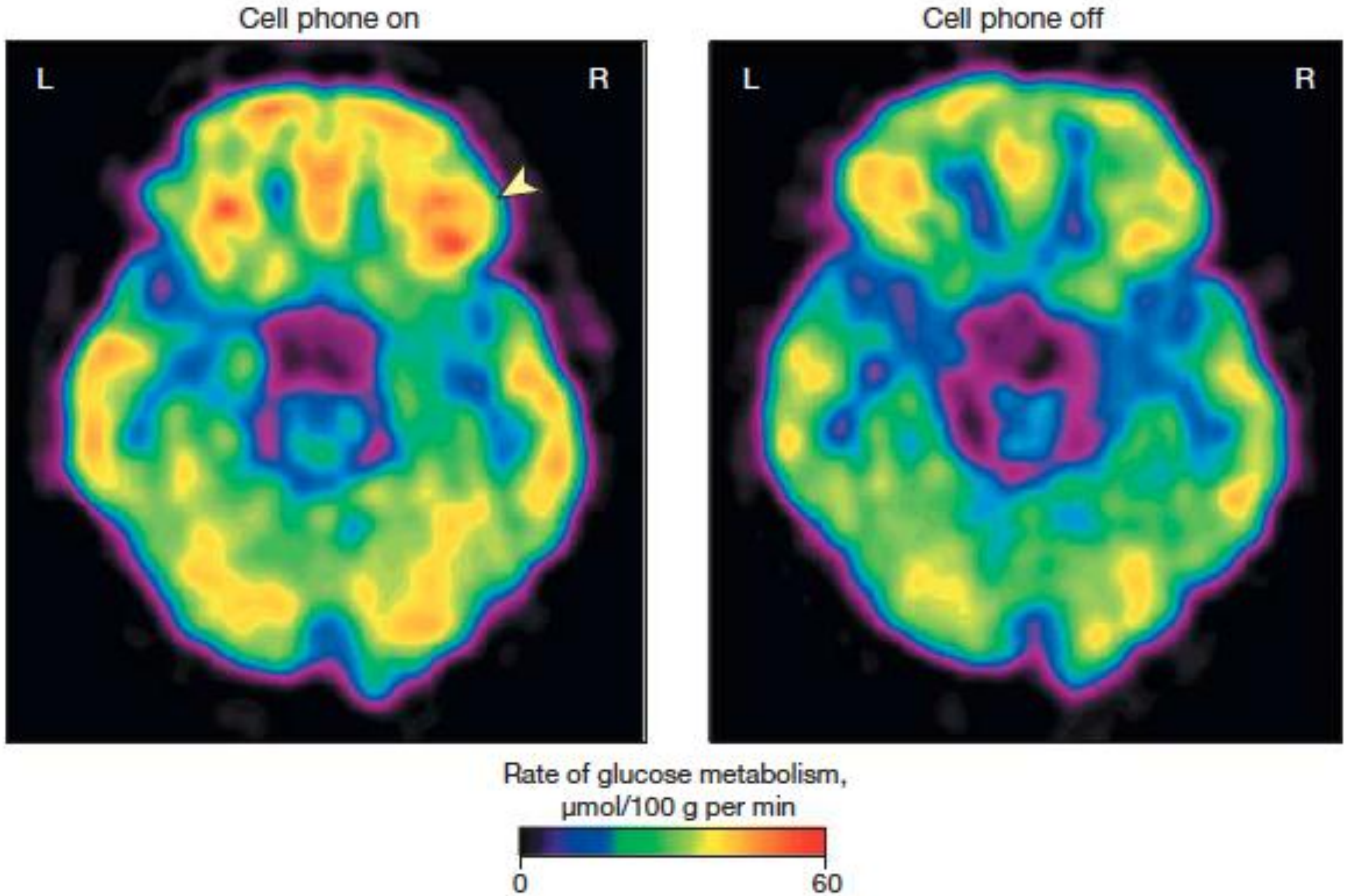

Images are from a single participant representative of the study population. Glucose metabolism in right orbitofrontal cortex (arrowhead) was higher for the "on" than for the "off" condition (see "Methods" for description of conditions).

Of Mice and Men … and Broken Hearts (MRI at UVA)
Structural medical images at its best – reference point

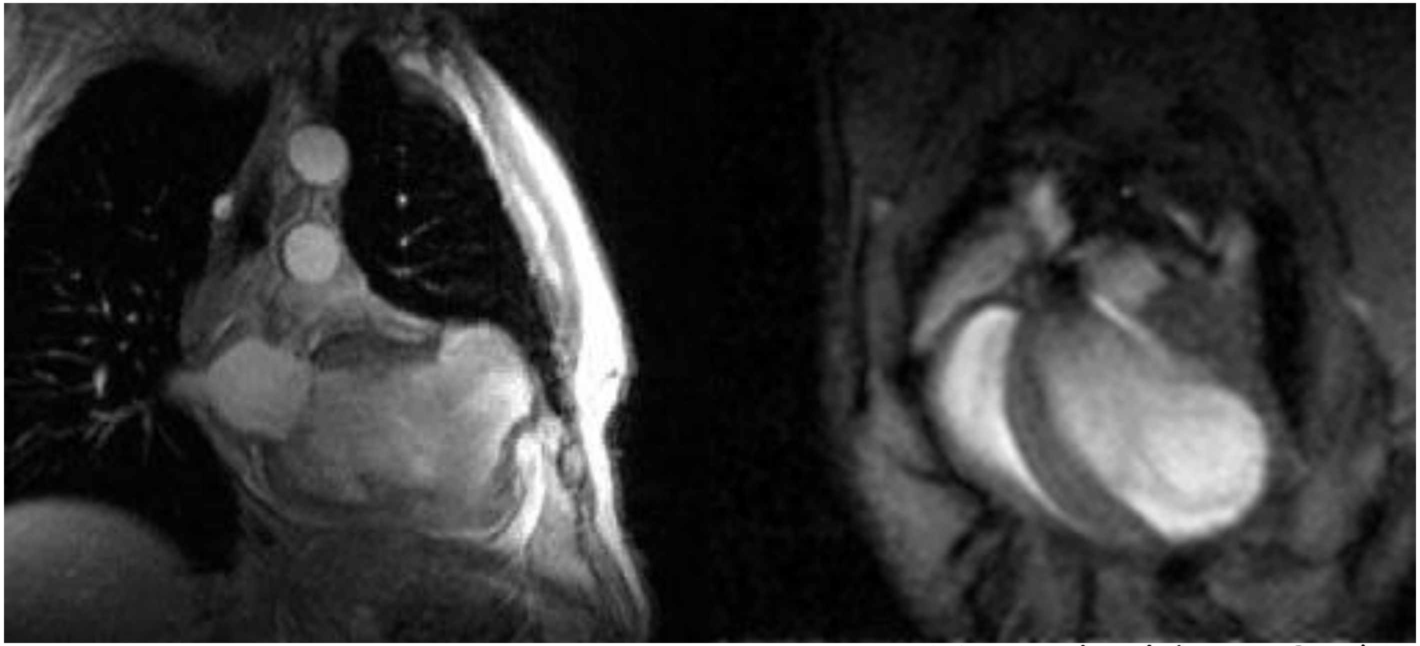

73-year-old man 7 years after an anterior MI.

14-week old C57BL/6N mouse 4 weeks after a reperfused, 2-hour occlusion of the major LAD.

(Courtesy of Dr. Stuart Berr, UVA)

microPET II Imaging in Mice

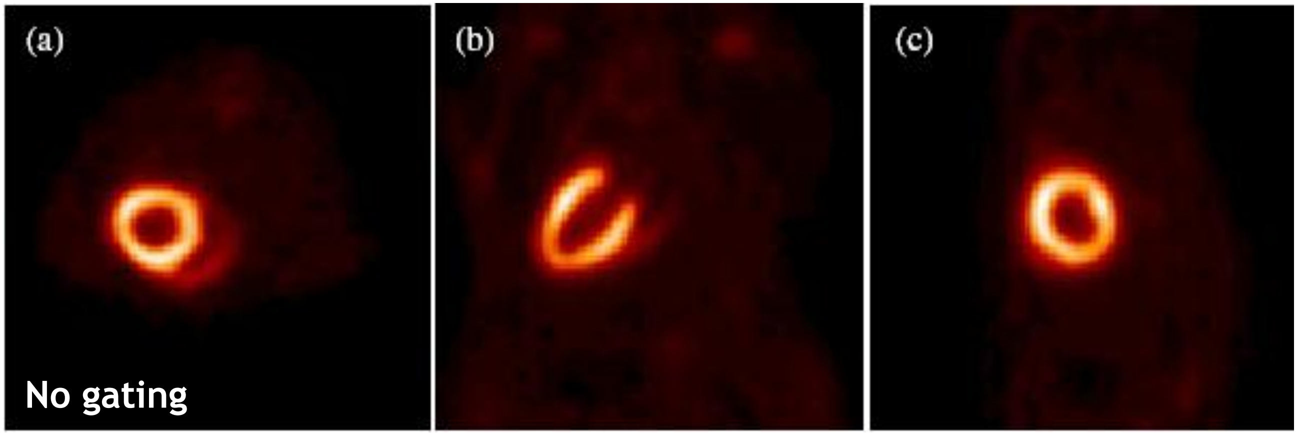

32 g mouse
580 μCi, 60 min

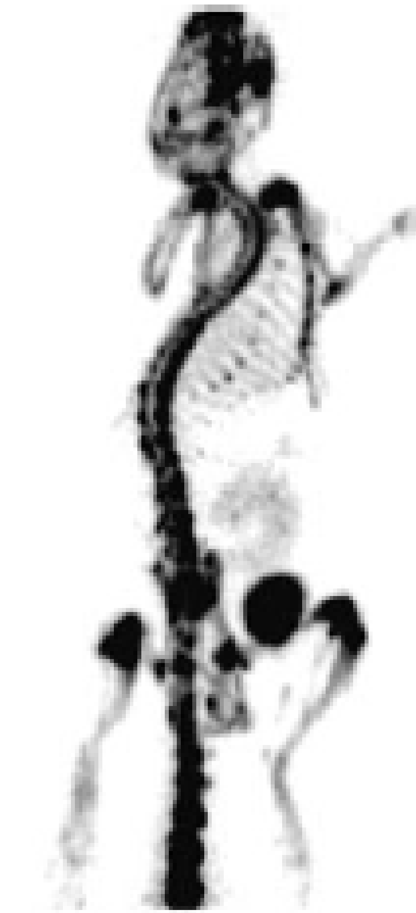

31 g mouse
1 mCi $^{18}F^{-}$

0.975 mm LSO
64-ch PMT + F.O.
X-Y Analog decoding
Resolution: 1.2 mm/2.3 μl
Efficiency: 2.26%
Peak NEC: 235 kcps

microPET II

Yang et al, PMB 2004
& IEEE NSS/MIC 2004

Tracers

- A radioactive biologically active substance is chosen in such a way that its spatial and temporal distribution in the body reflects a particular body function or metabolism.
- In order to study the distribution without disturbing the body function, only traces of the substance are administered to the patient.
- The radiotracer decays by emitting gamma rays or positrons (followed by annihilation gamma rays).
- The distribution of the radioactive tracer is inferred from the detected gamma rays and mapped as a function of time and/or space.

Spin-offs from particle physics

- new dense and fast scintillating crystals or direct conversion materials
- finely segmented and compact photodetectors
- low noise and highly integrated electronics
- data acquisition systems based on highly parallelized architecture with efficient data recording and storage
- filtering algorithms
- modern and modular simulation software based on universally recognized standards
- high performance image reconstruction and analysis algorithms

(Paul Lecoq, CERN)

From HEP to Medical

Where ***techniques*** *are transfered to developments in bio- medical field*
Medical Imaging has only partially benefited from new technologies developed for telecommunications and High Energy Physics detectors

- **New scintillating crystals and detection materials →**
  - CMS (WPbO4) → Luap ...(Crystal Clear col),
- Photodetectors : **Highly segmented and compact** → PMT → APD → SiPM
  - APD : SSC/SDC (1991) → CMS (1996) → MicroTEP→ TEP
- Electronics & signal treatemnt→ Highly integrated
  - Fast, low noise,low power preamp
  - Digital filtering and signal analysis
- Trigger/DAQ →
  - **High level of parallelism and event filtering algorithms**
  - Pipeline and parallel read-out, trigger and on-line treatment
- Computing
  - Modern and modular simulation software using worldwide recognized standards (GEANT)

<u>Detector technologies used in medical imaging:</u>

- Silicon, Selenium - (X-ray)
- CdTe, CdZnTe – (X-ray, gamma, PET)
- Crystal scintillators (gamma, PET)
- Cherenkov – (TOFPET)
- Vacuum Photomultipliers (including MCP based, position sensitive, etc)
- PIN diodes
- Avalanche photodiodes (APD)
- "Silicon photomultipliers" – SiPMs, Geiger avalanche diodes
- Time of Flight PET
- Compton gamma imaging

Areas of involvement

-The most obvious field: nuclear medicine: SPECT and PET

-Diagnostic tools (early detection of abnormalities, such as cancer)

-Beam radiation therapy (proton and ion beams, and the latest promise of antiprotons !)

-Monitoring chemo- and radio-therapy

-Organ specific imagers:

-Breast

-Prostate

-Brain

-Small animal SPECT and PET imagers

Special features: MRI compatibility, Time of Flight (TOF) PET

Selected detector technologies used in medical imaging as the best particle physics spin-off :

- APDs and SiPMs
- Crystal scintillators
- Fast electronics, ASICS
- Fast simulation and reconstruction software
- TOF

"Among the many applications of nuclear energy and ionising radiation, medical imaging certainly is least subject to negative perception or outright opposition from the general public. Proponents of nuclear power correctly refer to it as an example of a very positive use of nuclear technology." - **By Frank Deconinck, 2006.**

Photon detection

The detection of the photons is based on the transfer of their energy to the detector through the photo-electric and the Compton effect.

Examples are

- Scintillators, e.g. NaI, BGO and LSO **(cfr. talk by C. van Eijk)**
- Semiconductor detectors, e.g. Si, Ge
- Gas detectors, e.g. with a wire chamber read-out (MWPC, HIDAC, …)

Multi Wire Proportional Chamber

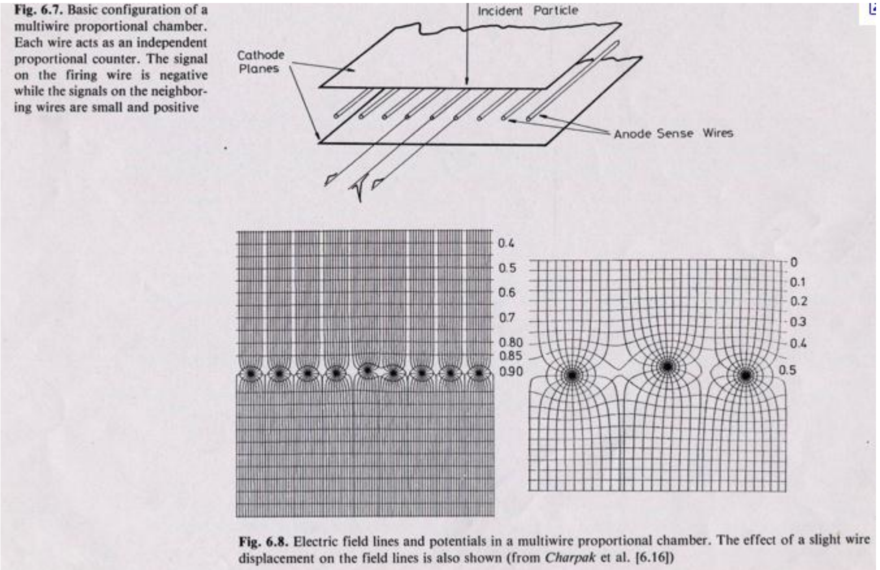

Fig. 6.7. Basic configuration of a multiwire proportional chamber. Each wire acts as an independent proportional counter. The signal on the firing wire is negative while the signals on the neighboring wires are small and positive

Fig. 6.8. Electric field lines and potentials in a multiwire proportional chamber. The effect of a slight wire displacement on the field lines is also shown (from *Charpak* et al. [6.16])

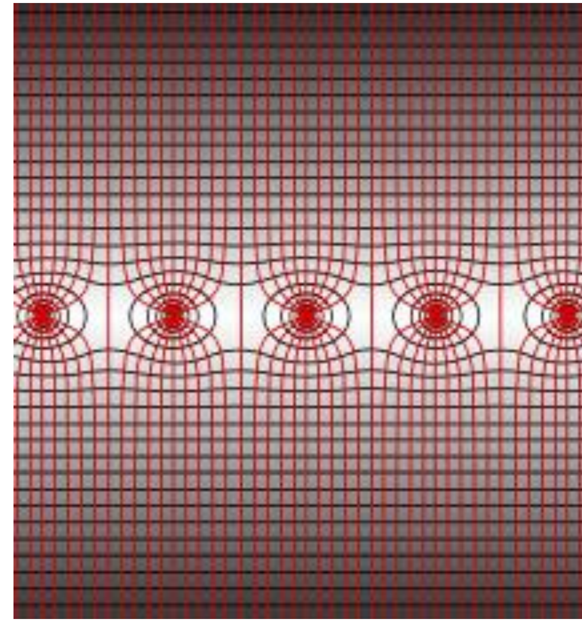

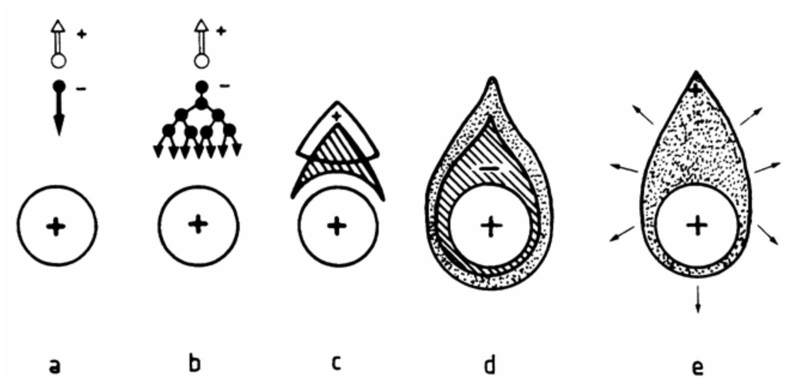

The first large multiwire proportional chamber built at CERN. Left to right, Georges Charpak, Fabio Sauli and Jean-Claude Santiard. (Photo CERN x8.8.70)

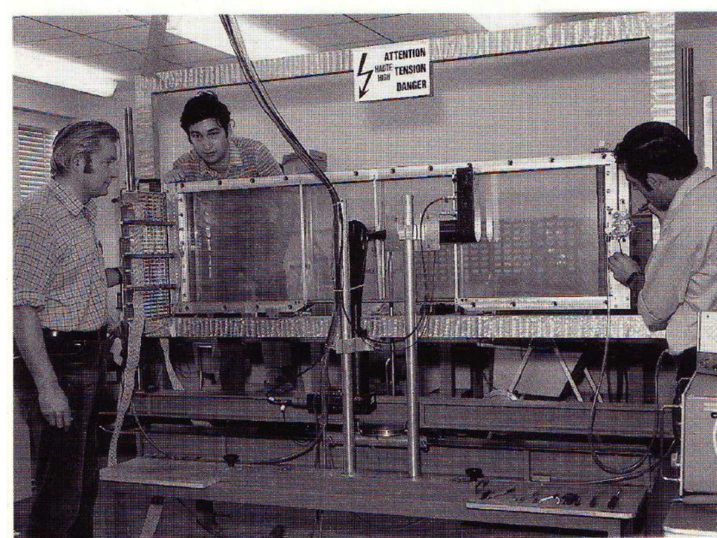

Important role played by Fabio Sauli

The Nobel Prize in Physics 1992

The Royal Swedish Academy of Sciences awards the 1992 Nobel Prize in Physics to **Georges Charpak** for his invention and development of particle detectors, in particular the multiwire proportional chamber.

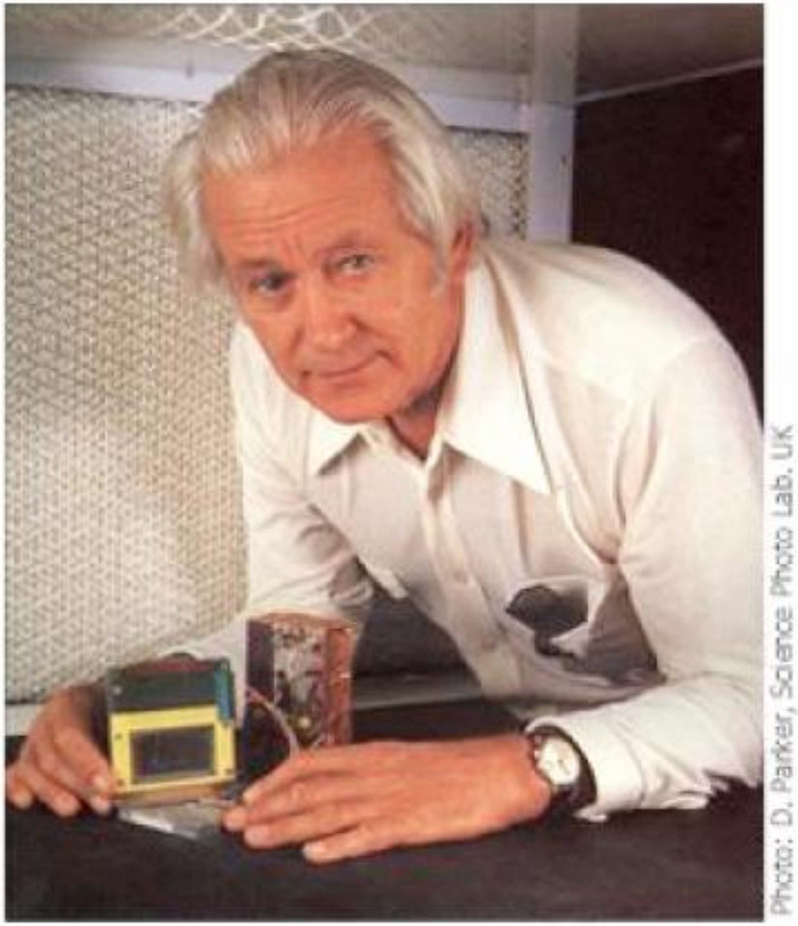

Georges Charpak
CERN, Geneva, Switzerland

X-RAY RADIOGRAPHY

PHOTOGRAPHIC EMULSION RÖNTGEN (1896):

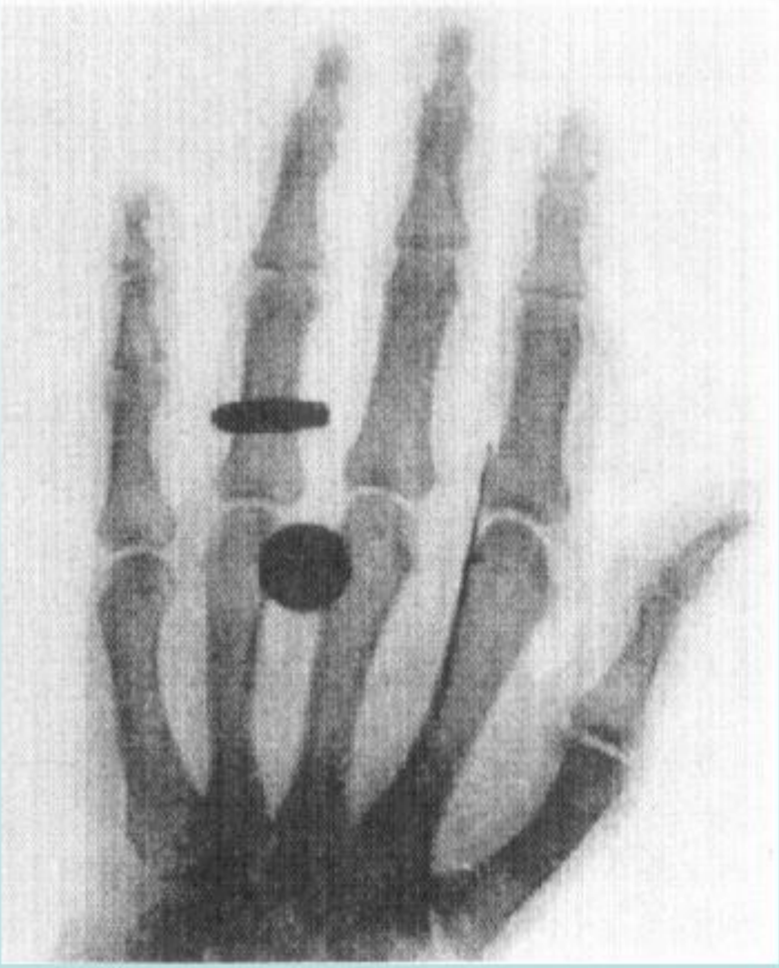

DIGITAL RADIOGRAPHY WITH MWPC:
CHARPAK'S HAND (2002):

An Efficient, Gaseous Detector with Good Low-energy Resolution for (≤50 keV) Imaging

Nguyen Ngoc Hoan, S. Majewski, G. Charpak, and A.J.P.L. Policarpo

Institut National de Physique Nucléaire et de Physique des Particules, Orsay, France,
University of Warsaw, Warsaw, Poland, and University of Coimbra, Coimbra, Portugal

An imaging detector with good energy resolution and reasonable spatial accuracy has been designed for biomedical applications. It is based on a scintillating proportional gas chamber. The energy resolution is typically 5.4% (FWHM) at 27 keV and the spatial resolution is 2.7 mm (FWHM) for 22-keV x-rays. The physical processes involved in this detector are discussed along with its main limitations and merits.

J Nucl Med 20: 335–340, 1979

FIG. 4. (A) Energy resolution and linearity of detector observed with radioactive sources and fluorescence spectra induced by 60-keV radiation from Am-241. (B) Energy resolution of camera. Spectrum of x-rays emitted at 130° relative to 60-keV beam emitted by Am-241, impinging on a 3% solution of KI in water. Shown are K_α and K_β lines of iodine (27.5 and 31.0 keV) with a resolution of 5.4%. Lower-energy peaks are $K_{\alpha,\beta}$ xenon escape peaks from the Compton radiation scattered at 130°.

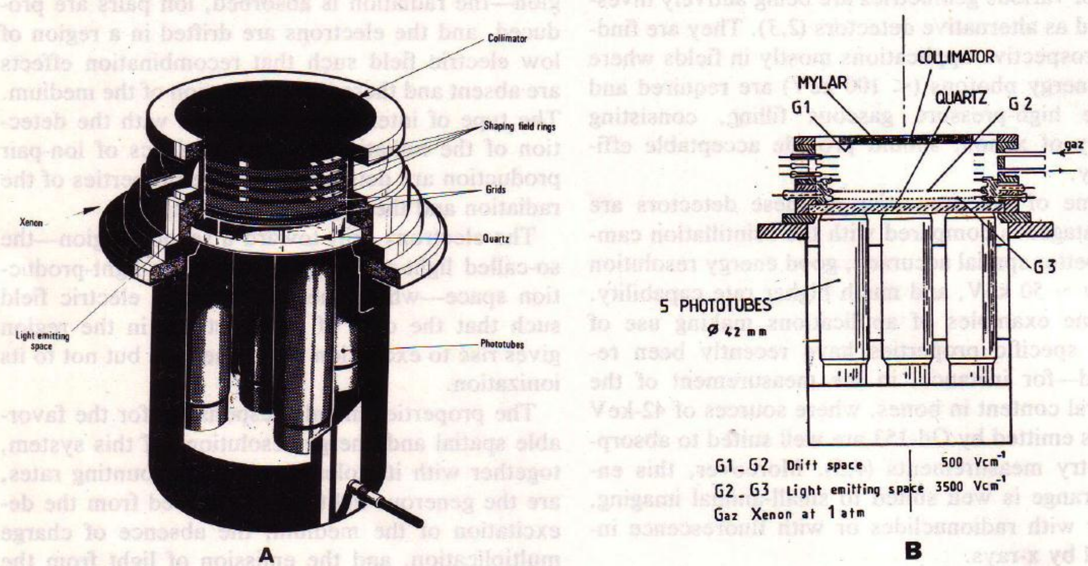

FIG. 1. (A) Detector of energy-sensitive x-ray camera using gas scintillator. (B) Photons absorbed in xenon in drift space produce photoelectrons that drift into light-producing space. Ultraviolet light is converted into visible light by wavelength shifter deposited on quartz window. Five photomultipliers view the scintillations. On-line computing based on microprocessor gives position of centroid of spatial position of light-emitting track.

FIG. 6. Image of thyroid phantom (Picker No. 3602) filled with 30 μCi of I-125. Collimator has 1-mm holes, septa 0.1 mm, length 20 mm, transmission 1.24×10^{-4}. Acquisition time 3 min.

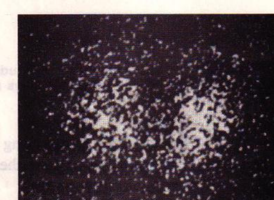

FIG. 7. Thyroid image from unanesthetized rabbit with 100 μCi of I-125 injected 24 hr before observation. Acquisition time 2 min.

PARALLAX ERROR WITH GASEOUS DETECTORS:

AT HIGH X-RAYS ENERGY, ONE NEEDS THICK LAYERS OF GAS TO ACHIEVE A REASONABLE EFFICIENCY OF CONVERSION

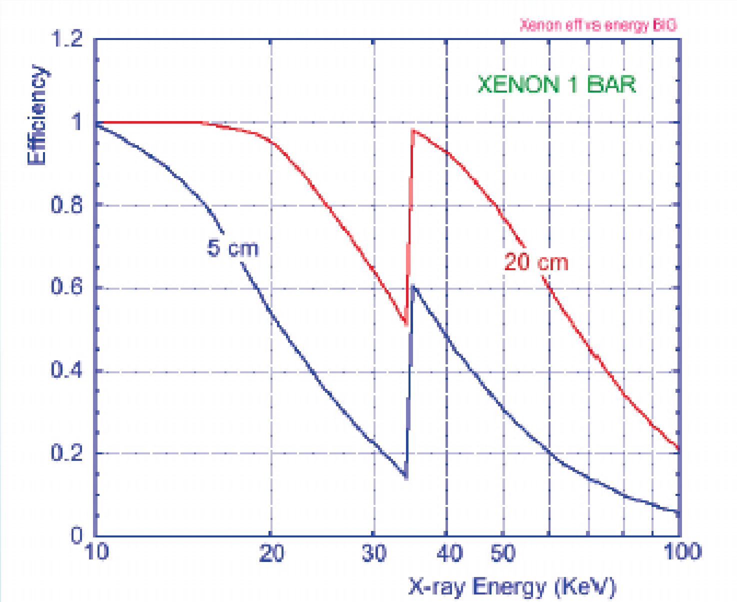

WITH POINT-LIKE X-RAY SOURCES, THIS INDUCES A LARGE PARALLAX ERROR (THE CONVERSION POINT IS UNKNOWN):

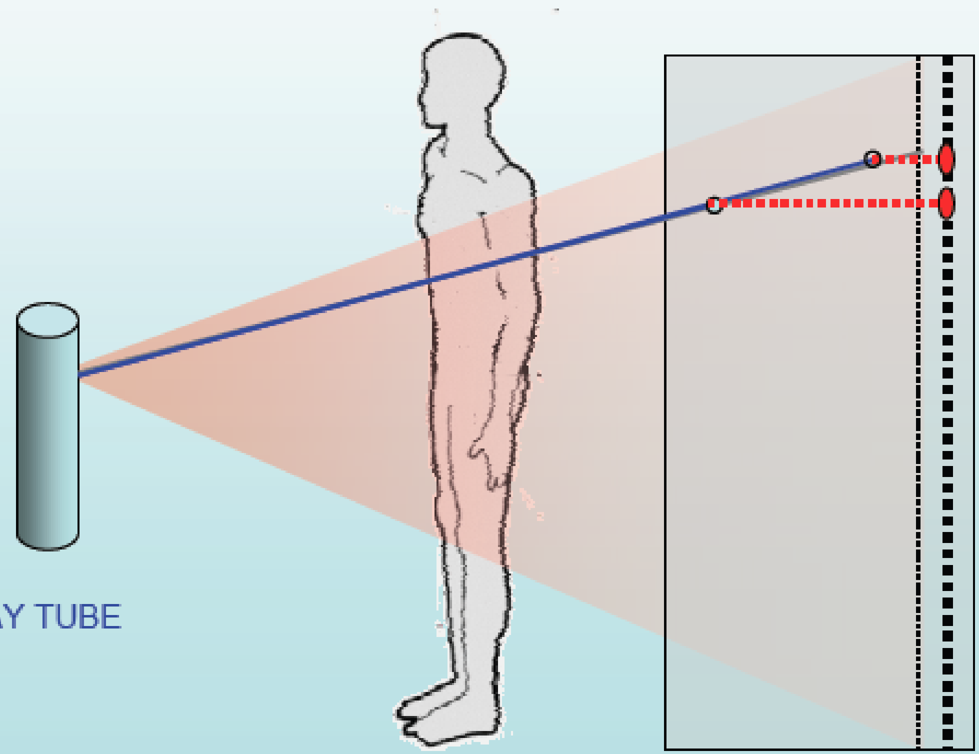

X-RAY TUBE

SIBERIAN DIGITAL RADIOGRAPHY SYSTEM
MWPC WITH RADIAL ANODE WIRES, AIMING AT THE EMISSION POINT:

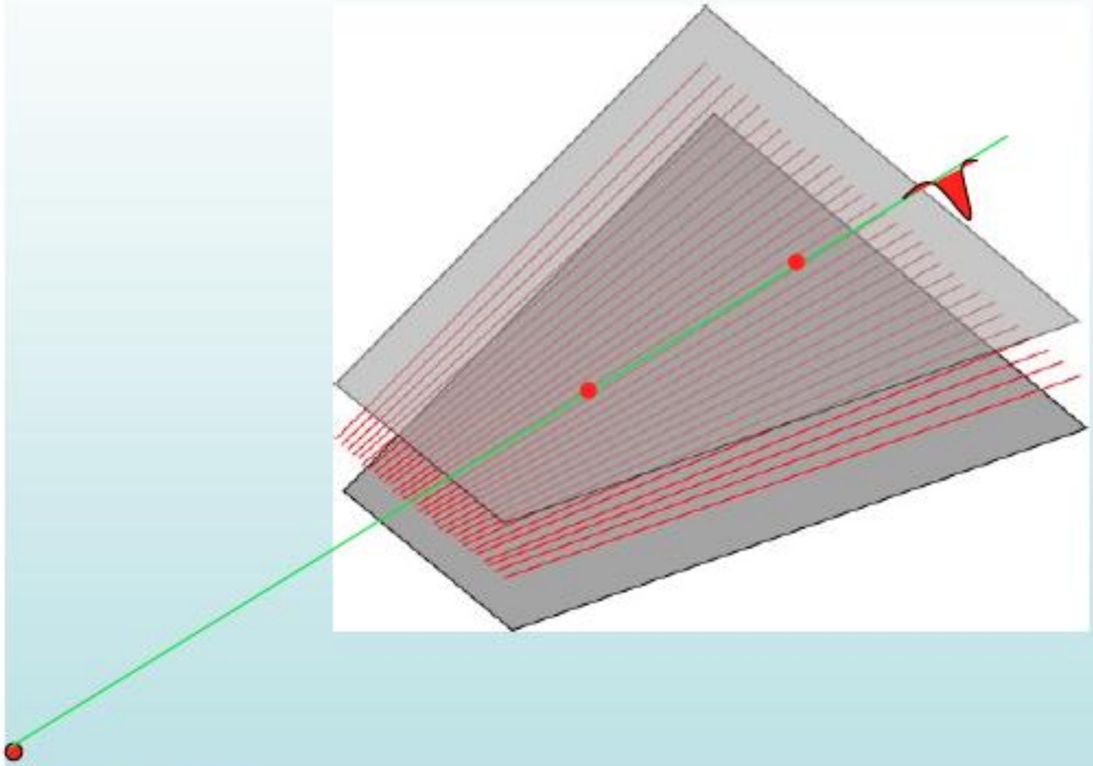

X-RAY TUBE

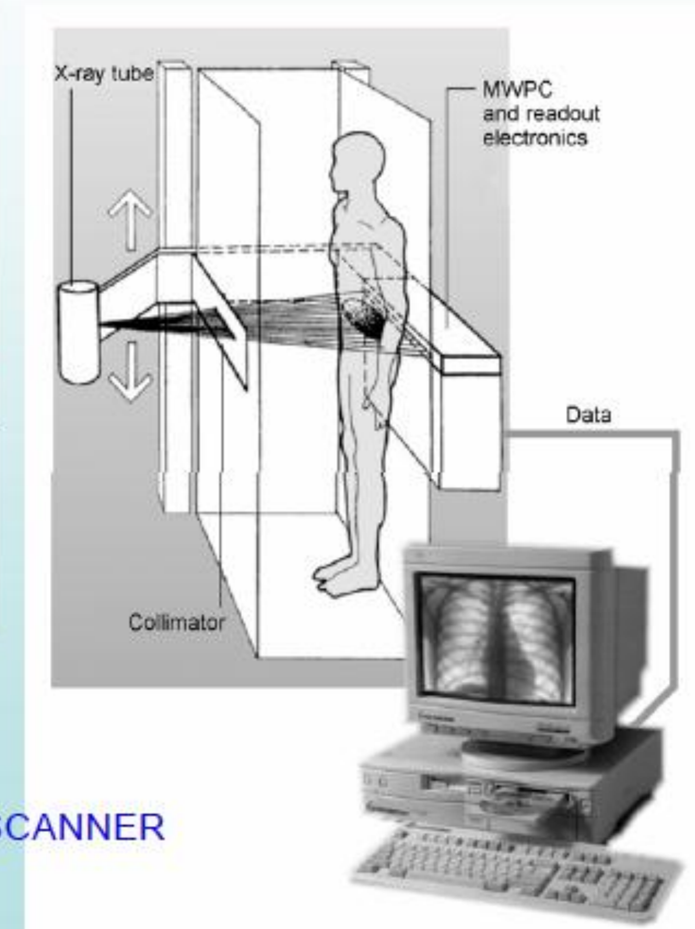

LINE SCANNER

DIGITAL RADIOGRAPHY
GOOD CONTRAST AT VERY LOW DOSES

THE HEAD OF ONE OF THE AUTHORS
(Lev Shekhtmann)

Quad-HIDAC Nano PET

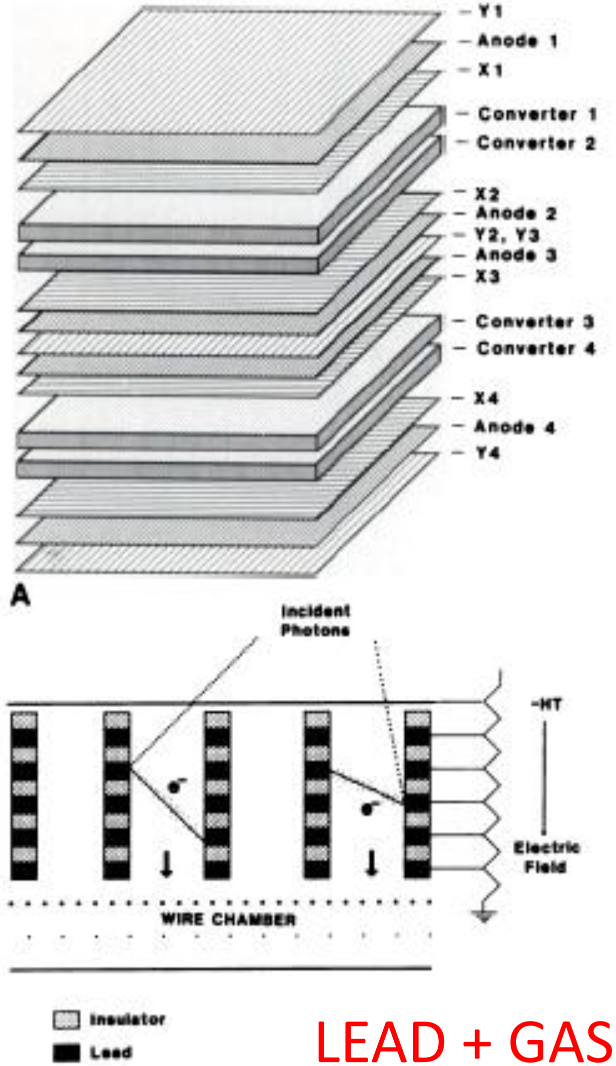

LEAD + GAS VOLUME

The HIDAC Camera Project, 1977-1982

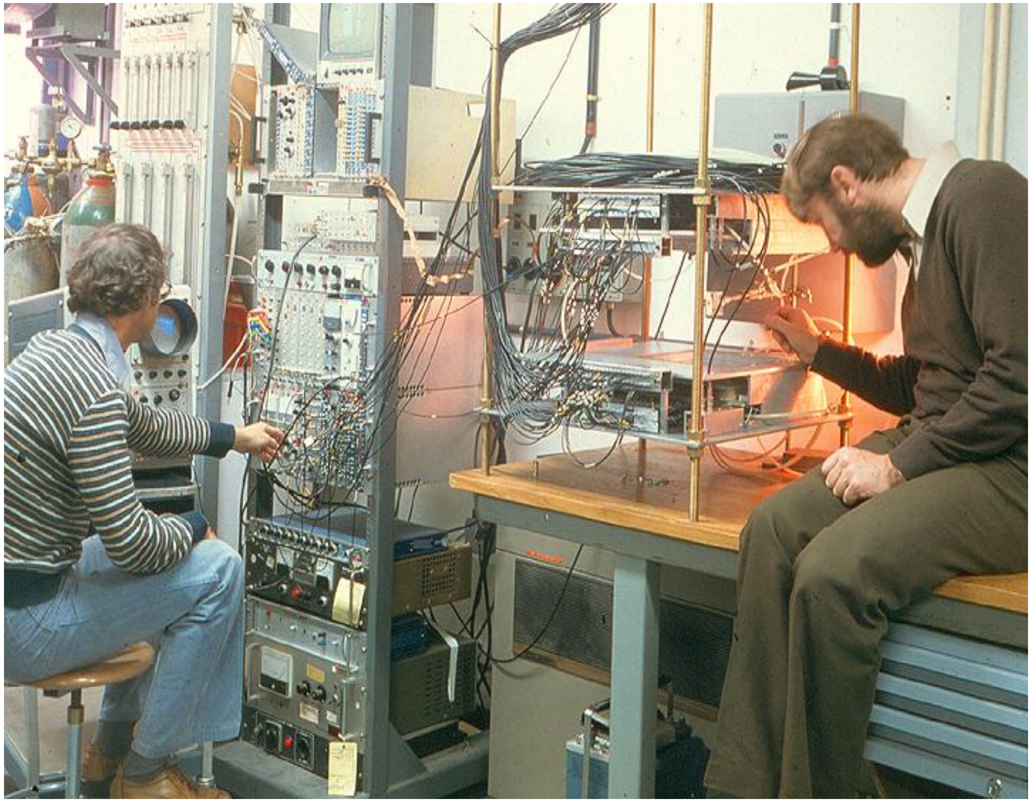

1978

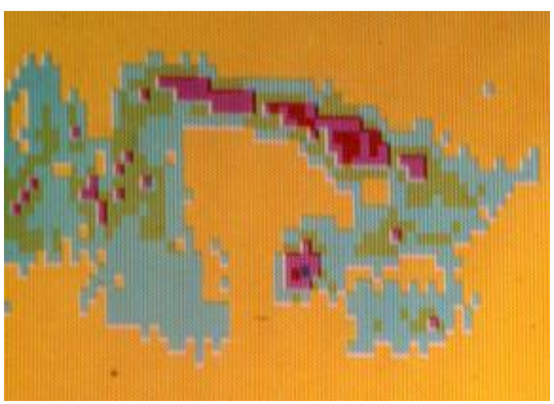

1982

The HIDAC Camera Project, 1983-1988

Une nouvelle technique pour soigner le cerveau et le cœur

Mieux voir pour mieux soigner

Le Courrier, January 1988

Tribune de Genève, January 1988

Scientists Press Plans for New Brain and Heart Research *UNI* News 1988

Thyroid imaging with ^{124}I

Financially supported by the Fonds National Suis

The HIDAC Camera: 25 years later…..

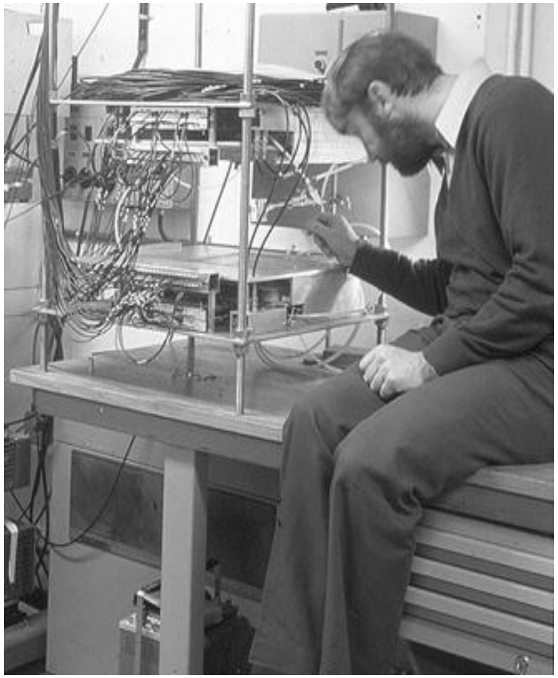

1978

2003

Quad-HIDAC Nano PET

- First & only PET imager with true nanolitre volumetric imaging capability
- Uniform sub-millimetre spatial resolution throughout FOV
- Compared with conventional microPET scanners
  - FOV nearly 4x larger
  - 10x intrinsic volumetric spatial resolution
- Used in small animal studies (mouse & rat)

PSI Switz/UMIST, UK

hrPET

100 MBq ^{18}F-fluoride administered

Imaging

Scanned image reconstructed

40 minutes post injection

20 minutes data acquisition

Image reconstruction

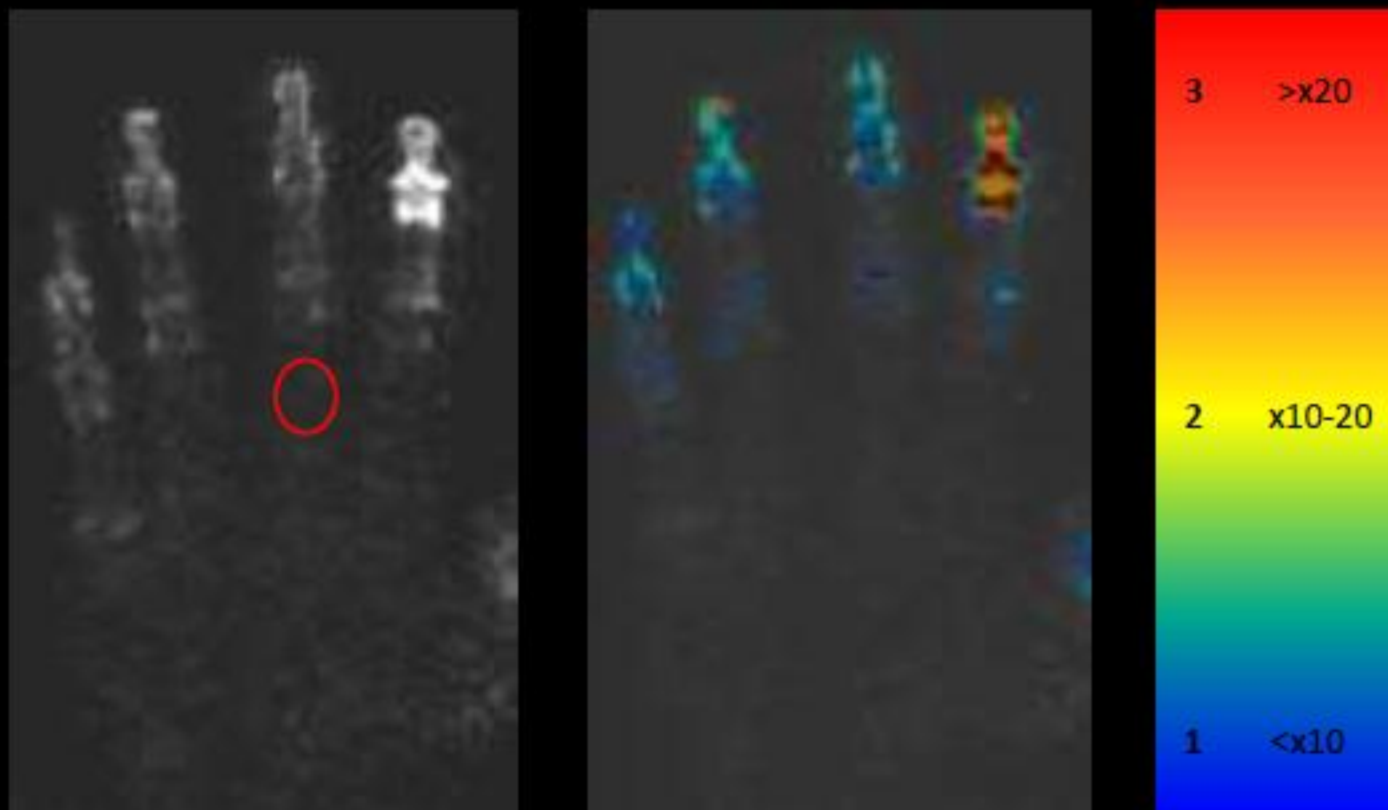

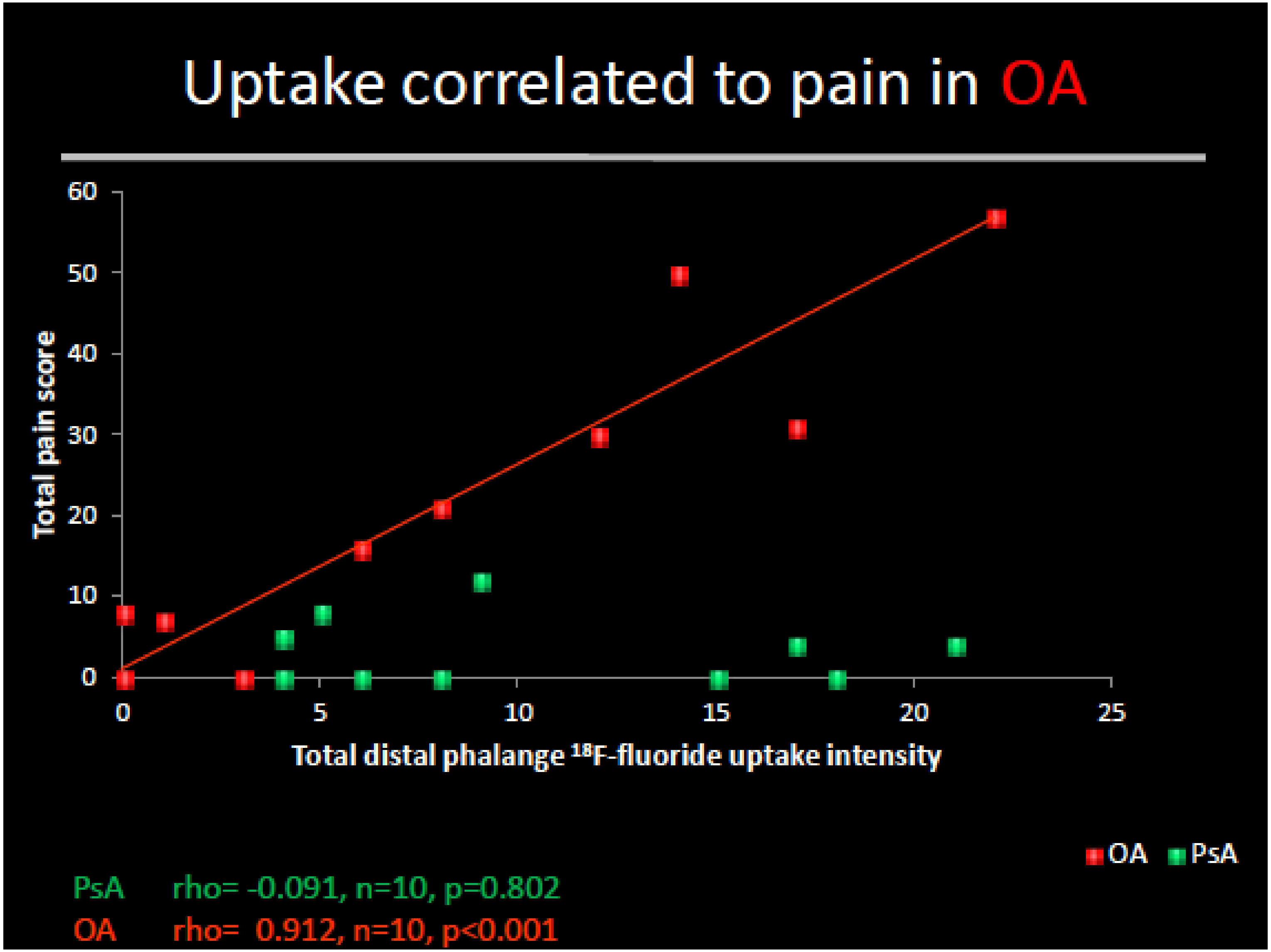

Uptake correlated to pain in OA
Total pain score
0
10
20
30
40
50
60
0
5
10
15
20
25
Total distal phalange 18F-fluoride uptake intensity
OA
PsA
PsA rho= -0.091, n=10, p=0.802
OA rho= 0.912, n=10, p<0.001

Proton Radiography

PHYS. MED. BIOL., 1976, VOL. 21, NO. 6, 941–948.

Further Results in Nuclear Scattering Radiography

G. CHARPAK, S. MAJEWSKI, Y. PERRIN, J. SAUDINOS, F. SAULI, D. TOWNSEND and J. VINCIARELLI

CERN, 1211 Geneva 23, Switzerland

Received 15 *April* 1976

ABSTRACT. A further investigation of the nuclear scattering of 500–1000 MeV protons is described. Three-dimensional information on the density distribution within carbon, CH and H_2O phantoms is obtained with a volume resolution of 2 mm³. The separation of scattering on hydrogen from that on heavier nuclei, such as carbon and oxygen, is demonstrated, providing the statistics are sufficient. Some preliminary measurements on animals are reported, but with a volume resolution limited by statistics to 43 mm³.

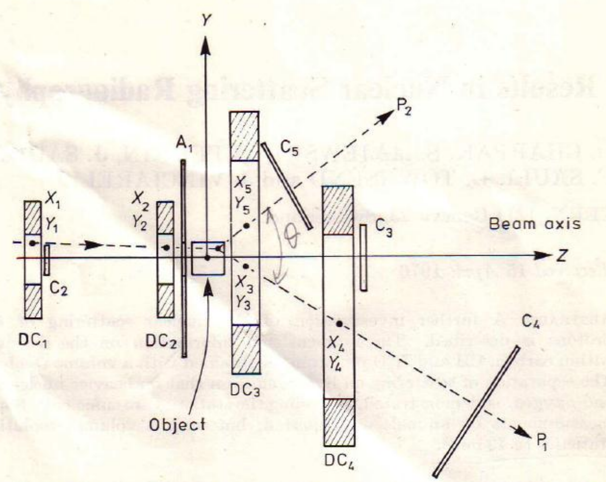

Fig. 1. Experimental set-up (vertical cut). The drift chambers DC_1, DC_2, DC_3 and DC_4 measure the trajectories of the incident and scattered protons.

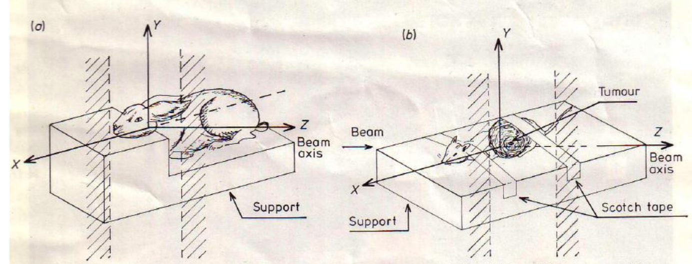

Fig. 6. Positions of the animals relative to the beam: (*a*) rabbit; (*b*) mouse with an abdominal tumour. The dashed lines give the limits in X of the useful area.

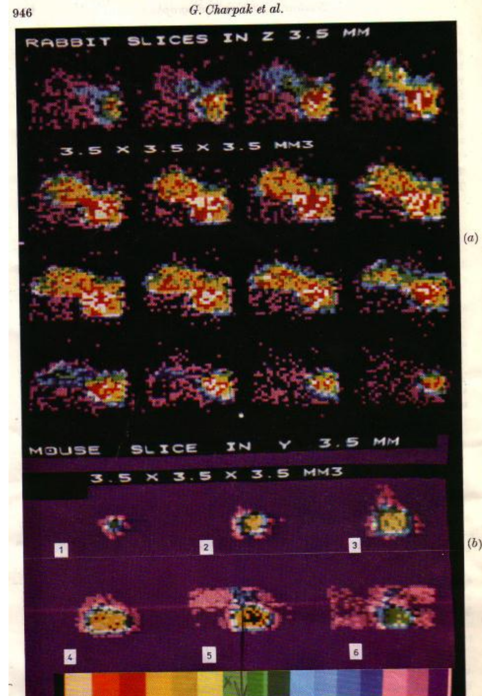

Fig. 7. Density distribution. (*a*) Rabbit, vertical slices (plane YX) of 3·5 mm, perpendicular to the beam direction; (*b*) mouse with tumour, horizontal slices (plane ZX) of 3·5 mm. The abcissa corresponds to the incident beam axis. The scale of 16 colours is given at the bottom of the figure. Colour 13 (orange) is changed to black in the figure in order to increase the contrast.

Gaseous Detectors

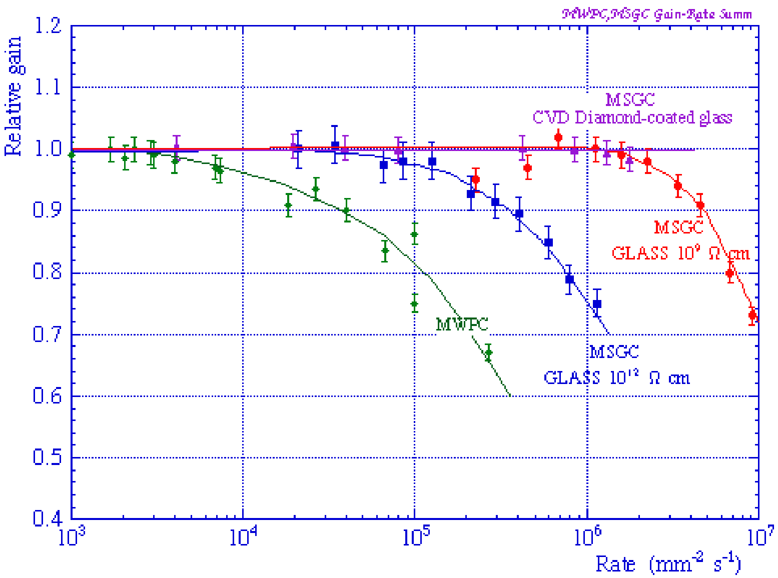

scale factor

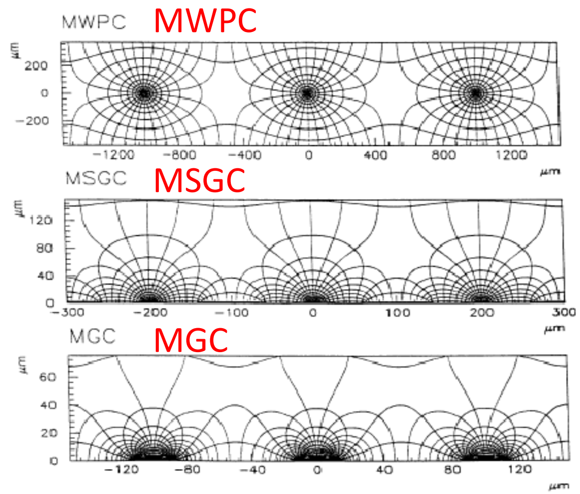

1	MWPC
5	MSGC
10	MGC

R. Bellazzini et al.

Advantages of gas detectors:

- low radiation length
- large areas at low price
- flexible geometry
- spatial, energy resolution …

Limitation:

- rate capability limited by space charge defined by the time of evacuation of positive ions

Solution:

- reduction of the size of the detecting cell (limitation of the length of the ion path) using chemical etching techniques developed for microelectronics and keeping at the same time similar field shape.

Field Configurations

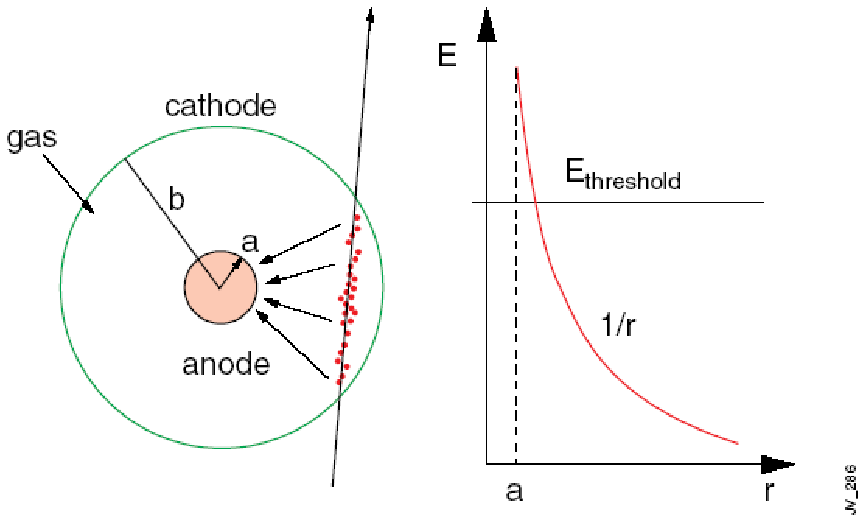

Electrons liberated by ionization drift towards the anode wire.

Electrical field close to the wire (typical wire Ø ~few tens of μm) is sufficiently high for electrons (above 10 kV/cm) to gain enough energy to ionize further → avalanche – exponential increase of number of electron ion pairs.

anode

e^-
primary electron

$$E(r) = \frac{CV_0}{2\pi\varepsilon_0} \cdot \frac{1}{r}$$

$$V(r) = \frac{CV_0}{2\pi\varepsilon_0} \cdot \ln \frac{r}{a}$$

C – capacitance/unit length

Cylindrical geometry is not the only one able to generate strong electric field:

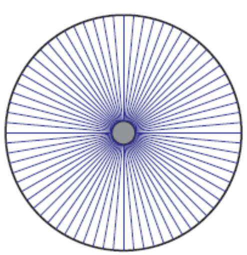

wire

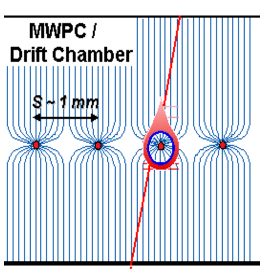

mwpc

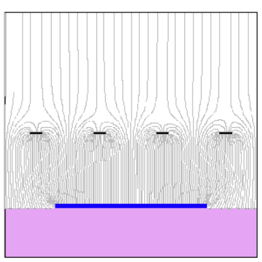

parallel plate

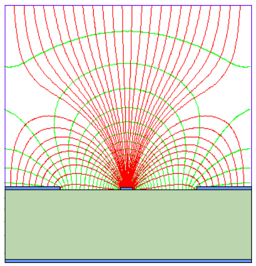

strip

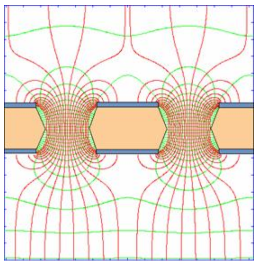

hole

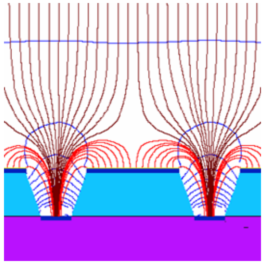

groove/well

Current Trends in Micro-Pattern Gas Detectors (Technologies)

Semiconductor Industry technology:

- Photolithography
- Etching
- Coating
- Doping
- Wafer postprocessing

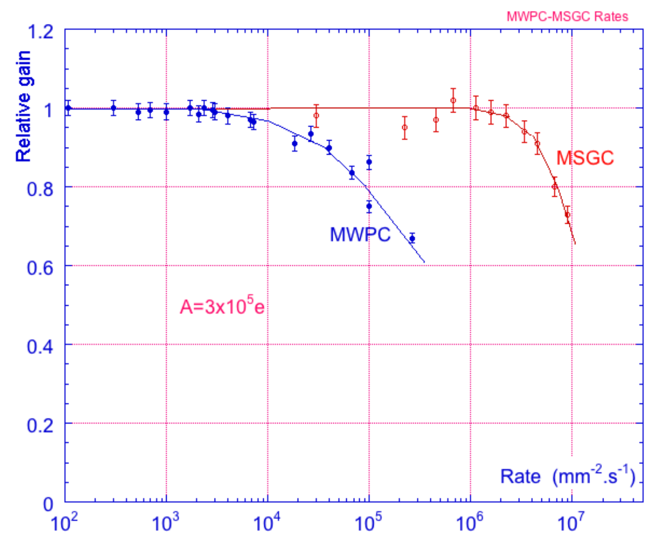

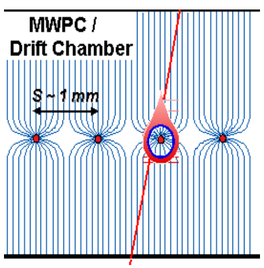

Amplifying cell size reduction by factor of 10

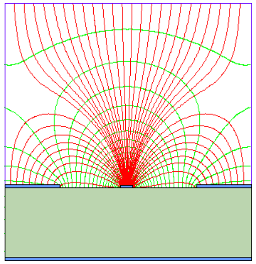

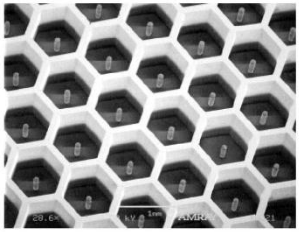

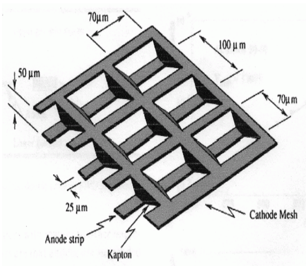

Operational instabilities:

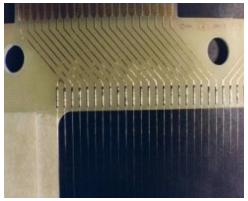

Rate Capability>10^6/mm^2
Position Resolution ~40µm
2-track Resolution ~400µm

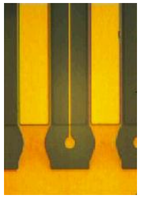

Substrate charging-up
Discharges
Polymer deposition (ageing)

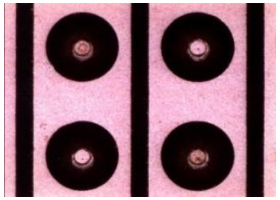

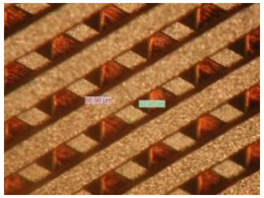

MWPC

MSGC

Current Trends in Micro-Pattern Gas Detectors (Technologies)

- MSGC
- Micromegas
- GEM
- Thick-GEM, Hole-Type Detectors and RETGEM
- MPDG with CMOS pixel ASICs
- Ingrid Technology

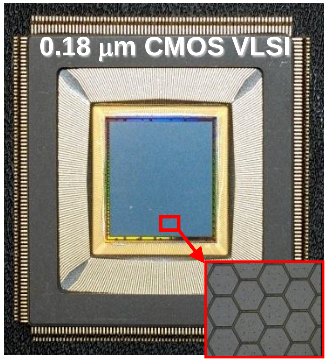

CMOS high density readout electronics

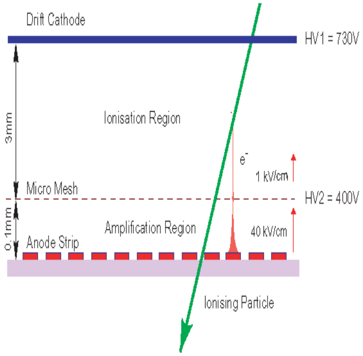

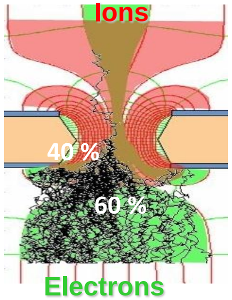

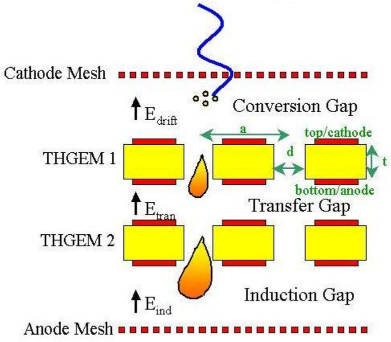

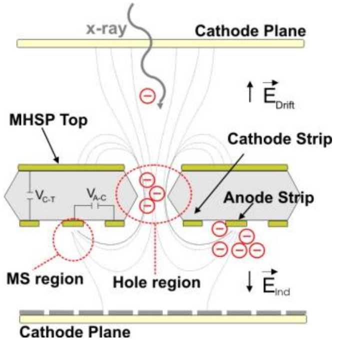

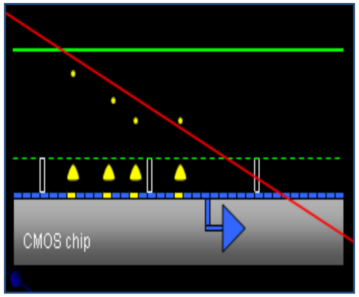

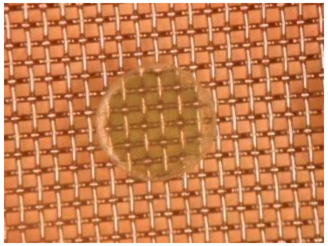

Micromegas

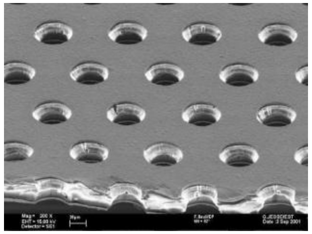

GEM

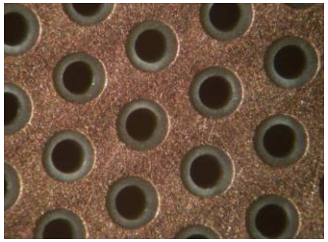

THGEM

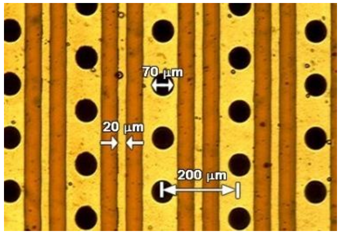

MHSP

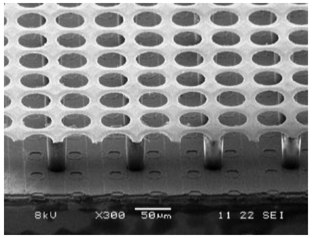

Ingrid

GEM – Gas Electron Multiplier

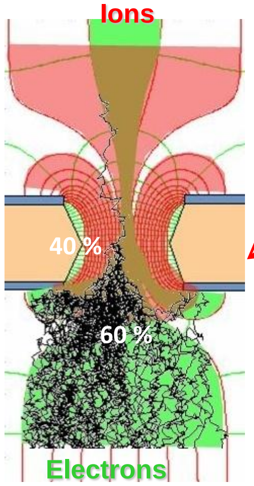

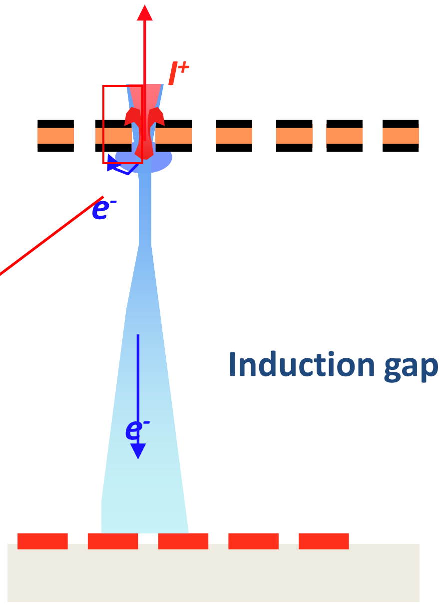

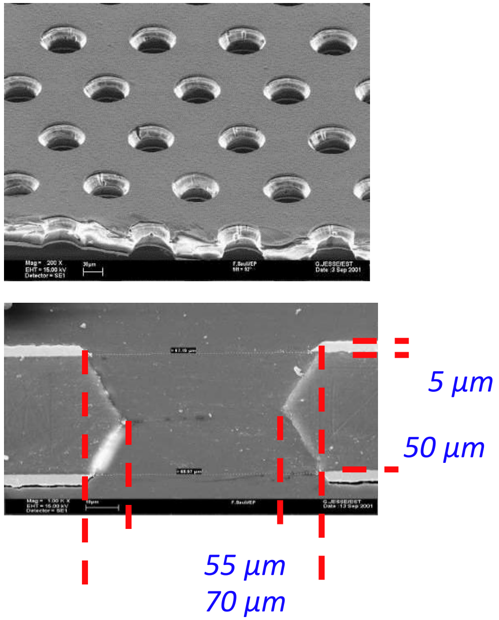

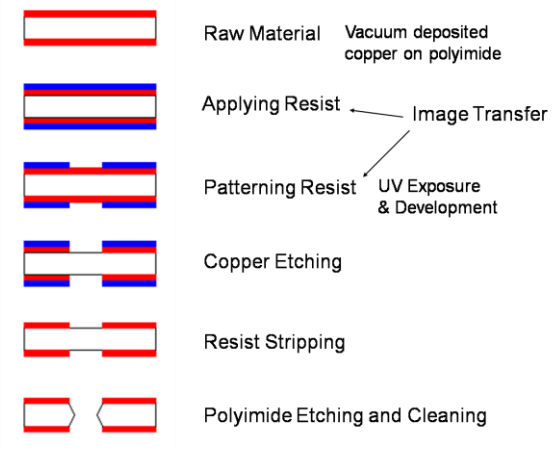

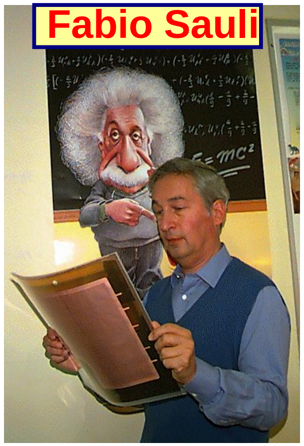

Thin, metal coated polyimide foil perforated with high density holes.

Electrons are collected on patterned readout board.
A fast signal can be detected on the lower GEM electrode for triggering or energy discrimination.
All readout electrodes are at ground potential.
Positive ions partially collected on the GEM electrodes.

THGEM – Thick GEM

Standard GEM

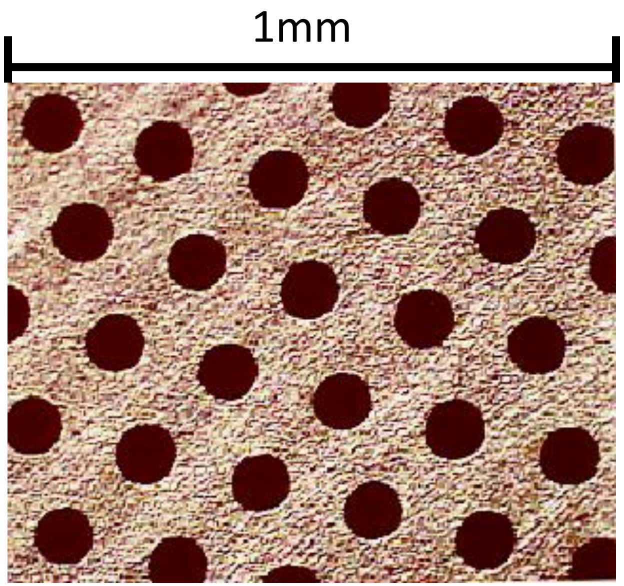

- Microlithography + etching
- High Spatial resolution (tens of microns); V_{GEM}~400V
- >10^3 gain in single GEM
- 10^6 gain in cascaded GEMs
- Fast (ns)
- Low pressure – gain~30

THGEM

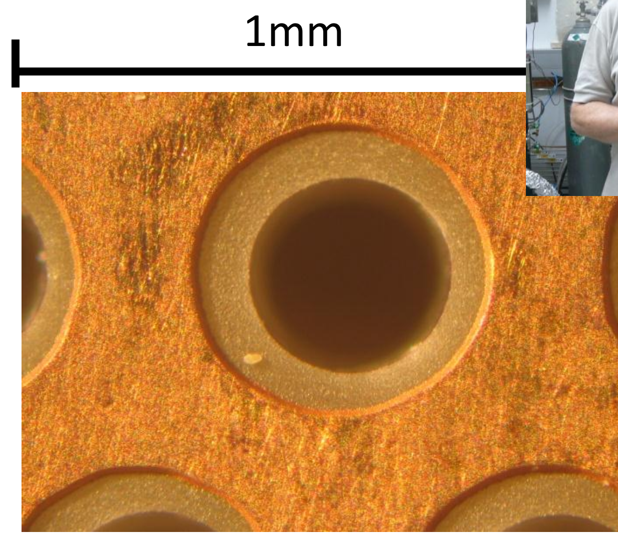

Thick GEM
A. Breskin

- PCB tech - etching + drilling
- Simple and robust
- V_{TGEM}~2KV (at atmospheric pressure)
- 10^5 gain in single- & 10^7 double-TGEM
- Sub-mm to mm special resolution
- Fast (ns)
- Low pressure (<1Torr) gain 10^4

V. Peskov, A. Breskin …

MICROMEGAS

Y. Giomataris, Ph. Rebourgeard, J.P. Robert, Charpak, NIMA376(1996)29

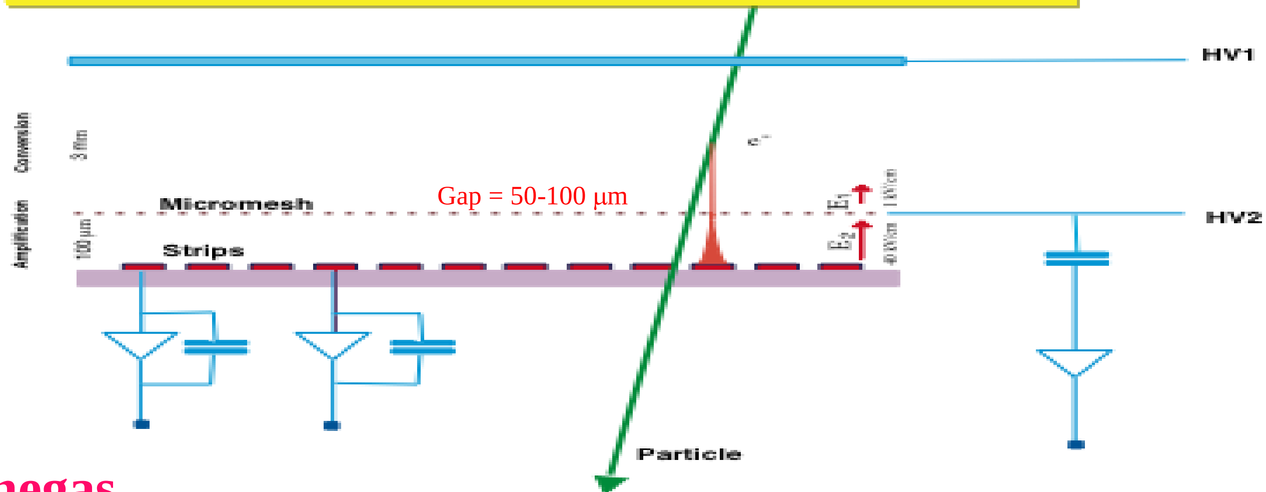

In 1st Micromegas
Fishing line spacers have been used

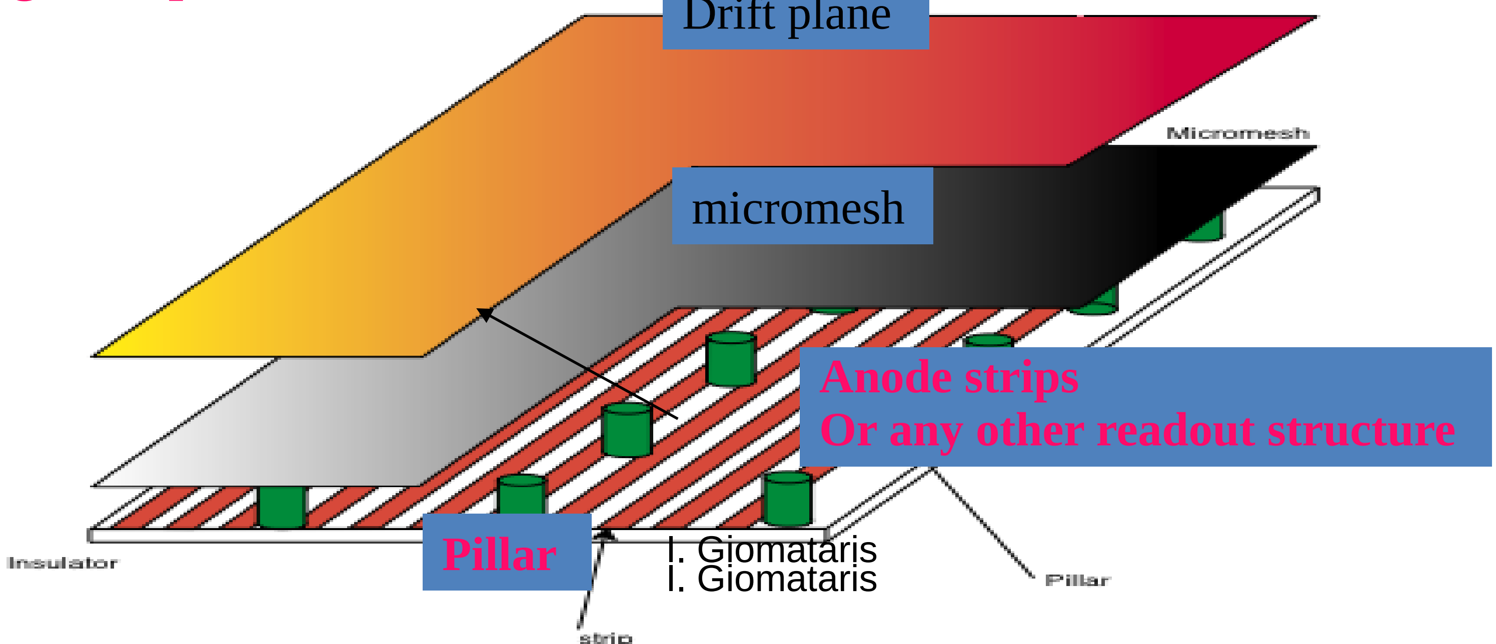

Micromegas performance

High radiation resistance : > 30 mC/mm2 > 25 LHC years
G. Puill, et al., IEEE Trans. Nucl. Sci. NS-46 (6) (1999)1894.

Good energy resolution

Signal discrimination

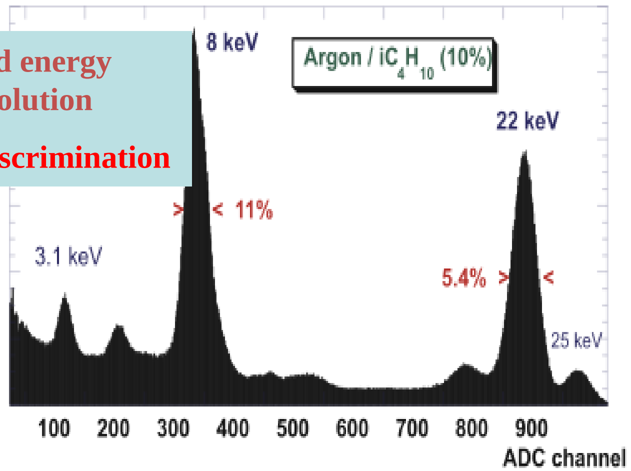

A. Delbart, ***Nucl.Instrum.Meth.A461:84-87,2001***

Sub-nanosecond time resolution

Time of flight, fast TPC

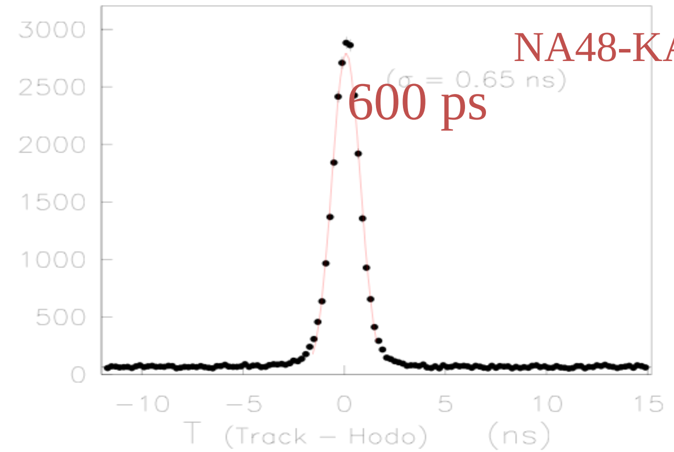

Excellent single electron resolution

UV photodetector

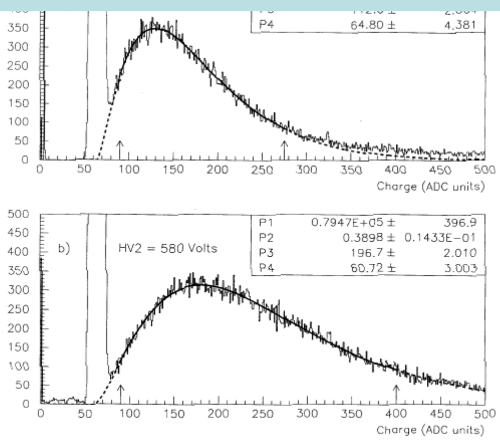

Spatial resolution	<12 μm
Time resolution	<0.2ns
Energy resolution (FWHM)	11% (στα 5.9 keV)
Rate capability	> 10^6/mm^2/s

Large Atlas muon detector Half-size Chamber

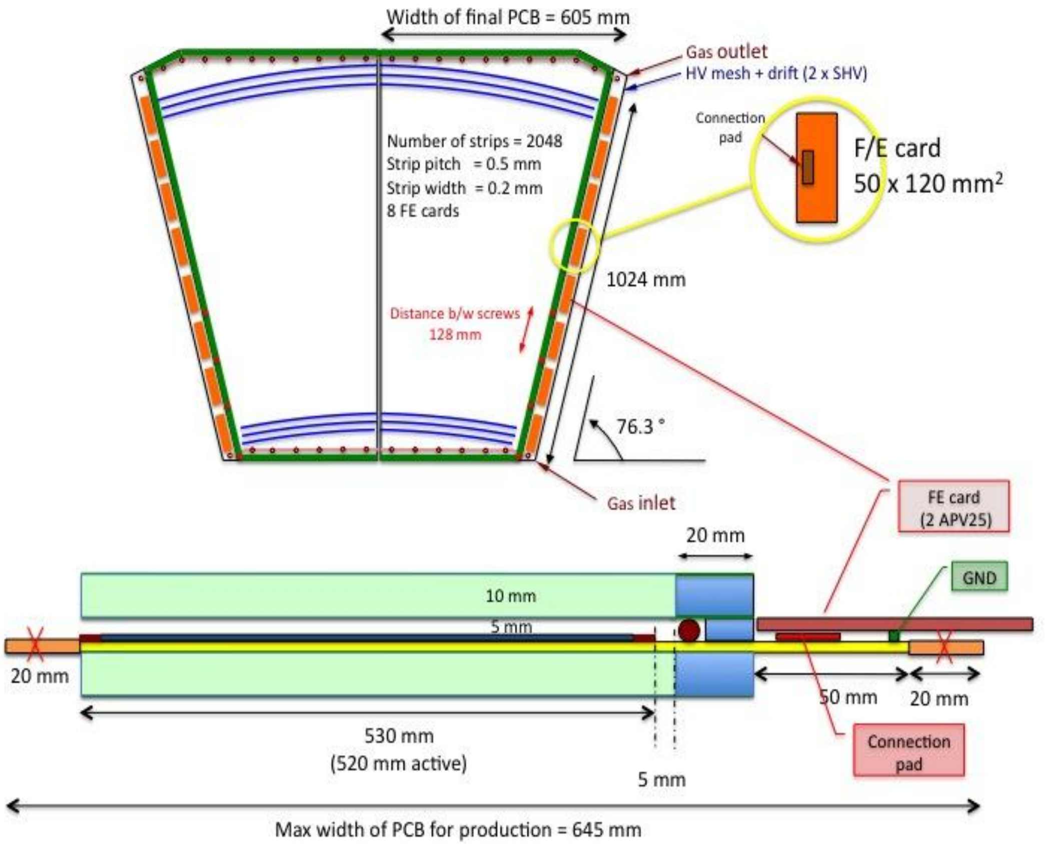

Large chambers 2x1 m^2
- **CERN new infrastructure**
- **Transfer to industry under way**

COMMERCIAL SYSTEM

SMART SOLUTIONS for biomedical IMAGING

BIOSPACE

BIOSPACE

(FOUNDED BY CHARPAK)

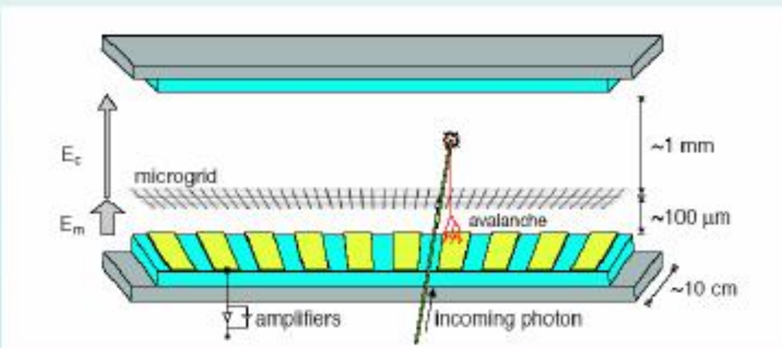

xray **imaging**

EOS™ low irradiation 2D-3D X-ray scanner

EOS™ is an equipment dedicated to the orthopedic practice, that performs head to toes, low dose, 2D and 3D digital X-ray imaging. EOS™ takes by scanning two simultaneous, perpendicular planar X-ray views in the standing position and provides the clinician with the corresponding digital planar radiographs together with a three dimensional bone envelope image.

2D

- spine exam within 5 to 10 seconds.
- full body scan in less than 25 seconds.
- patient irradiation dose 5 to 10 fold below dose received in conventional, CR (computed radiology) or DR (digital radiology) exams.
- High image dynamics allowing the simultaneous observation of soft and bone tissues.

The three dimensional bone envelope, calculated using a proprietary technology, can be derived from the two digital radiographs for the spine, knee and hip. It replaces the three dimensional image obtained from highly irradiating CT scan exams multiplanar digital imaging.

3D

- 3D images with patient irradiation dose 100 to 500 fold below those received during full spine CT exams

EOS™ provides a unique digital, low dose solution for exams routinely performed in the orthopedic practice combined with the 3D capability up to now achievable with CT scans only.

EOS™ is under clinical trials at Hôpital St Vincent de Paul, Paris and will be tested in the Hôpital Erasme (Brussels) and the Hospital Vall d'Hebron (Barcelona) within a clinical trial programme funded by the European Union.

EOS™ is developed in collaboration with ENSAM/LBM (Laboratoire de Biomécanique de l'Ecole Nationale Supérieure des Arts et Métiers), Paris, and ETS/LIO (Laboratoire de recherche en imagerie et Orthopédie de l'Ecole de Technologie Supérieure), Montréal

For more information about EOS™: info@biospace.fr

Georges' Company - Low Dose X-ray

EOS imaging

COMPANY OVERVIEW | EOS PRODUCTS | NEWS & EVENTS | HEALTH PROFESSIONALS | PATIENTS | CONTACT

HOME › COMPANY OVERVIEW › HISTORY

Biospace Radiologie

COMPANY OVERVIEW
- History
- Management team
- Board of directors
- Partners

History

The 1992 Nobel Prize for Physics was awarded to a revolutionary invention: a high energy particle detector.

This detector design gave birth to EOS: it enabled X-ray imaging to be performed at a much lower dose, with an expanded dynamic range and without the vertical distortion inherent in today's long length film and digital imaging systems. A collaboration between a team of world-class physicists, engineers and most importantly orthopedic surgeons and radiologists brought EOS from proof-of-concept to a fully operational machine. All thanks to a radically new vision of what imaging could and should bring to orthopedics.

- **2005** Clinical testing in Paris and Brussels hospitals completed with first EOS prototype
- **2006** biospace med is created and has received its first venture capital round
- **2007** EOS has received market approval in Europe and North America
- **2010** EOS equips hospitals and private clinics in the USA, Canada and 5 European countries
- **2010** The company changes its corporate name to EOS imaging

EOS imaging development and production facilities are located in central Paris. The company has subsidiaries in Cambridge, USA and Montreal, Canada.

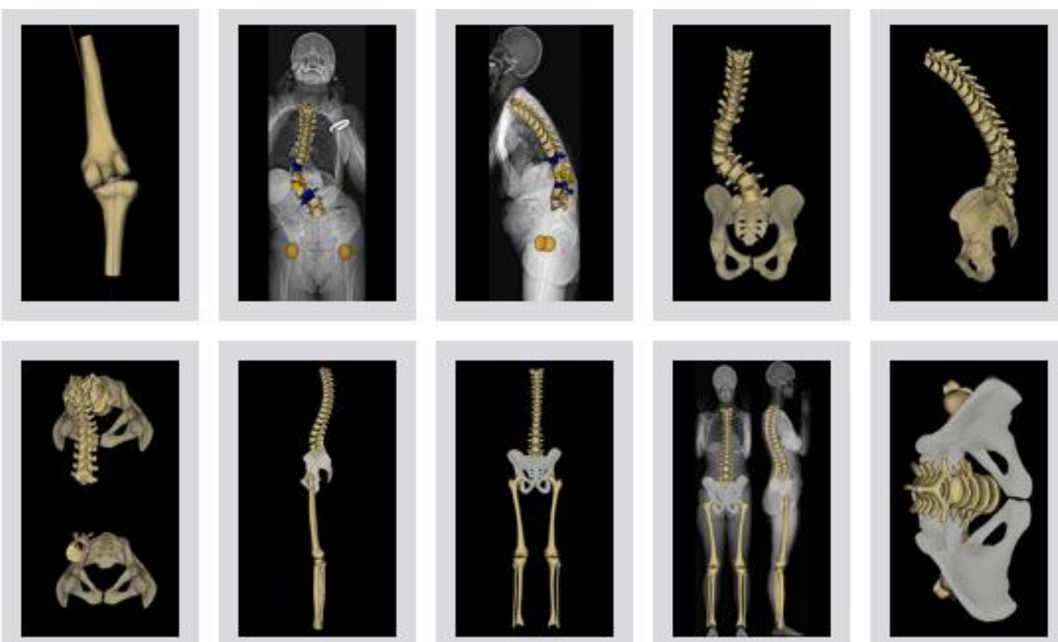

Fig. 1: EOS 2D/3D System

Gas Chambers

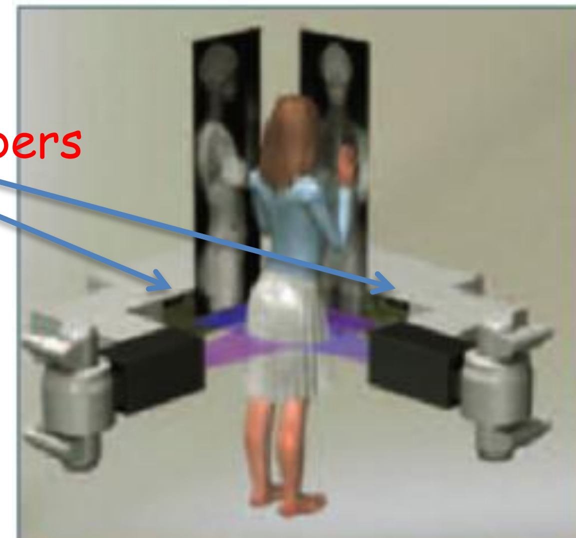

Fig. 2: EOS Scanning Technique
Vertical linear scanning allows the acquisition of long length images without being limited by the detector's vertical dimension. This is particularly important when treating patients whose global balance and posture must be observed.

See, measure, and treat like never before

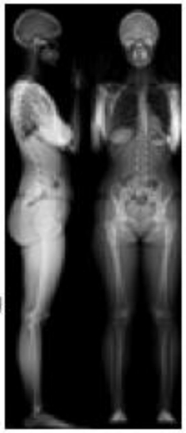

Biospace Radiologie

EOS captures whole body images of a standing patient in a single scan without any stitching or vertical distortion. Frontal and Lateral digital images of any length may be obtained simultaneously, with an outstanding image quality.

This was unavailable until EOS.

10 X Lower Dose X-ray

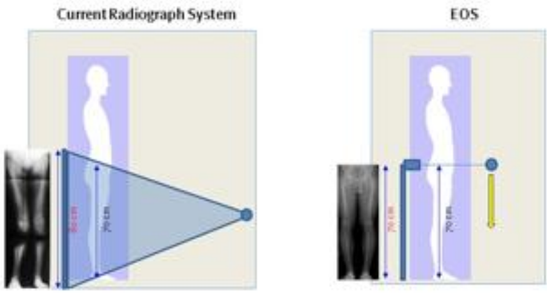

The lack of vertical distortion - thanks to the EOS slot scanning technology and its unique reference plane positioning- provides true size images, in 1:1 scale, for highly accurate surgical planning measurement.

This was unavailable until EOS.

Special Focus: Pediatric

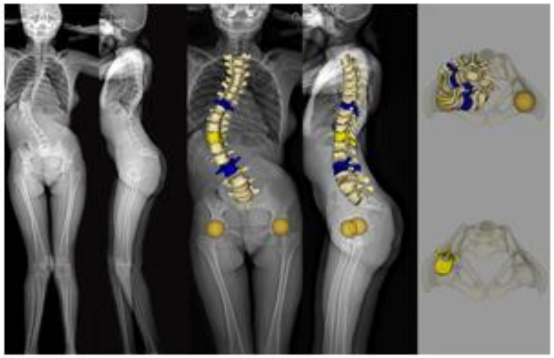

The 3D bone-modeling is unique because it is in a weight-bearing position.

A 3D rendering of specific skeletal anatomies may be made at any time after frontal and lateral scans are performed. These 3D renderings give both a weight-bearing 3D model as well as the automatic calculation of clinical parameters, enabling new ways to globally evaluate a patient's postural abnormality, in the natural UPRIGHT 3D environment.

This was unavailable until EOS.

EOS radically changes the way radiologist/orthopedist teams can now diagnose and treat musculoskeletal pathologies on all age groups, from children to geriatric patients.

DIGITAL RADIOGRAPHY WITH GEM DETECTORS:

QuickTime™ and a GIF decompressor are needed to see this picture.

2-D READOUT

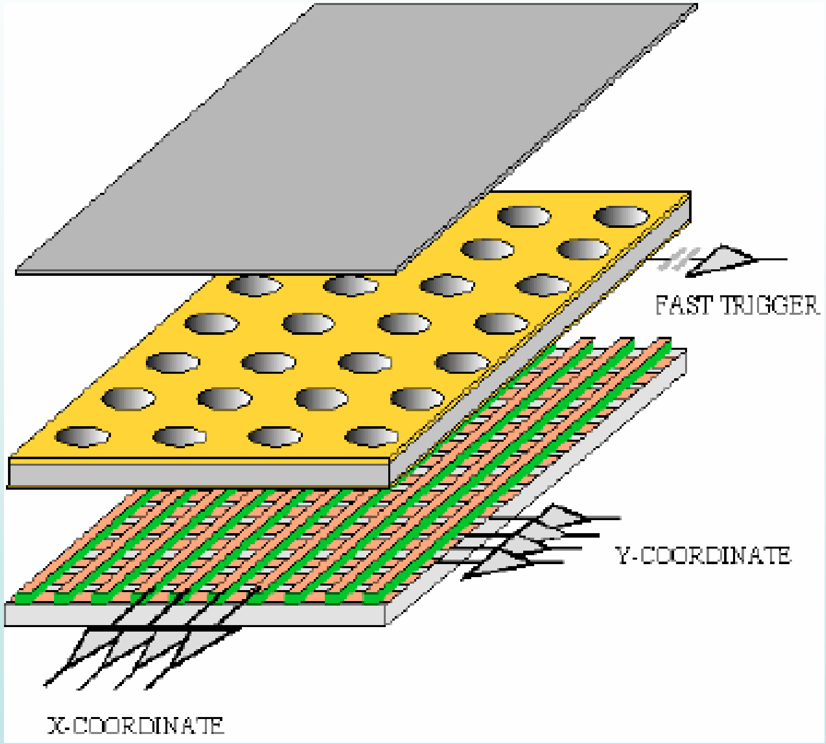

RADIOGRAPHY OF A SMALL MAMMAL (A BAT)

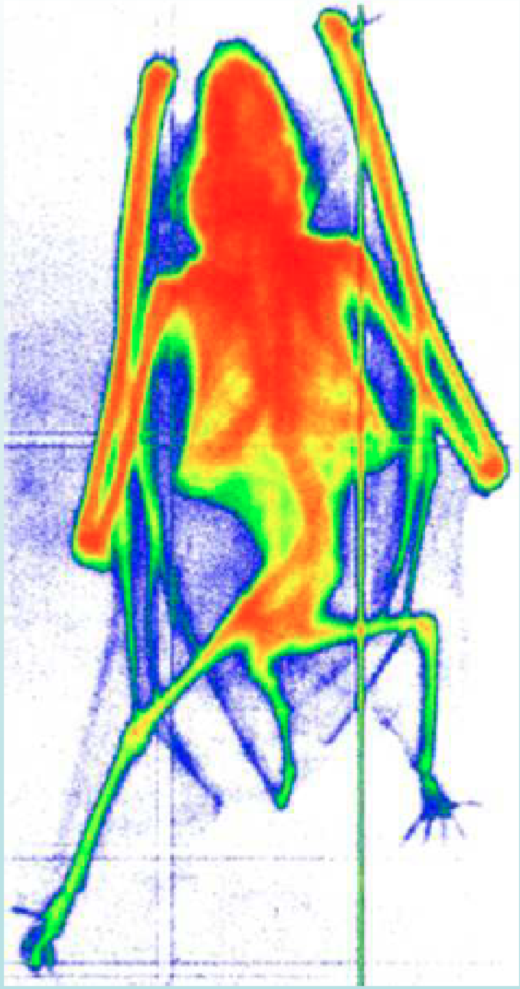

VERY HIGH RATE IMAGING: PORTAL IMAGING WITH GEM

(ADVANCED PROJECT AT KAROLINSKA HOSPITAL, STOCKHOLM) :

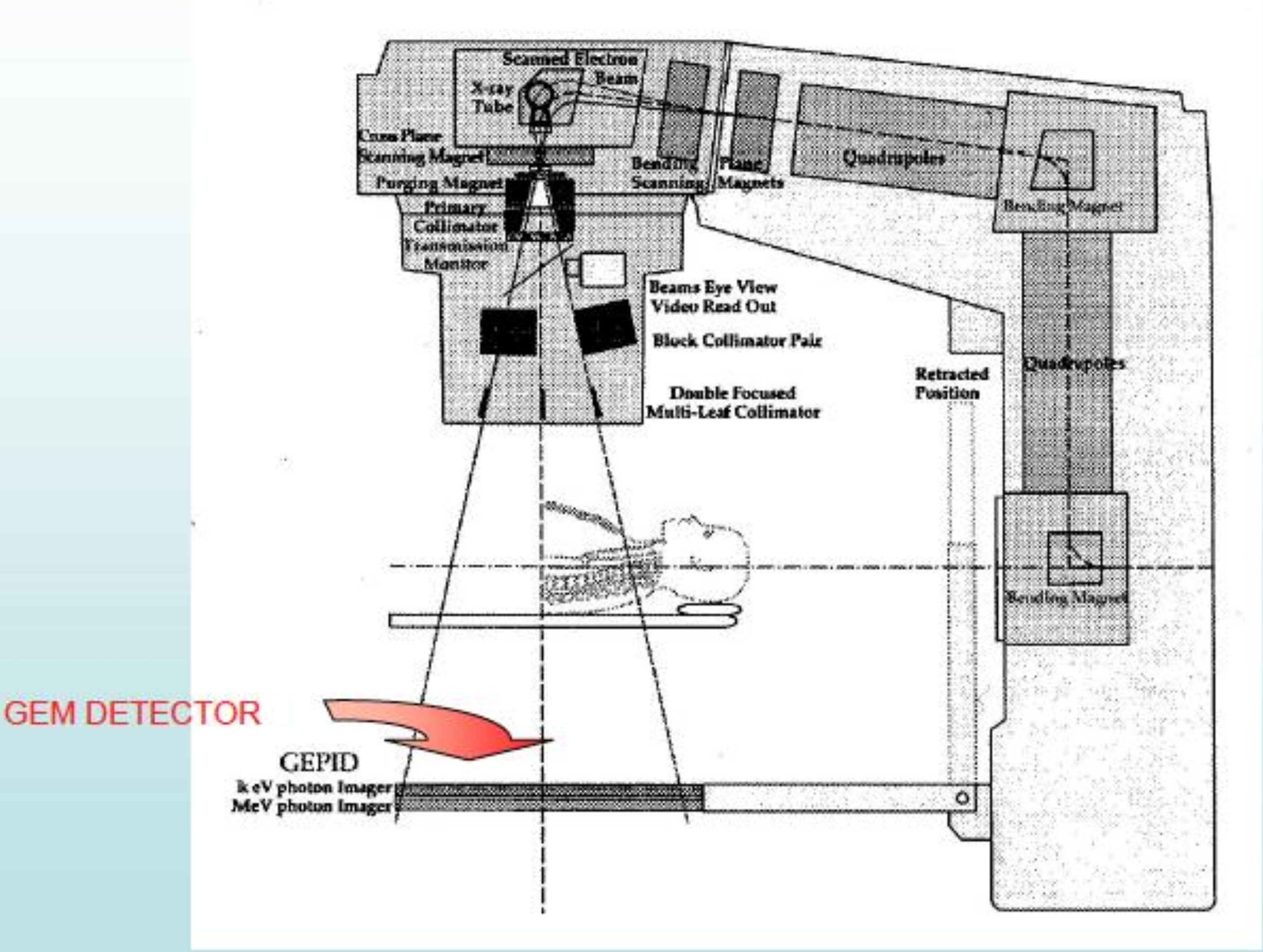

ON-LINE FAST IMAGE ALLOWS TO MODIFY THE TREATMENT PLAN DURING THERAPY

Why Semiconductors ?

- Presently most medical devices are based on photo-imaging (film) => excellent resolution but low sensitivity and lack of image uniformity => long exposure times in β- and x-ray imaging and development time.

- Lately, digital imaging based on integrating devices (i.e. MWPC (multi-wire proportional chambers, gas devices). Sensitivity better than film but resolution poorer (~400 μm)

- New idea: single particle counting using semiconductor detectors has the following advantages:
  - High sensitivity (low exposure time)
  - High dynamic range and excellent linearity
  - Energy discrimination of particles
  - Direct digital imaging and online image display
  - Very good resolution (< 50 μm)

Which Semiconductors ?

- Generally available: Ge, Si, GaAs, CdTe
- Ge needs liquid nitrogen cooling to yield good resolution
- GaAs and CdTe have higher X-ray absorption efficiency than Si in relevant range (<E>=10-70 keV) At 20 keV the detection efficiency for a 200 μm thickness GaAs layer is 98%, which is four times higher than the equivalent efficiency in Silicon.
- GaAs is more advanced than CdTe but both technologies are in their prototype stages compared to Silicon.

Photon Absorption Efficiencies

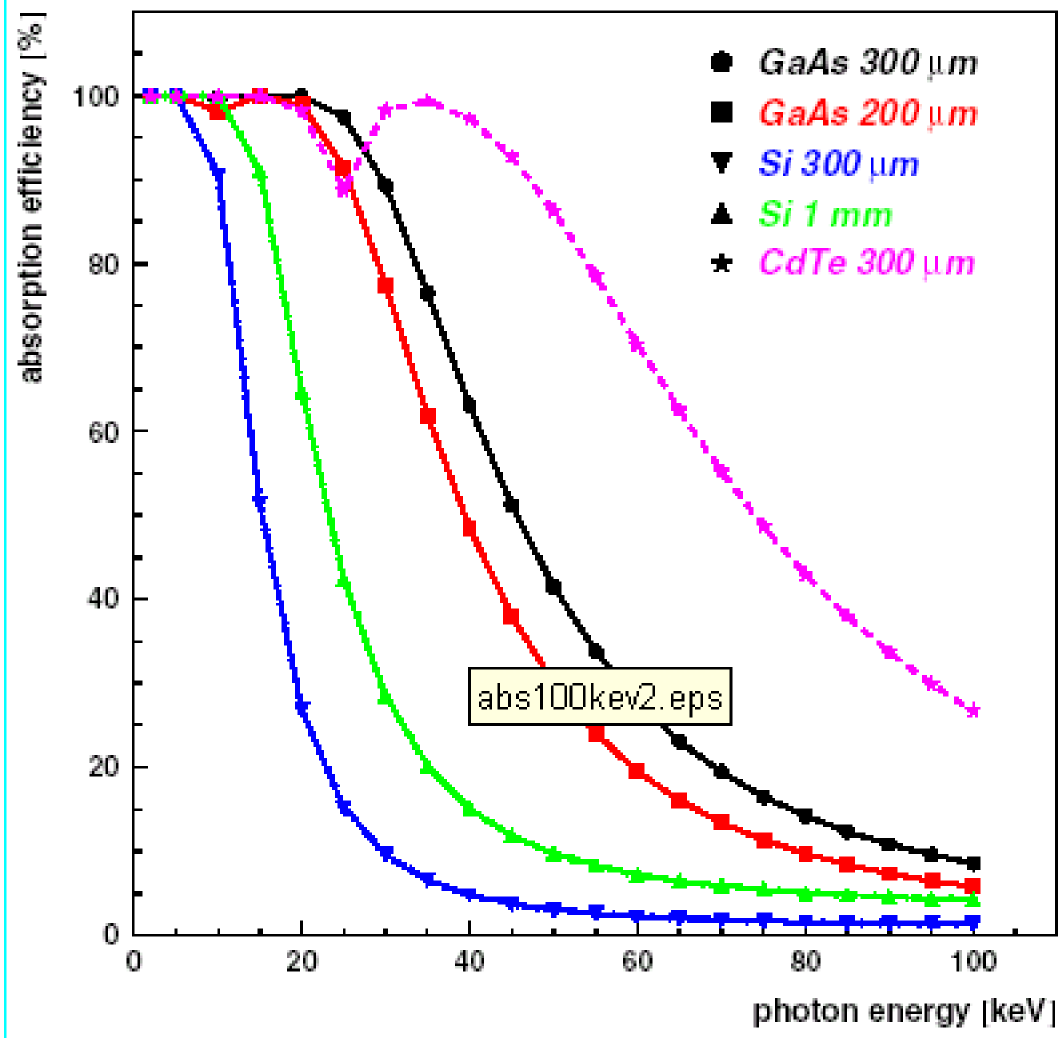

Face on detectors

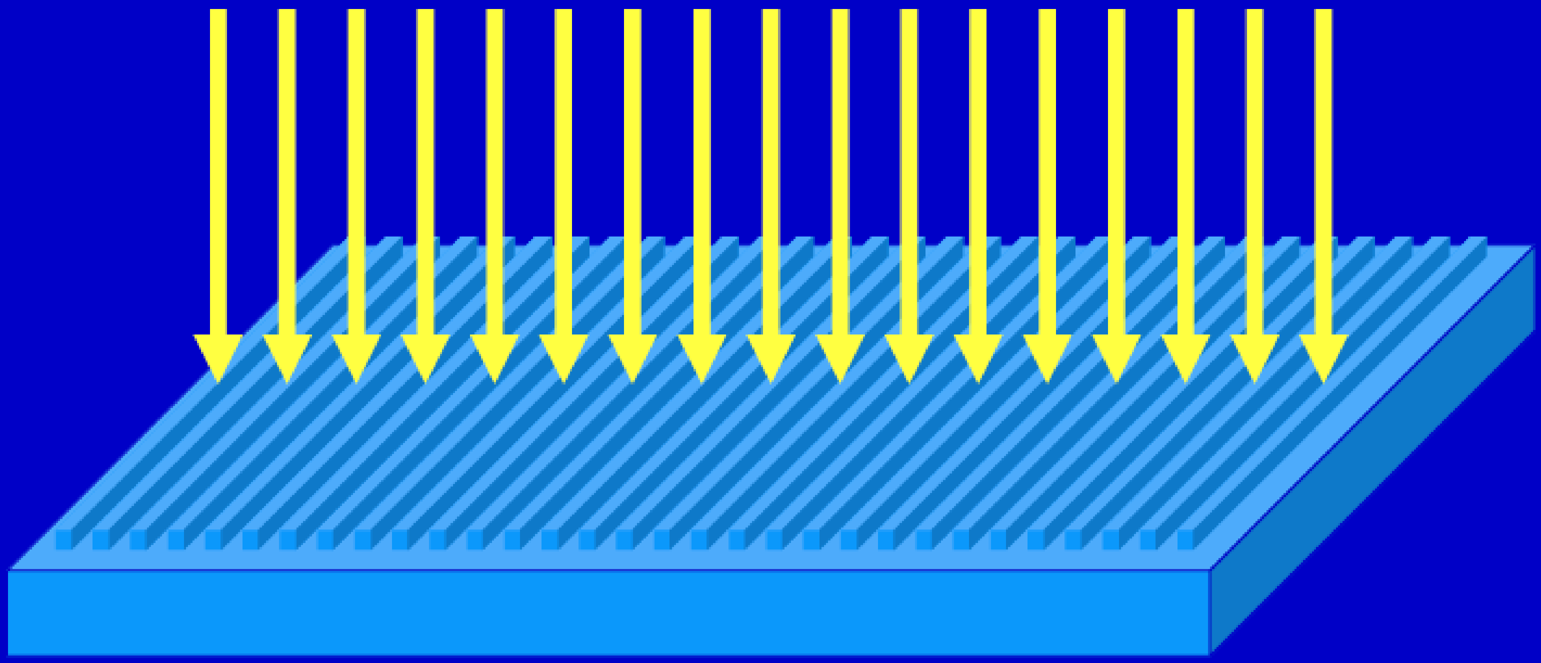

✓ A 20 keV photon has only 25% probability of being absorbed in 300 μm of silicon

✓ A 2-D detector is required for imaging

Edge on detectors

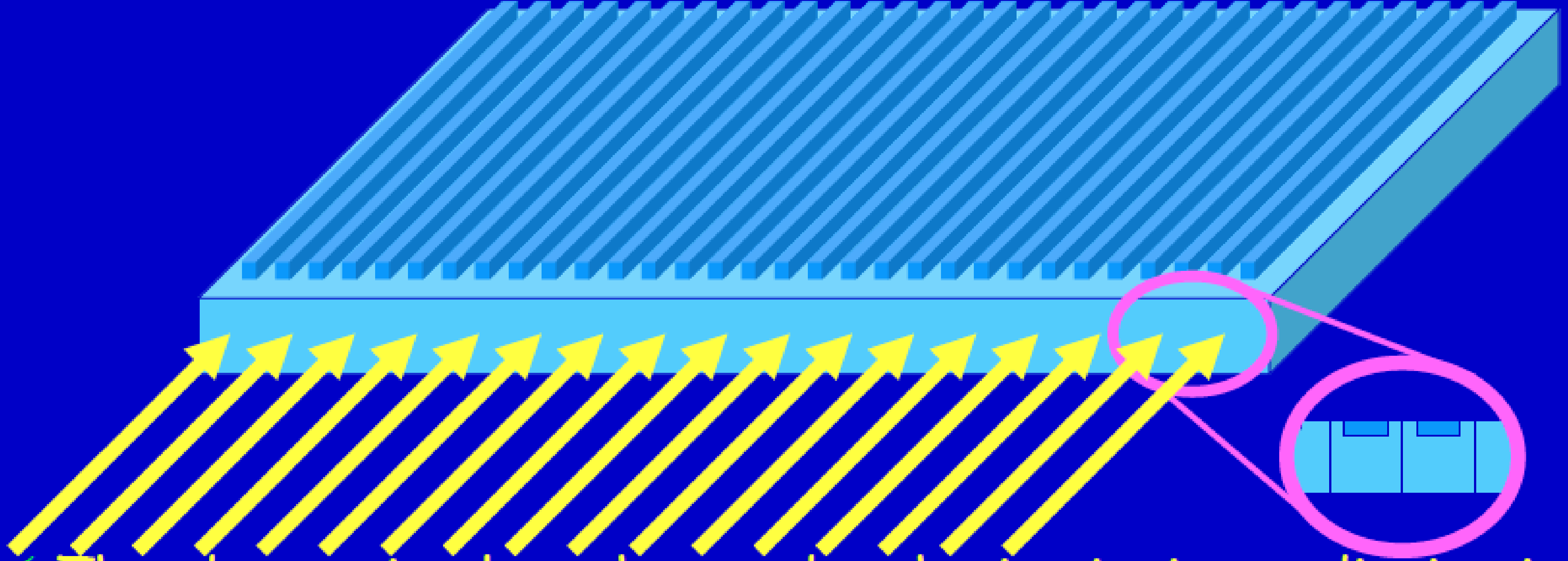

✓ The absorption length seen by the impinging radiation is given by the strip length

- ➢100% absorption probability in 1 cm of silicon for 20 keV photons

✓The pixels of size is determined by the strip pitch times the detector thickness

✓Almost complete scattering rejection

Arfelli et al., Physica Medica Vol IX, pp. 229-233, 1993

Edge on vs. Face on

Edge on

- ✓ High absorption efficiency
- ✓ Good scattering rejection
- ✗ Needs scanning
  - Long acquisition time
- ✓ Small number of channels

Face on

- ✗ Limited quantum efficiency
- ✗ Scattered radiation detection
- ✓ No scanning required
- 2D detectors
  - Double sided silicon microstrip detectors
    - ✗ Fast read out electronics to avoid ambiguities
  - Pixel detectors
    - ✗ Large number of channels

Medical Applications

X-ray applications

- Digital mammography <E> = 20 keV
- Dental X-ray tube <E>= 35 keV
- Fast frame medical diagnostics

Nuclear medicine

- Thyroid measurements, <E> = 60-140 keV photons
- DNA probe array, β-emitter (^{32}P, ^{14}C, ^{35}S), <E> = 50-700 keV

Digital Mammography (DM)

- **Main features**
  - Linear response with X-ray exposure
  - Wide dynamic range ($10^4 – 10^5$)
    - Mammography of dense breast
  - Reduced radiation dose
    - Exposure determined as a function of the Signal to Noise Ratio (SNR) not of the Optical Density of the film (OD)
      - Dose reduction from 20 to 80 %
  - Image processing
  - time required for the examination ($t_{exp}<1s$; T_{proc}~minutes)

- Limitations (?)
  - Spatial resolution
    - Film-screen systems $\geq$ 20 lp/mm
    - Digital systems $\leq$ 5 lp/mm (spatial frequency is smaller, but image is sharper)
  - Monitor resolution
    - Monitor 2000x2500 pixels, resolution 0.1 mm

Detection Quantum Efficiency

$DQE = SNR_{out}^2/SNR_{in}^2$ **Noise of the detection process**

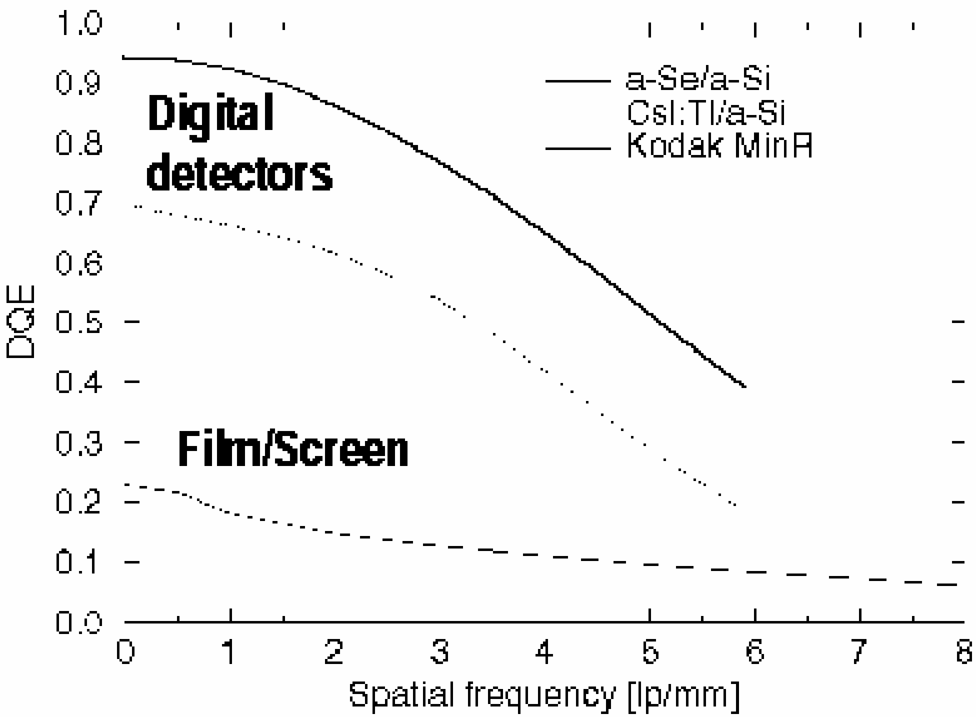

DQE(v) for mammography conditions:

- simulated (cascaded linear systems model) a-Se (350µm) on a-Si with 85 µm pixel pitch
- simulated (cascaded linear systems model) Cs:I:Tl (140µm) on a-Si with 85 µm pixel pitch
- measured Kodak MinR film-screen system

Figure 1. Direct vs Indirect Detectors

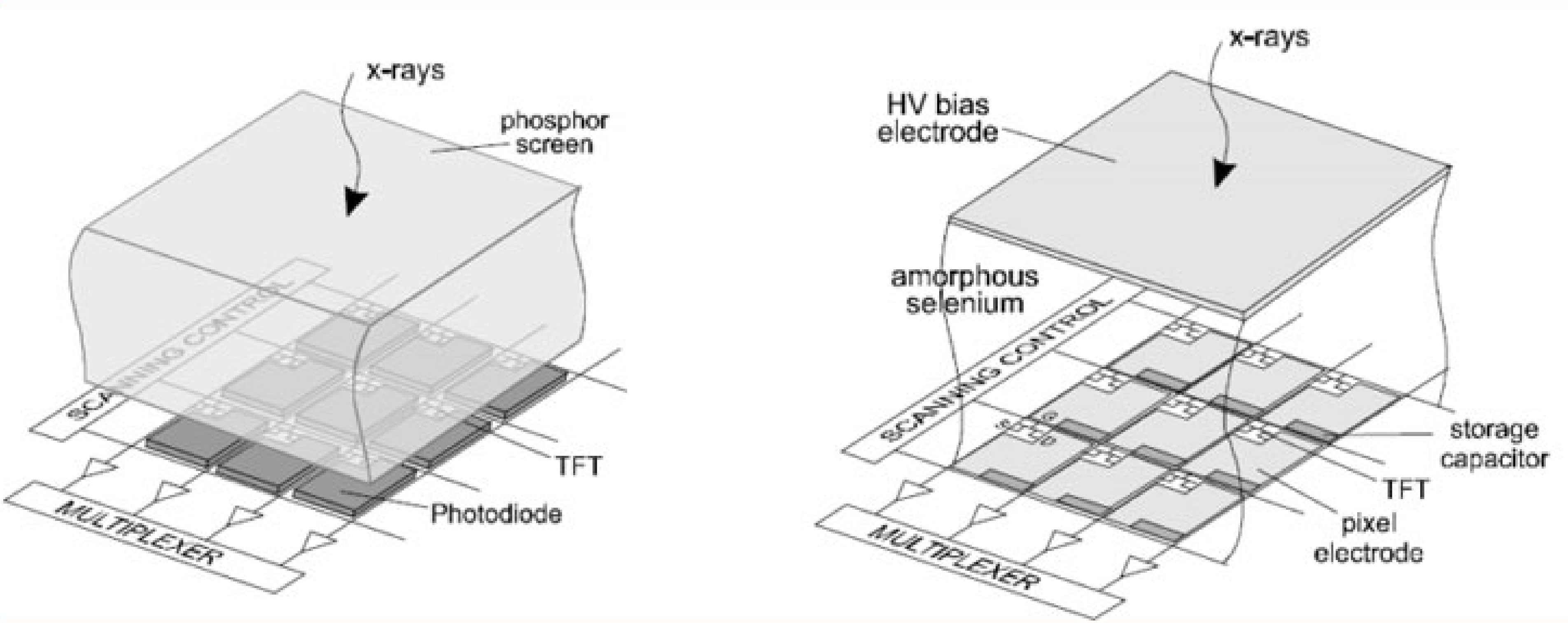

TFT = thin-film transistor.
Reprinted with Rowlands. Flat panel detectors for medical X-ray: physics and technology. Available at: http://hepwww.rl.ac.uk/Vertex03/Talks/Row/Rowlands.pdf. Accessed December 20, 2010.[1]

The Emergence of Portable Flat-Panel DR Detectors in Medical Imaging
George Tsoukatos, BPS, RT(R)

http://www.eradimaging.com/site/printerfriendly.cfm?ID=760

Amorphous vs. crystalline semiconductors

- Advantage of amorphous semiconductors:
  Can be produced into any size detectors (i.e. a-Si can match film detector size)

- Disadvantage of amorphous semiconductors:
  Charge carrier lifetimes are orders of magnitude lower than in crystalline semiconductors. High voltages have to be applied to collect charges fast.

Figure 5. Dual-Energy Subtraction

Images courtesy of Francois Nicholas. GE Medical Systems.

Figure 4. Flat-Panel Detector Signal Chain

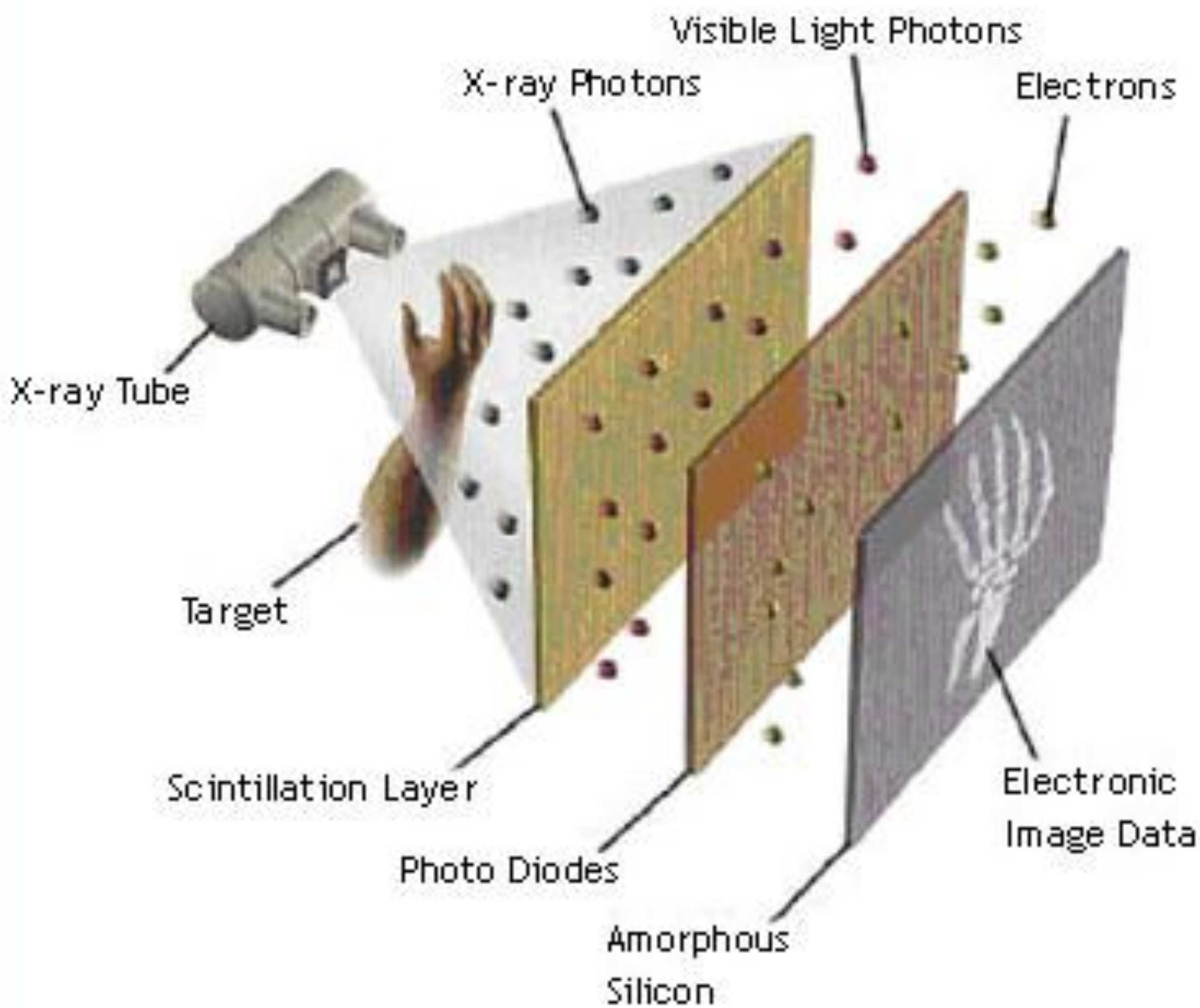

Reprinted with permission from Varian Medical Systems. PaxScan. Flat-panel X-ray imaging [brochure]. November 11, 2004.[13]

Digital Tomosynthesis

Digital Tomosynthesis

enhances X-ray equipment

- Principle: limited angle tomography
- With digital acquisition retrospective choice of slice
- Algorithm/SW empowers systems towards 3-D
- Adaptive sampling @ minimum dose

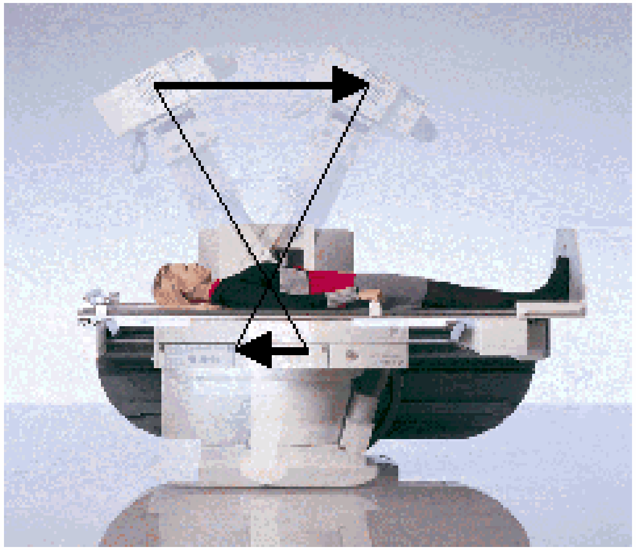

Image quality in digital tomosynthesis

PET Application

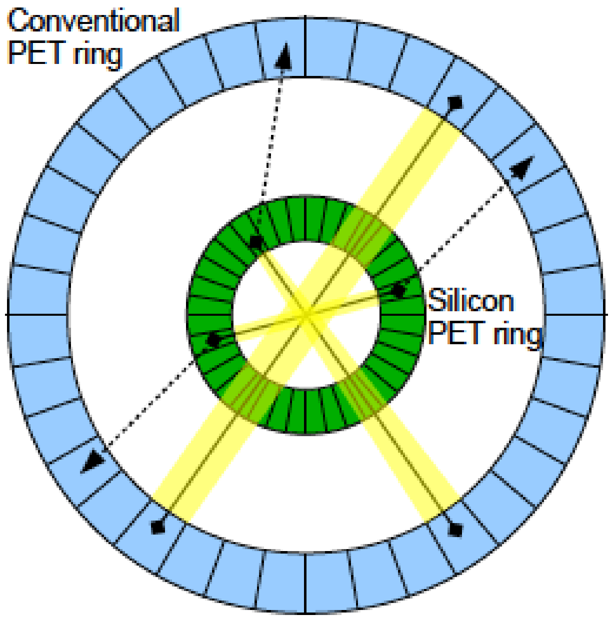

Figure 5.3: Diagram of the dual ring PET concept and the three potential ty
PET coincidences. In order of highest resolution to lowest (and lowest sensitiv
highest), they are: standard PET events in the silicon ring, hybrid events be
the silicon and conventional ring, and standard PET events in the conventiona
Nearly all silicon interactions are Compton scatters followed by the absorption
photon in the scintillator ring.

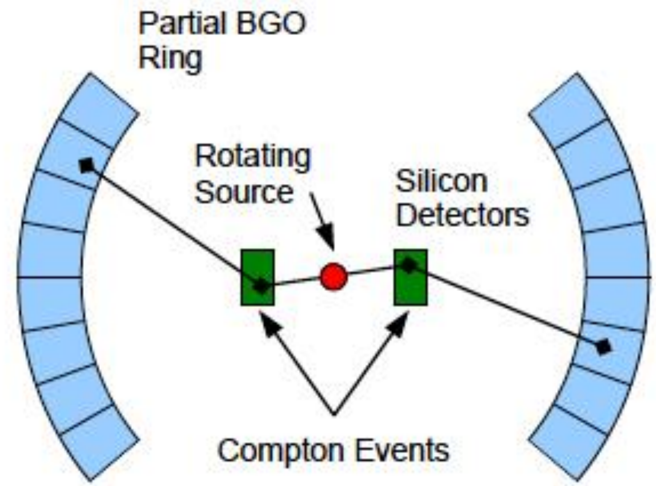

Figure 5.4: Diagram of the partial ring setup with rotating source to simulate a full ring.

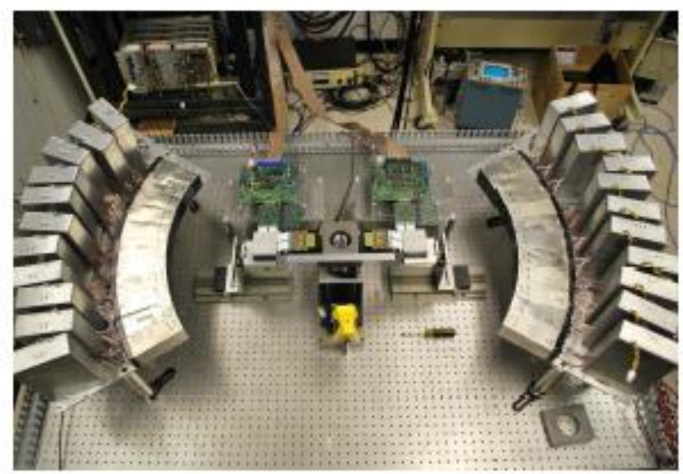

Figure 5.5: Image of the high resolution PET partial ring setup during final assembly.

Eric R. Cochran, M.S. Thesis, Ohio State.

Silicon Drift Detectors ?

- Generally available: CCD, Si pixels, Si strip, Si drift
- CCD (charge-coupled devices) are slow and not very radiation resistant.
- Silicon pixels are fast and have high resolution but they are very expensive and the connection to the electronics (bump bonded) is a difficult technical process, but the main electronics development (PCC) is optimized for bump-bonding
- Silicon strip detectors have relatively poor resolution and are not cost competitive to drift detectors.

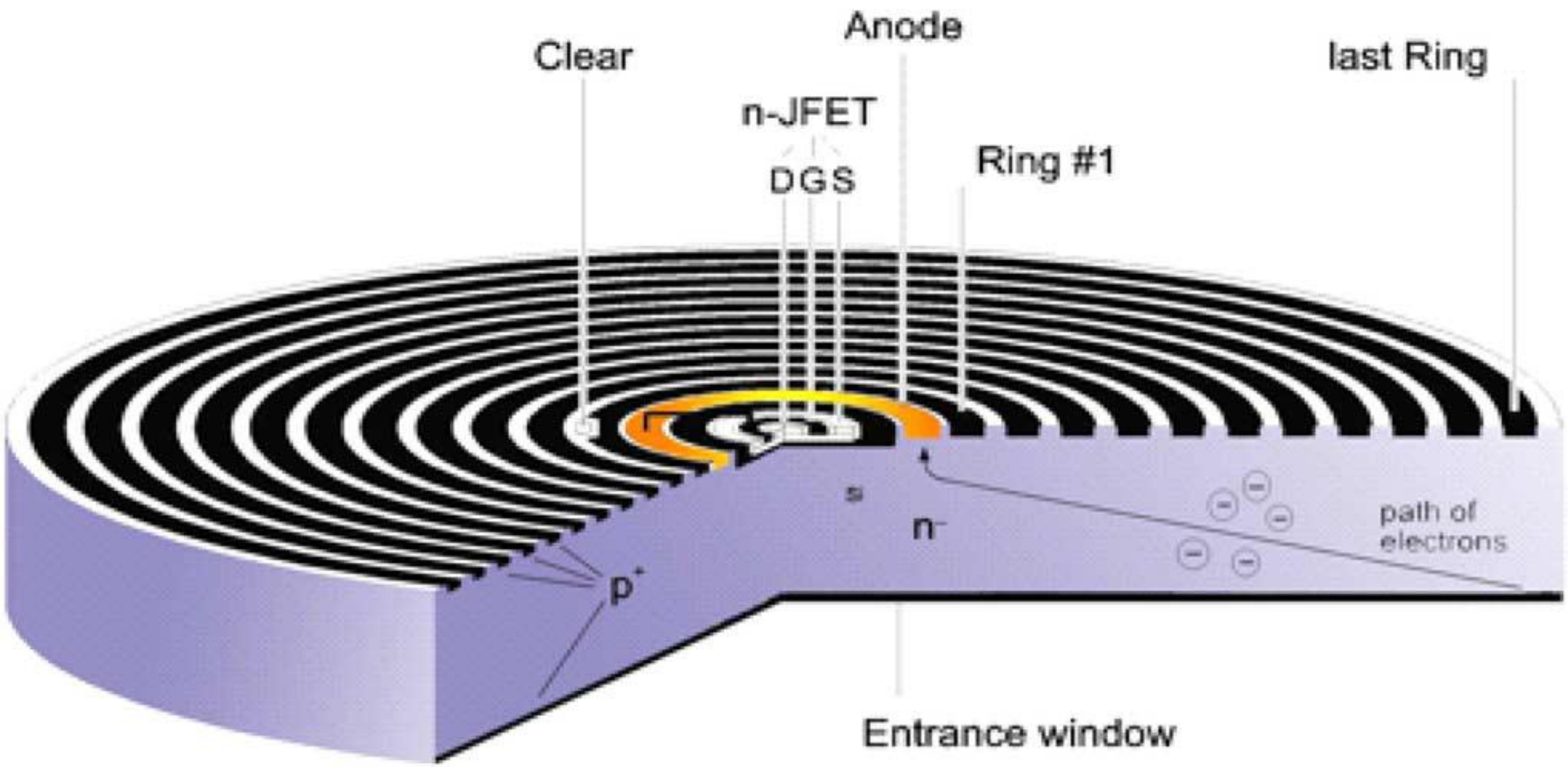

Cross section of a Silicon Drift Detector with the integrated n-channel JFET, showing the contacts and corresponding doping type.

Present status of technology

STAR (detector at Relativistic Heavy Ion Collider (RHIC) at BNL on Long Island)

- 4in. NTD material, 3 kΩcm, 280 μm thick, 6.3 by 6.3 cm area
- 250 μm readout pitch, 61,440 pixels per detector
- SINTEF produced 250 good wafers (70% yield)

ALICE (future detector at Large Hadron Collider (LHC) at CERN in Geneva, Switzerland)

- 5in. NTD material, 2 kΩcm, 280 μm thick, 280 μm pitch
- CANBERRA produced around 100 prototypes, good yield

Future (potentially for detector at Next Linear Collider (NLC) in ?)

- 6in. NTD, 150 micron thick, any pitch between 200-400 μm
- 10 by 10 cm wafer
- low radiation length, low cost for large area

Actual Collision in STAR (central)

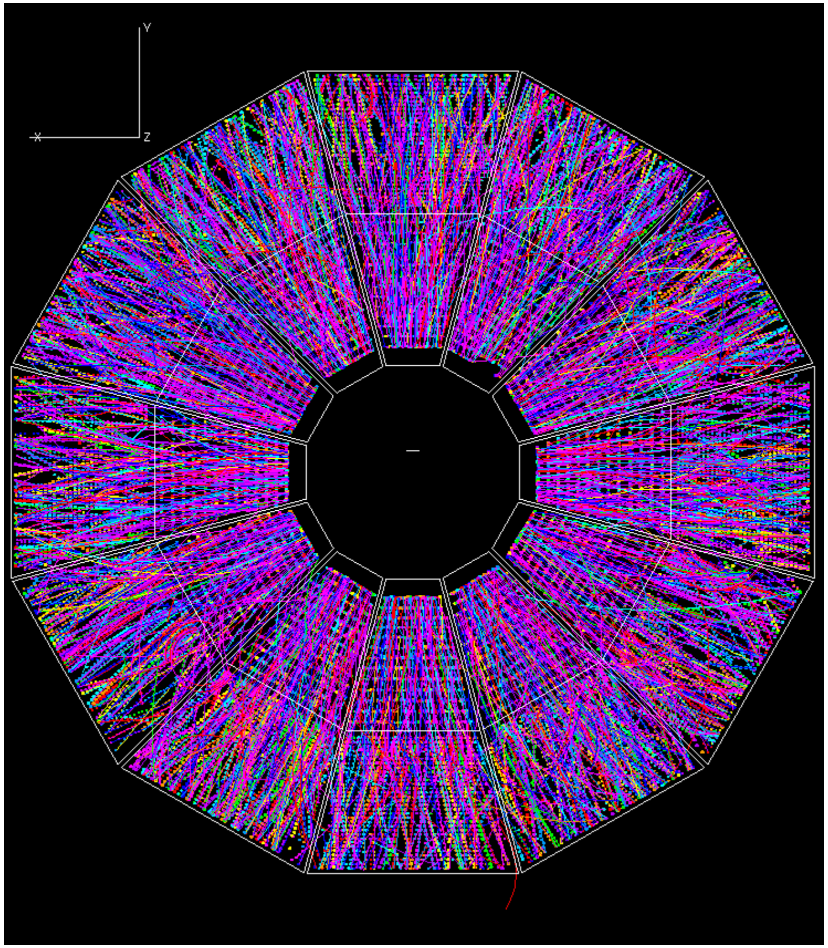

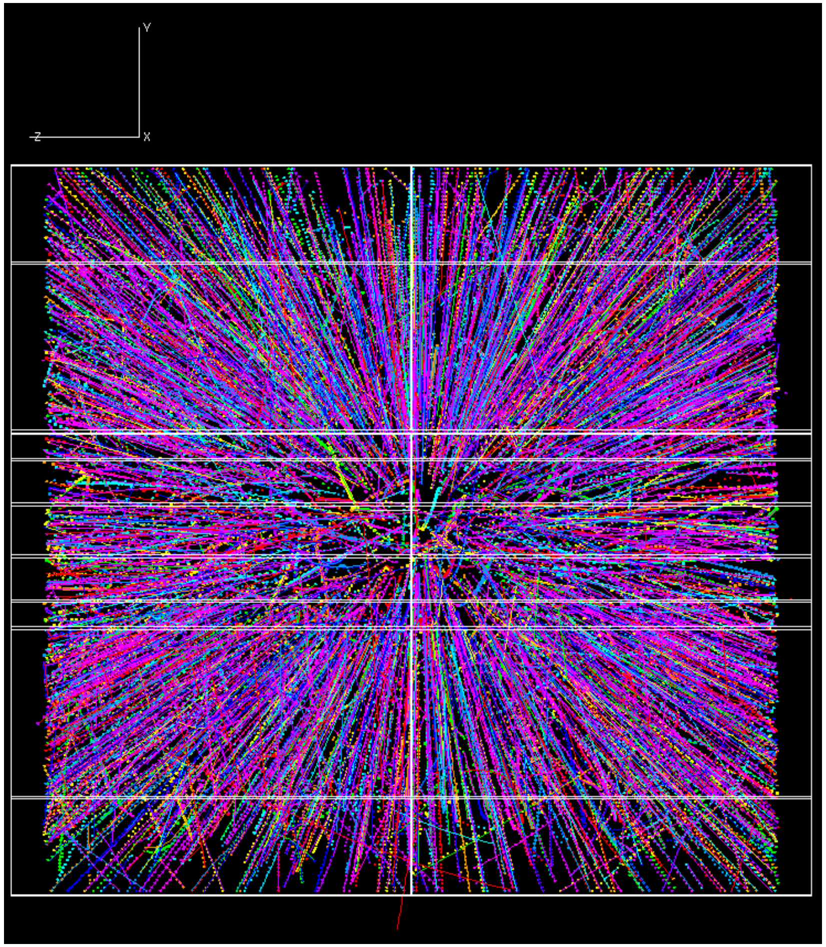

HICAM

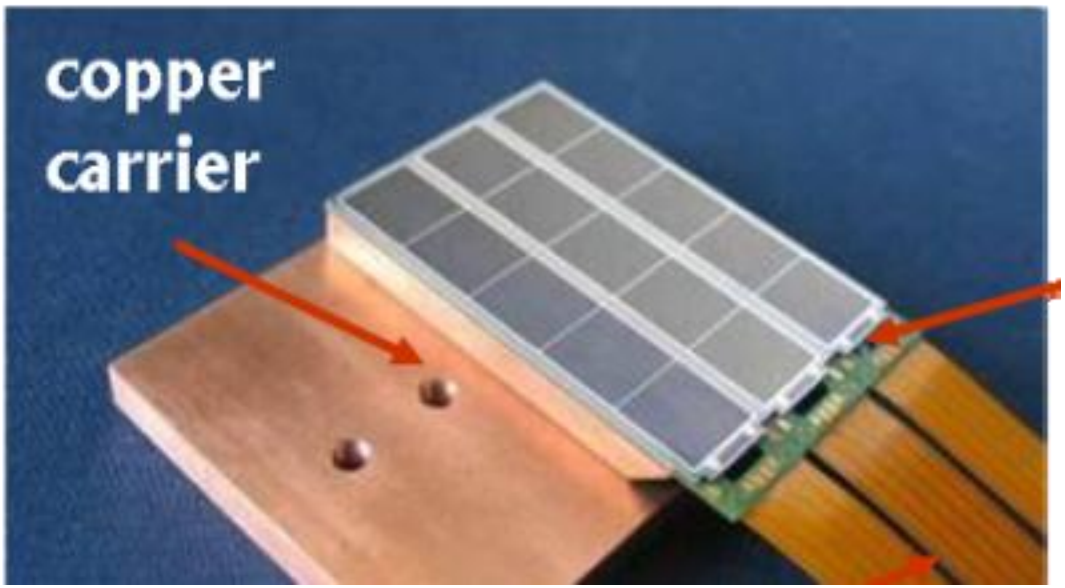

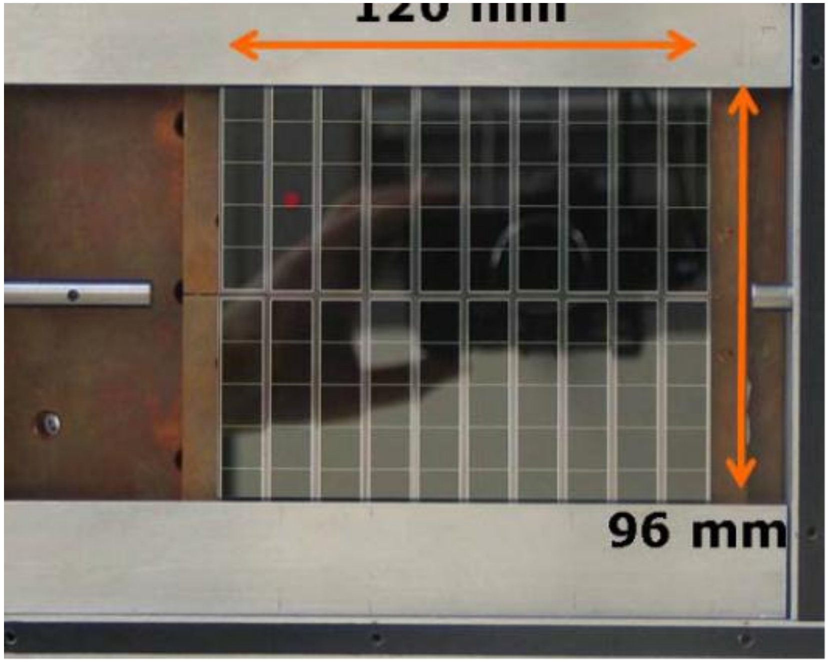

P.Busca, R.Peloso, C.Fiorini, A.Gola, A.Abba, K.Erlandsson, B.F.Hutton, C.Bianchi, G.L.Poli, U.Guerra, G.Virotta, L.Ottobrini, C.Martelli,
G.Lucignani, A.Pedretti, P.Van Mullekom, S.Incorvaia, F.Perotti

HICAM

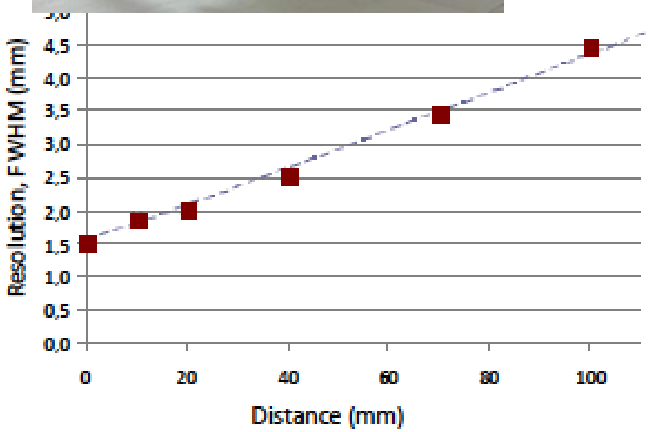

Fig.2. Spatial resolution in function of source-collimator distance. Estimated intrinsic resolution ~ 0.8 mm.

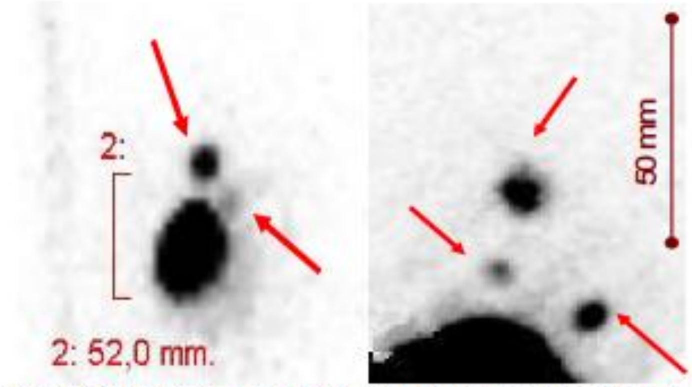

Fig.5. Image of the lymphoscintigraphy to localize the sentinel node. Left acquisition is performed with E.CAM gamma camera, the arrows indicate the two visible nodules. Same patient acquired with HICAM is shown on the right, the arrows indicate the three visible nodules.

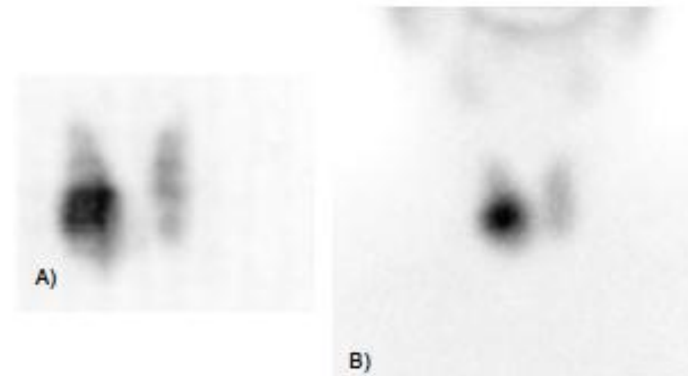

Fig.6. An example of hyper fixation at the right thyroid lobe. A) image acquired with HICAM; B) the same patient acquired with E.CAM gamma camera.

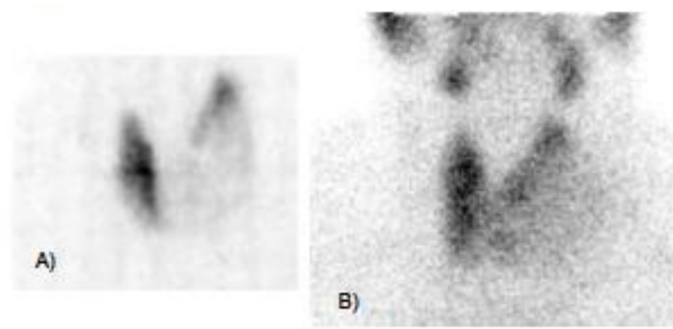

Fig.7. An example of hypo fixation at the left thyroid lobe. A)image acquired with HICAM; B) the same patient acquired with E.CAM camera.

SPECT "Anger Camera" Detector

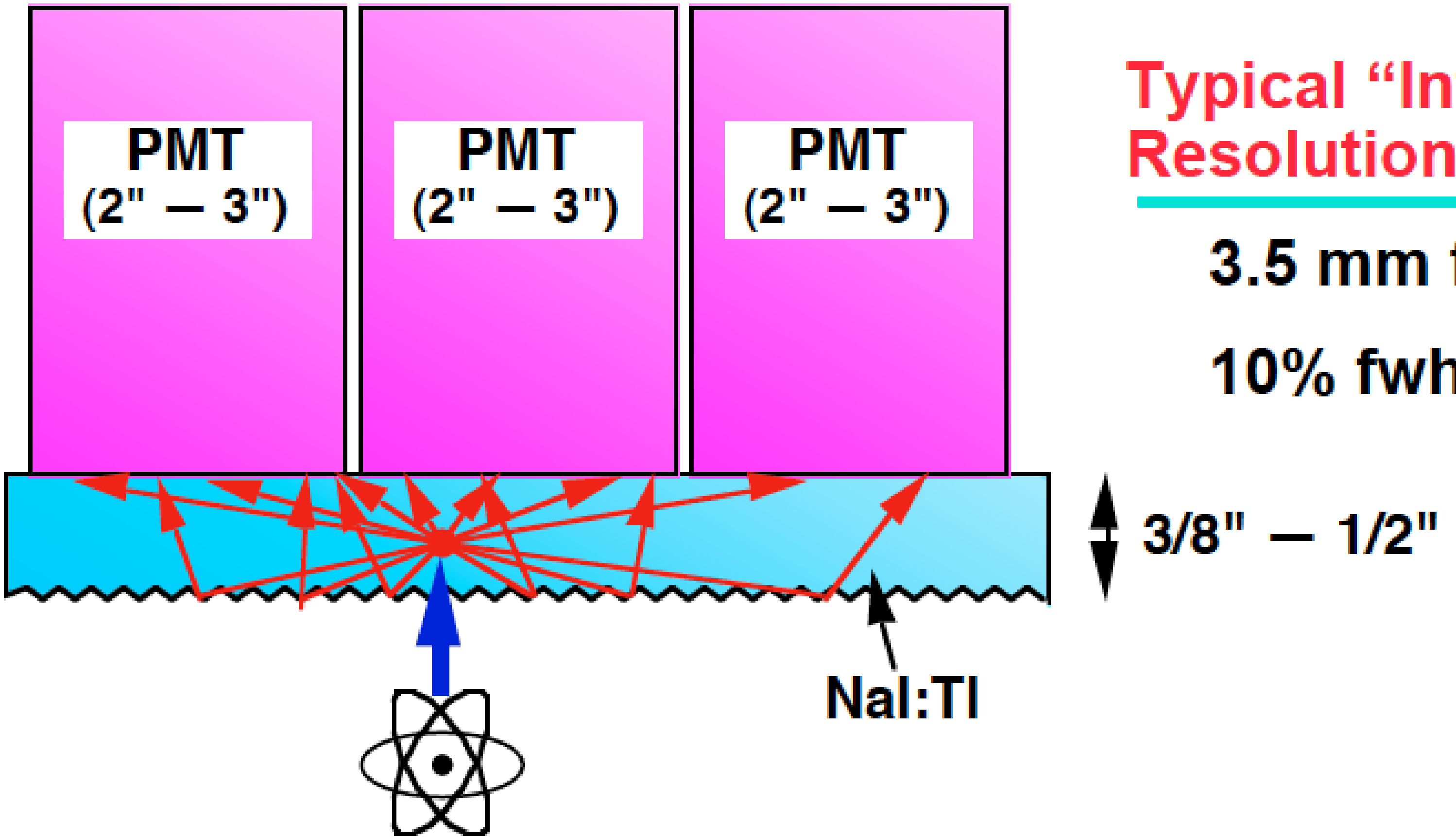

Typical "Intrinsic" Resolution:

3.5 mm fwhm

10% fwhm

Position Measured by PMT Analog Signal Ratio

SPECT Detector Requirements

At 140 keV:

- **High Efficiency** (>85%)
- **Good Energy Resol.** (<15 keV fwhm)
- **High Spatial Resol.** (<4 mm)
- **Low Cost** (<\$15/cm^2)
- **"Short" Dead Time** (<2000 μs cm^2)

Based on the "Anger Camera"

*Image courtesy of L. Shao, Philips Medical Systems

NaI crystal

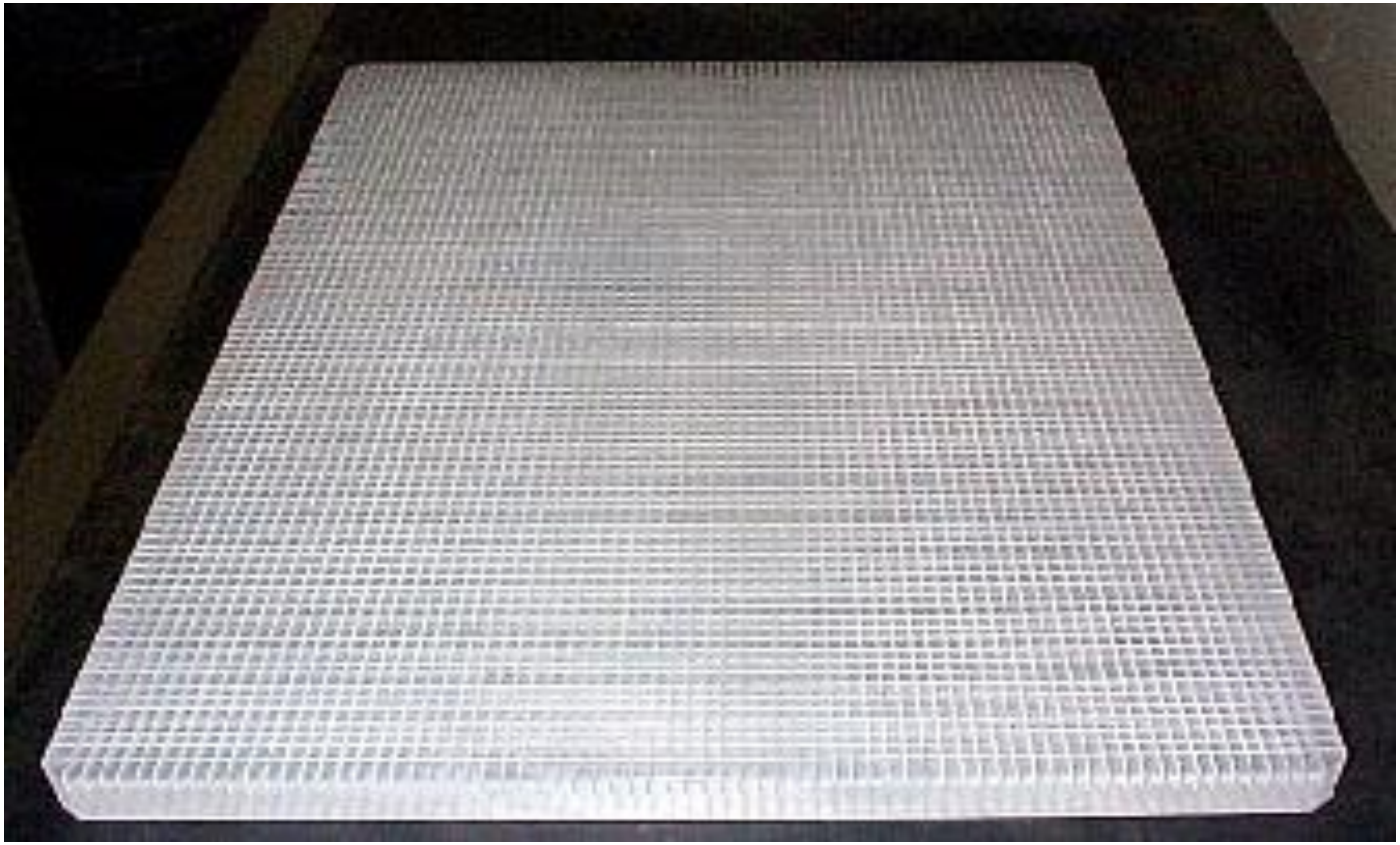

Detector and PM's

Detector size up to 60x40 cm (single crystal); up to 100 PM's.

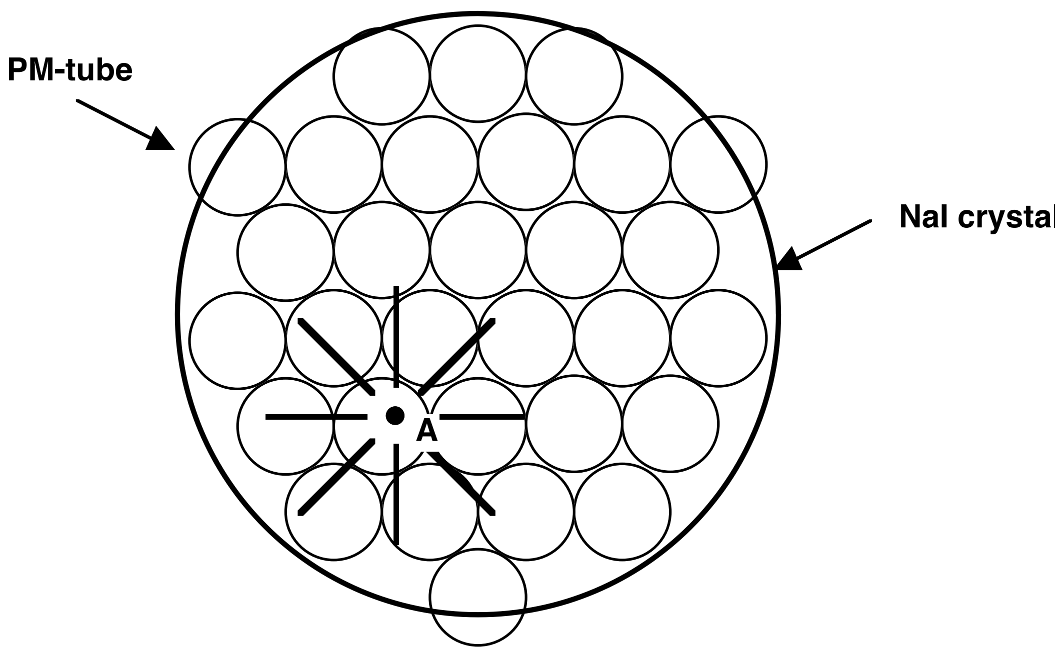

Position determination by light distribution centroide method

$$DRF = n(r,z) = \int dxdyP(x,y)PSF\left\{\left[(x-r)^2 + y^2\right]^{1/2}, z\right\}$$

DRF = Detector Response Function

P(x,y) = PSPMT gain uniformity response

Anger camera principle

$$\sigma_x = \frac{\sigma\,(\mathrm{DRF})}{\sqrt{\mathrm{N}}}$$

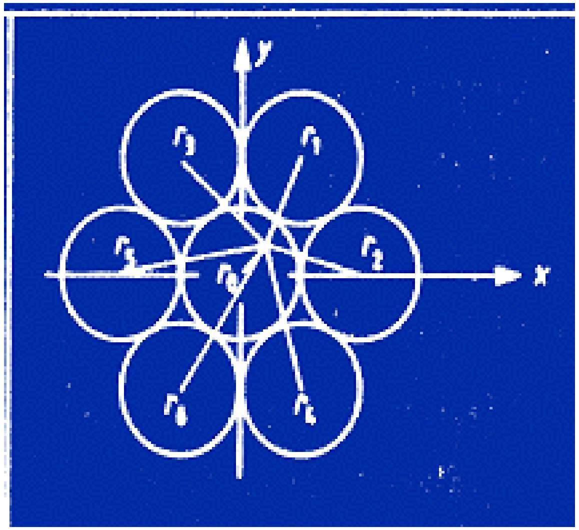

Spatial resolution = Standard error of the mean value

Collimator

No lenses exist for X- or γ-rays. To form a γ-ray image on the detector plane, one has to use either a pinhole collimator (camera obscura principle) or a multihole collimator.

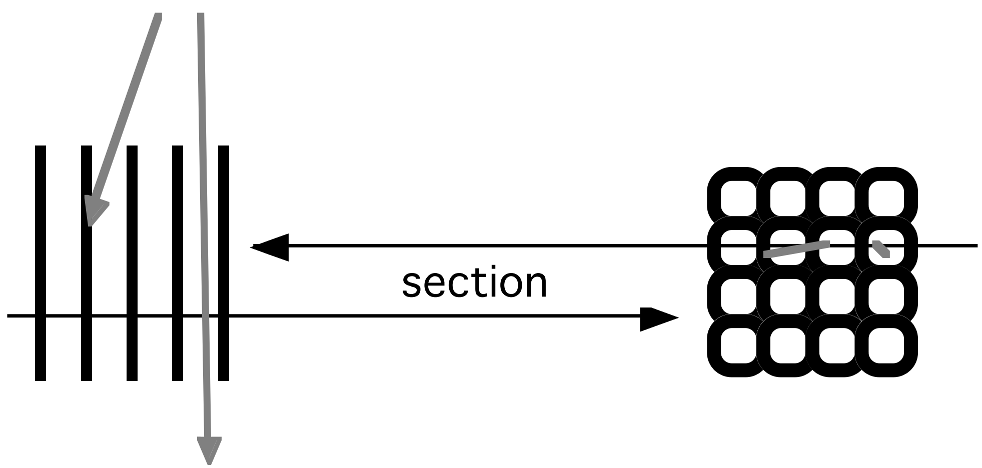

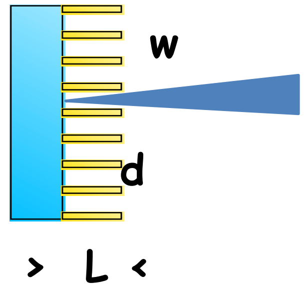

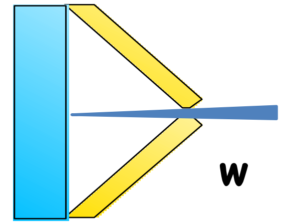

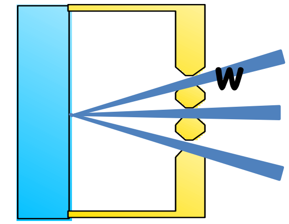

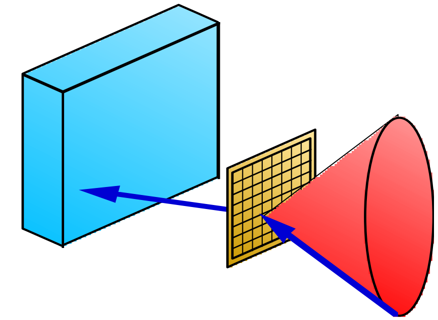

Collimator
Thin Cone

Pinhole
Thin Cone

Coded Aperture
Thin Cones

Compton
Cone Surface

$$\text{Resolution } (R) = 2\frac{w}{L}\left(d+\frac{L}{2}\right)$$

$$\text{Efficiency} \propto \left(\frac{w}{L}\right)^2$$

changing L,d

efficiency vs sp.res.

$$\text{Resolution} = w$$

$$\text{Efficiency} \propto \left(\frac{w}{d}\right)^2$$

better res.
small FOV
lower eff.

$$\text{Resolution} = w$$

$$\text{Efficiency} \propto n\left(\frac{w}{d}\right)^2$$

- res. Similar to p.h.
- higher eff.
- reconstruction complicated

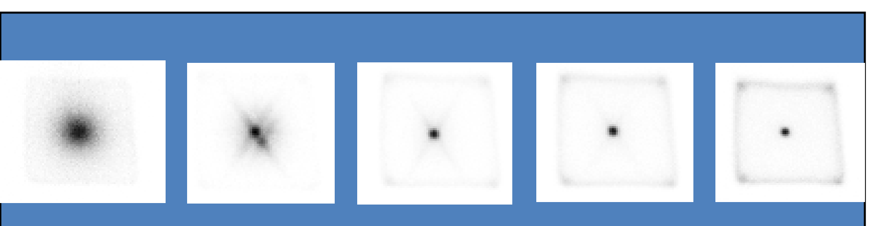

0 - 20 mm
1 - 0.009 %

Compton Cameras

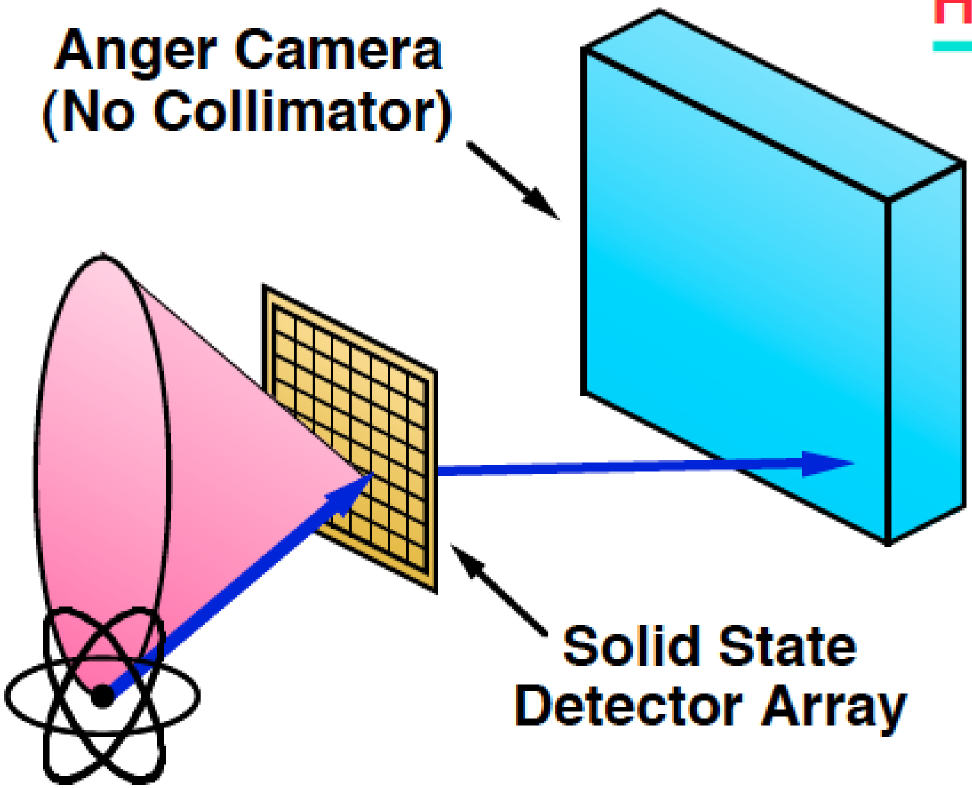

How They Work:

- Measure first interaction with good *Energy* resolution.
- Measure first and second interaction with moderate *Position* resolution.
- Compton kinematics determines scatter angle.
- Source constrained to lie on the surface of a cone.

- No Collimator, but Reconstruction Difficult
- Progress, but the Jury is Still Out...

Collimator Tradeoffs

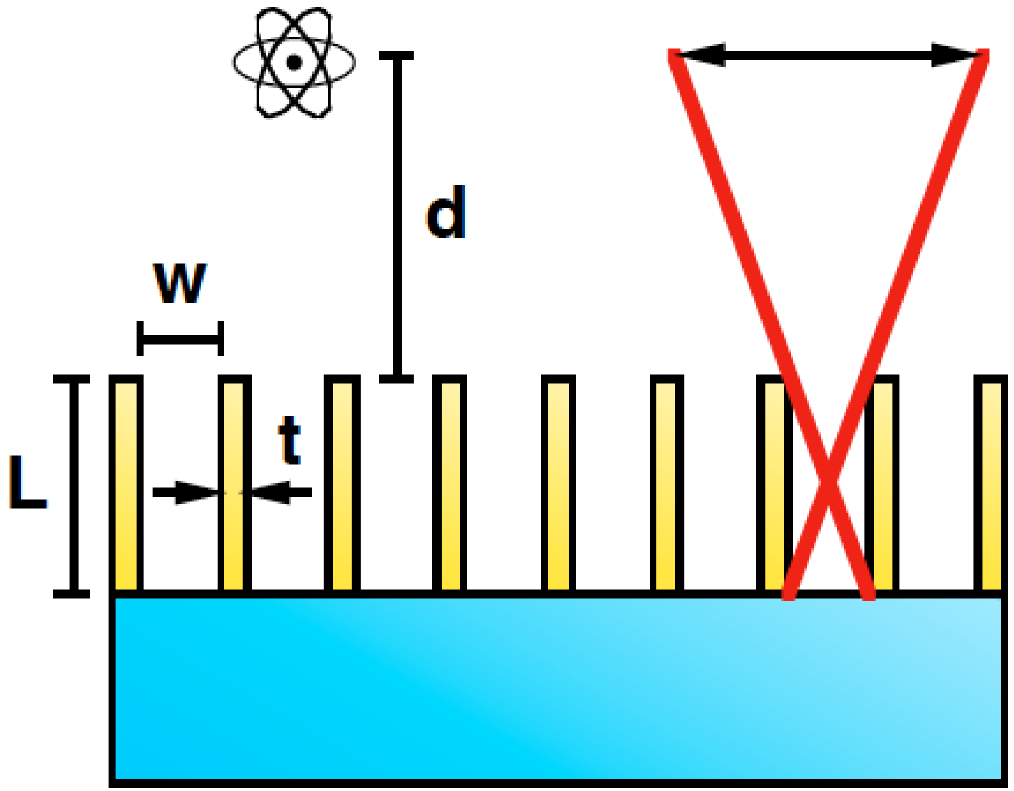

$$\text{Resolution} = 2\frac{w}{L}\left(d + \frac{L}{2}\right)$$

$$\text{Efficiency} \propto \left(\frac{w}{L}\right)^2$$

Typical Values:

w= 2 mm
L= 30 mm
t= 0.25 mm

Resol. (@5 cm) = 6 mm
Efficiency = 0.02%

Collimator Dominates Imaging Performance

Tc-99m

- Tc-99m decays by emitting a 140 keV gamma ray. Its half life is 6 hours.
  - The γ-rays can be detected and the original tracer distribution directly visualised as projections by means of a gamma camera;
  - By measuring projections over an adequate set of angles (π or 2π), tomographic reconstructions can be performed to generate images of the tracer distribution in virtual slices through the body.
- Tc-99m is used in more than 90% of all ‘single photon’ nuclear medicine studies.

γ Imaging: Single Photon Detector Module

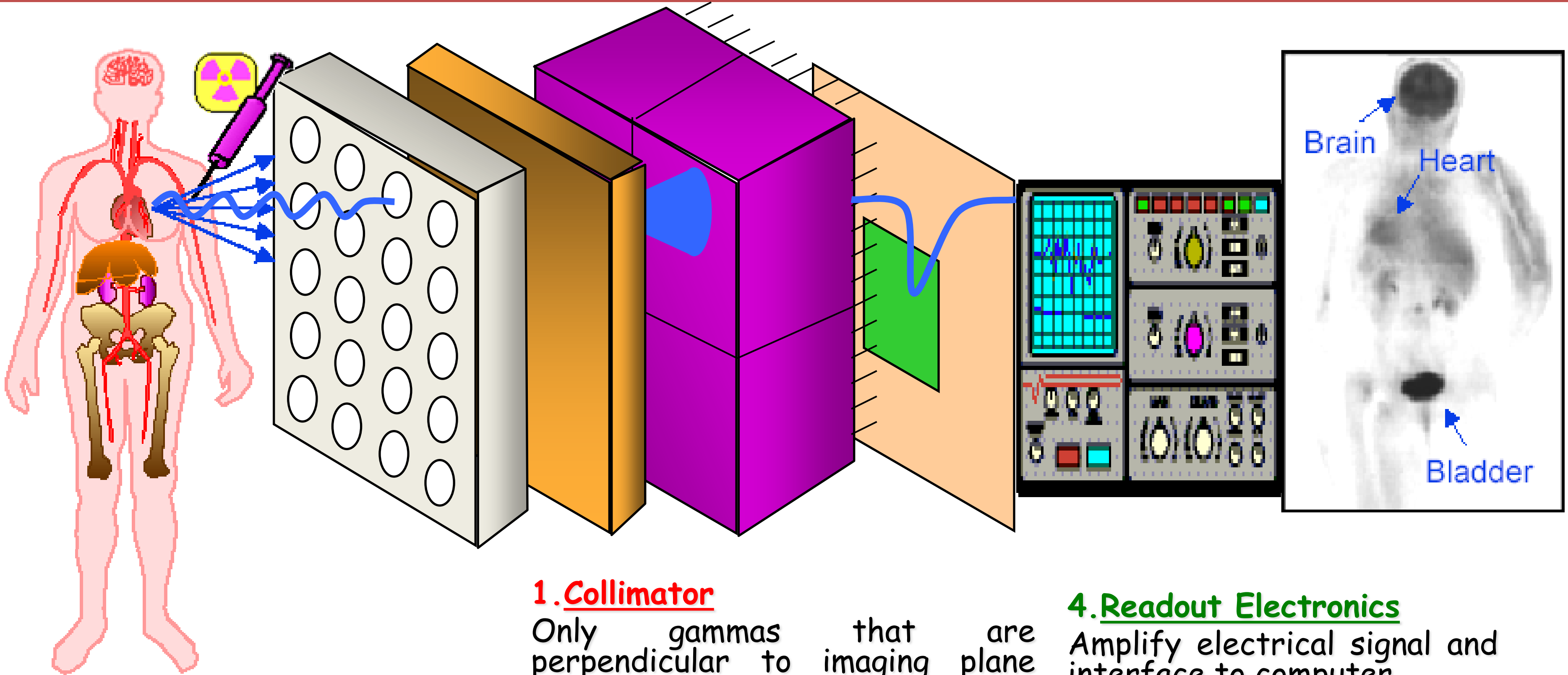

Patient injected with radioactive drug.
Drug localizes according to its metabolic properties.
Gamma rays, emitted by radioactive decay, that exit the patient are imaged.

1. **Collimator**
Only gammas that are perpendicular to imaging plane reach the detector

2. **Scintillator**
Convert gammas to visible light

3. **Photomultiplier**
Convert light to electrical signal

4. **Readout Electronics**
Amplify electrical signal and interface to computer

5. **Computer decoding procedure**
Elaborate signal and gives image output

Single Photon Emission Computed Tomography (SPECT)

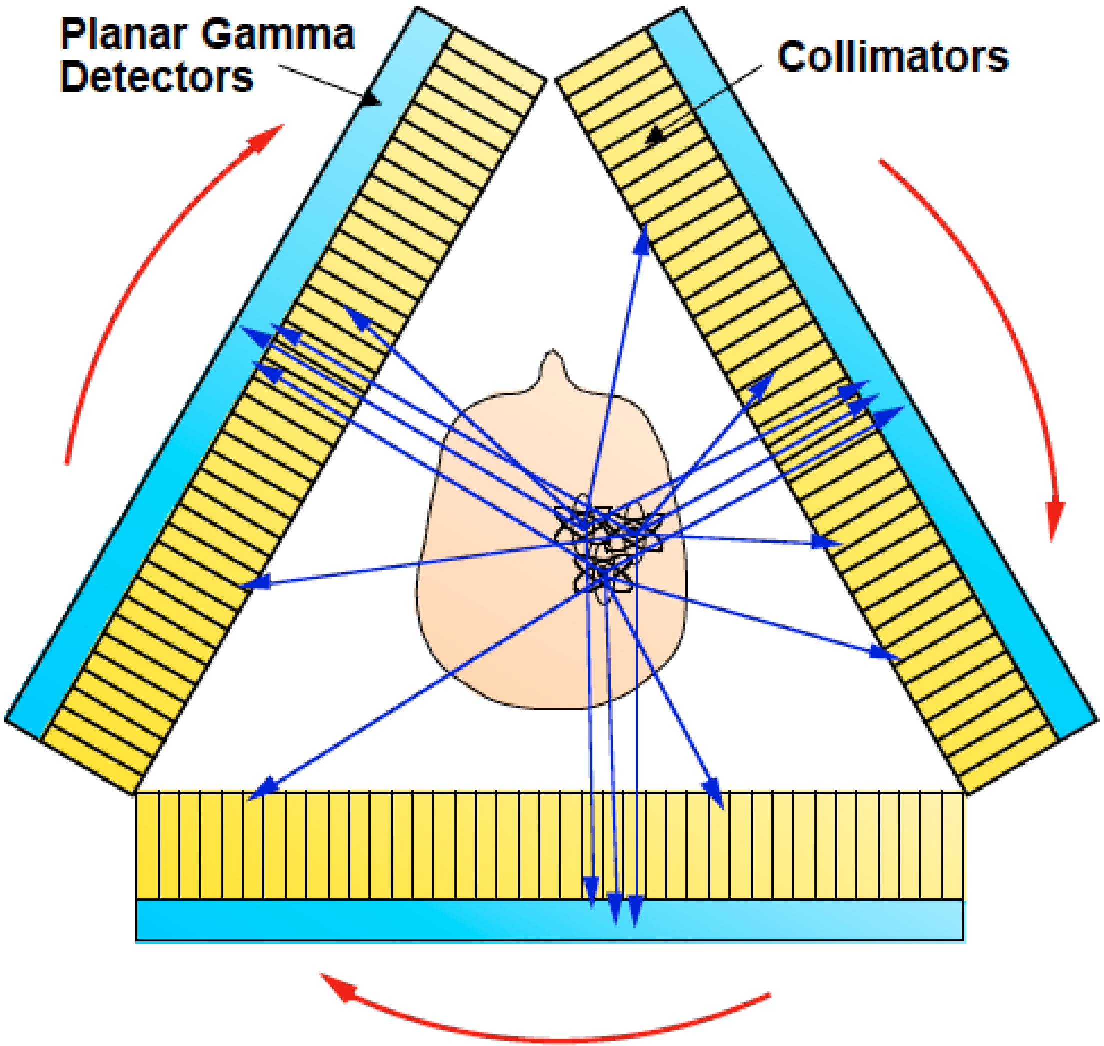

- One, two, or three imaging heads (cost / performance tradeoff)
- Parallel hole collimators.
- Multiple views obtained by rotating the imaging heads around the patient.

Predicting the survival of patients with breast carcinoma using tumor size, JS Michaelson, M Silverstein, J Wyatt, et. al. *Cancer* 2002; 95: 713-723

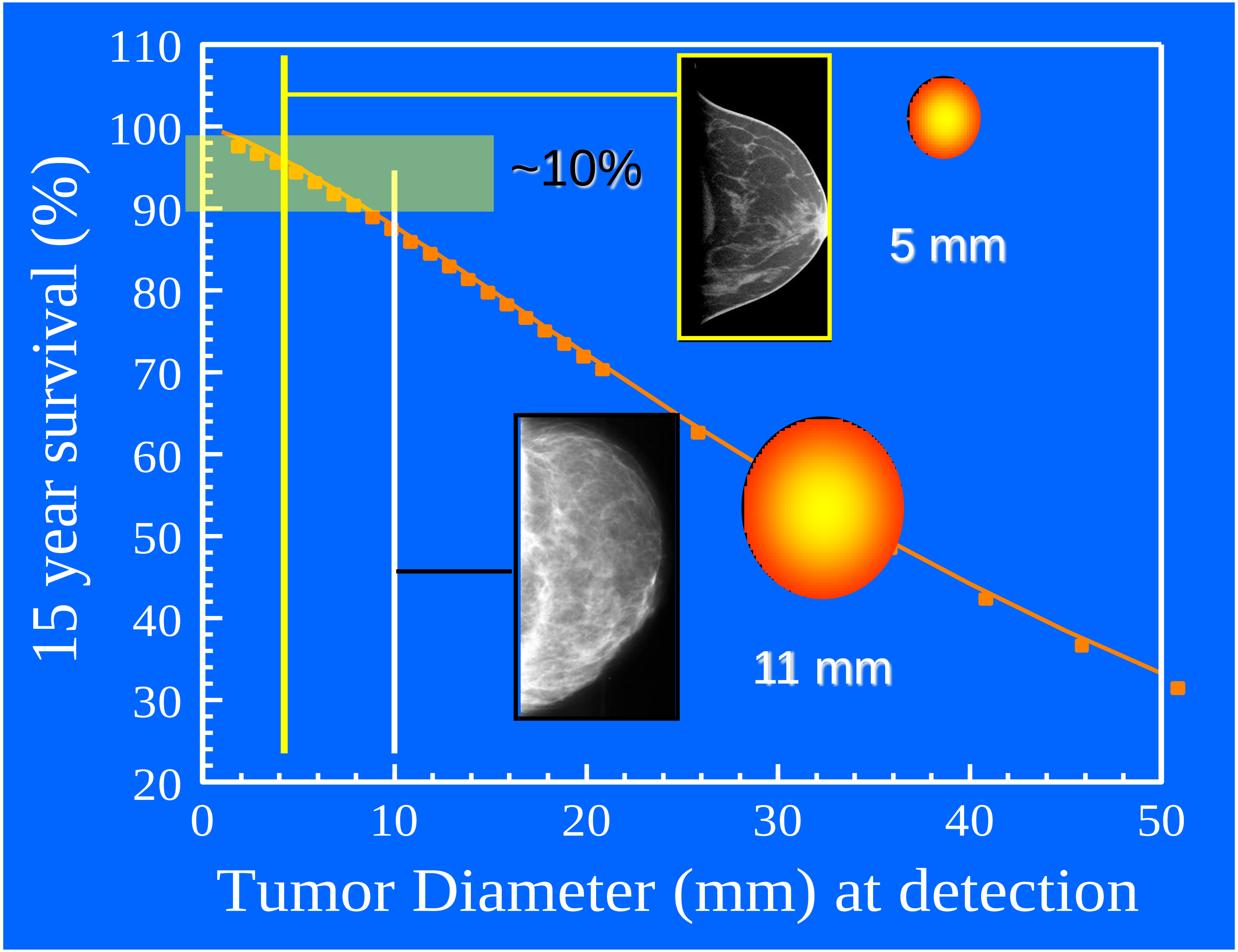

(slide provided by Dr Simon Cherry, UC Davis)

Camera Comparison: Patient Positioning

Large field-of-view gamma camera - not designed to image the breast

Dilon 6800 small field-of-view gamma camera (anatomically specific)

Advances in PSPMT Photodetector Technology

Compact position sensitive PMTs:
Hamamatsu's R8520, H8500, and Burle's 85002.

Metal channel dynode PSPMT

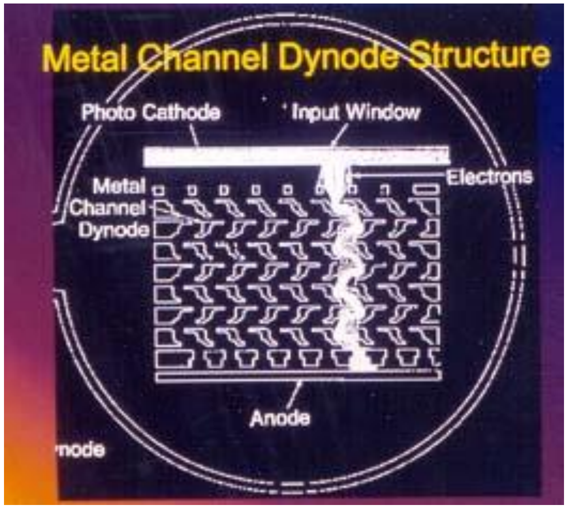

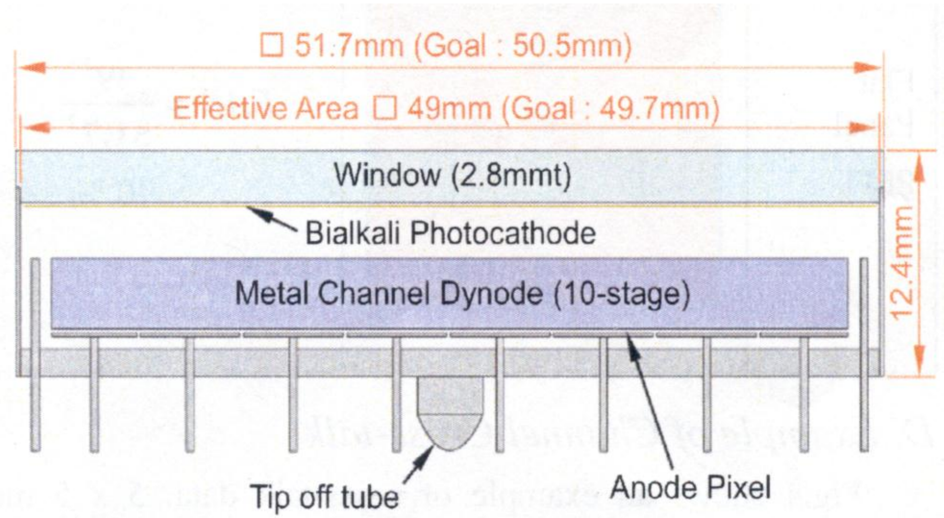

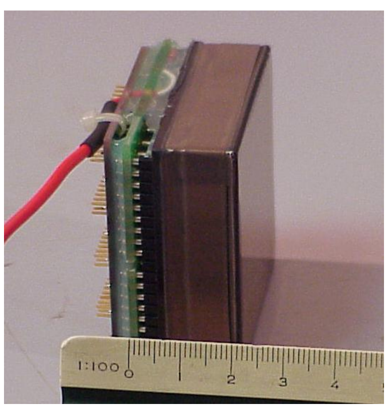

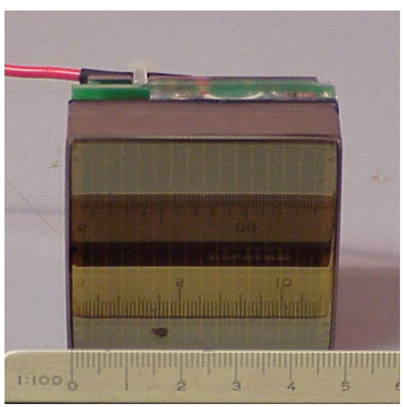

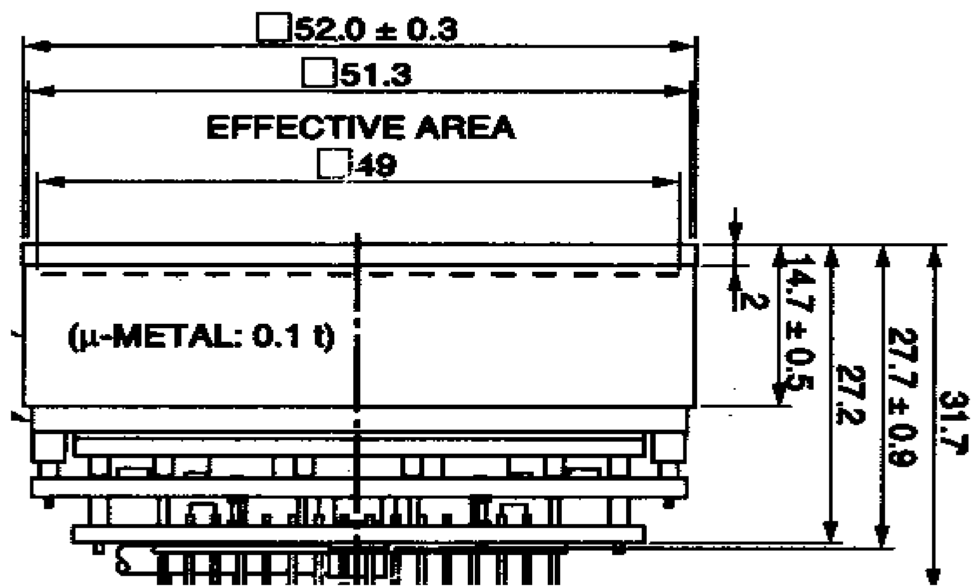

IMI Project: INFN Technological Transfer for a large FoV gamma imager dedicated to scintimammography

PSPMT array closely packed coupled to a NaI (Tl) scintillation matrix

Position is determined by light distribution centroid method

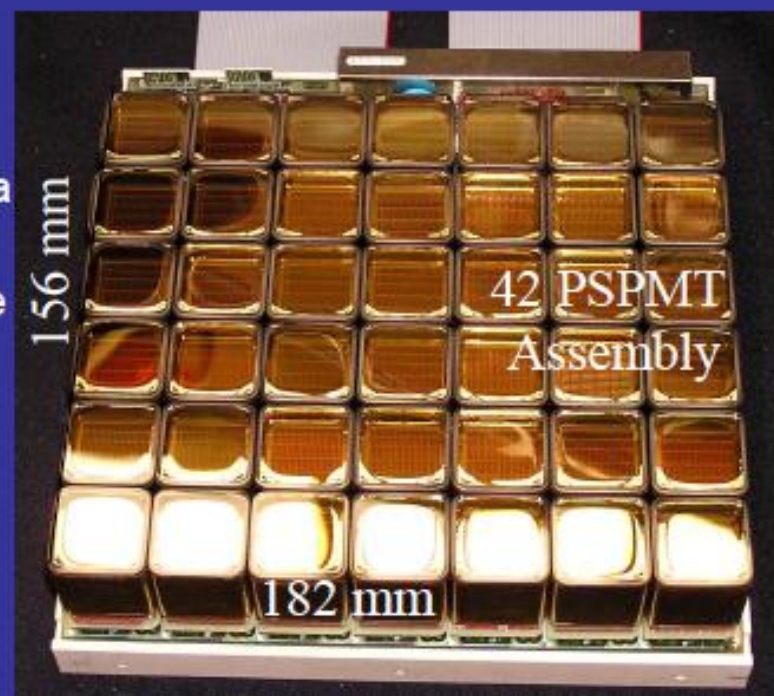

42 PSPMT independent images

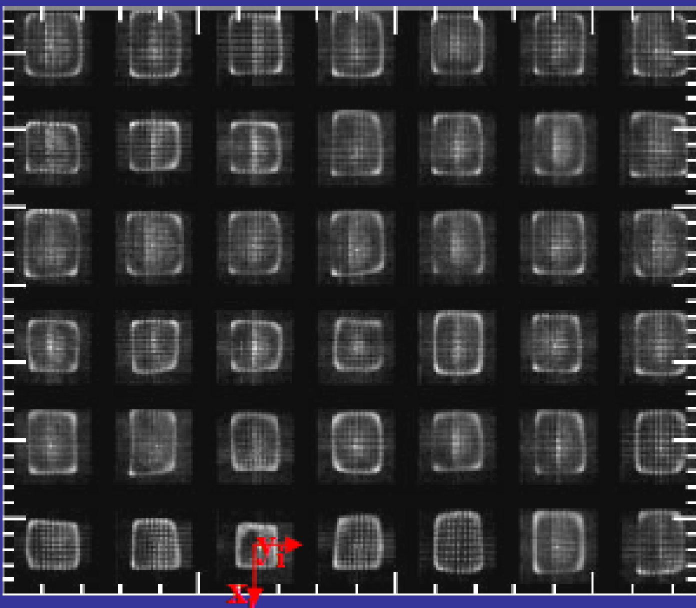

42 PSPMT reconstructed raw image

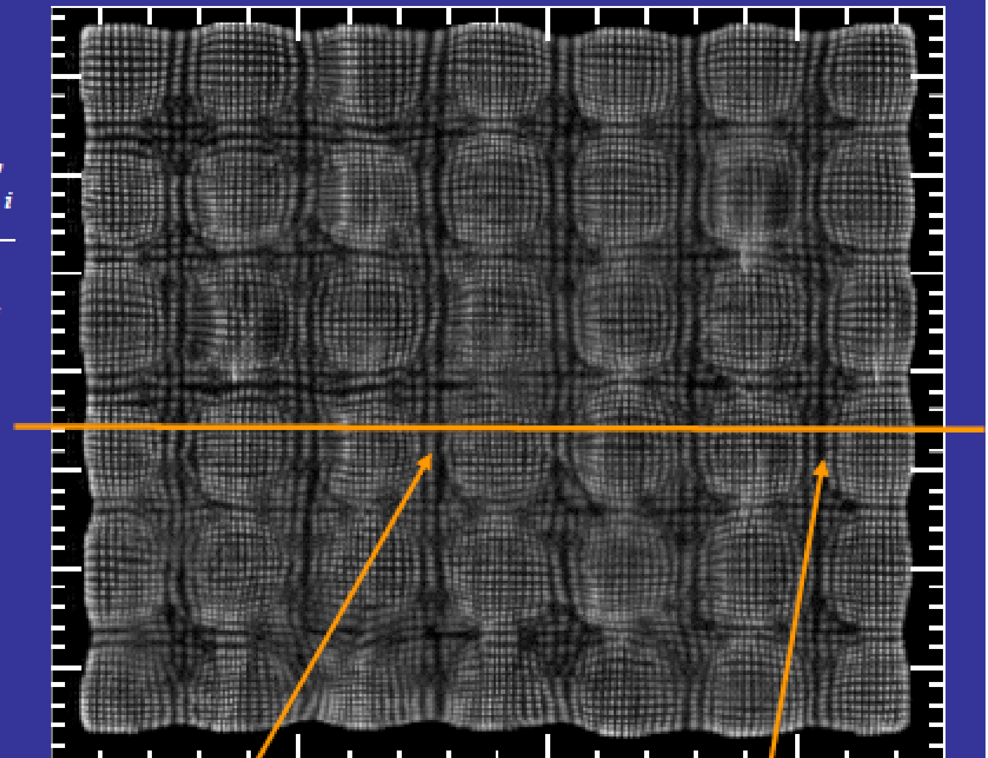

$$Y = \frac{\sum_{i=1}^{16} y_i E_i}{\sum_{i=1}^{16} E_i}$$

$$X = \frac{\sum_{i=1}^{16} x_i E_i}{\sum_{i=1}^{16} E_i}$$

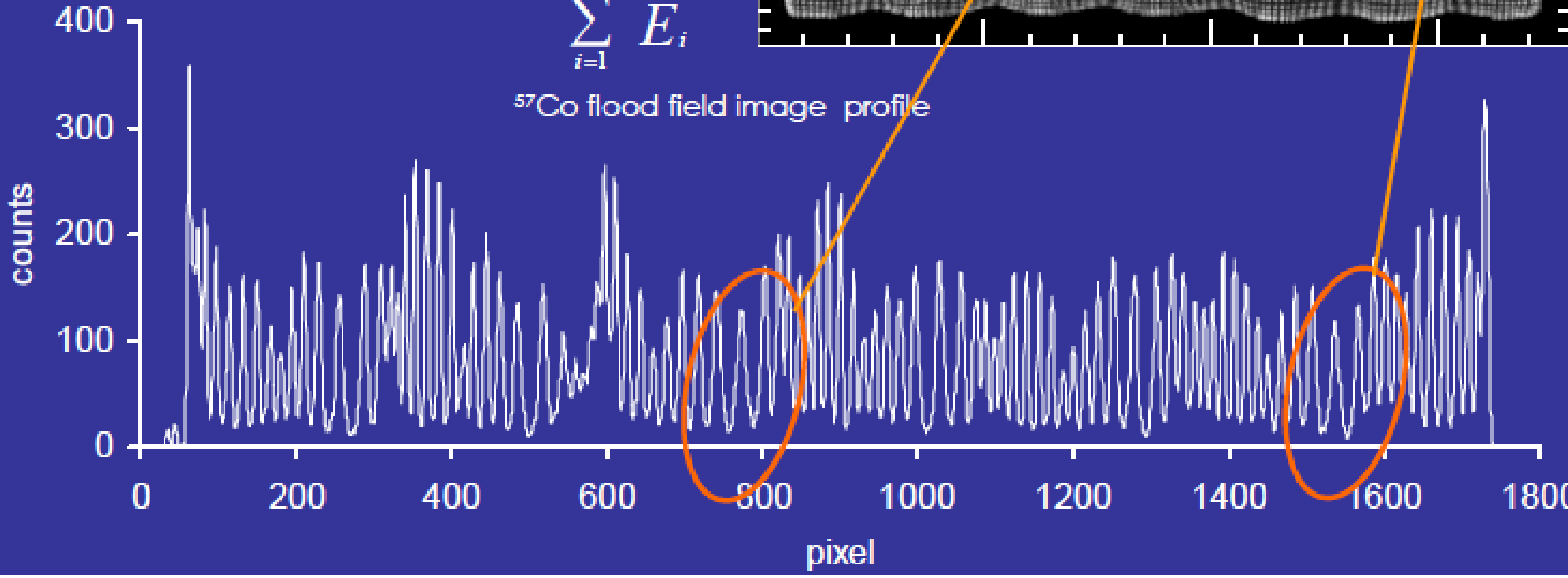

Detector performances

6930 NaI(Tl) individual crystals identification

Ce^{144} flood field image

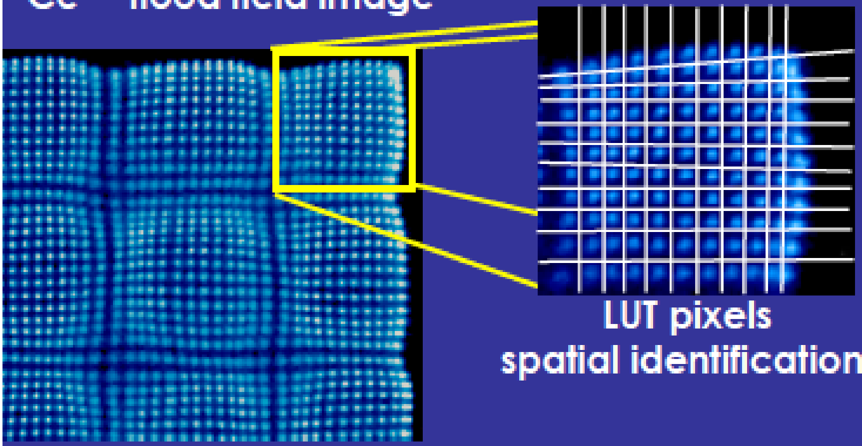

LUT pixels
spatial identification

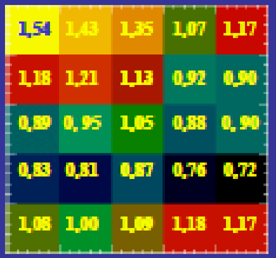

LUT counts uniformity

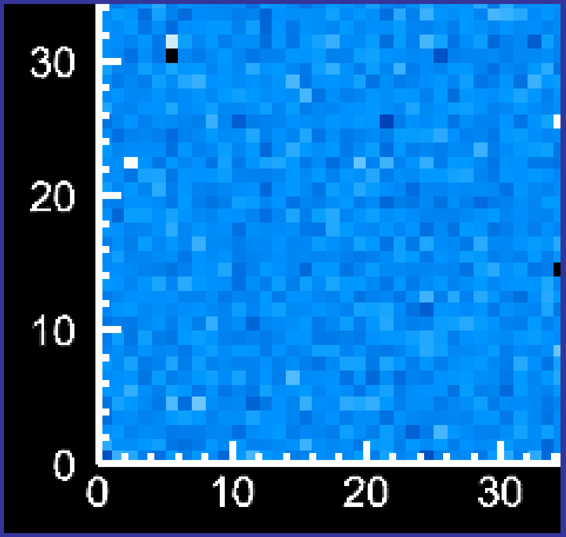

LUT Reconstructed image

Integral uniformity = ± 16.9 %
Differential uniformity = ± 4.5 %
Intrinsic (pixel ID) spatial resolution = 0.9 ± 0.2 mm
Final Intrinsic spatial resolution about 2 mm

	Active area	Dead area between 4 PSPMT	Outer area
Energy Resolution	(15±1)%	(22±2)%	(30±2)%

Camera spatial resolution
LEGP collimator

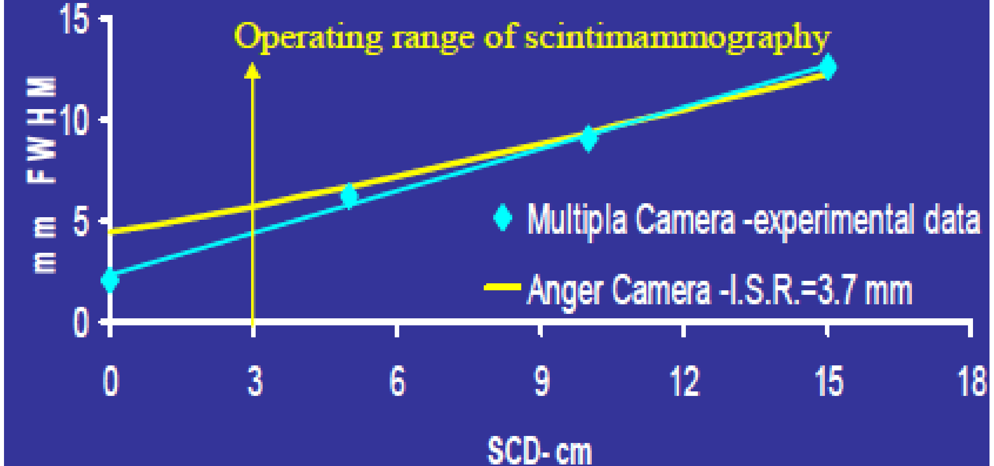

Pulse height distributions

Reconstructed spectra after L U T application

^{99m}Tc Flood Field irradiation

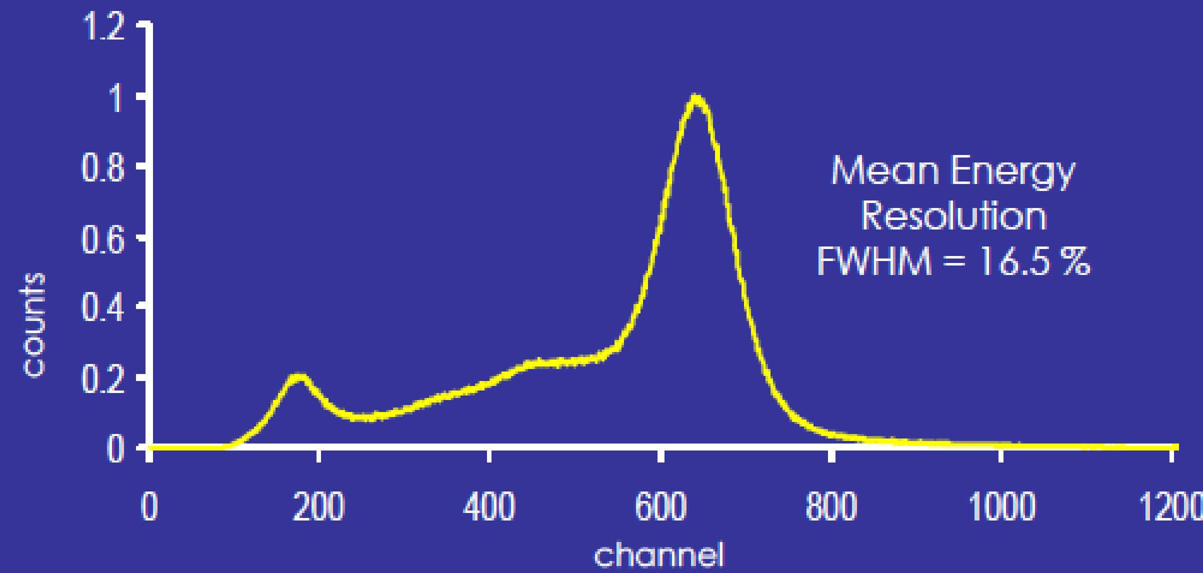

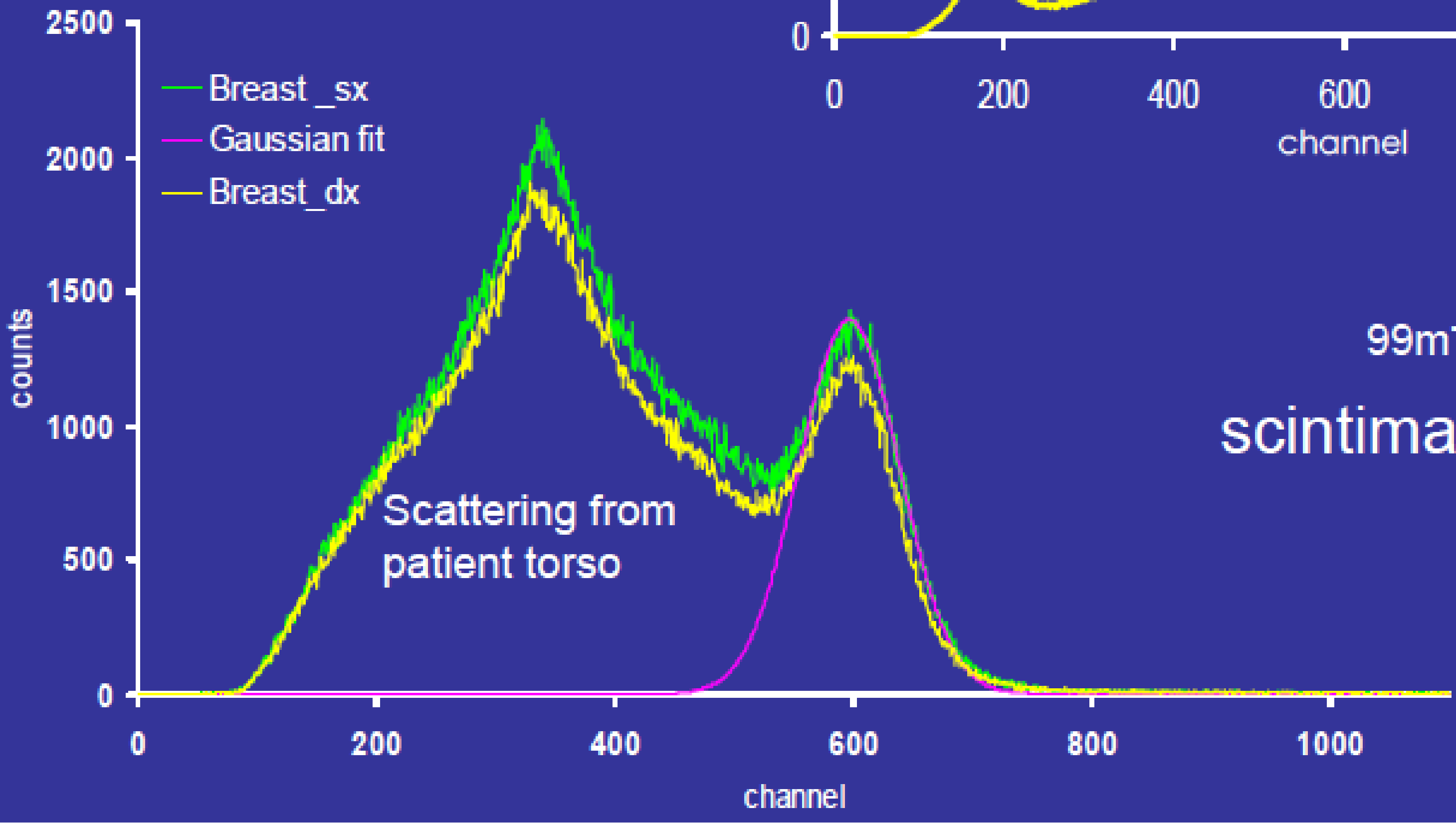

^{99m}Tc MIBI scintimammography

JLab Imaging Detector Technology

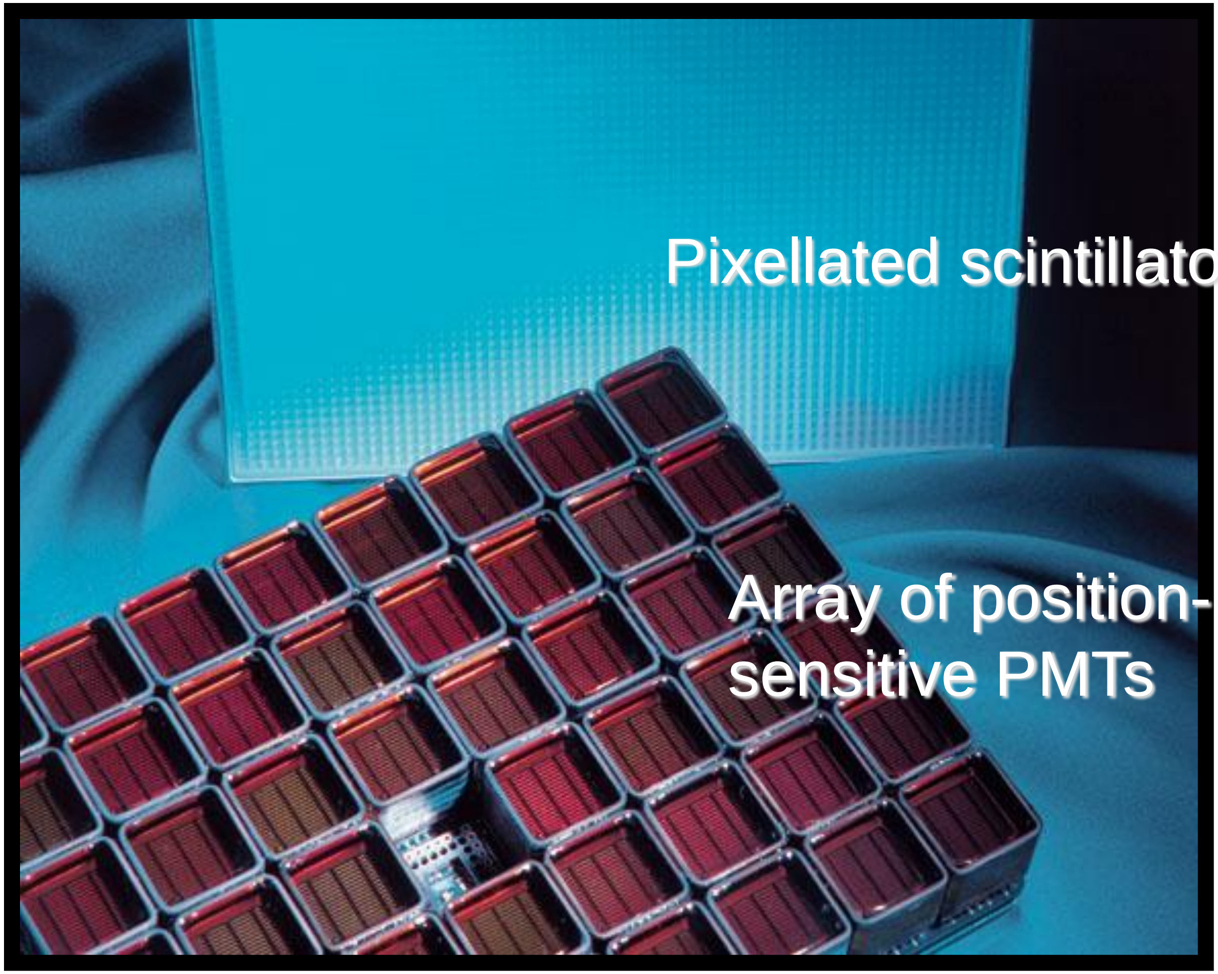

Dilon 6800 Gamma Camera

Removable Smart Shield™ modified to accommodate biopsy hardware.

Removable sliding slant-hole collimator system for stereo viewing.

Microcalcifications with Previous Benign Biopsy

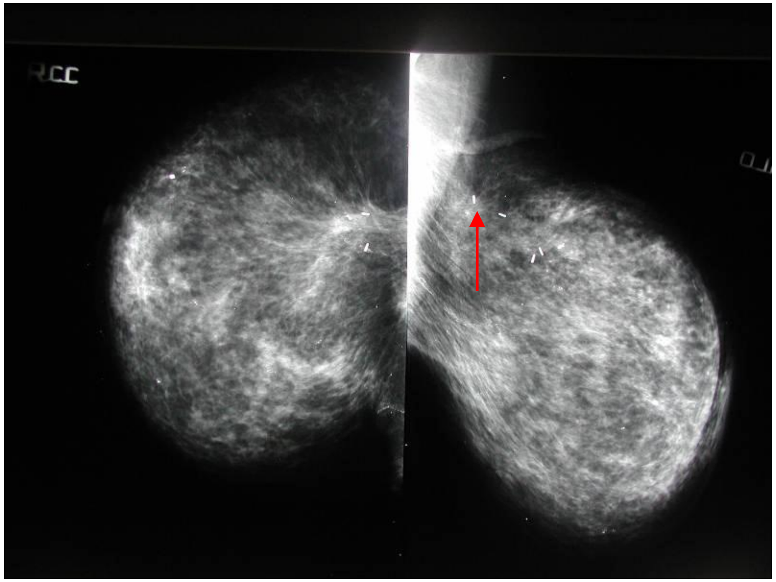

Mammogram: right breast shows area of microcalicifications (see arrow). Previous needle biopsy of this area was negative.

BSGI: demonstrated a high-uptake region highly suspicious and the patient was sent for open biopsy. Ductal Carcinoma.

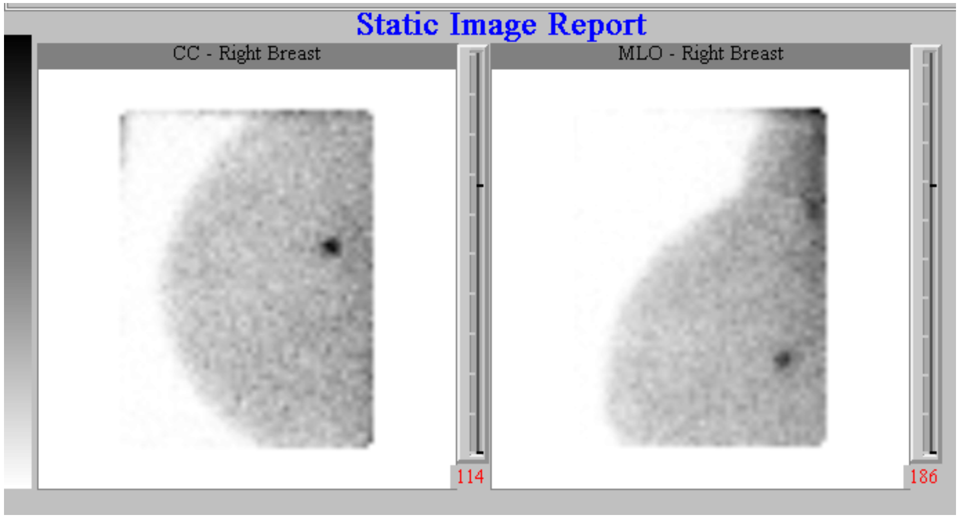

Courtesy of West Valley Imaging

Dense Breast - Negative BSGI

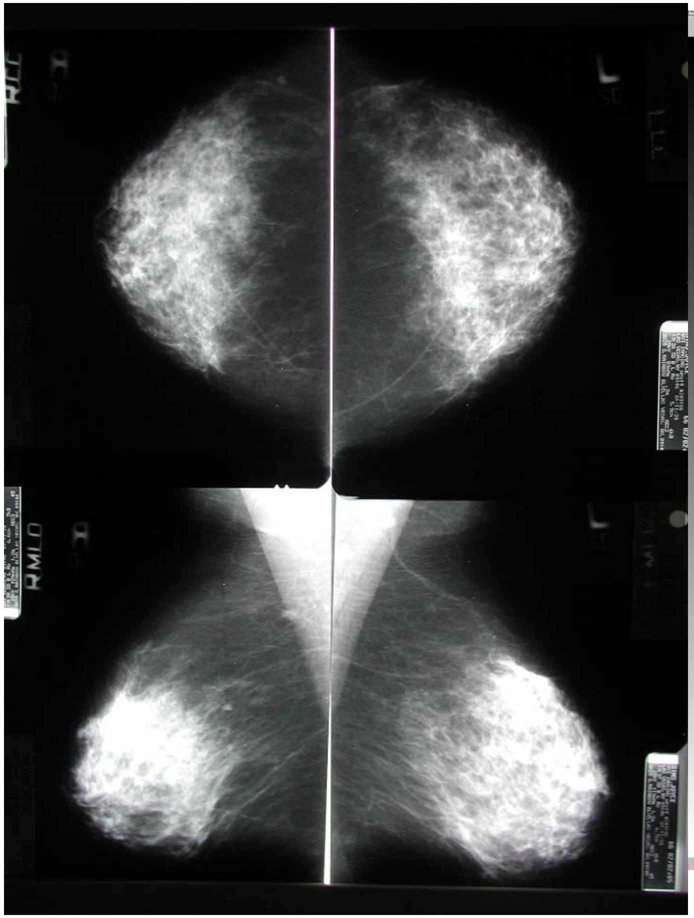

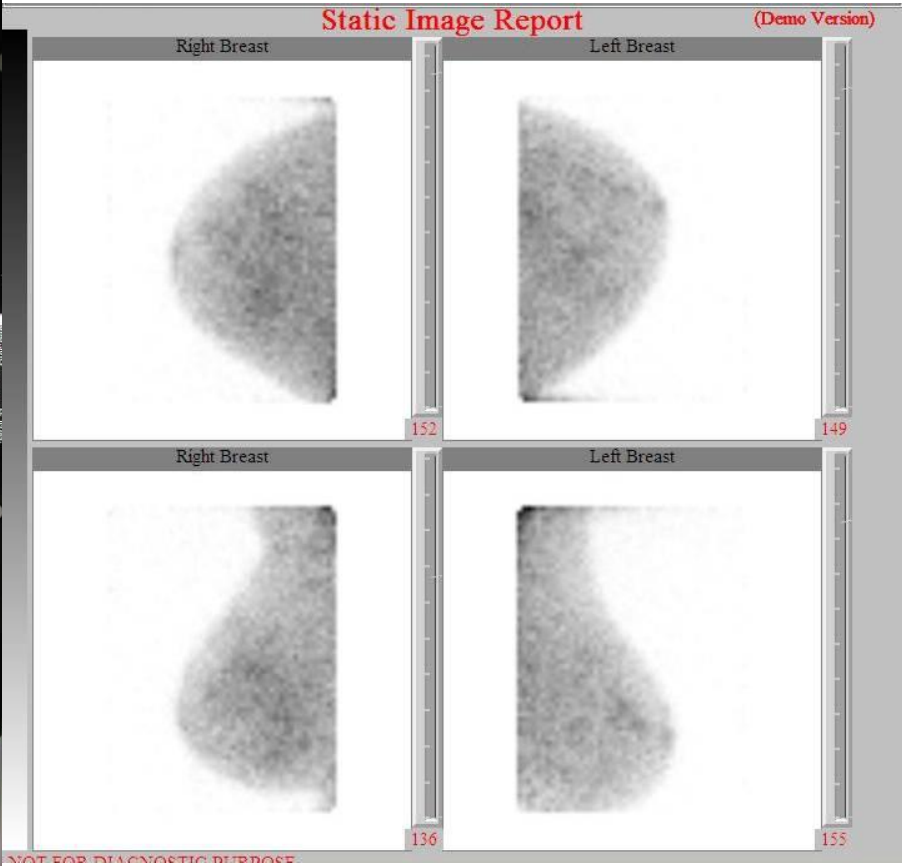

The slightly heterogeneous pattern seen in the BSGI image closely correlates with the bilateral dense parenchyma tissue seen in the mammogram. Negative.

Courtesy of West Valley Imaging

Lantanium Tribromide Crystal
Saint Gobain Brillance380:

- **High Light yield: 63000 ph/MeV**
- Scintillation decay time: 16 ns
- Detection Efficiency @ 140 keV 70%
- Spectral emission max 380 nm

Hamamatsu Flat Panel PMT H8500:

- **64 anodes**
- Bialkali Photocatode (QE= 0.27)
- Spectral response: 300 nm – 650 nm
- Active area: 49 mm x 49 mm (89%)
- Gain: 2 x 10^6

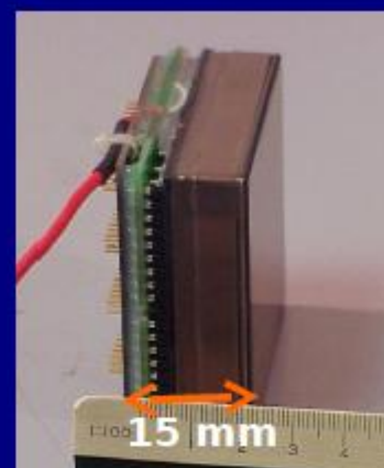

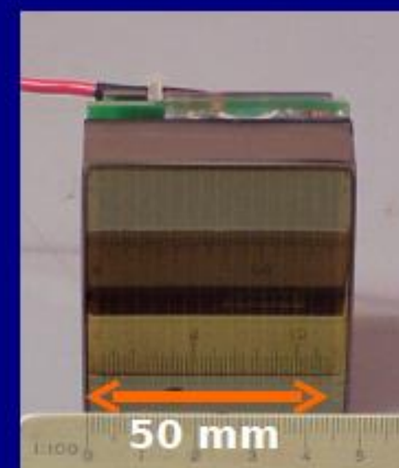

Valentino Orsolini Cencelli[a], F. de Notaristefani[a], A. Fabbri[a], F. Petullà[a], E. D'Abramo[a],R. Pani[b], M.N. Cinti[b], P. Bennati[b], P. Boccaccio[c], N. Lanconelli[d], G. Moschini[c], F. Navarria[d]

Monolithic scintillator detectors

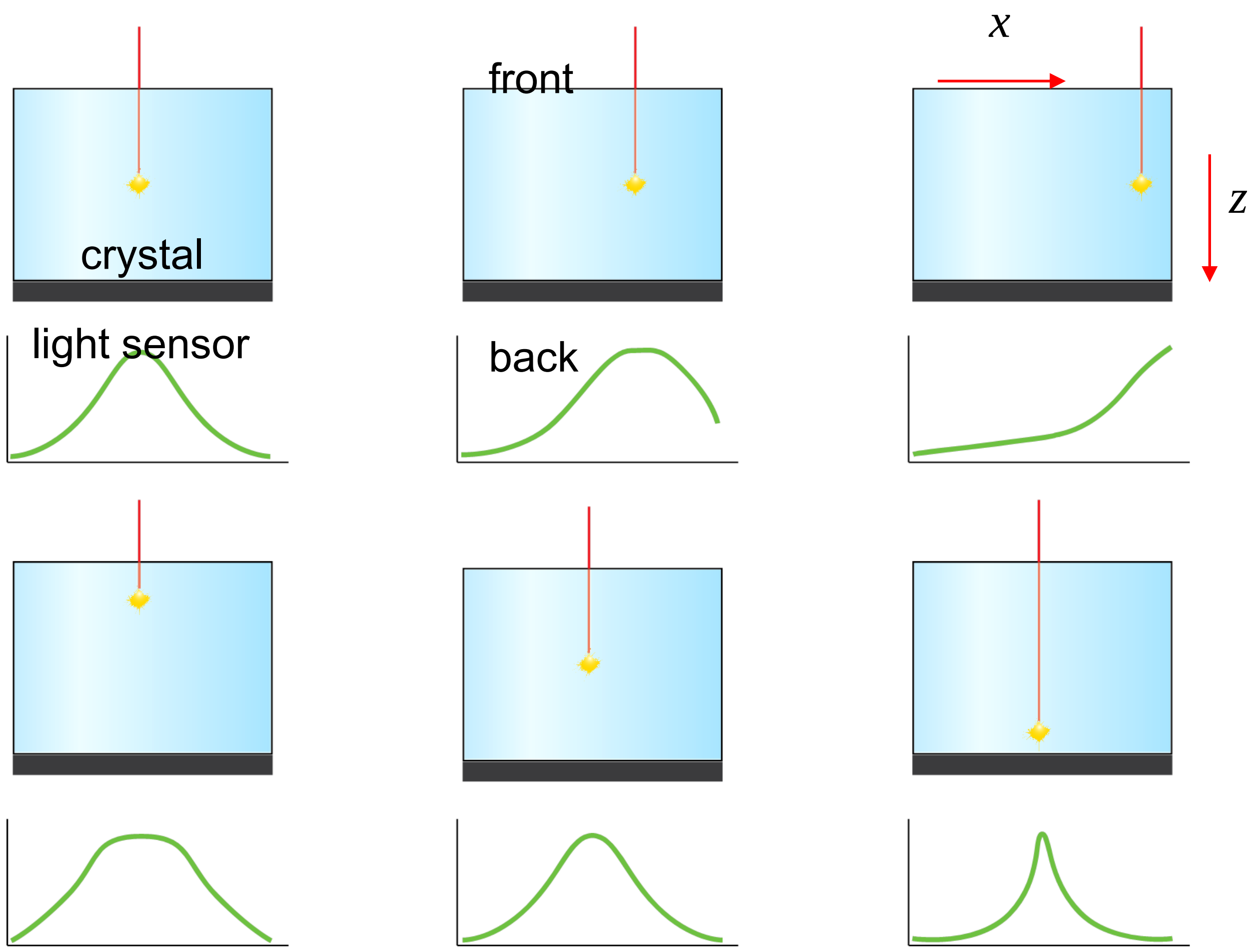

Light distribution depends on the entry point on the front surface…

and on the depth of interaction (DOI).

Data courtesy by D.Schaart

The Algorithm:

✗ The point of interaction within the crystal is determined via an iterative estimate;

✗ A reference light distribution is assumed and it's parameters estimated with the steepest descent method in the parameter space;

✗ The search is stopped when the difference between the function and the estimation is lower then a target value;

Objective Function

$$\min_{x_0, y_0, r, I_0} \left\{ \sum_{i,j=1..8} \left(C_{ij} - \frac{I_0}{\left[1 + \frac{[(x_0 - x_i)^2 + (y_0 - y_j)^2]}{r^2} \right]} \right)^2 \right\}$$

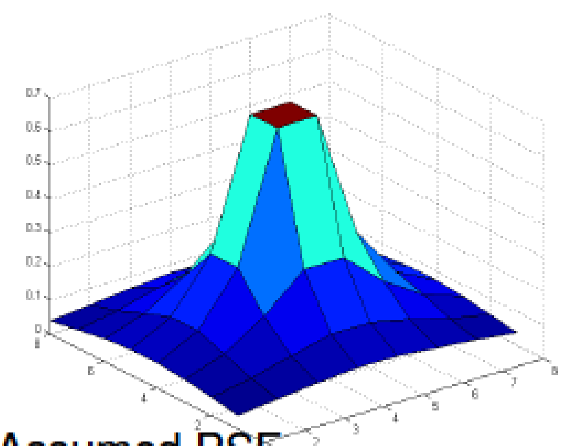

Assumed PSF

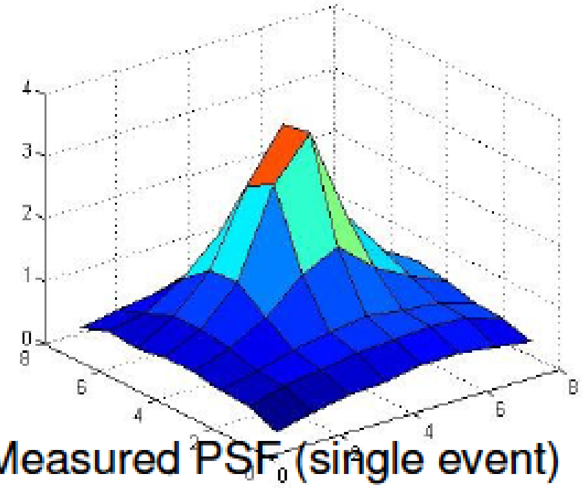

Measured PSF (single event)

Valentino Orsolini Cencelli[a], F. de Notaristefani[a], A. Fabbri[a], F. Petullà[a], E. D'Abramo[a], R. Pani[b], M.N. Cinti[b], P. Bennati[b], P. Boccaccio[c], N. Lanconelli[d], G. Moschini[c], F. Navarria[d]

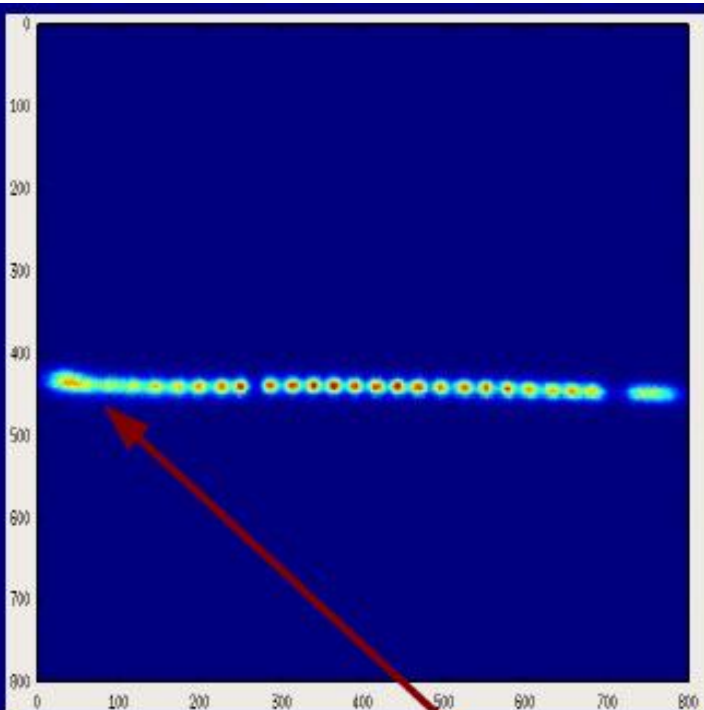

- spot scanning
- 0.4 mm collimator
- 1.5 mm pitch
- 140 KeV
- 20K events

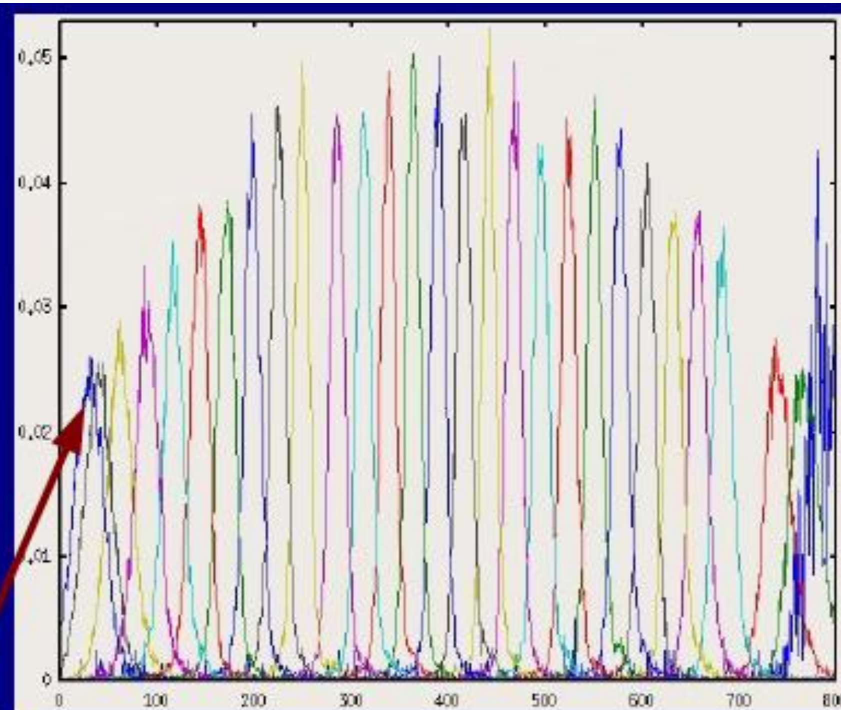

Spot profiles.

Border resolution loss.

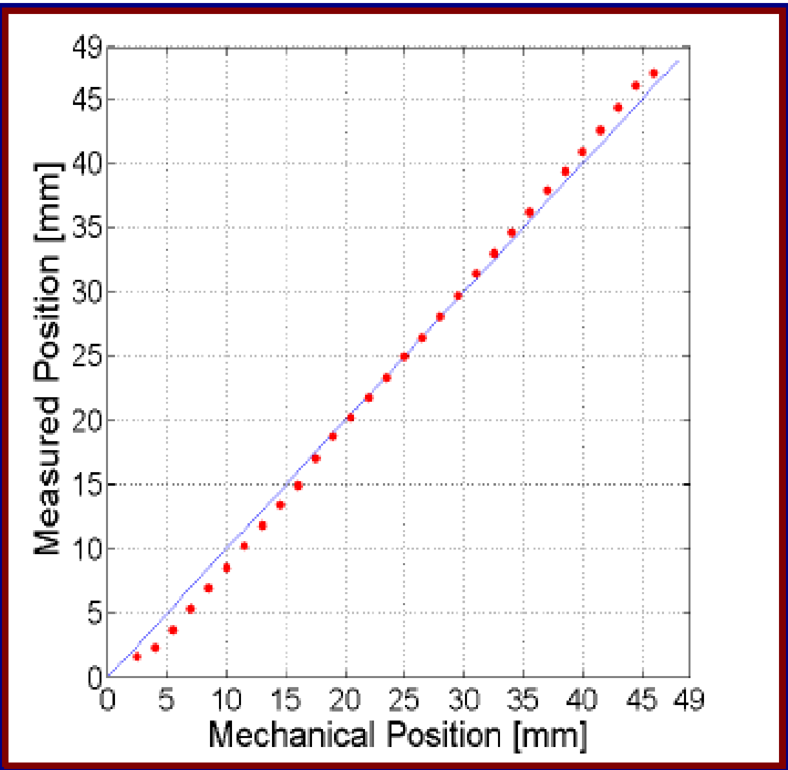

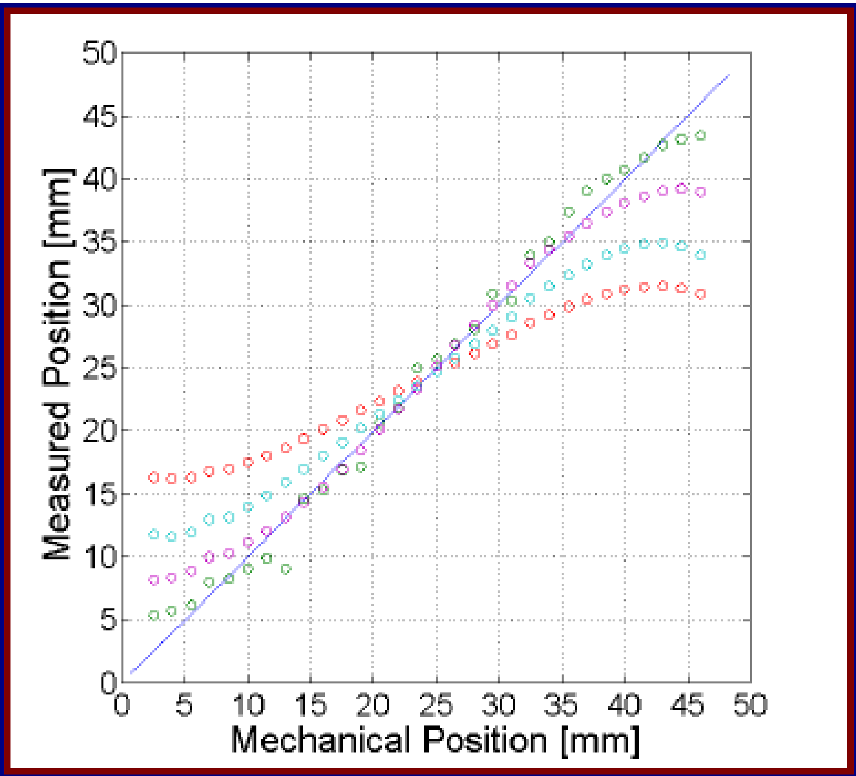

LS Algorithm

$$X = \sum_{i=1..64} \frac{x_i C_i}{\sum C_i} \qquad Y = \sum_{i=1..64} \frac{y_i C_i}{\sum C_i}$$

Valentino Orsolini Cencelli[a], F. de Notaristefani[a], A. Fabbri[a], F. Petullà[a], E. D'Abramo[a], R. Pani[b], M.N. Cinti[b], P. Bennati[b], P. Boccaccio[c], N. Lanconelli[d], G. Moschini[c], F. Navarria[d]

Why PET ?

Similarities and differences

Calorimeter

HEP

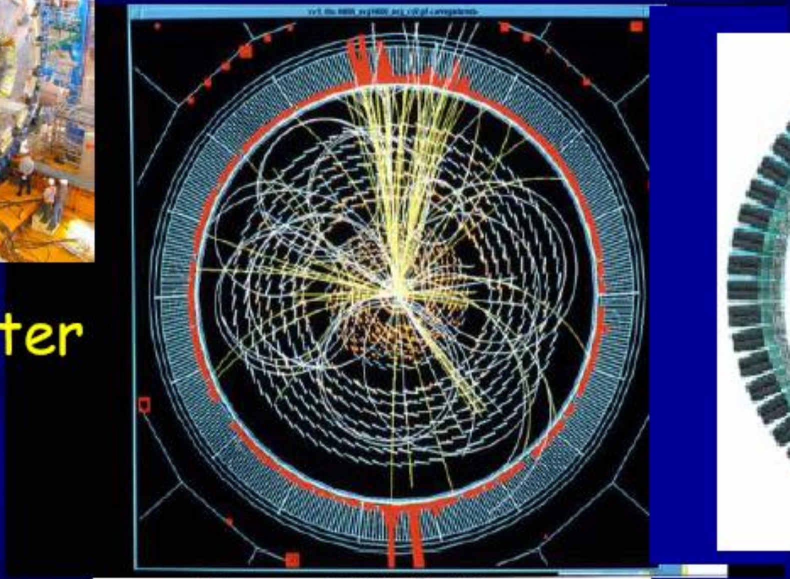

M_{Higgs} = 100 GeV

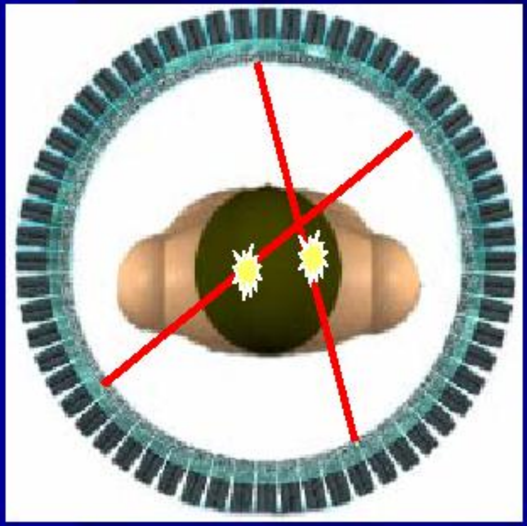

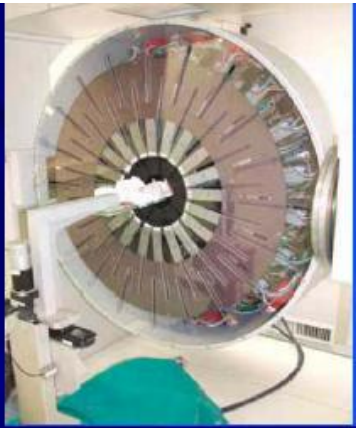

PET Camera

Biomedical Imaging

Similarities

Geometry and granularity
Detector (Crystals & scintillator)
Photo Sensor (PM,APD)
Electronics:Fast and compact
Event rate & Data volume

Differences

Energy range (10GeV-511keV)
No synchronisation
--> free running
electronics

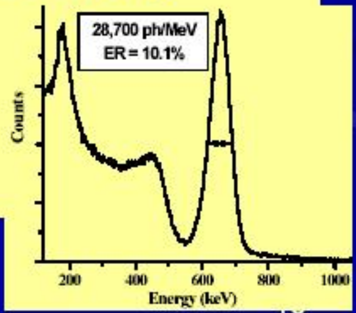

Producing Images

Principles of functional (PET) imaging

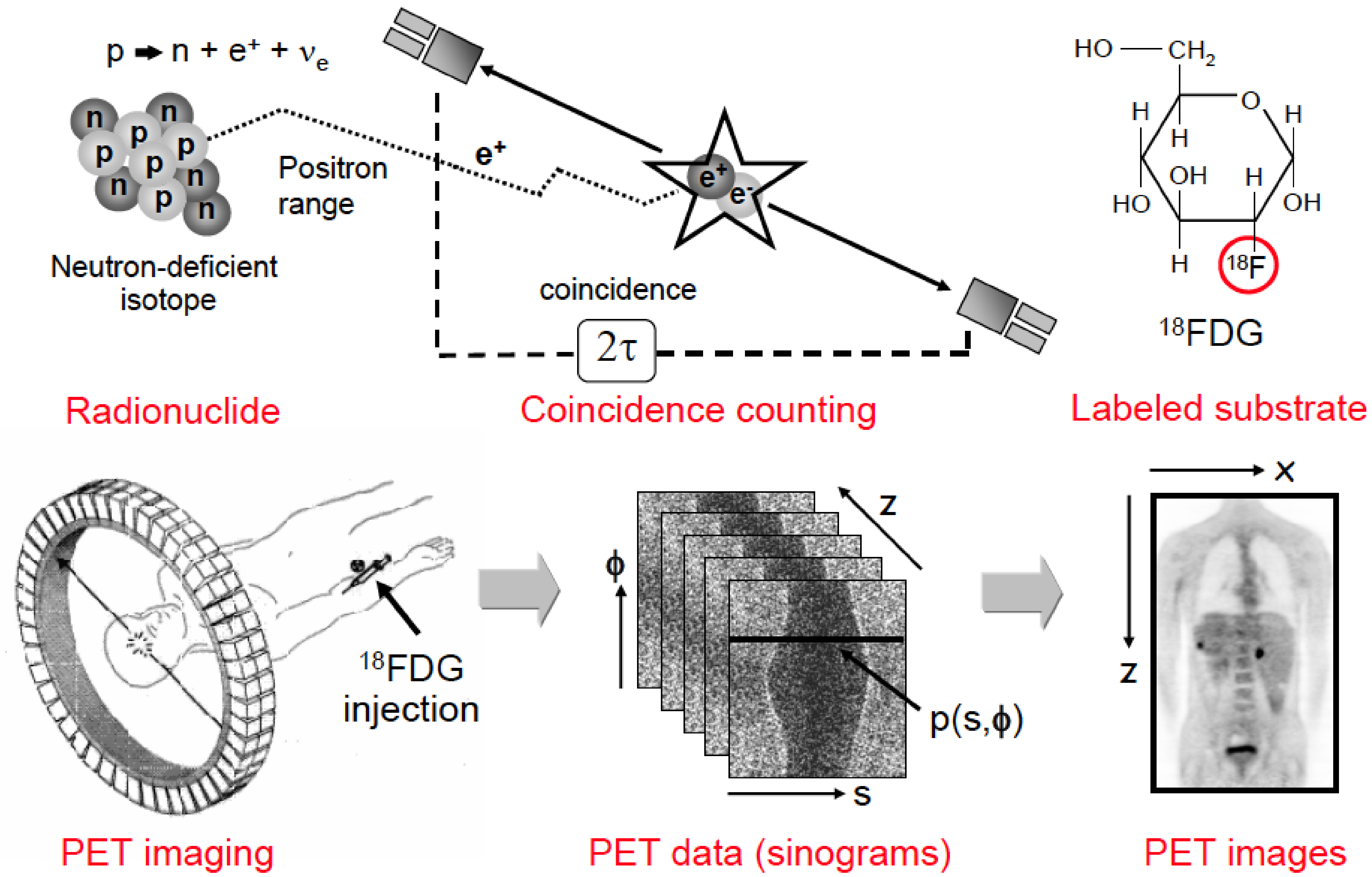

F-18

F-18 decays by emitting a positron

- The positron travels in tissue for < 1 mm before colliding and annihilating with an electron;
- The rest energy of the particles (the energy equivalent to the mass of both electron and positron: $E=mc^2x2$) is liberated in the form of two oppositely directed (space) coincident (time) gamma rays of 511 keV.
- By detecting a large number of coincident photons over a 2π geometry, tomographic reconstruction techniques yield images of the original tracer distribution.

Combined Resolution Effects

$$r_{tot} = \sqrt{r_{\det}^2 + r_{acol}^2 + r_{\beta}^2 + r_{mot}^2 + r_{rec}^2}$$

- Detector resolution (3D)
- Acolinearity (0.5° FWHM – 2.2mm / 1000mm)
- Positron range (<1mm for F-18, ~5mm for Rb-82)
- Subject motion during scan
- Additional blurring in reconstruction

Acolinearity

$$r_{acol} \approx 0.0088 \times D\alpha(1-\alpha)$$

- 0.0088 radians is angular uncertainty in soft-tissue
- For D = 40 cm and α = 0.1, r_{acol}= 0.32 mm FWHM
- Compare with 1.76 mm FWHM at center of 80 cm ring

Advances in PET

PET in 1986

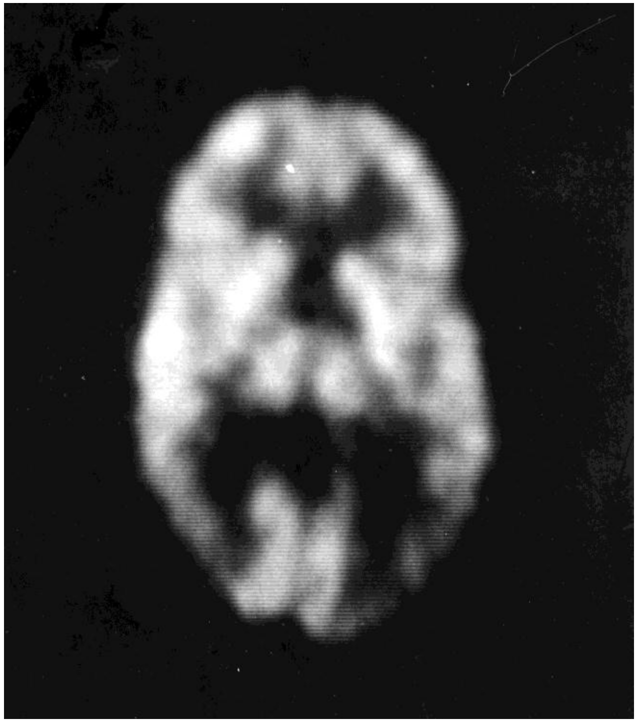

- 8 mm Resolution
- 5 cm Axial Extent
- Cardiology / Neurology
- Academic Research

PET in 2010

- 4 mm Resolution
- >15 cm Axial Extent
- Oncology
- Routine Clinical

Contributions from “Physics”

-Physics concepts: positron range, annihilation, imaging via efficient detection of two 511 keV annihilation gamma rays, two gamma rays co-linearity, TOF, etc

-Instrumentation: detectors, electronics

-Radioactive labels (in radiopharmaceuticals)

-Simulations (modeling) of the detection process and electronics

-Reconstruction, filtering algorithms (tomography, inlcluding limited angle)

PET Detectors

- **Scintillation Detector**
  - Photomultiplier tube (PMT)
  - Avalanche photodiode (APD)
  - Silicon photomultiplier (SiPM)

- **High Density Semiconductors**
  - CdTe or CZT
  - Ge
  - TlBr

Historically: BGO "Block Detector"

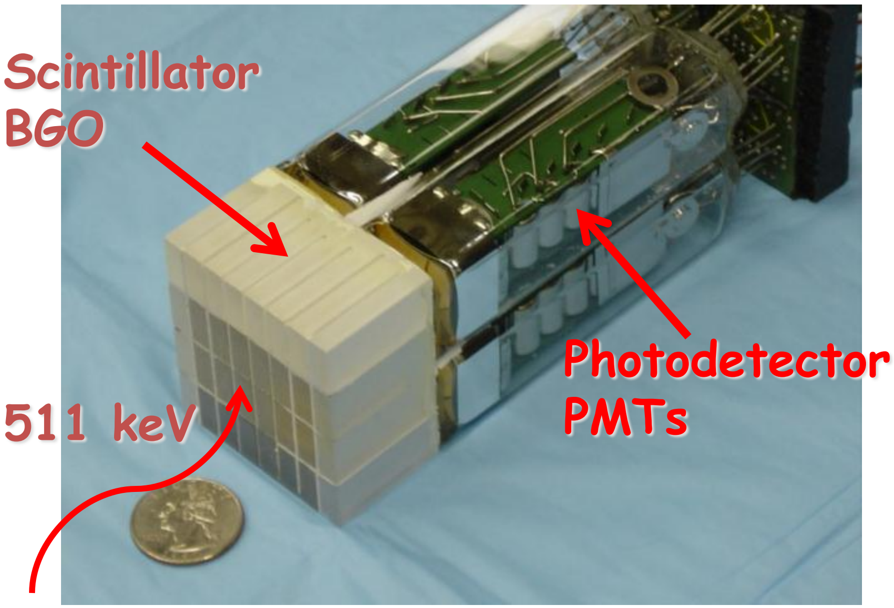

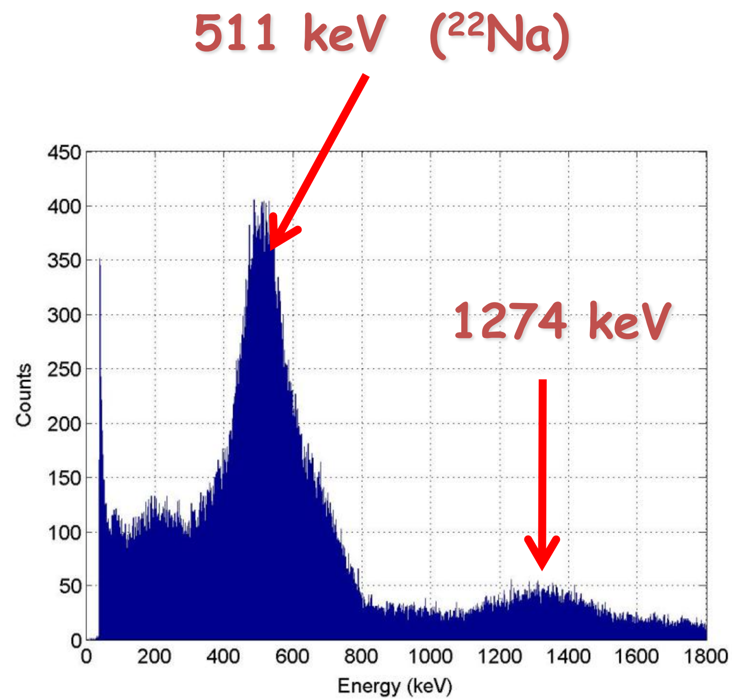

5.3 cm × 5 cm and 3 cm thick
8×4 array, 12.5 mm × 5.25 mm crystal size

(Bill Moses, LBL)

Block Detectors Use "Light Sharing"

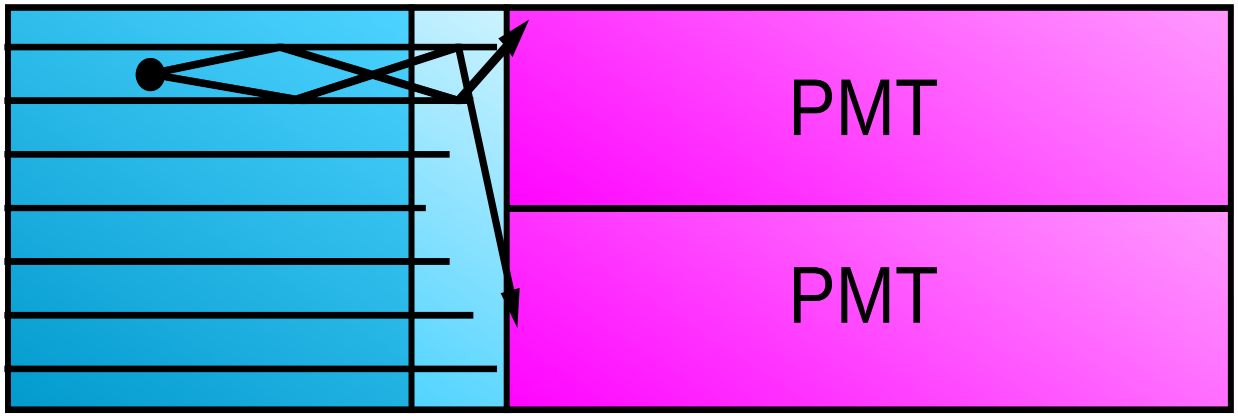

Light Sharing Degrades Timing Resolution

The block detector 1984

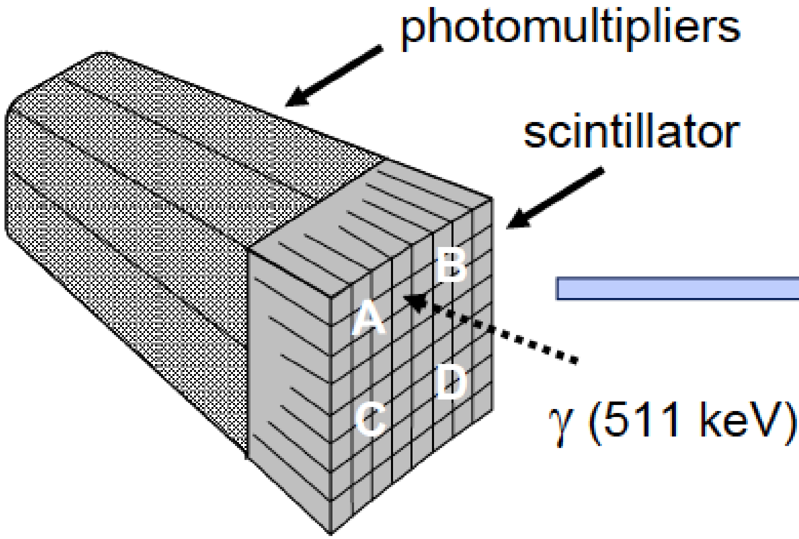

Casey and Nutt, 1986

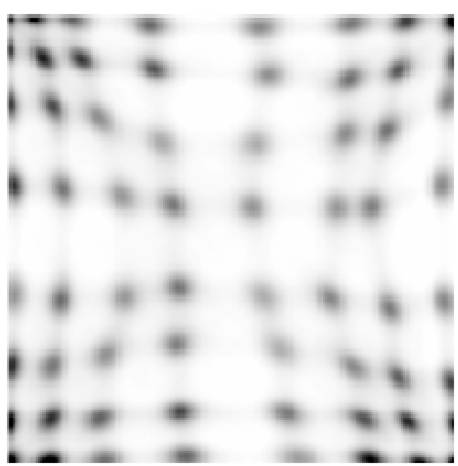

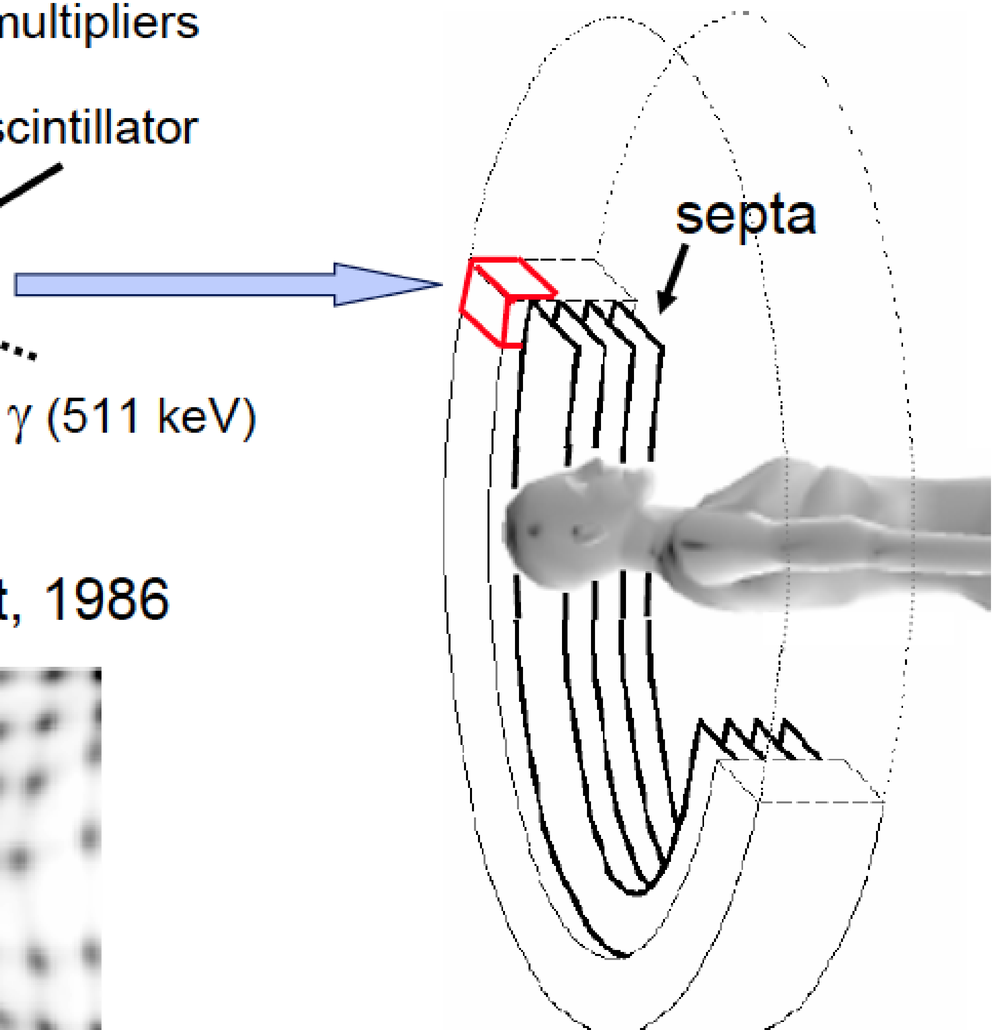

Multi-ring scanner

PET Scintillators

Scintillator	90% efficiency (cm)	Light output (photons/MeV)	Decay time (nsecs)
BGO	2.4	7,000	300
BaF_2	5.1	2,000	0.8
CsF	5.4	1,900	4
LSO, LYSO	2.6	25,000	42
$LaBr_3$	4.9	60,000	27
LuI_3	4.1	100,000	30

PET Electronics

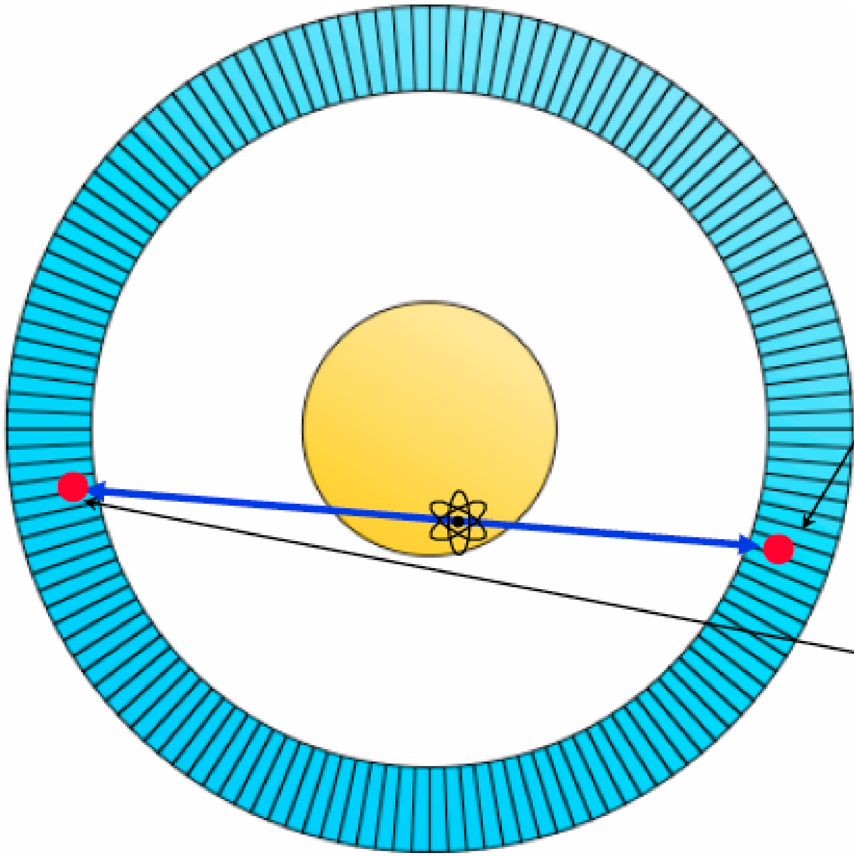

"Singles Event"

- Position (crystal of interaction)
- Time Stamp (arrival time)
- Energy Deposit

Δt

"Singles Event"

- Position (crystal of interaction)
- Time Stamp (arrival time)
- Energy Deposit

- Identify "Singles Events"
- Find Time Coincidences Between Singles Events w/ Δt
- "Coincident Event" = Pair of Singles Events

The clinical importance of spatial resolution

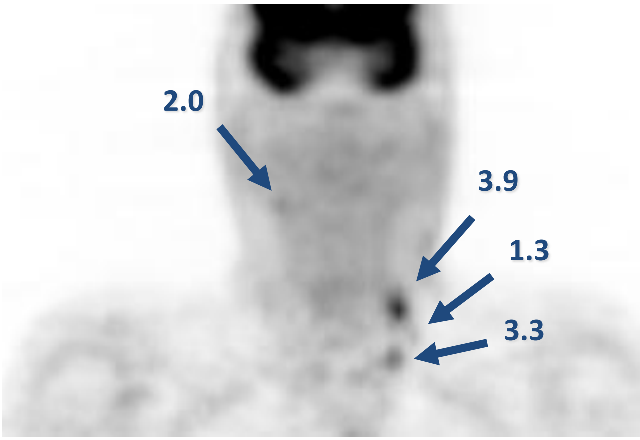

Low-REZ; 8.6 mCi; 60 min uptake

8 x 8 elements/block
6.4 mm x 6.4 mm

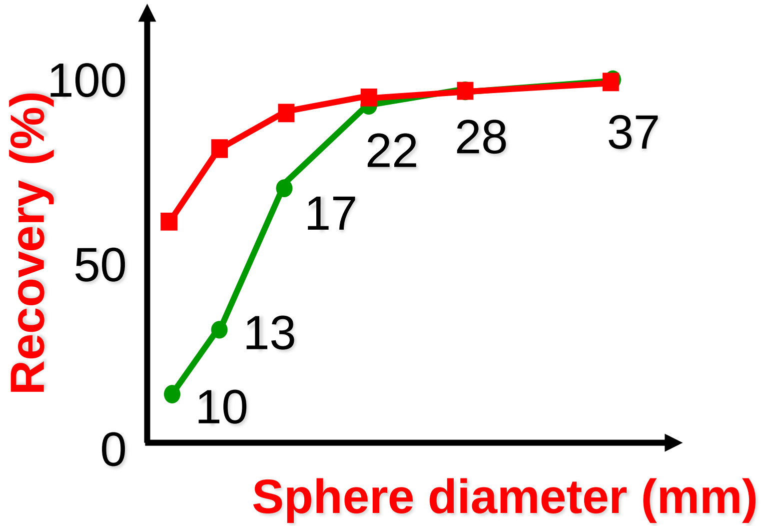

HI-REZ; 11.2 mCi; 90 min uptake

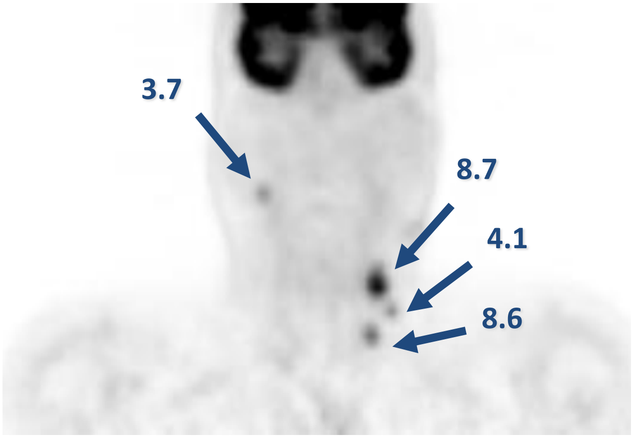

13 x 13 elements/block
4.0 mm x 4.0 mm

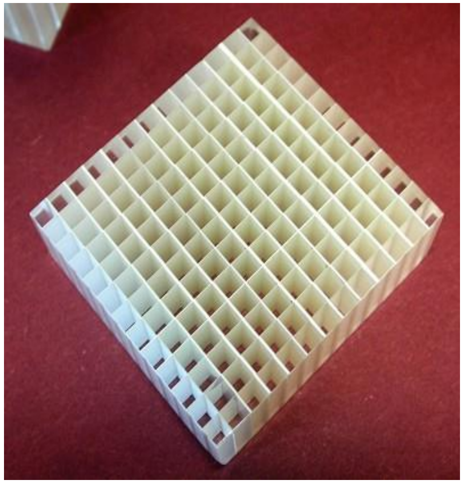

Courtesy of David Townsend, Ph.D.
University of Tennessee Medical Center

How to Detect Smaller Lesions with PET

- Improve spatial resolution
- Improve sensitivity (SNR)
- Improve reconstruction algorithms
- Synergistic use of PET and CT information
- New radiotracers for specific targets

(slide provided by Dr Simon Cherry, UC Davis)

Low Photoelectric Fraction

$\Rightarrow$ Low Coincidence Efficiency

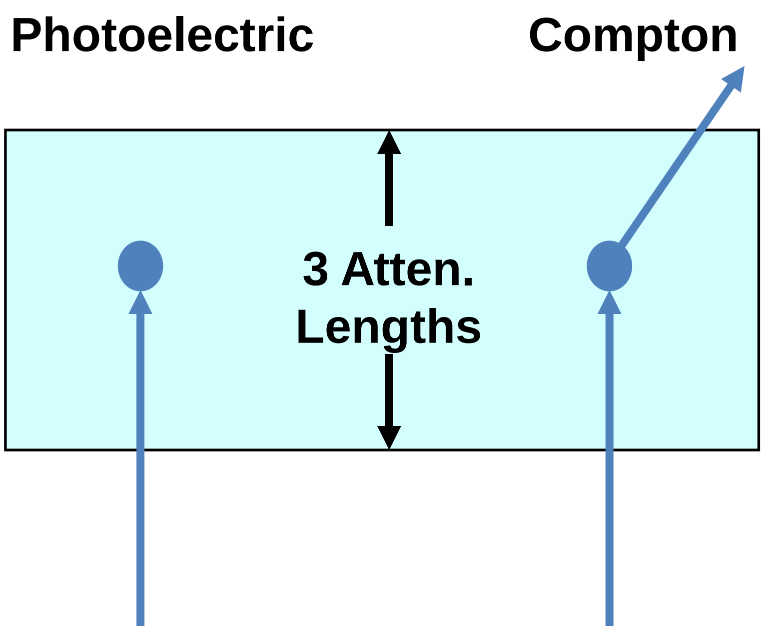

Both Photons Deposit >350 k

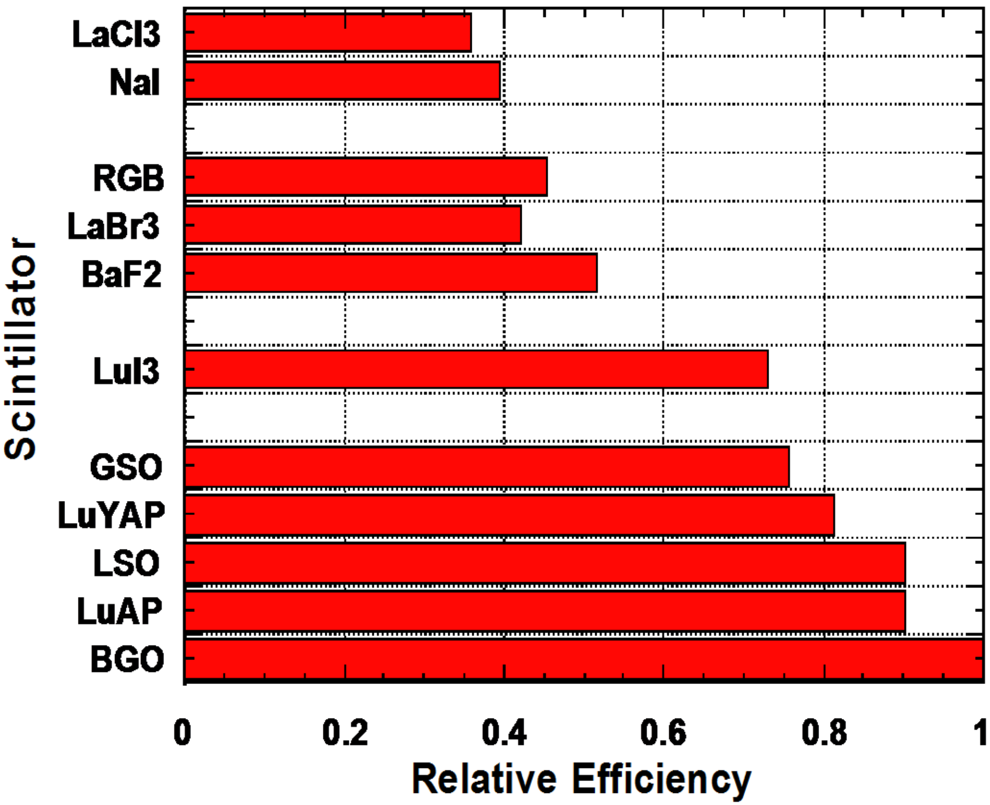

LSO Has Twice The Efficiency of $LaBr_3$

Effects of Detector Resolution

- Already large uncertainty along path of annihilation photons (undone by tomographic reconstruction)
- Resolution determined primarily by uncertainty *transverse* to the photon paths

$$R_D \approx 2.35\sqrt{\left((1-\alpha)^2\left(\sin^2\theta_1\sigma_{D1}^2+\cos^2\theta_1\sigma_{C1}^2\right)+\alpha^2\left(\sin^2\theta_2\sigma_{D2}^2+\cos^2\theta_2\sigma_{C2}^2\right)\right)}$$

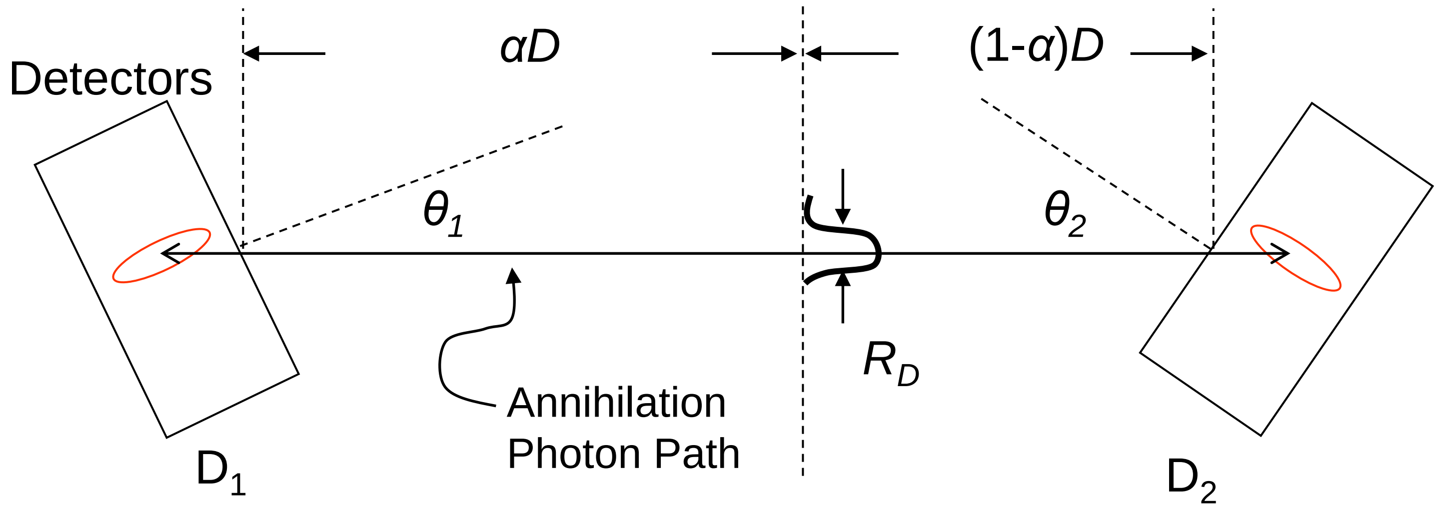

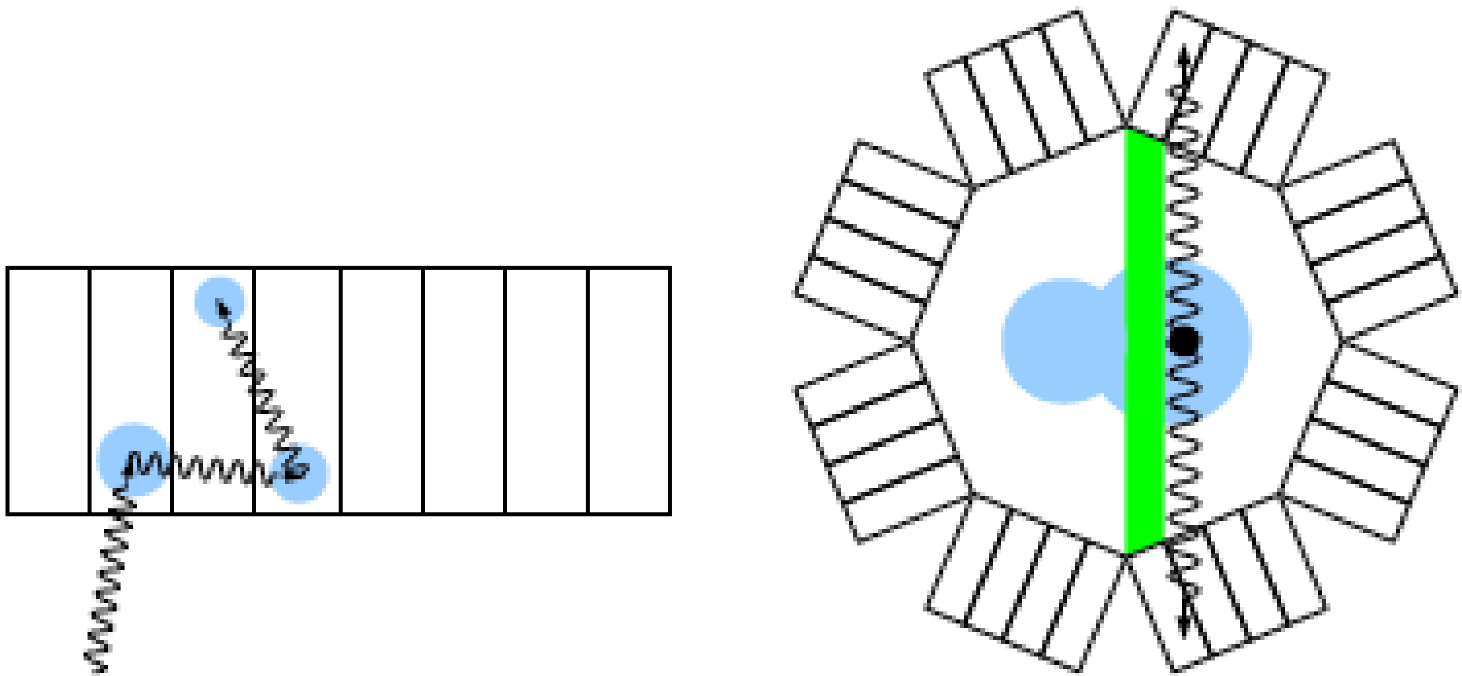

(a) (b)

Figure 5.1: Diagrams demonstrating loss of spatial resolution due to (a) inter-crystal scattering and (b) uncertainty in the depth of interaction.

Eric R. Cochran, M.S.

Low Density ⟹ Radial Elongation

Penetration Blurs Image

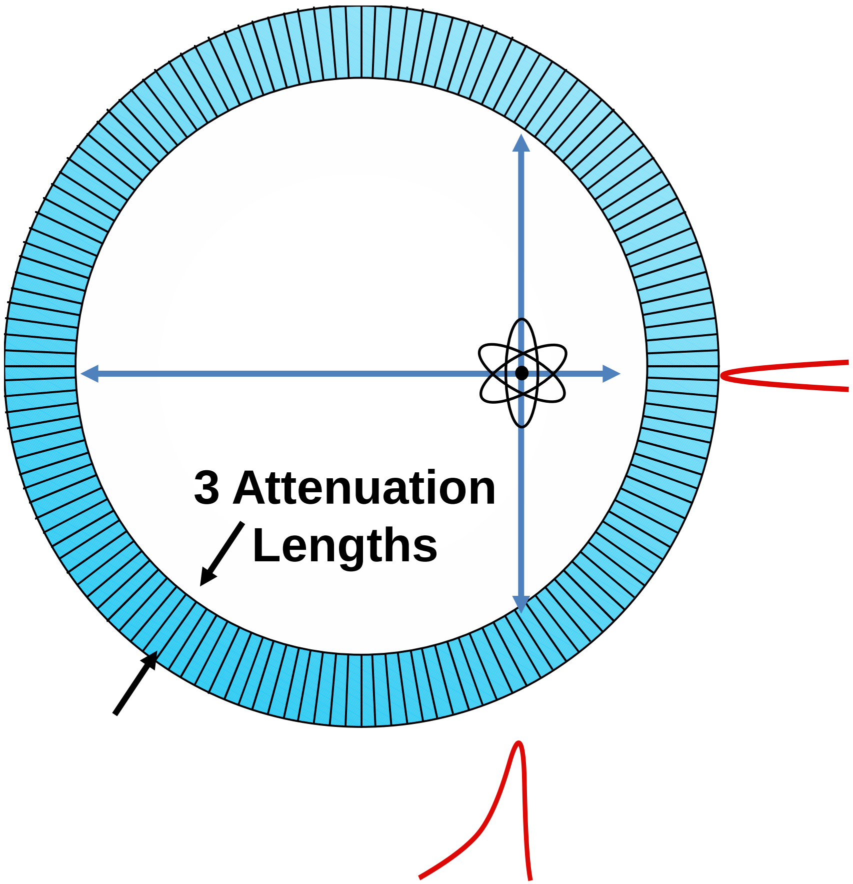

Resolution vs. Position

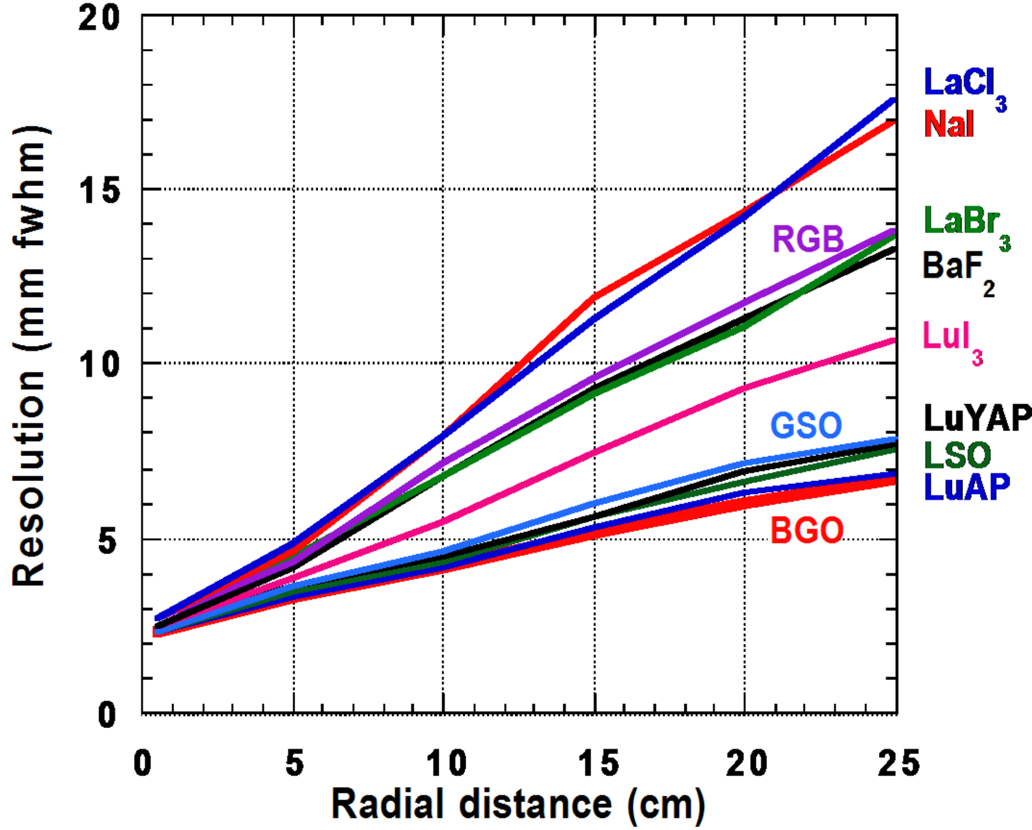

LaBr$_3$ (& BaF$_2$) Have More Degradation Than LSO

Concept of Zoom Resolution Improvement

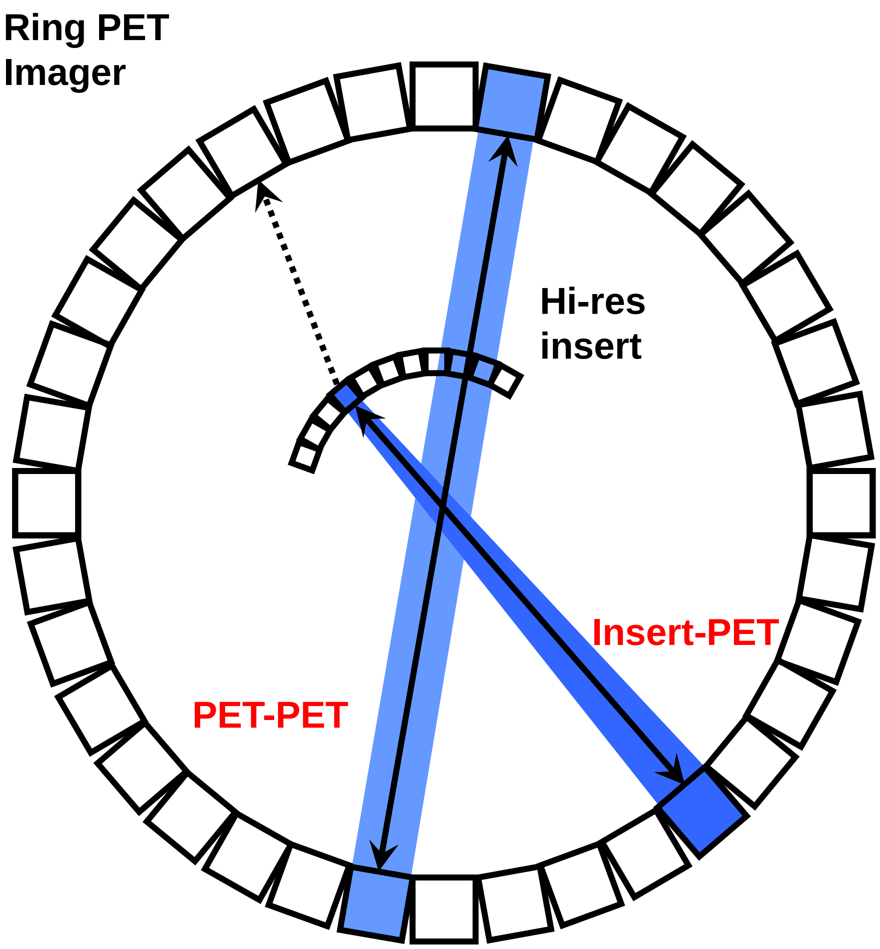

- High resolution is possible close to high resolution detector insert
- High resolution information is limited-angle
- Resolution improvement will not be isotropic, only local
- Time-of-flight information may reduce anisotropy

In Vivo Medical Imaging Technologies

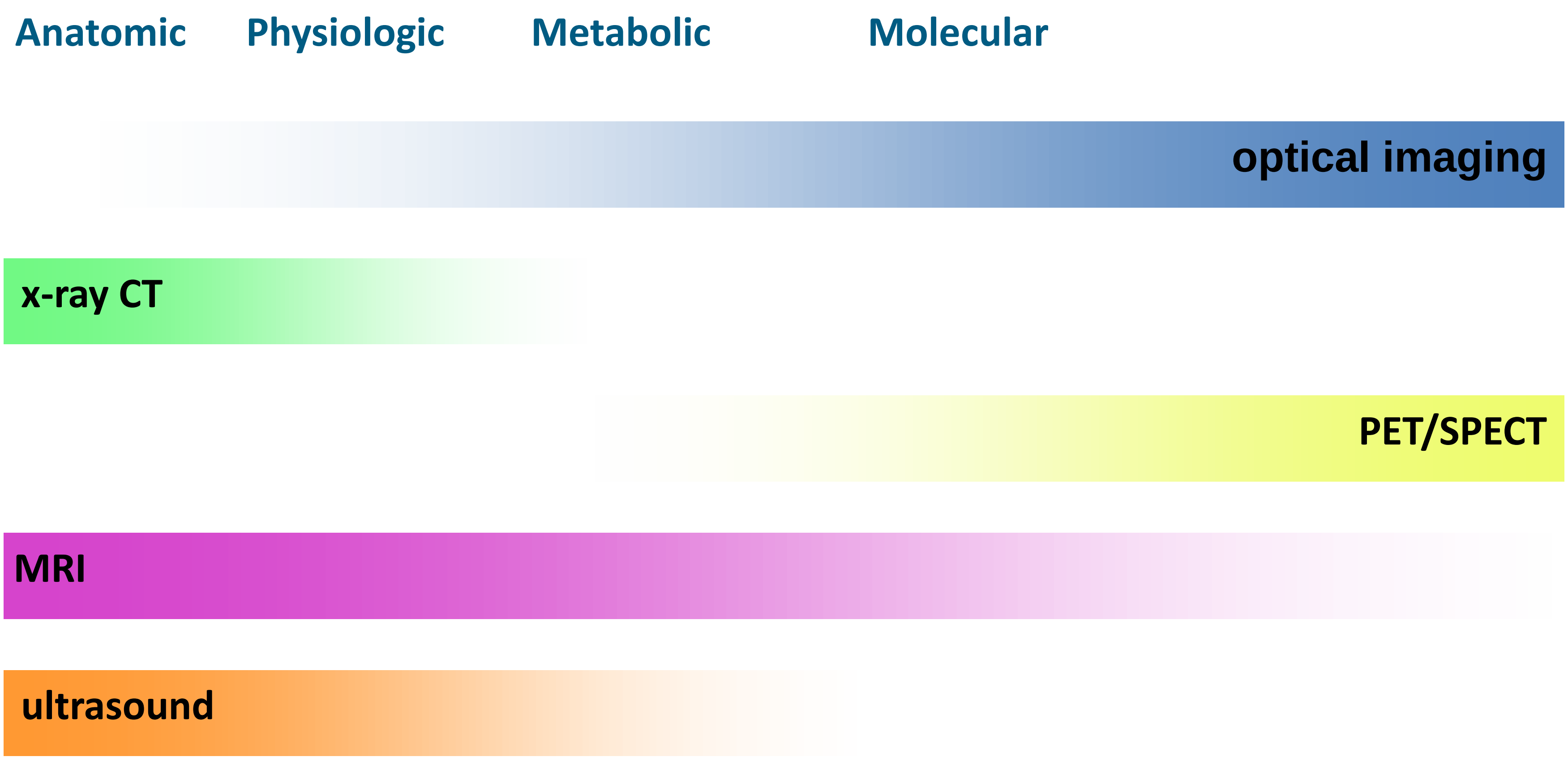

Fusing Anatomy and Function

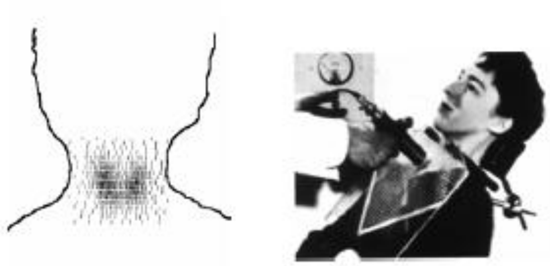

Hand-drawn contours

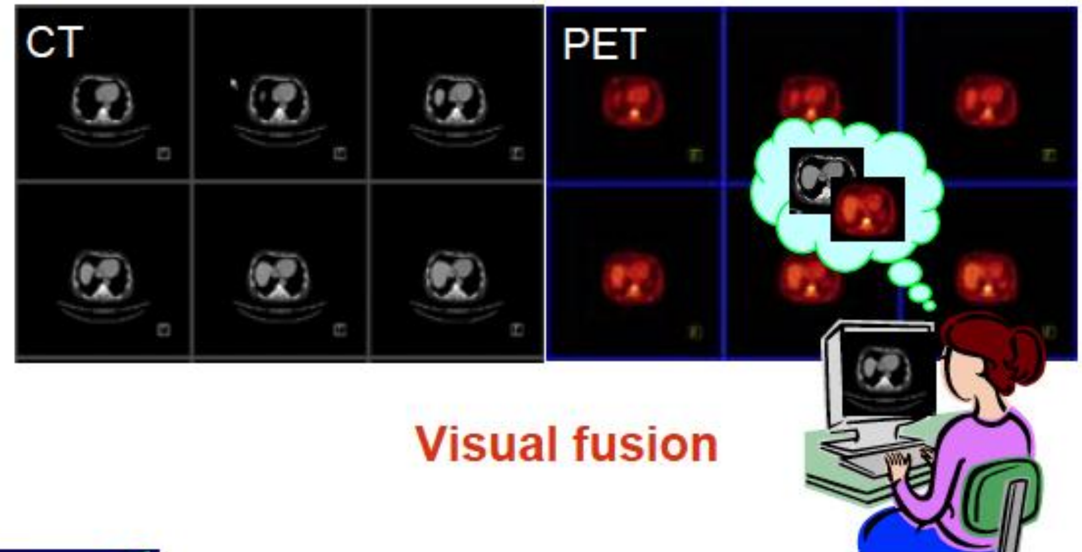

Visual fusion

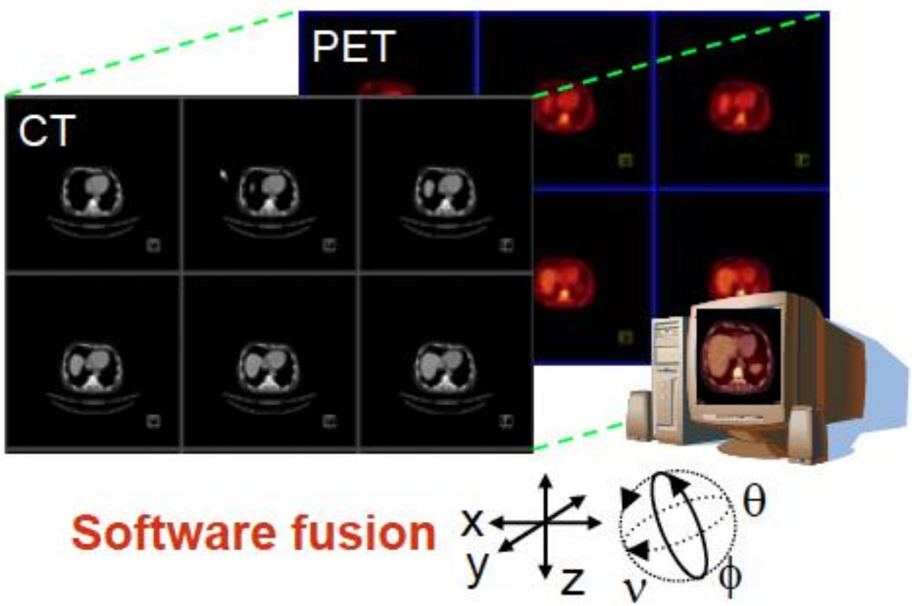

Software fusion

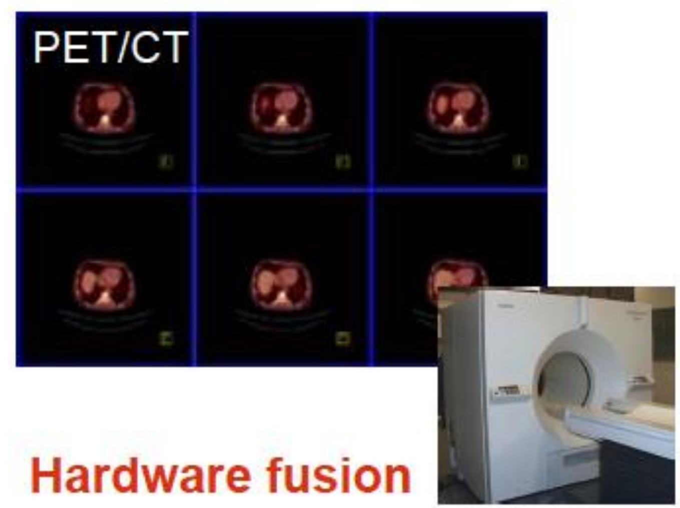

Hardware fusion

Dual-Modality PET/CT Imaging

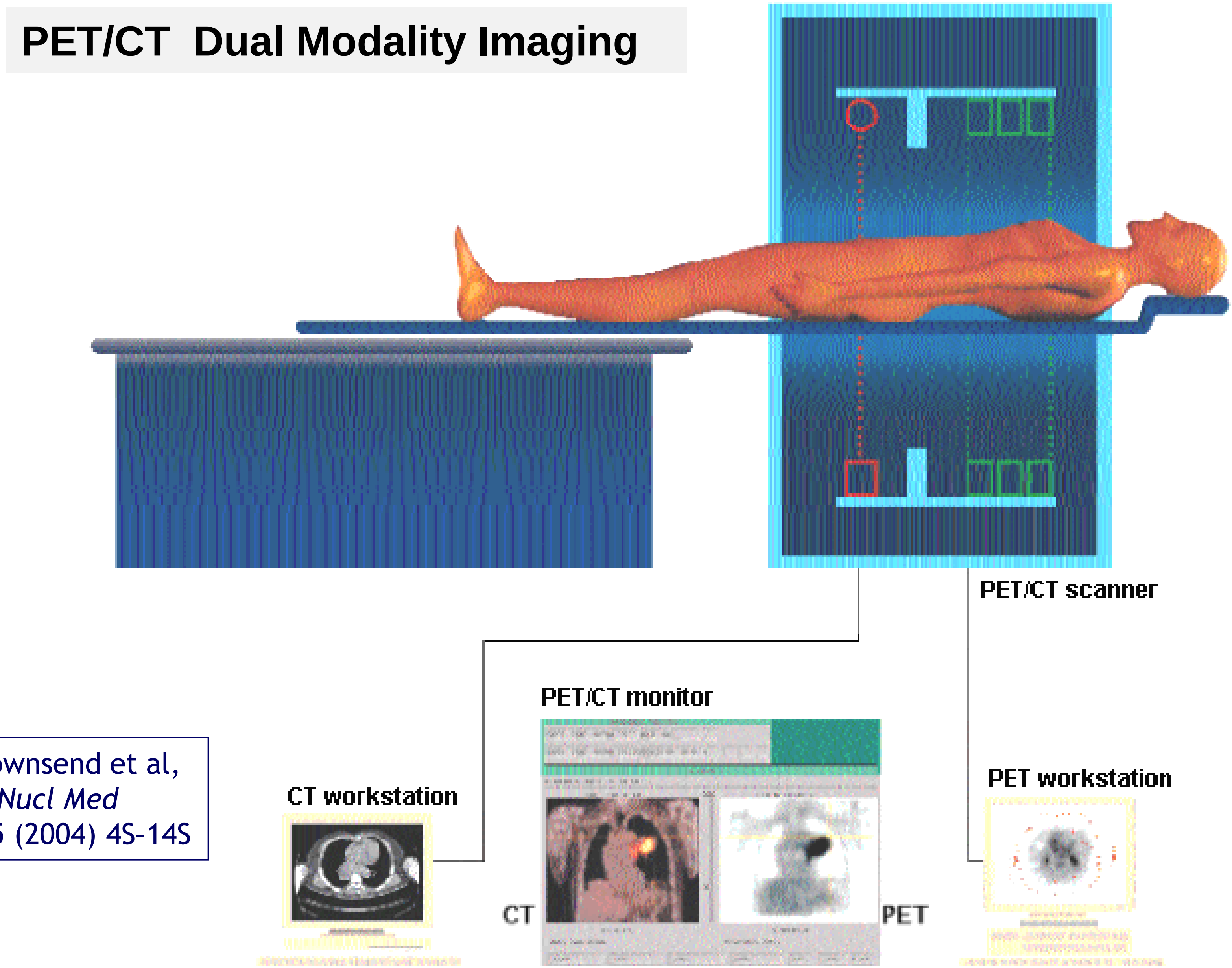

Townsend et al,
J Nucl Med
45 (2004) 4S–14S

Comparing anatomy and function

Cancer Imaging and Tracer Development

CT scan of anatomy

NaF-PET scan of function

Form + function

Fused image accurately localizes uptake into a lymph node and thus demonstrates spread of disease.

- to image different aspects of disease
- to identify tracer uptake
- to simplify the image interpretation
- to give added value to CT and PET

Why combine form and function?

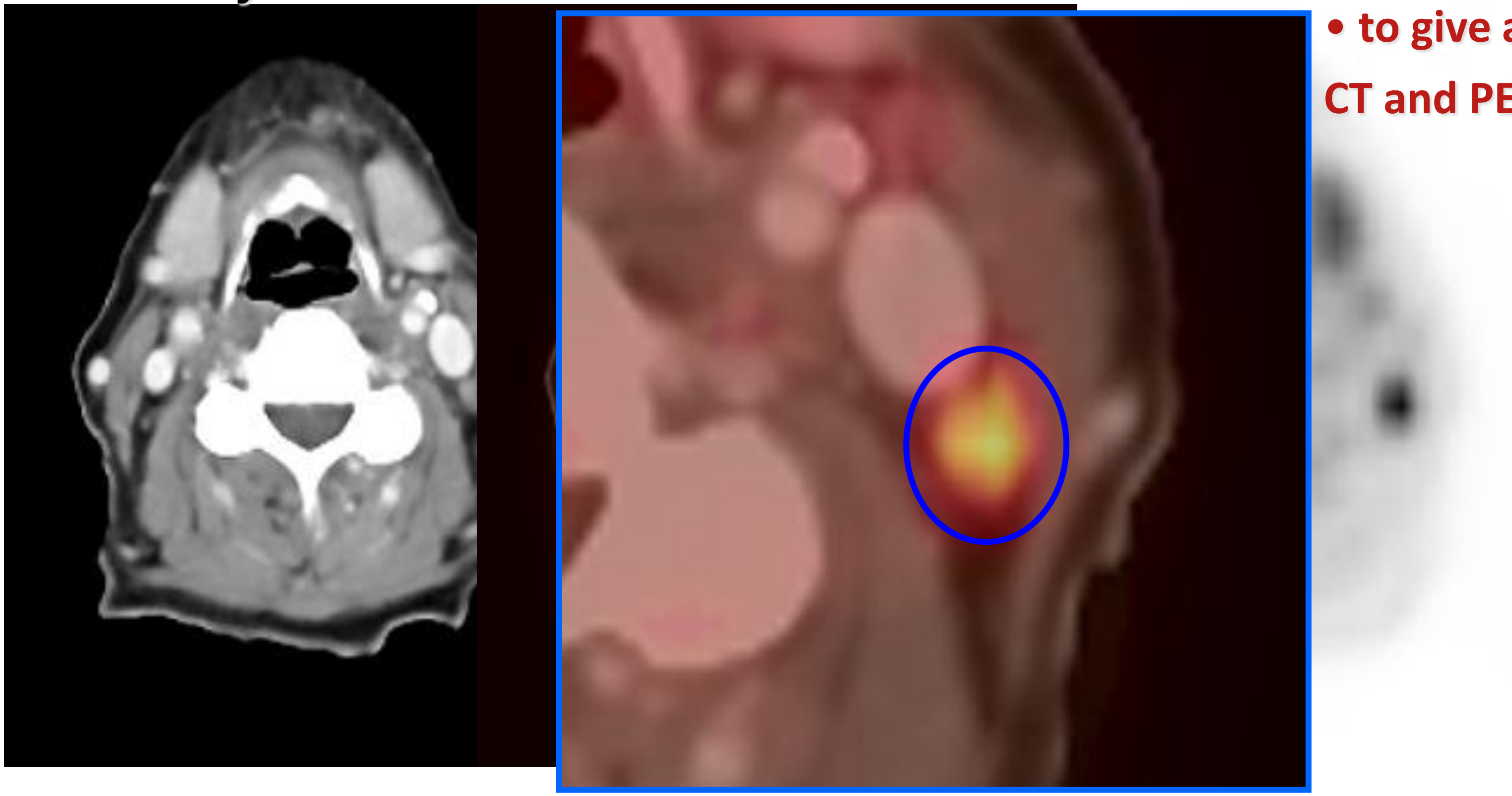

CT (anatomy) **PET/CT** **PET (function)**

Courtesy of David Townsend, Ph.D.
University of Tennessee Medical Center

Dynamic PET/CT imaging

PET image of seconds 4546

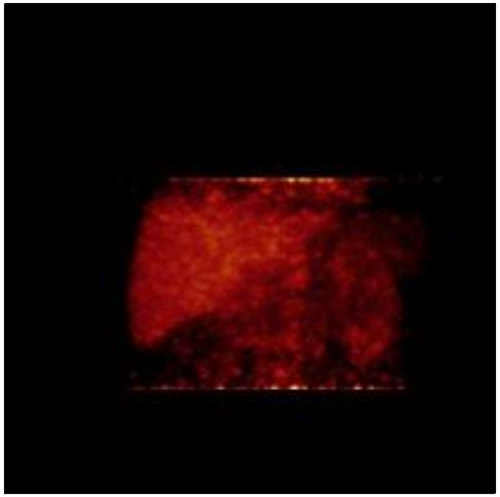

5 sec frames following bolus

Fused PET/CT

Motivation to Combine PET and MRI

- **Strengths**

- "Near-perfect" registration of structural and molecular imaging data
- Anatomically-guided interpretation of PET data
- Anatomic priors for PET reconstruction and data modeling
- PET can be combined with advanced MRI techniques such as DWI, DCE MR, MRS, cell tracking and MR molecular imaging agents

- **Weaknesses**

- Technically difficult and likely expensive
- Uncertainty regarding throughput, cost effectiveness and ultimate clinical role

Time-of-Flight in HEP

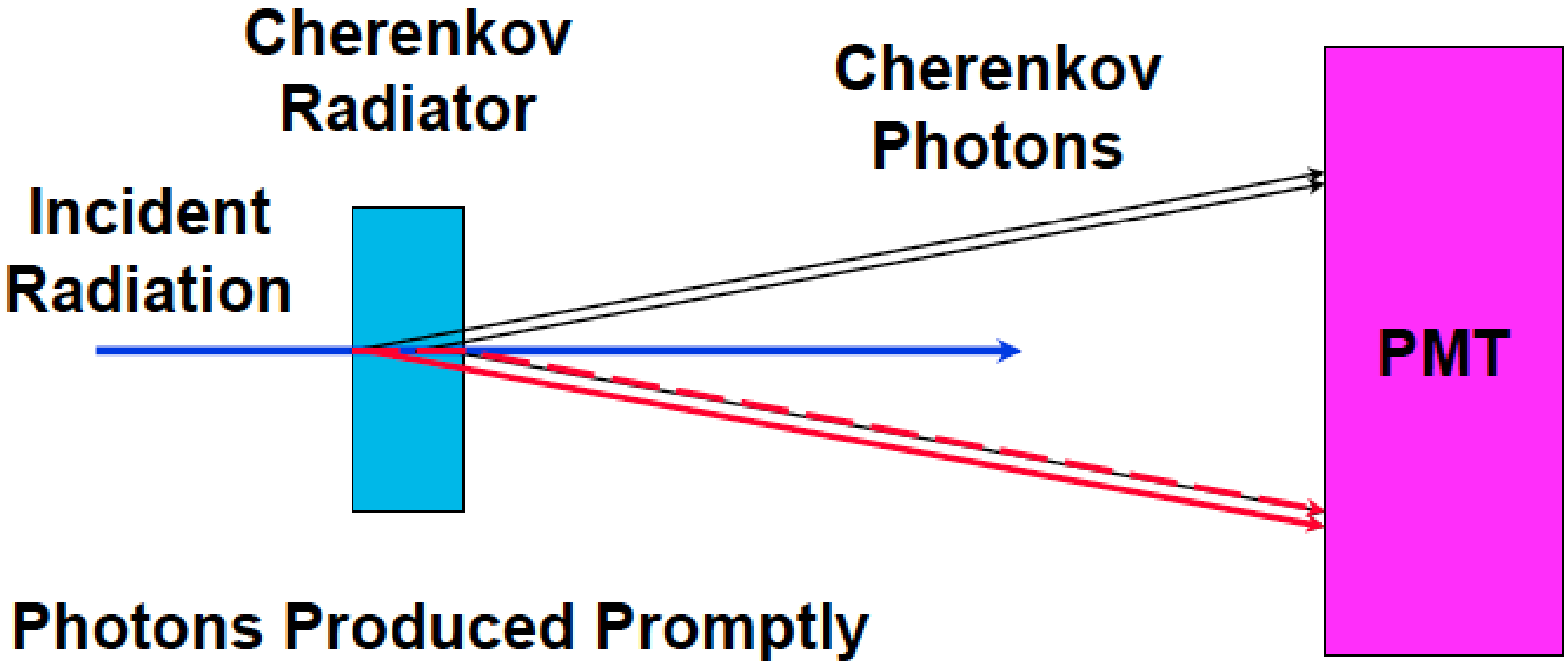

- Photons Produced Promptly
- Photons Travel in ~Same Direction
- Small Time Variations due to Path Length Difference
- Small Variations due to Photon Production Position

Time Spread Between Photons Arriving at PMT is Small

Time-of-Flight in PET

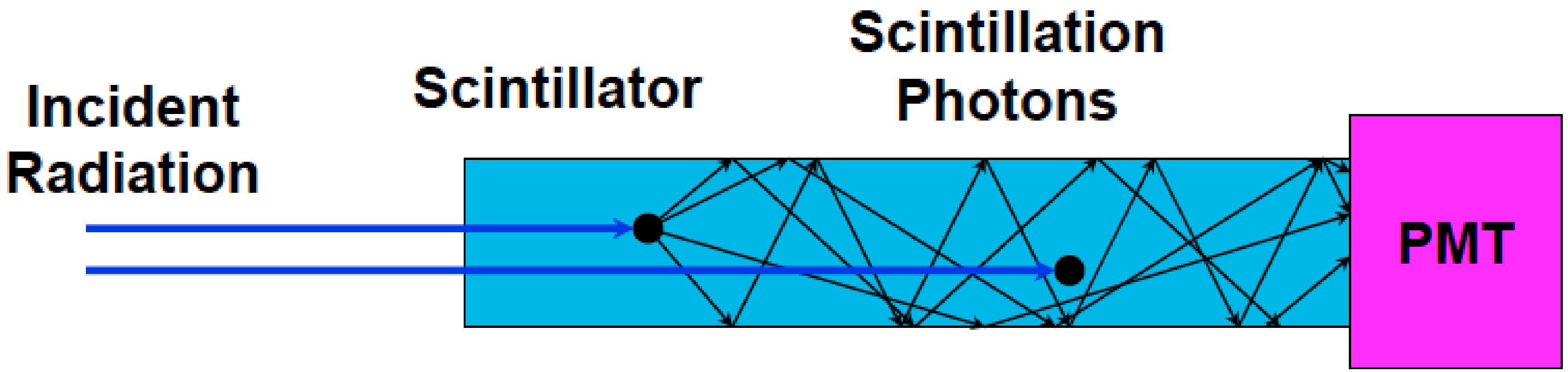

- Photons Produced with Scintillator Decay Time
- Photons Travel in All Directions
- Large Time Variations due to Path Length Difference
- Large Variations due to Photon Production Position

Time Spread Between Photons Arriving at PMT is Large

TOF PET Is An Old Idea…

- Extensive work on TOF PET *was* done in the 80's.
- Several TOF PET cameras were built & most of the advantages described here were experimentally verified.
- The scintillator materials used in the 80's (BaF_2 and CsF) had drawbacks (*e.g.,* low density, low photofraction) which required other performance compromises, so BGO dominated PET.
- PET has changed: whole body imaging $\Rightarrow$ larger objects, larger axial FOV $\Rightarrow$ randoms are a larger problem, etc.
- LSO (~200 ps) and $LaBr_3$ (<100 ps) can provide outstanding timing resolution *without* the other performance compromises.

TOF PET Is Experiencing a Rebirth!!!

Time-of-Flight in PET

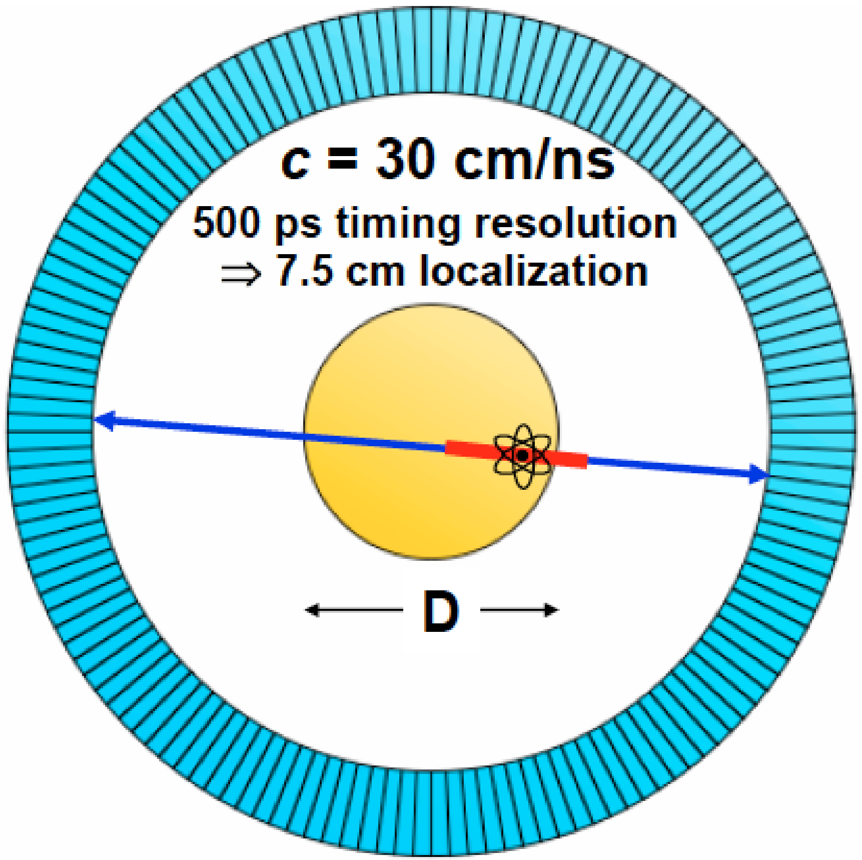

- Can localize source along line of flight.
- Time of flight information reduces noise in images.
- Variance reduction given by $2D/c\Delta t$.
- 500 ps timing resolution
  ⇒ 5x reduction in variance!

- Time of Flight Provides a *Huge* Performance Increase!
- Largest Improvement in Large Patients

Adding Time-of-Flight to Reconstruction

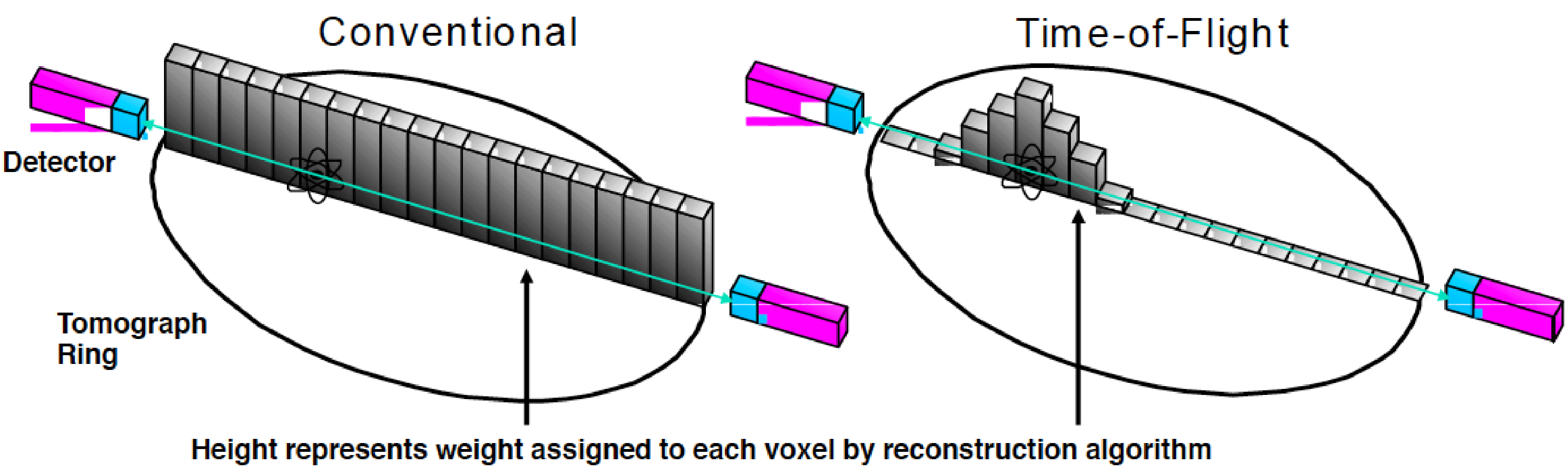

Data courtesy by W.Moses

Conventional:
- Detected event projeted to all voxels between detector pairs
- Lots of coupling between voxels

→ Many iterations to converge

Time-of-Flight:
- Detected event projeted **only to** voxels consistent w measured time
- Little coupling between voxels

→ Few iterations to converge

Principles of TOF PET

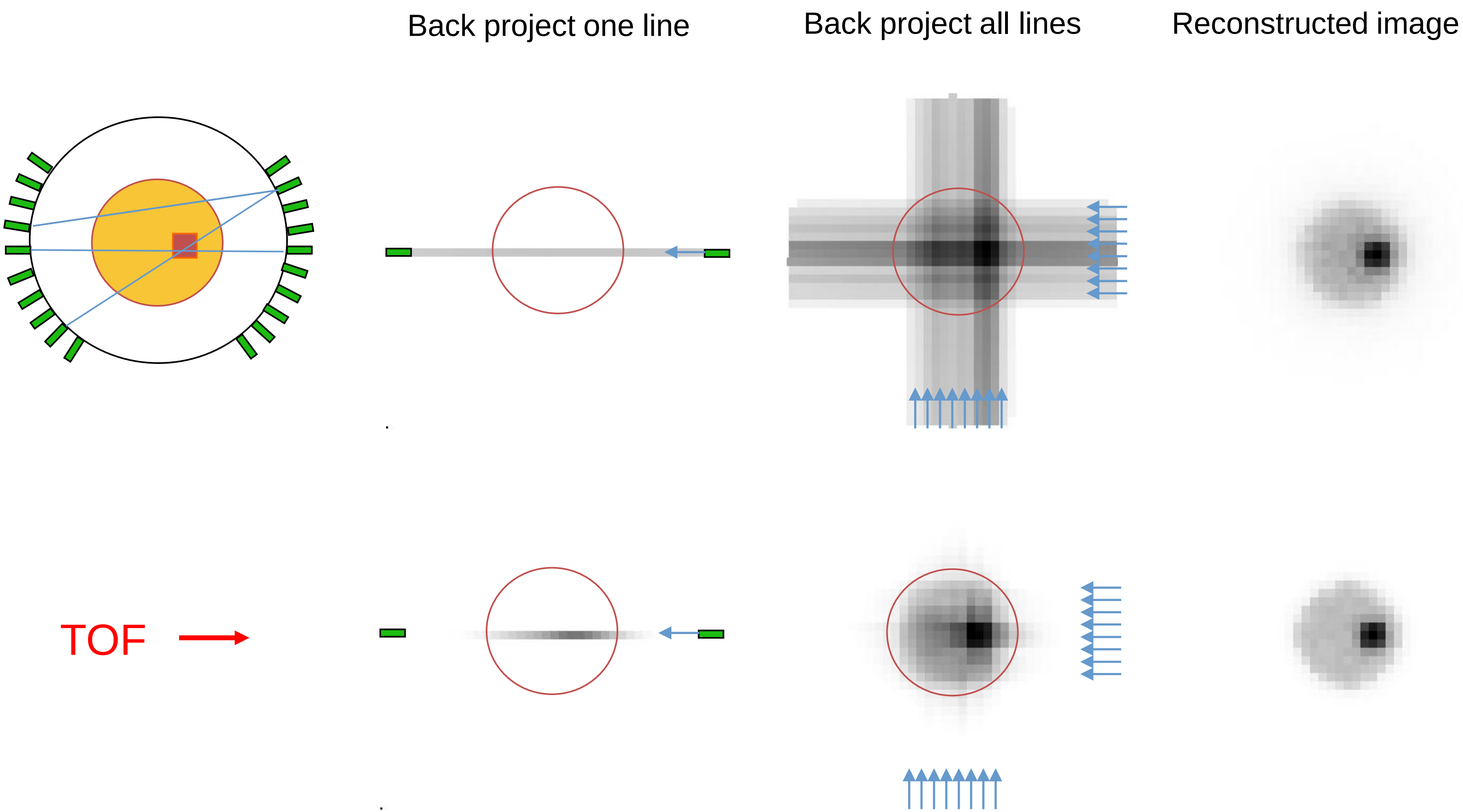

PET: Impaired Image Quality in Larger Patients

Slim Patient

Large Patient

- For an equivalent data signal to noise ratio, a 120 kg person would have to be scanned <u>2.3 times</u> longer than a 60 kg person [1)]

1) Optimizing Injected Dose in Clinical PET by Accurately Modeling the Counting-Rate Response Functions Specific to Individual Patient Scans. Charles C. Watson, PhD et al Siemens Medical Solutions Molecular Imaging, Knoxville, Tennessee, JNM Vol. 46 No. 11, 1825-1834, 2005

A clinical problem: Patient body size [1)]

Histogram of the patient body diameter for 65 randomly selected patients

Average patient diameter = 27 cm

Large patient diameter = 35 cm

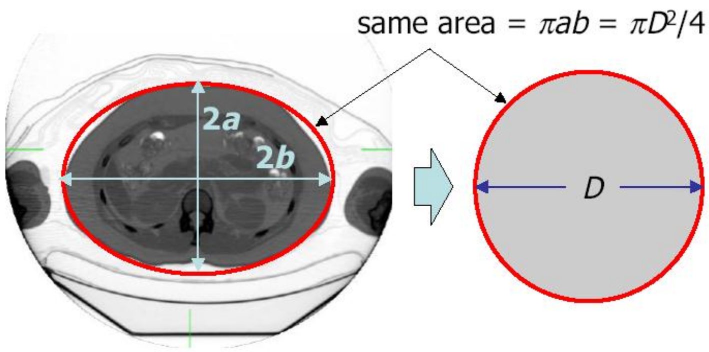

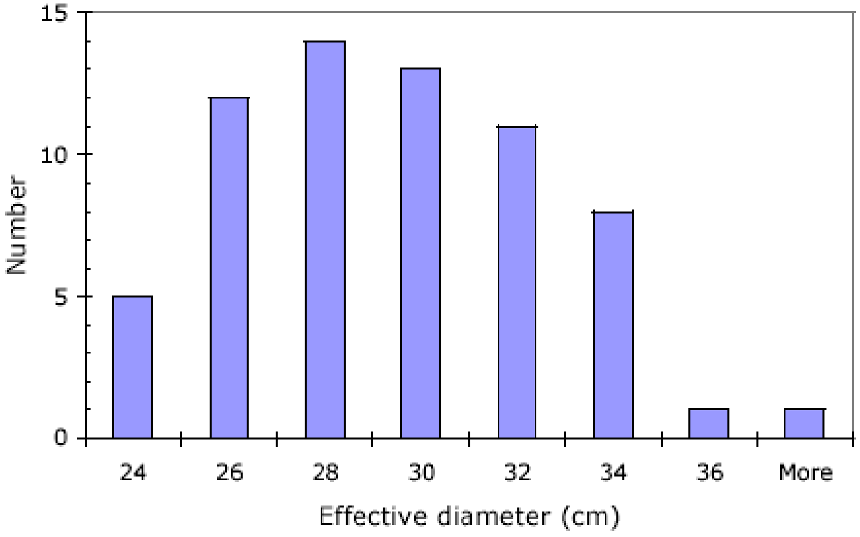

1) A Quantitative Approach to a Weight-Based Scanning Protocol for PET Oncology Imaging. Paul Kinahan, Phillip Cheng, Adam Alessio, Tom Lewellen, University of Washington, Seattle. Presented at MIC conference 2005. Data used with authors permission.

Dutch clinics under strain from obese patients

Wed Jan 18, 2006 5:11 PM GMT

AMSTERDAM (Reuters) - Dutch hospital beds and operating tables could buckle under the strain of obese patients, doctors have complained, adding some patients barely fit into scanning machines.

TruFlight™: Enhanced Diagnostic Confidence

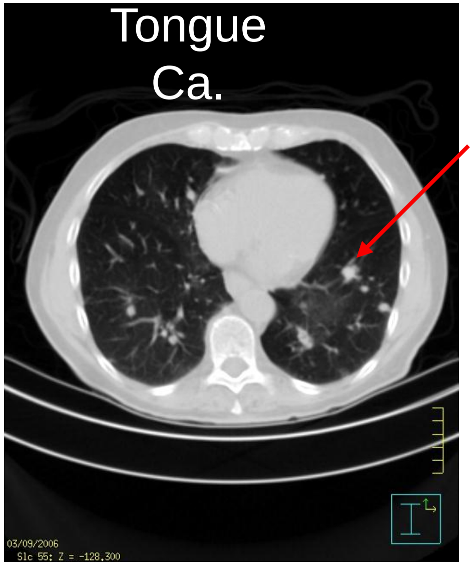

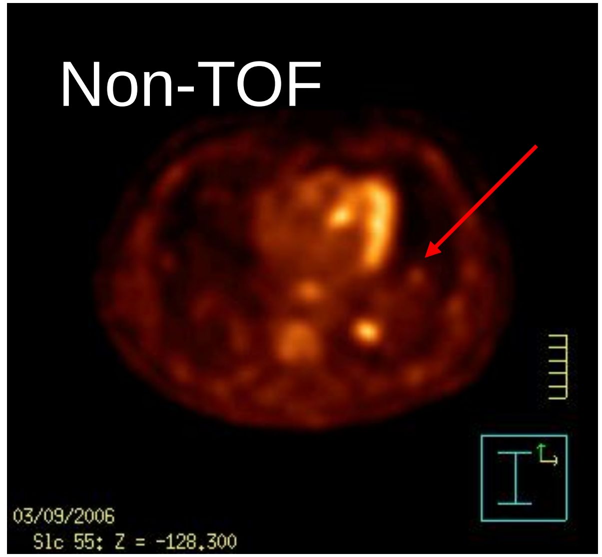

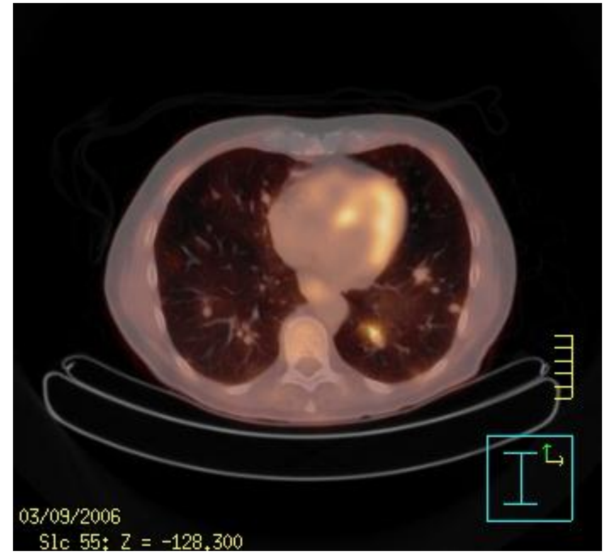

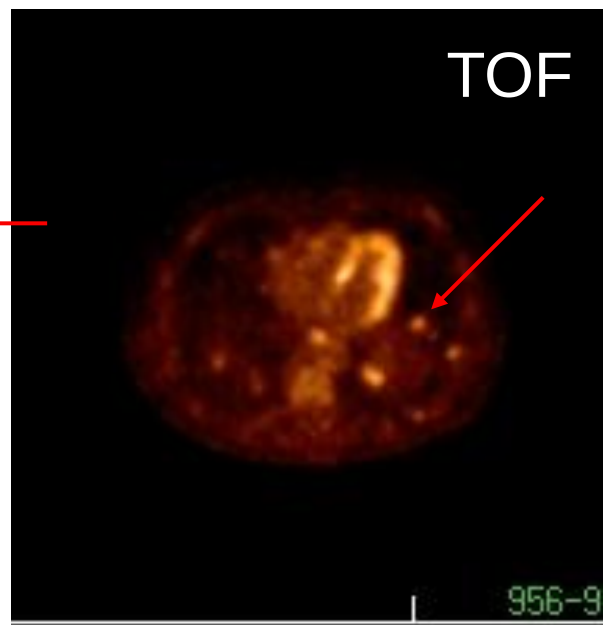

improved detectability of small mets in lung

67 kg; BMI = 29.0
9.8 mCi; 1 hr post-inj. (2min/bed)

Data courtesy of J. Karp, University of Pennsylvania

TruFlight™: Enhanced Diagnostic Confidence

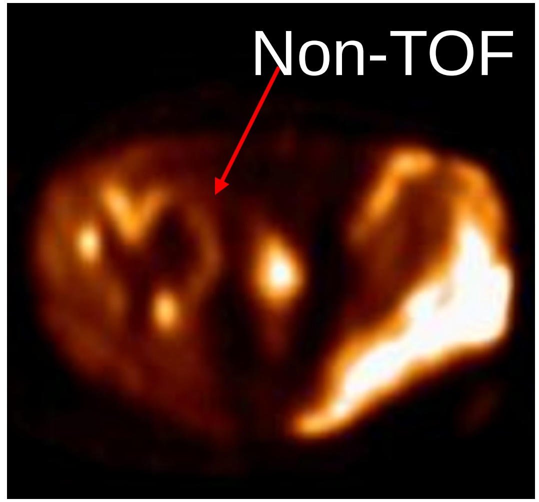

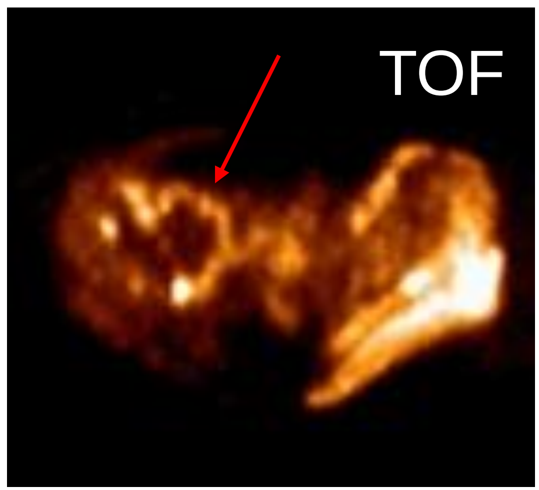

116 kg; BMI = 31.2
14 mCi; 2 hr post-inj

Lymphoma within right iliopsoas muscle with central area of necrosis

improved delineation of lymphoma activity

Data courtesy of J. Karp, University of Pennsylvania

TOF Gain for Whole-Body PET (35 cm)

Hardware	Δt (ps)	TOF Gain
BGO Block Detector	3000	0.8
LSO Block (non-TOF)	1400	1.7
LSO Block (TOF)	550	4.2
$LaBr_3$ Block	350	6.7
LSO Single Crystal	210	11.1
LuI_3 Single Crystal	125	18.7
$LaBr_3$ Single Crystal	70	33.3

Incredible Gains Predicted…

Future instrumentation: New scintillators

- Dense
- Bright
- Fast

dense

bright

$$\eta \approx \varepsilon^2 \cdot G_{TOF} \approx \varepsilon^2 \cdot \frac{1}{\Delta t} \approx \varepsilon^2 \cdot \frac{\sqrt{N}}{\tau}$$

fast

Conventional sensitivity

TOF amplifier

LSO/LYSO is dominating now….

Future, questions and challenges: Improving time resolution

$$\tau^2 = \tau_0^2 \frac{1}{N_0}\frac{1}{QE}\frac{1}{\alpha_{crystal}}\frac{1}{\alpha_{BLK}} + \Delta\tau^2_{PL-crys} + \Delta\tau^2_{PL-LG} + \Delta\tau^2_{PMT-TTS} + \Delta\tau^2_{PMT-\mathrm{var}} + \Delta\tau^2_{DISCR} + \Delta\tau^2_{TDC} + \Delta\tau^2_{SysNoise} + \ldots.$$

Scintillator timing

Scintillator Light output

Light sensor properties (PMT)

Crystal losses

Block losses

Path length spread in crystal

Path length spread in light guide

Transit time spread in PMT

PMT variations

Discriminator Time spread

TDC Time spread

System noise contributions: Power supplies, clocks, cables, etc

Statistical part

Signal From Scintillator

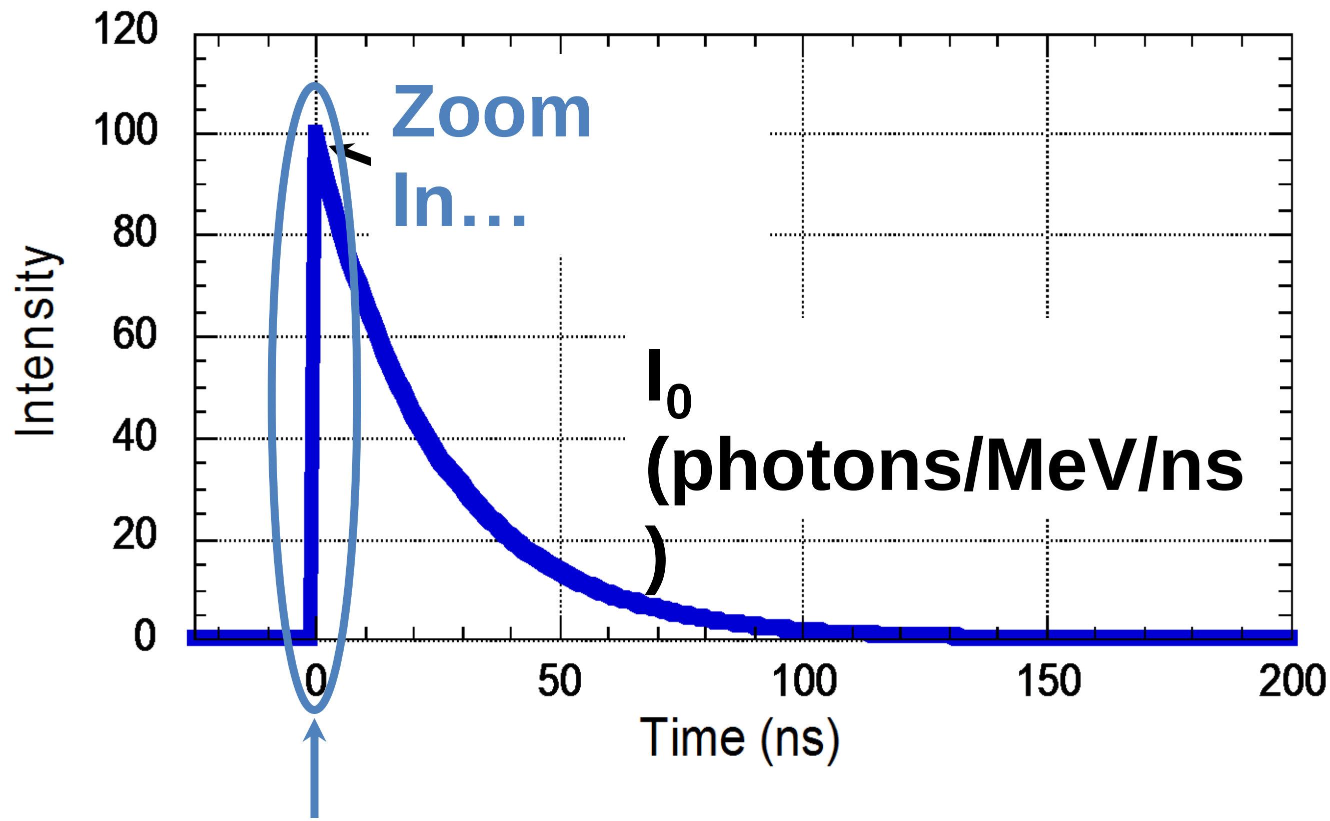

Interaction Happens at This Time…

Initial Intensity Governs Timing Resolution

Signal From Scintillator

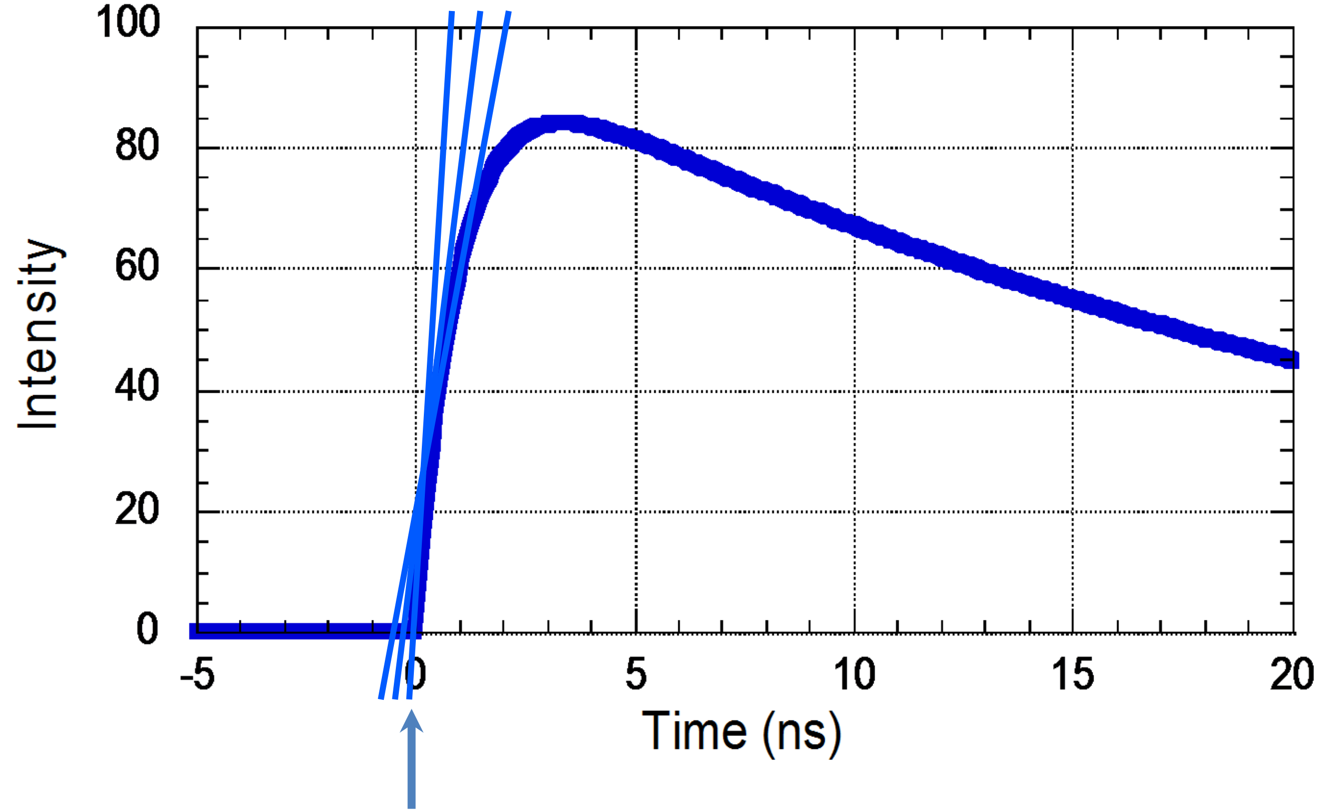

Interaction Happens at This Time…

Steep Initial Slope (High I_0) Improves Timing

Signal From Scintillator

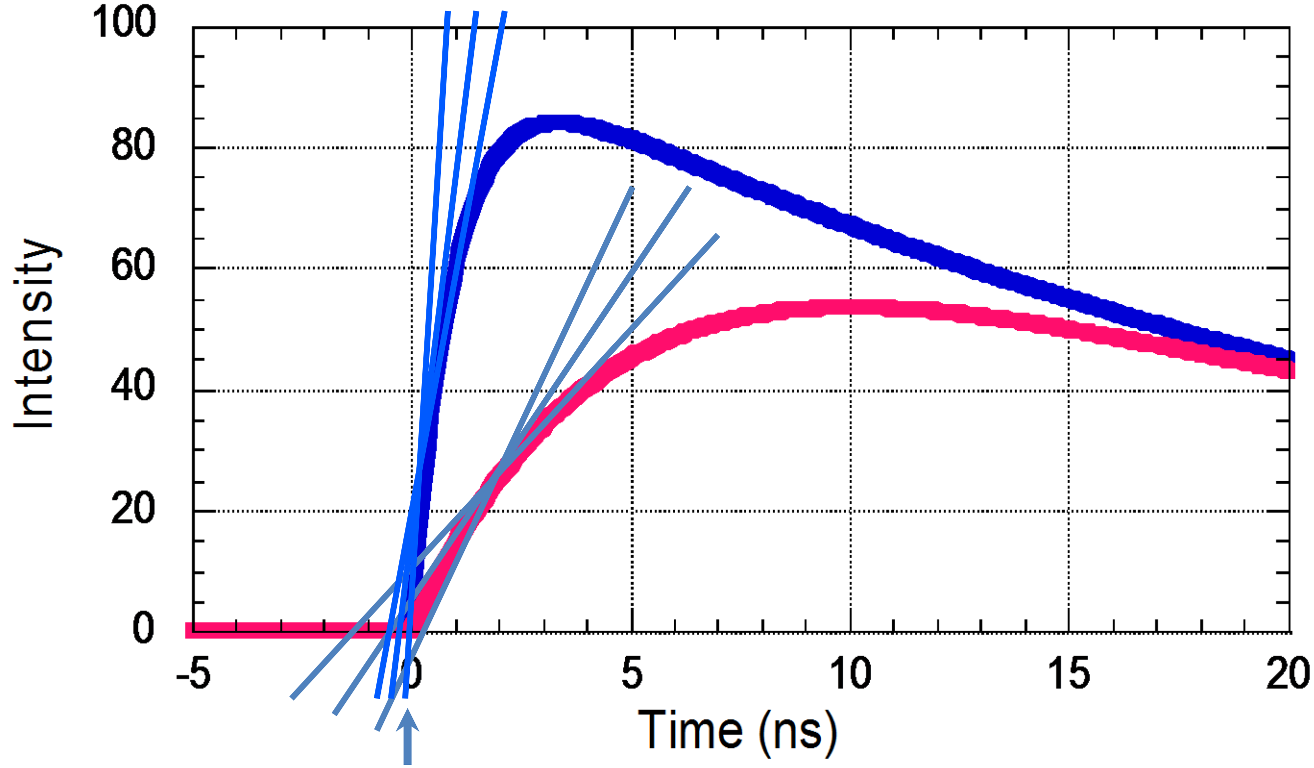

Interaction Happens at This Time…

Steep Initial Slope (High I_0) Improves Timing

Signal From Scintillator

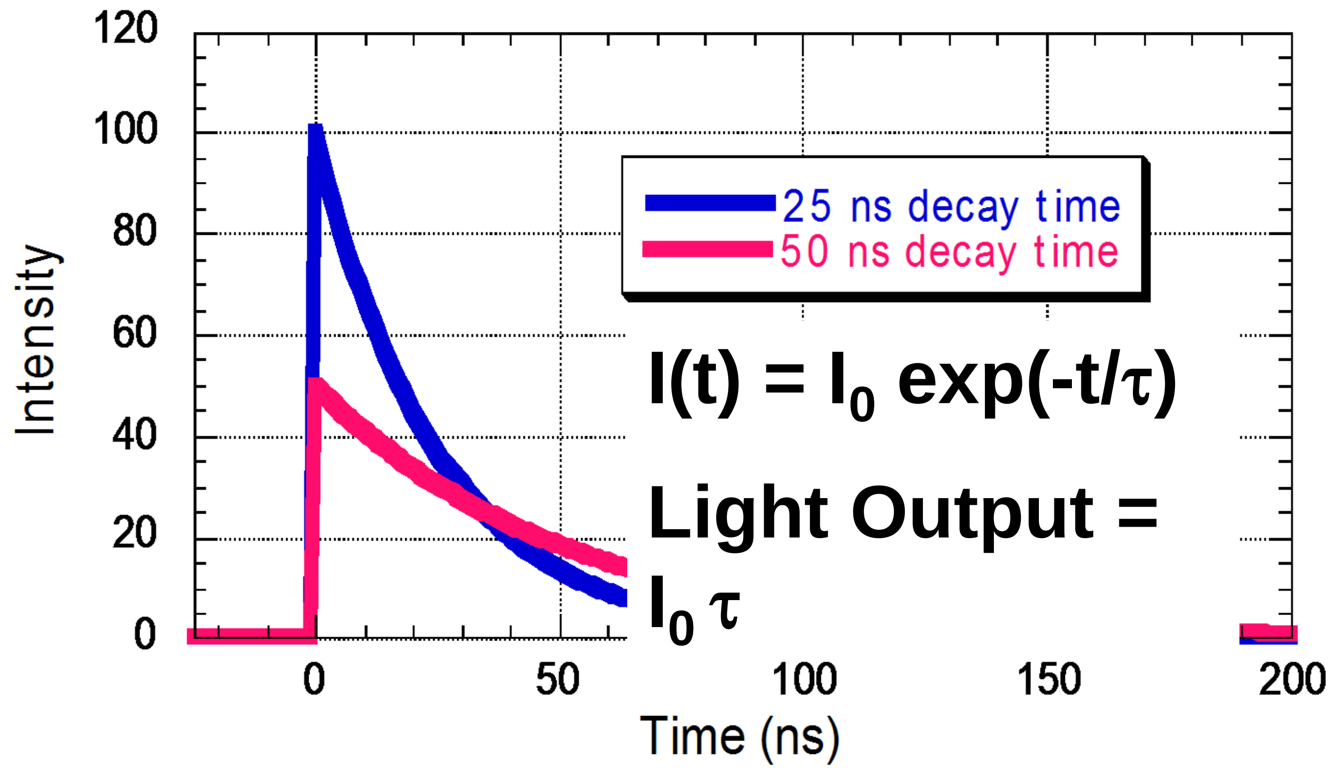

$$I(t) = I_0 \exp(-t/\tau)$$

Light Output = $I_0\,\tau$

- Both Scintillators Have Same Light Output (photons/MeV)
- Red Decay Time is 2x Longer Than Blue Decay Time

Want High Total Light Output & Short Decay Time

Scintillators

TOF PET systems in 1980's with BaF_2 achieved system TOF of 500-700 ps, but low light output led to poor energy and spatial resolution
Did not match overall performance of BGO systems with higher sensitivity

Scintillator	NaI(Tl)	BGO	BaF_2	GSO	LSO/LYSO	$LaBr_3$
τ (ns)	230	300	**2**	60	**40**	**27**
μ (cm^{-1})	0.35	0.95	**0.45**	0.70	**0.86**	**0.47**
photons (per MeV)	41,000	7000	**2000**	10,000	**26,000**	**60,000**

- high stopping -> better sensitivity & better spatial resolution
- high light output -> better energy resolution & better spatial resolution
- fast decay & high light -> better timing resolution (TOF) & lower deadtime

PET Scintillators

•from a pixelated to a monolithic block concept

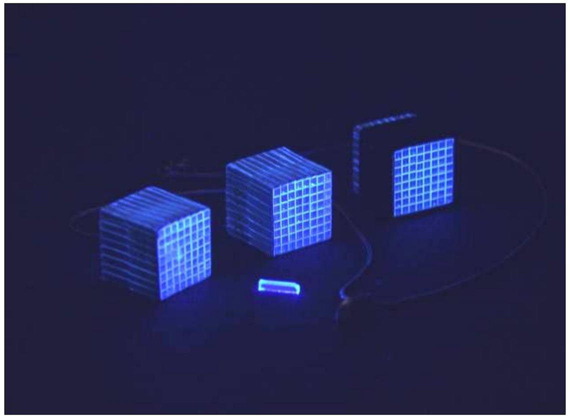

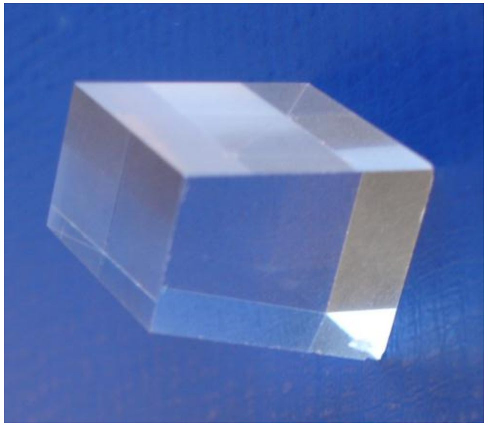

- Increase sensitivity (no inter-crystal separations, reduced dead space)
- 3D position information embedded in the light distribution
- extract parallax-corrected incidence coordinates with good accuracy
- continuous coordinates
- easy to manufacture and to assemble

Impact on the dynamic range of a photon detection system
(from a few photons up to 1000ph/event)

Timing parameters

- General assumption , based on Hyman theory

$$\Delta t \propto \frac{\sqrt{\tau}}{\sqrt{N_{phe}/ENF}}$$

decay time of
the fast component

Photodetector
excess noise factor

number of photoelectrons generated by the fast component

- For the scintillator the important parameters are
  – Time structure of the pulse
  – Light yield
  – Light transport
    - affecting pulse shape, photon statistics and LY

Statistical limit on timing resolution

W(Q,t) is the time interval distribution between photoelectrons

= the probability density that the interval between event Q-1 and event Q is t

= time resolution when the signal is triggered on the Q^{th} photoelectron

$$W_Q(t) = \frac{N_{phe}^{Q} \times \left(1 - e^{-\frac{t}{\tau_d}}\right)^{Q-1} \exp\left[-N_{phe}\left(1 - e^{-\frac{t}{\tau_d}}\right)\right] e^{-\frac{t}{\tau_d}}}{\tau_d (Q-1)!}$$

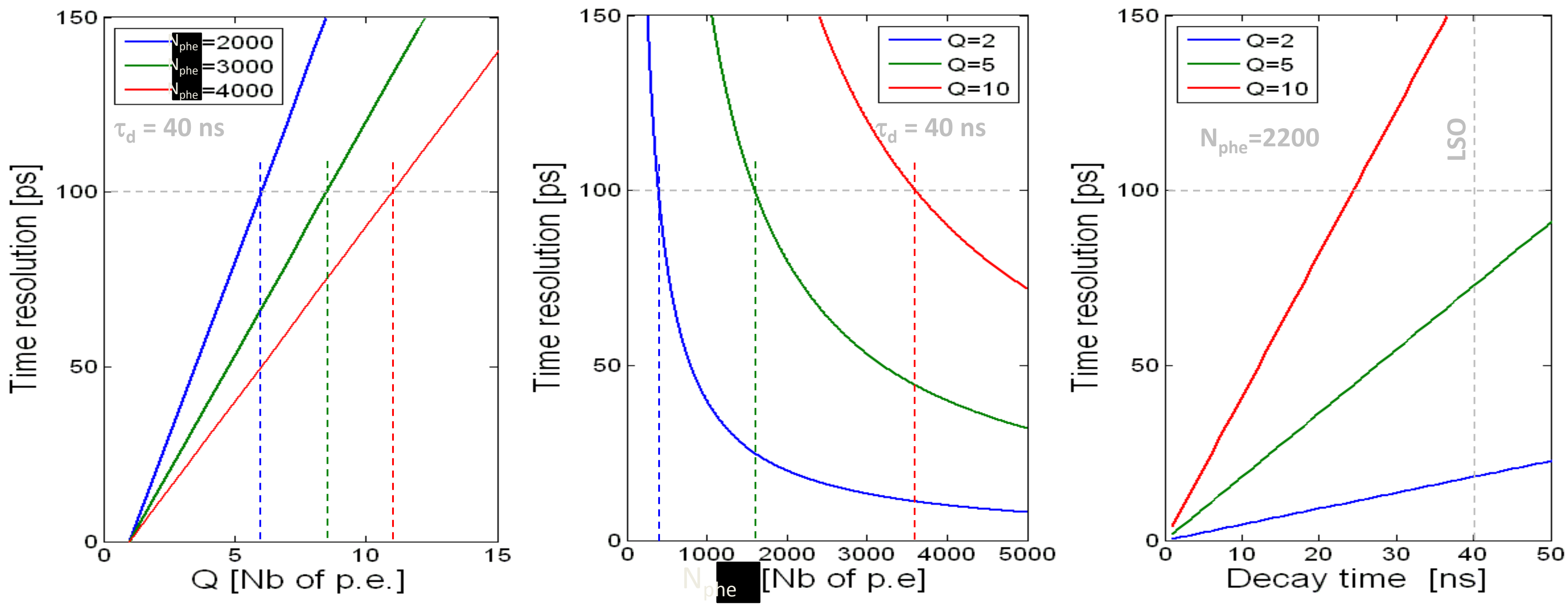

Crystal Geometry Affects Light Transport

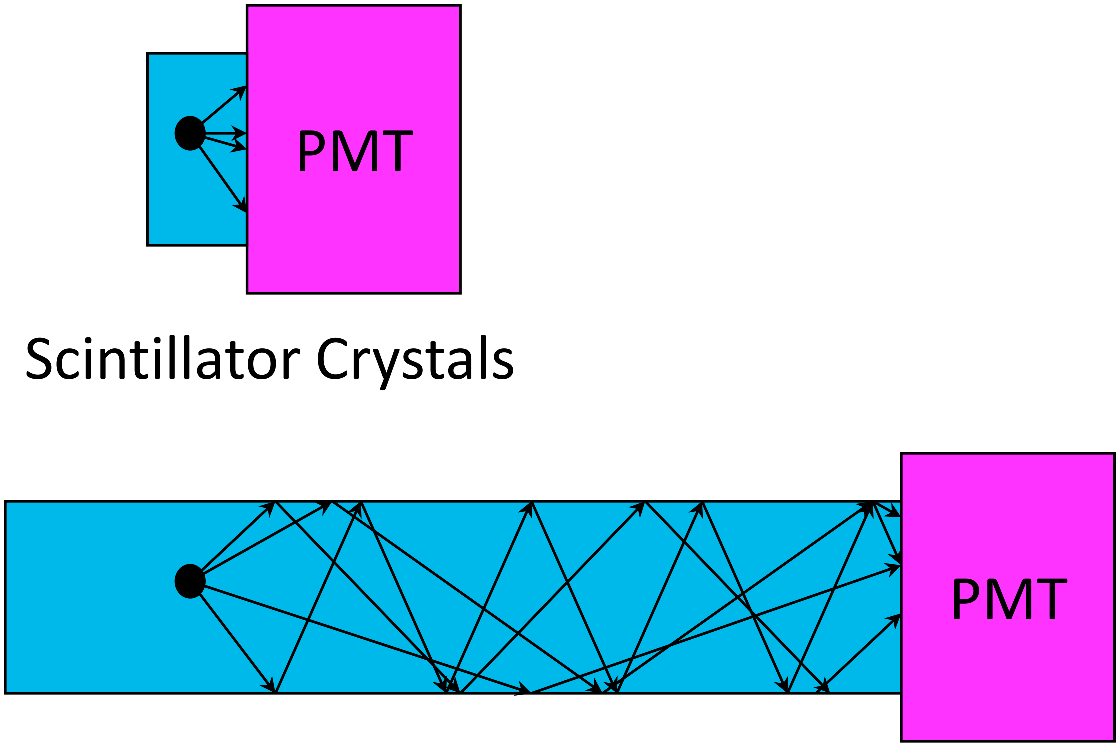

More Reflections in Long, Thin Crystals

Light Transport Affects Timing Resolution

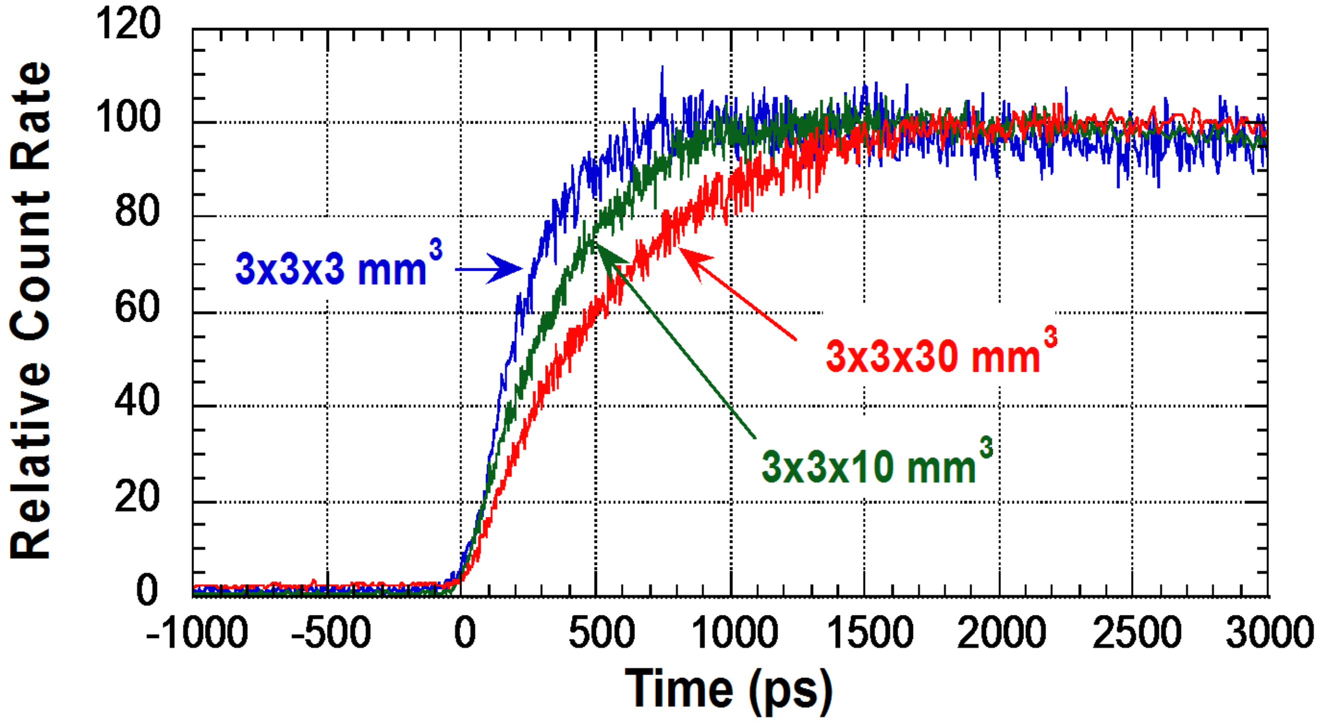

Long, Thin Crystals Have Slower Rise Time

Rise time

- Rise time is as important as decay time

$$I(t) = A\left(1 - e^{-t/t_r}\right)e^{-t/t_d}$$

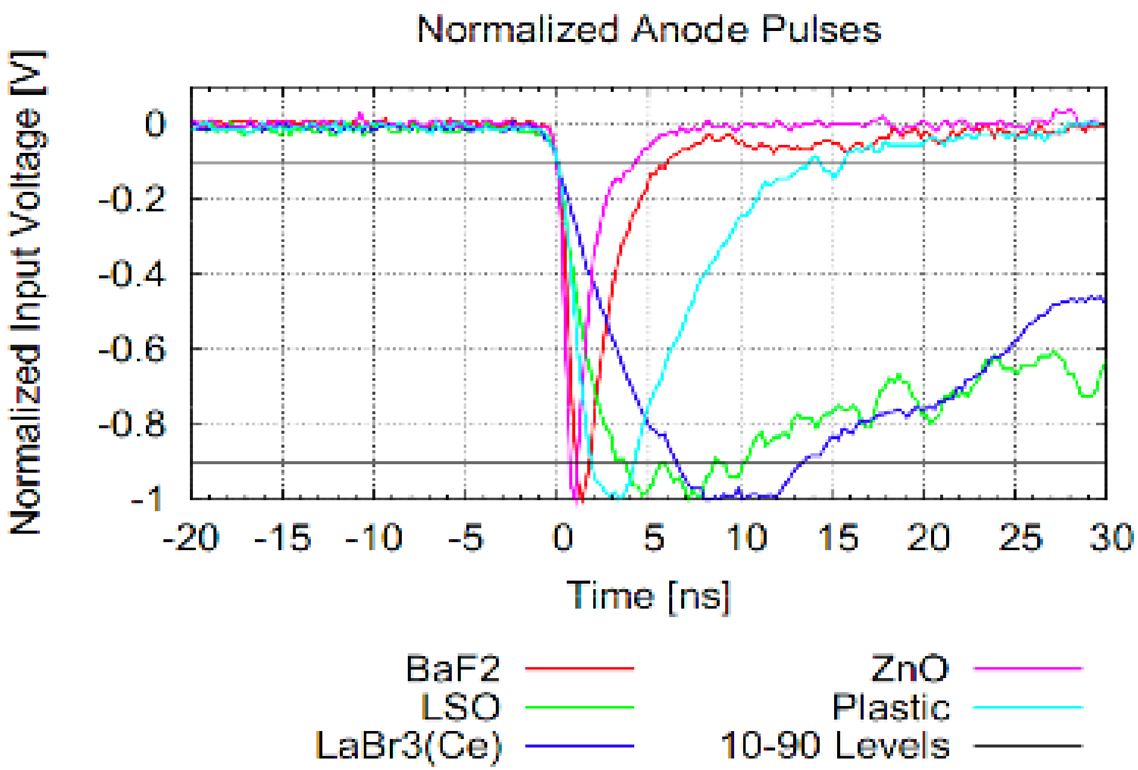

- Anode pulses are digitized by 8 GS/s and 3 GHz bandwidth
- measured with standard Hamamatsu H3378-50 PMT (rise time 0.7 ns)

Time resolution with rise time

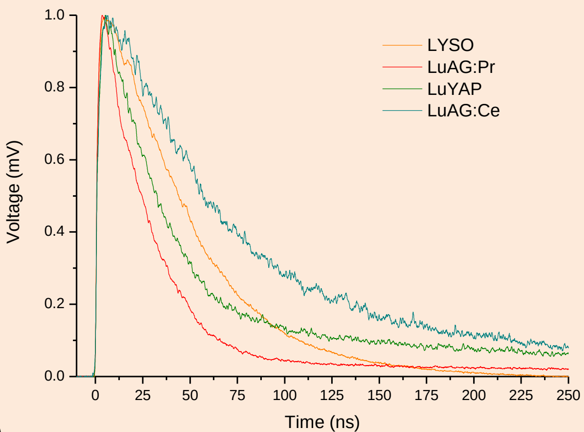

The intensity of light signal of a scintillating crystal can be described by the Shao Formula

$$I(t) = \frac{N_{phe}(t_r + t_d)}{t_d^2}(1 - e^{-t/t_r})e^{-t/t_d}$$

The number of photo-electrons firing the photo-detector N(t) between 0 and t after simplifications is given by :

$$N(t) = \int_0^t I(t) = \frac{N_{phe}}{t_d} * \frac{t^2}{2t_r}$$

Arrival time of first photon :

$$\mathbf{t_{1st}} = \sqrt{2 * t_d \frac{t_r}{\mathbf{Nphe}}}$$

Coincidence time resolution CTR :

$$CTR = 2.36 * \sqrt{2} * t_{1st} = 2.36 * \sqrt{2} * \sqrt{2 * t_d \frac{t_r}{N_{phe}}}$$

Leading Edge Discriminator

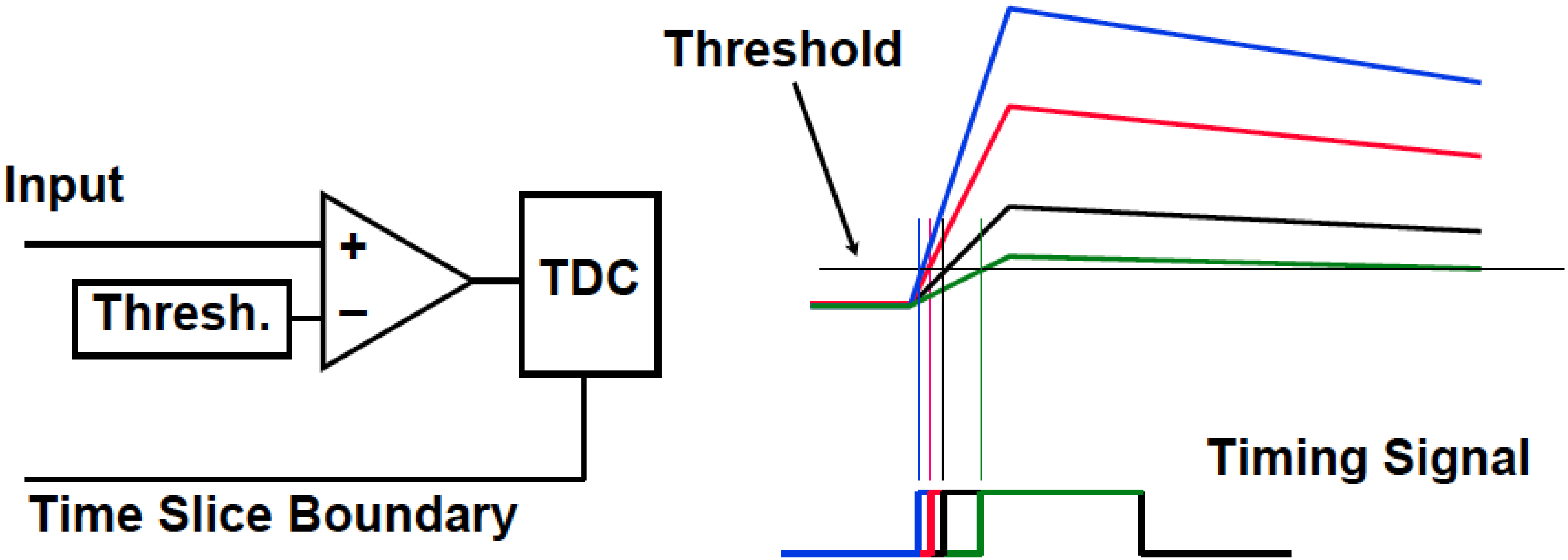

- Very Simple
- Sensitive to Amplitude Variations
- Minimized by Low Threshold & Small Dynamic Range
- Amplitude-Based Correction Possible

Constant Fraction Discriminator

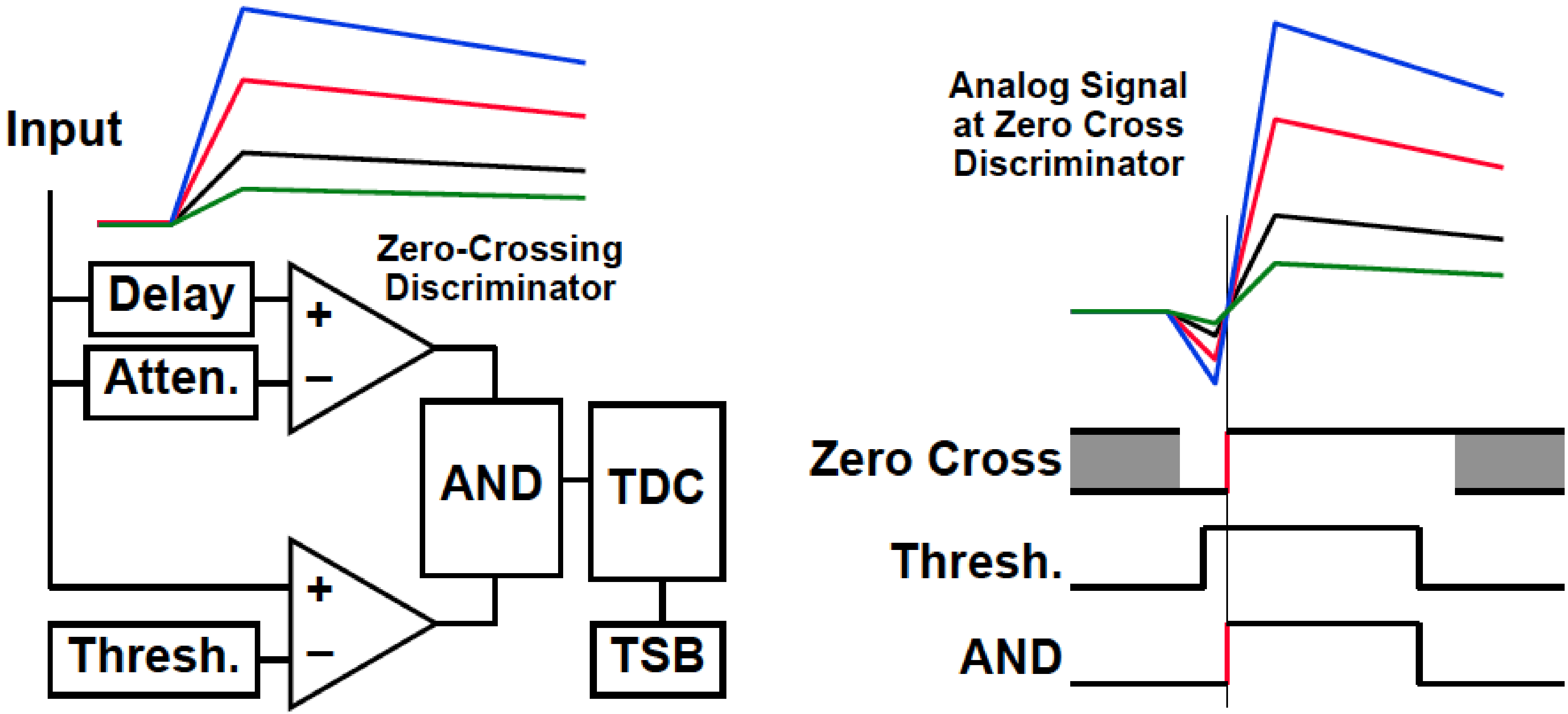

- Simple
- Insensitive to Amplitude Variations
- Present Standard for PET Systems

Comparison of CFD to Leading Edge

Simulation: CFD

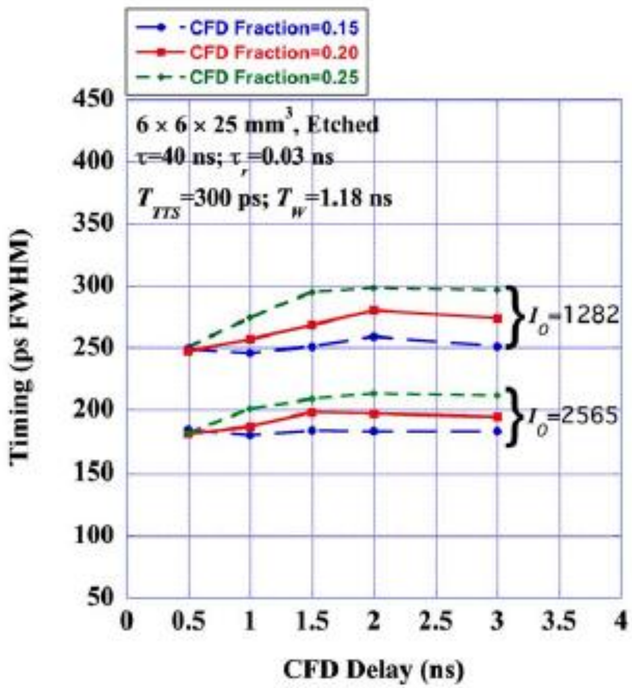

Simulation: Leading Edge

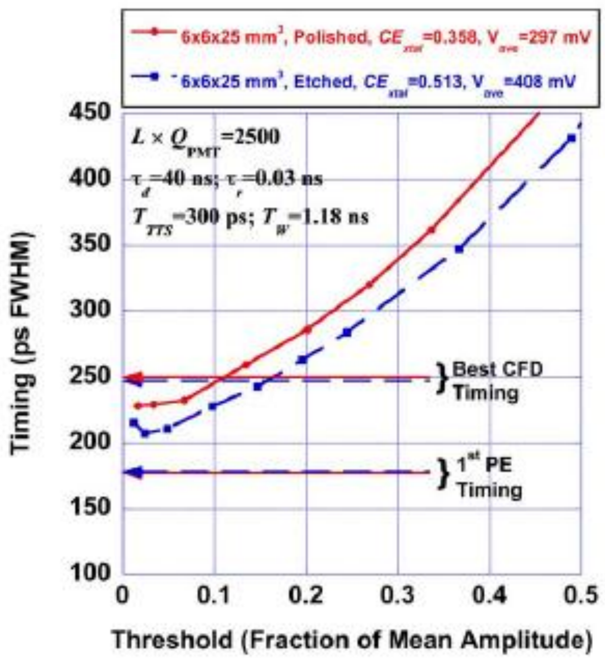

Experiment

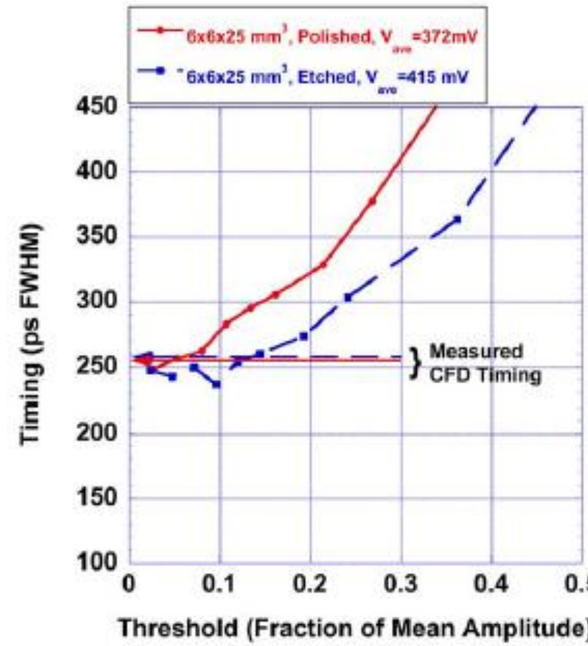

- Simulation: Leading Edge Slightly Superior to CFD
- Experiment: Minimal Difference

Courtesy of Woon-Seng Choong, LBNL

Multi-Threshold Discriminator

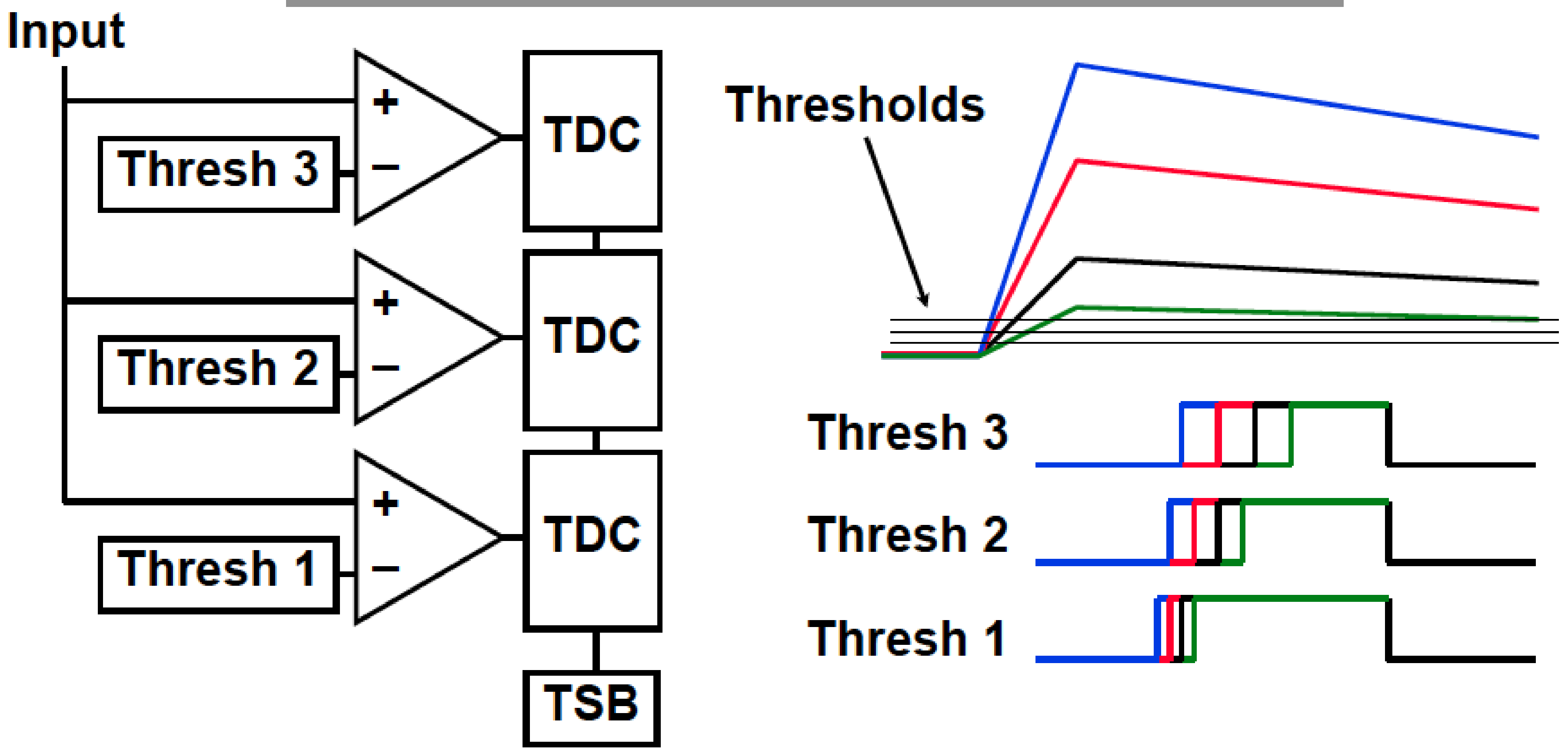

- Fit to Leading Edge, then Compute Intercept with Baseline
- Sensitivity to Amplitude Variations Reduced

Digitize Waveform

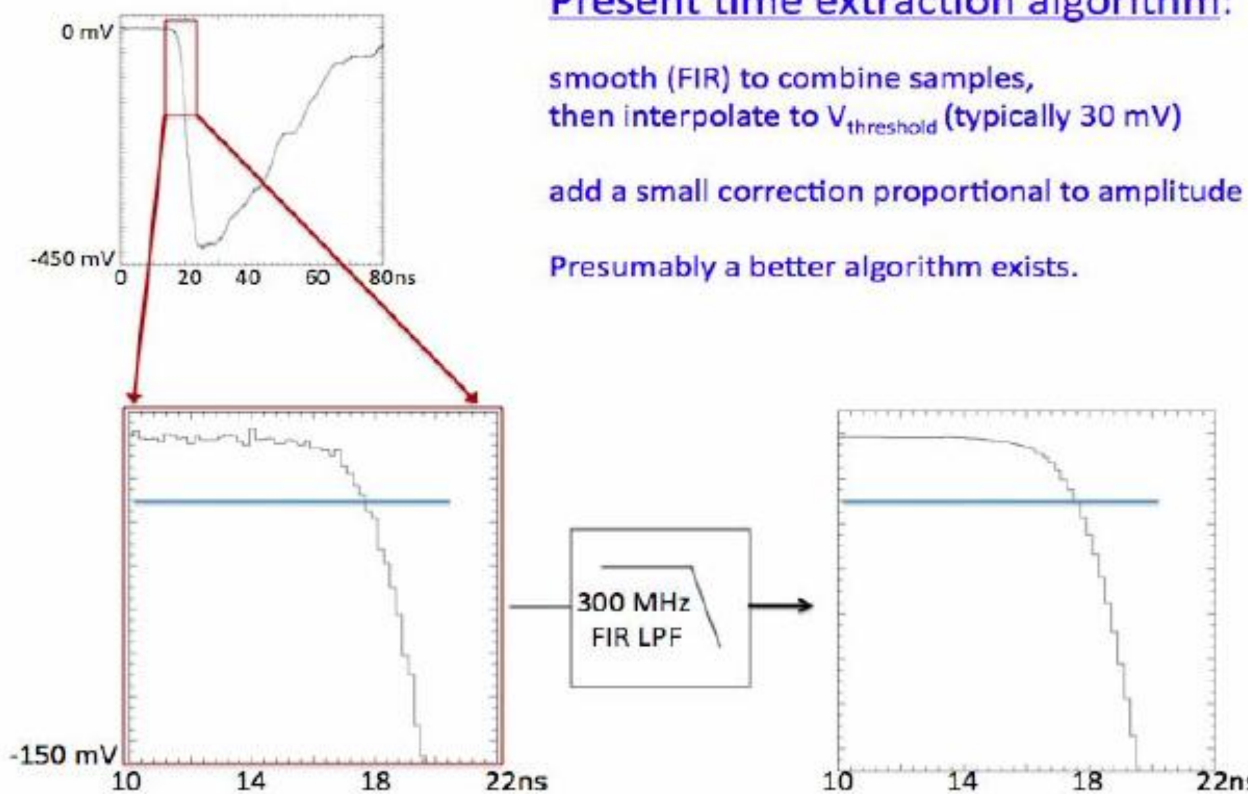

Present time extraction algorithm:

smooth (FIR) to combine samples,
then interpolate to $V_{threshold}$ (typically 30 mV)

add a small correction proportional to amplitude

Presumably a better algorithm exists.

- Fit Leading Edge, then Compute Intercept with Baseline
- Many Potential Fitting Algorithms Exist

Courtesy of Joel Karp & Bill Ashmanskas, U. Penn

Conclusions

- Timing resolution improves with lower threshold
- Ultimate resolution implies single photon counting
- High light yield is mandatory
  - 100’000ph/MeV achievable with scintillators
- Short decay time
  - 15-20ns is the limit for bright scintillators ($LaBr_3$)
  - 1ns achievable but with poor LY
    - Crossluminescent materials
    - Severely quenched self-activated scintillators
- SHORT RISE TIME
  - Difficult to break the barrier of 100ps

What Timing Can An LSO Module Achieve?

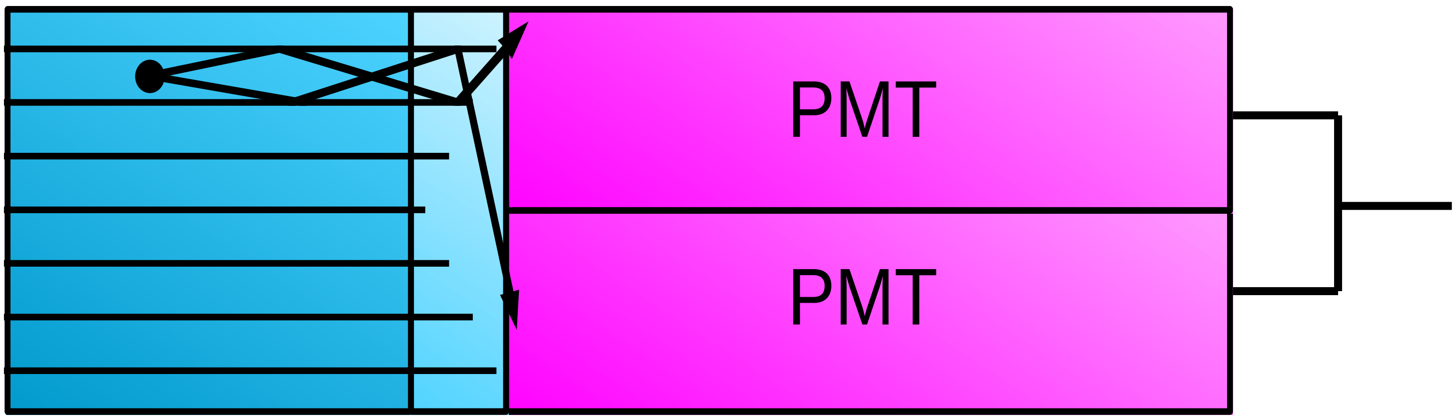

Crystal Geometry · **Light Sharing** · **PMT Quality** · **Multiple PMTs**

Predicted Limit	**550 ps**
Measured Value	**575 ps**

Already Near LSO Block Detector Theoretical Limit

Optimization: LSO Composition

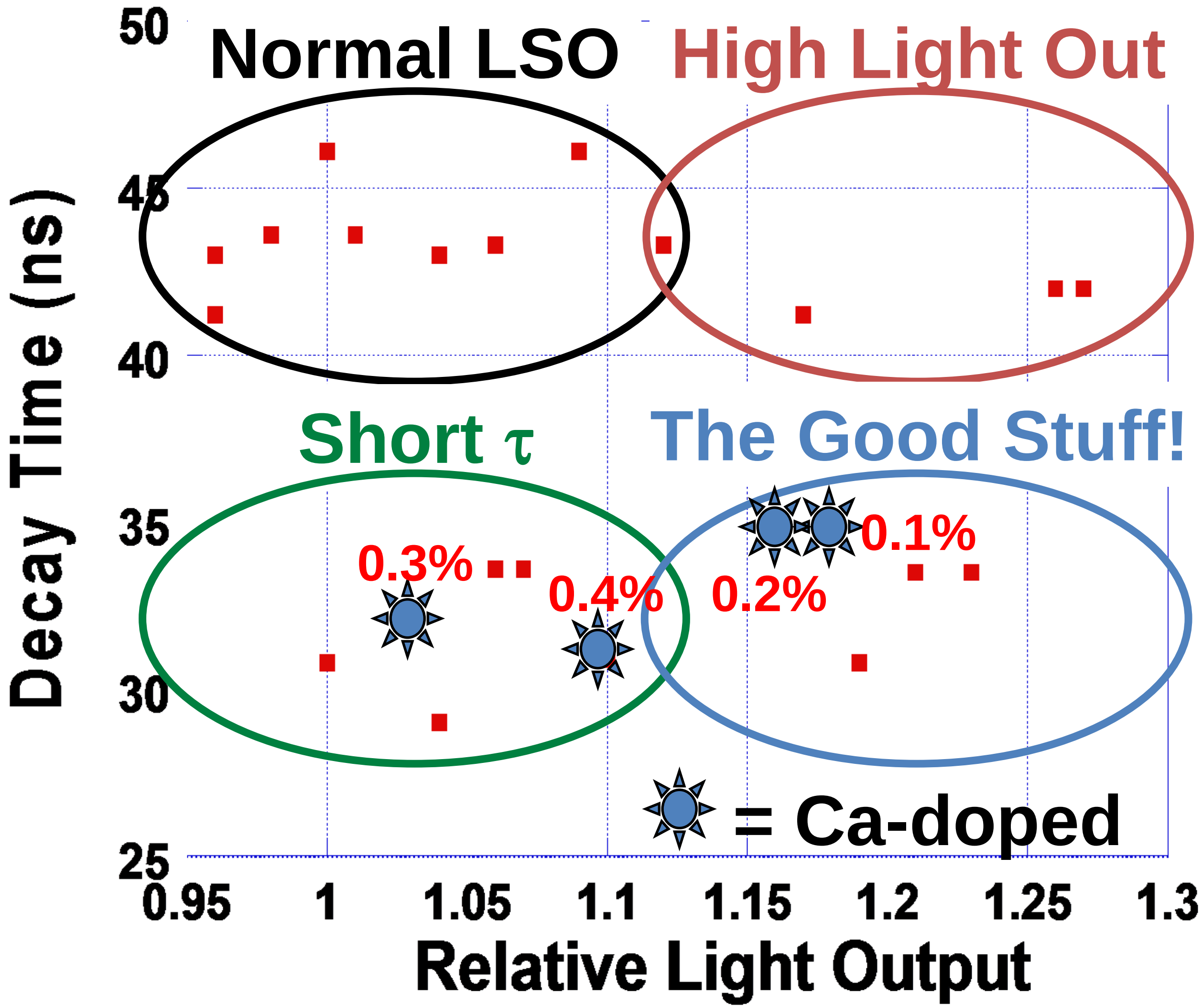

Ca-Doping Gives High Light Output & Short τ

Measured Results: LSO Composition

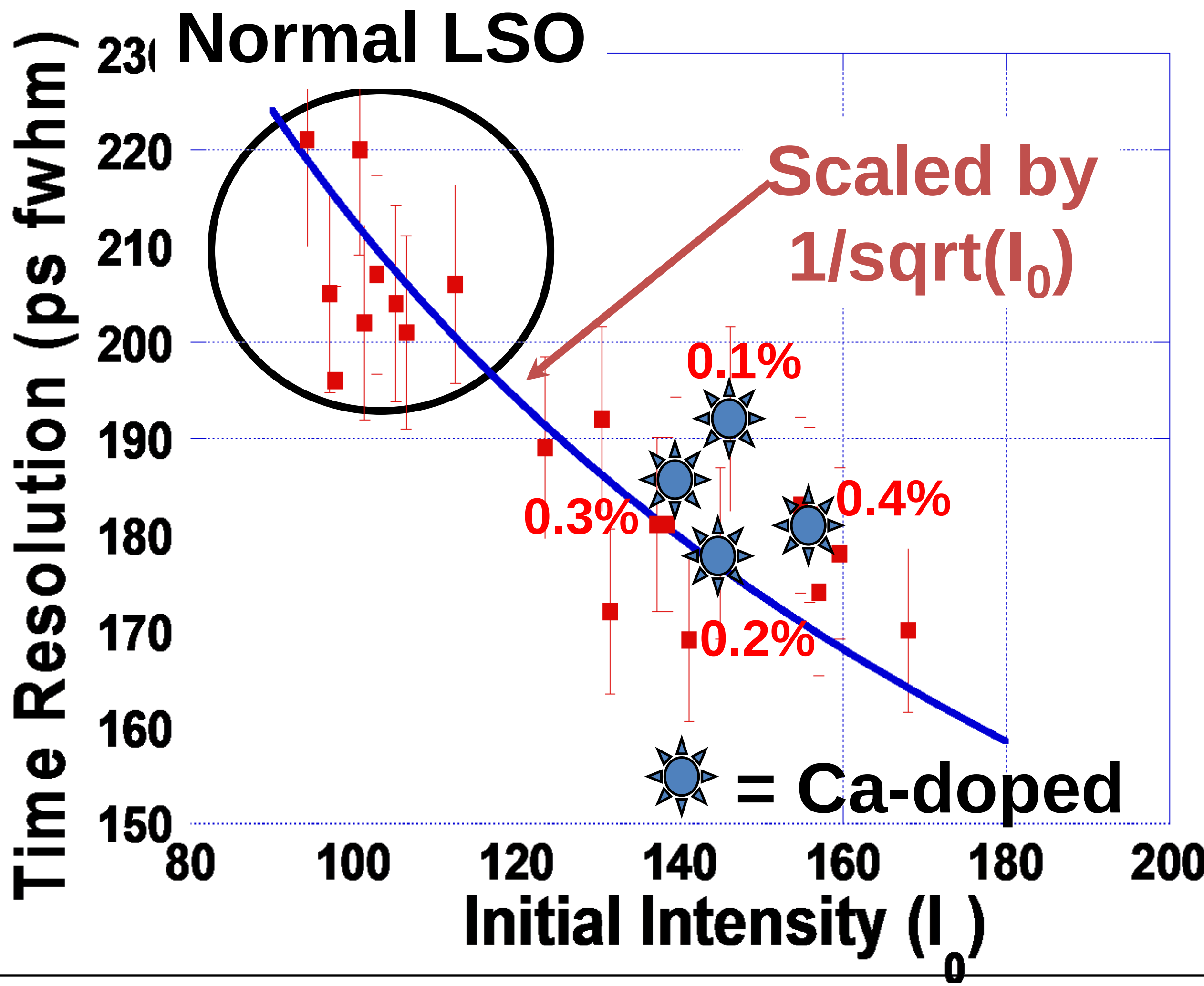

- Ca-Doping Gives Good Timing Resolution
  - ~15% Improvement Over Normal LSO

Measured Results: High QE PMTs

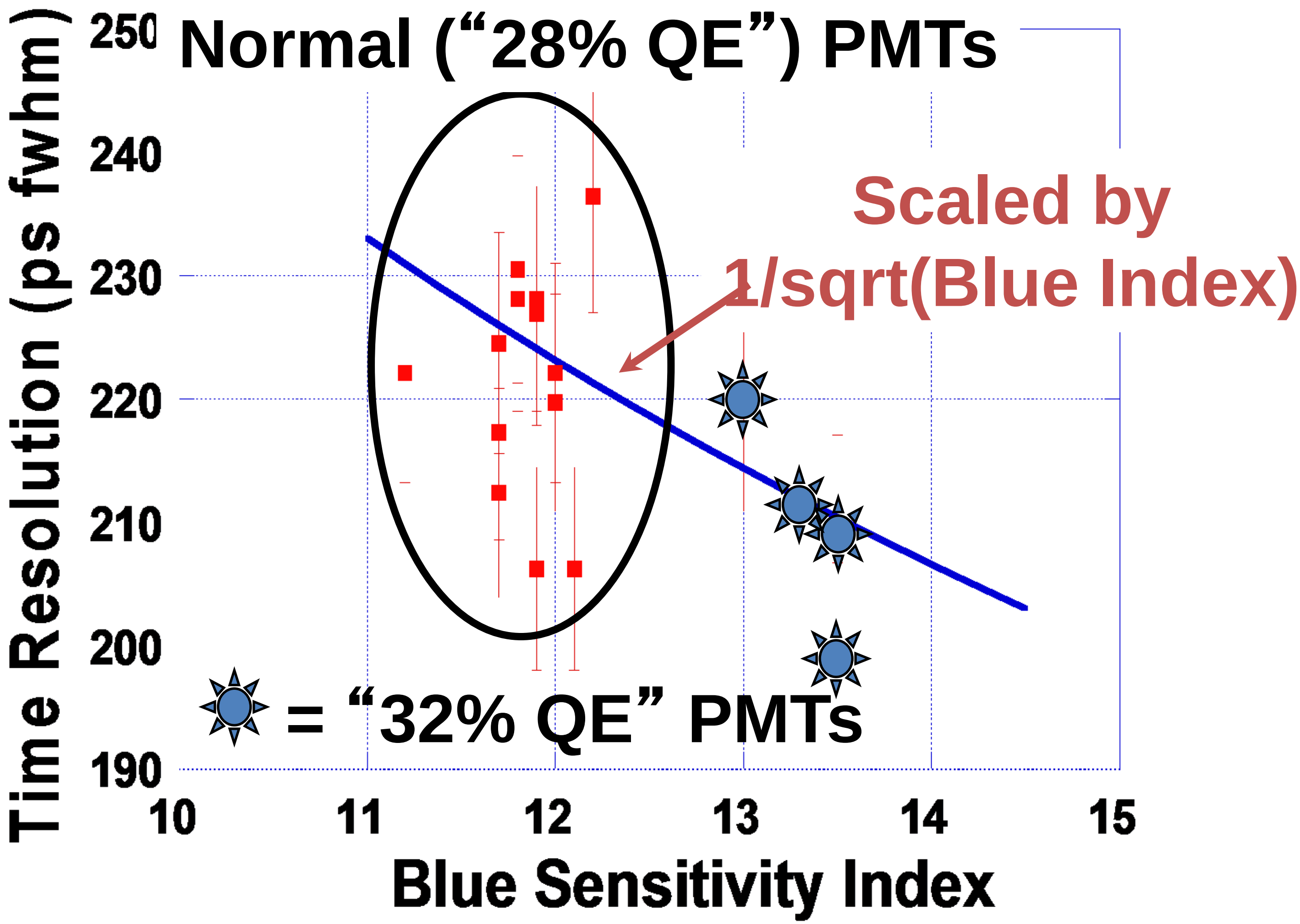

- Increased QE Improves Timing Resolution by 7%
  - Expect 10% Improvement with 35% SBA PMT

Additional Improvements

Hardware	Coinc. (ps fwhm)	TOF Gain
End-Coupled Crystal	543	4.3
Side-Coupled Crystal	309	7.6
Co-Doped LSO	258	9.1
32% QE PMT	219	10.6

- TOF PET with *Significantly* Better Timing is Possible
- To Achieve, We Must "Think Outside the Block Detector"

Side-Coupled Design

543 ps (coincidence)

309 ps (coincidence)

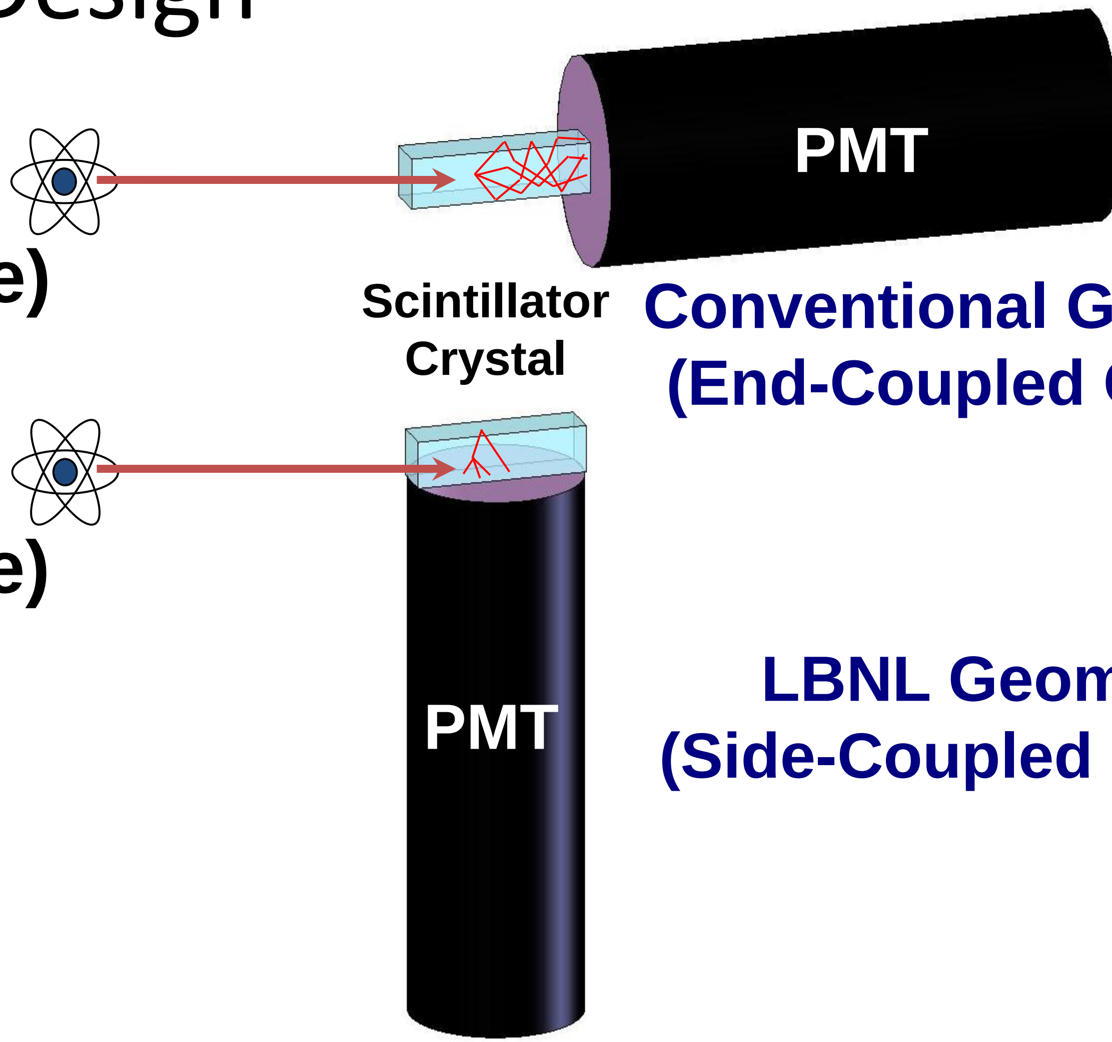

Conventional Geometry (End-Coupled Crystal)

LBNL Geometry (Side-Coupled Crystal)

Shorter Optical Path Length & Fewer Reflections

Detector Module Design

Two LSO Crystals

(each 6.15 x 6.15 x 25 mm^3)

Reflector

(on all five faces of each crystal, including the face between the two crystals)

Optical Glue

(between lower crystal faces and PMT)

Hole in Reflector On Top Face of Crystals

PMT

(Hamamatsu R-9800)

Two Side-Coupled Scintillator Crystals per PMT

Detector Ring Geometry

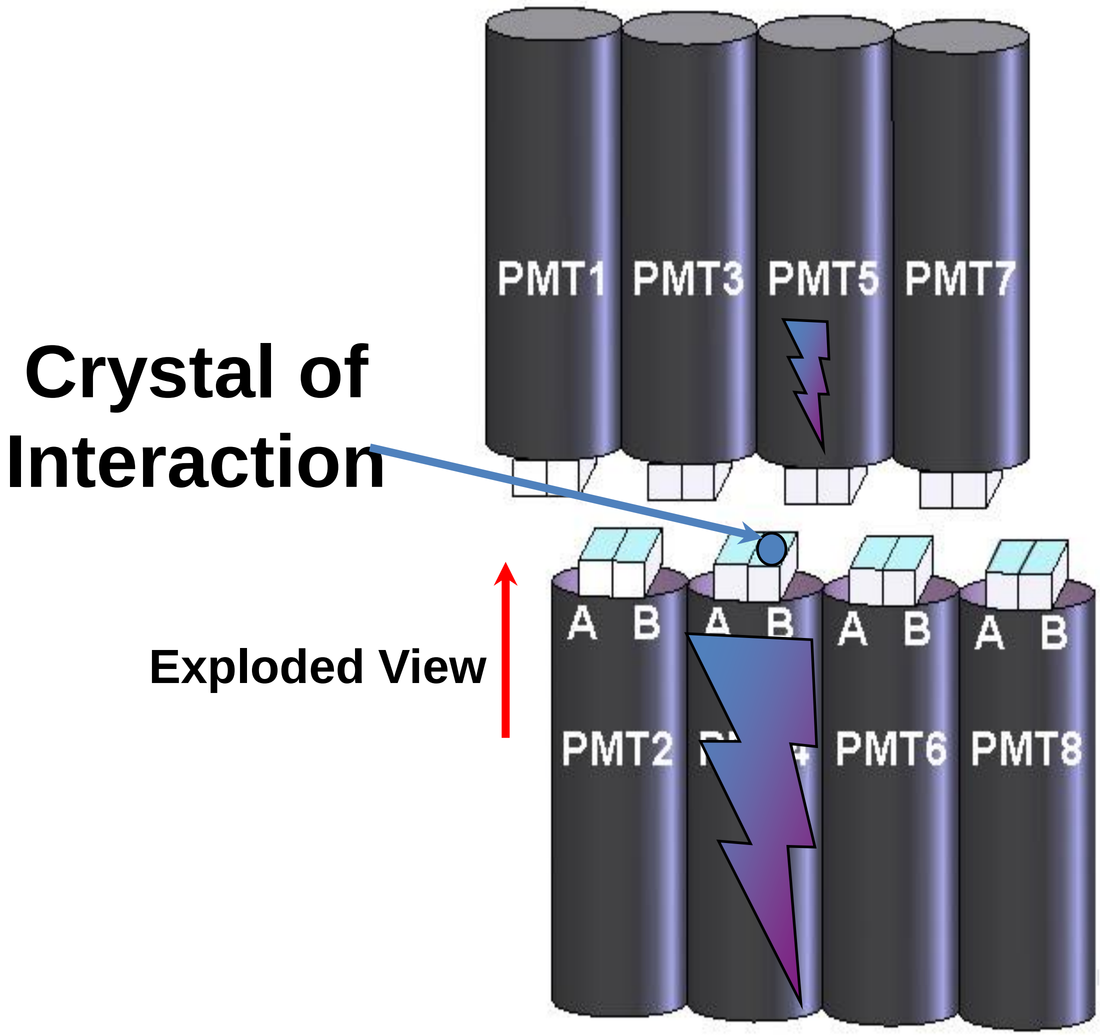

Crystals Decoded by Opposing PMT

- Top face of each crystal (with hole in reflector) is coupled via a small (<1 mm) air gap to the edge of one opposing PMT.
- Light seen by the opposing PMT is used to decode the crystal of interaction.

Camera Construction Status

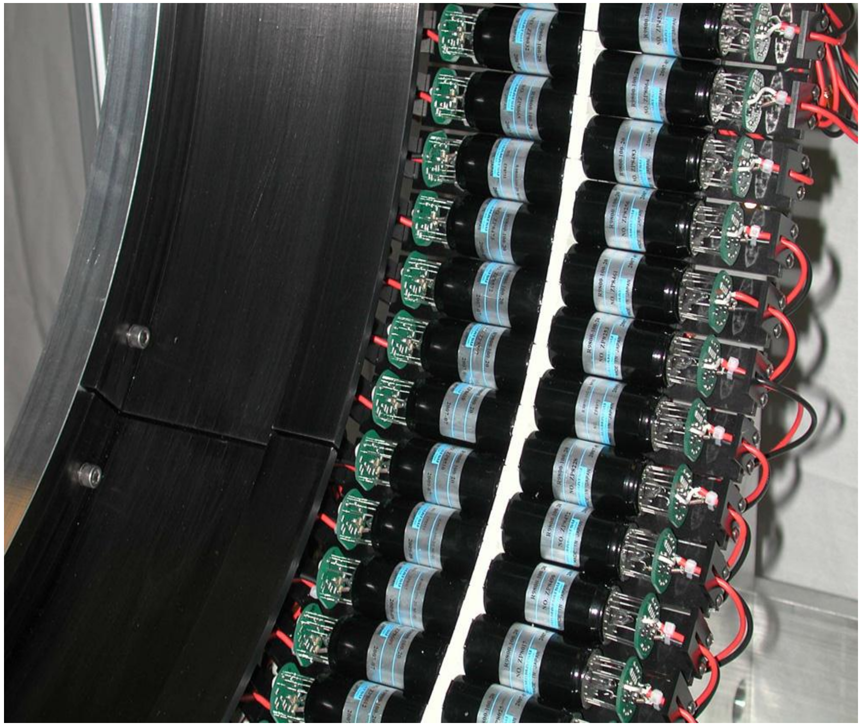

- Module Construction Complete
- Camera Assembly Complete

MCP-PMT

K. Inami (Nagoya univ.)
on behalf of Belle-II PID group

- Micro-Channel-Plate
  - Tiny electron multipliers
    - Diameter ~10μm, length ~400μm
  - High gain
    - ~10^6 for two-stage type

  → Fast time response

    Pulse raise time <400ps, TTS < 50ps
  - can operate under high magnetic field (~1T)

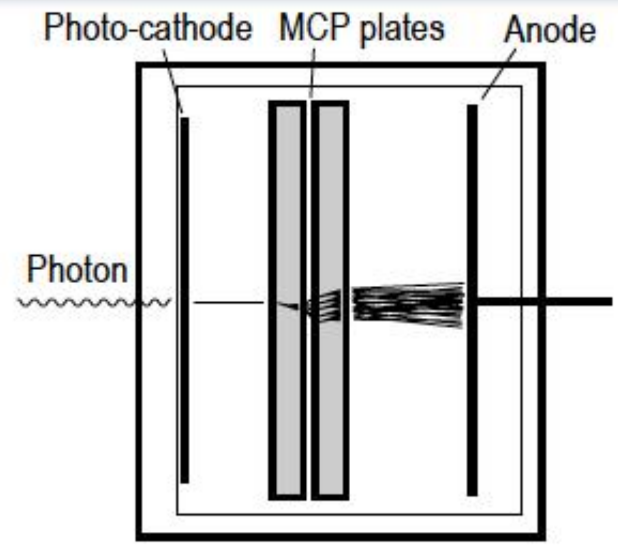

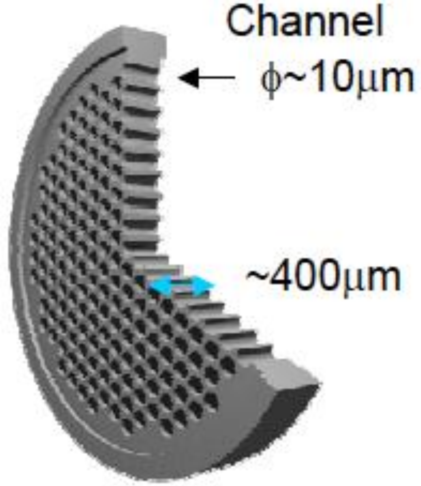

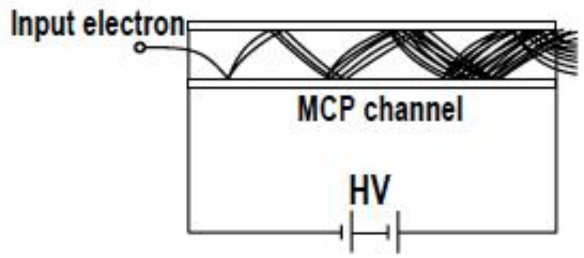

Single photon

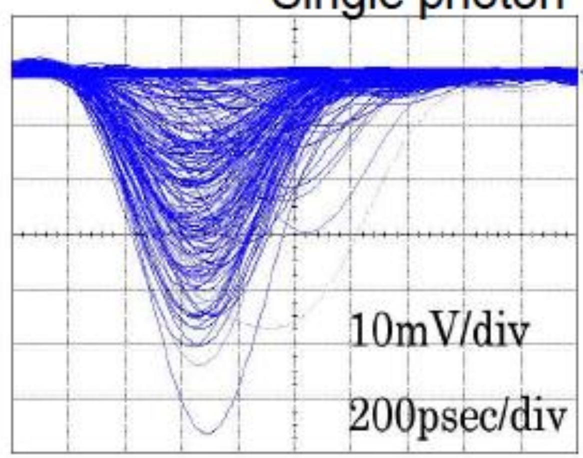

Square-shape MCP-PMT

K. Inami (Nagoya univ.)
on behalf of Belle-II PID group

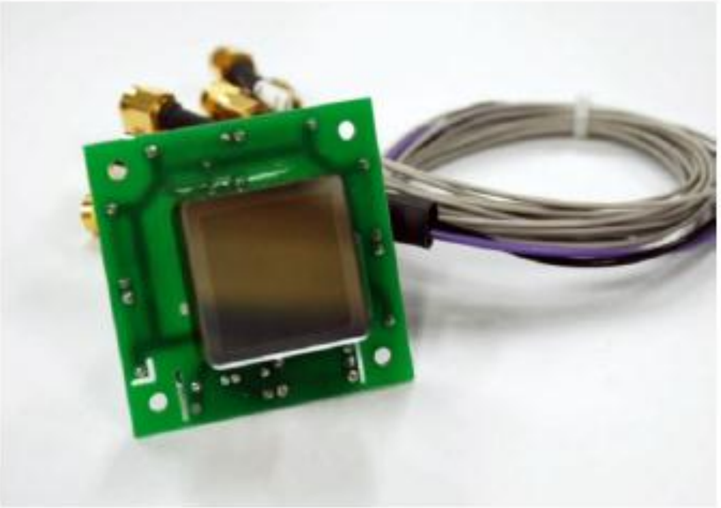

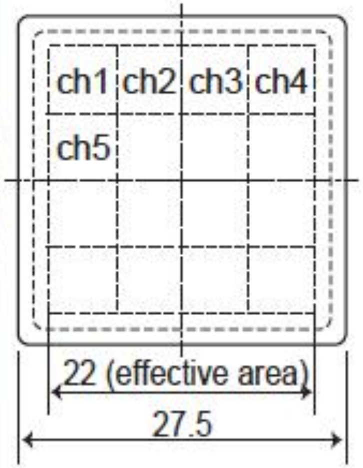

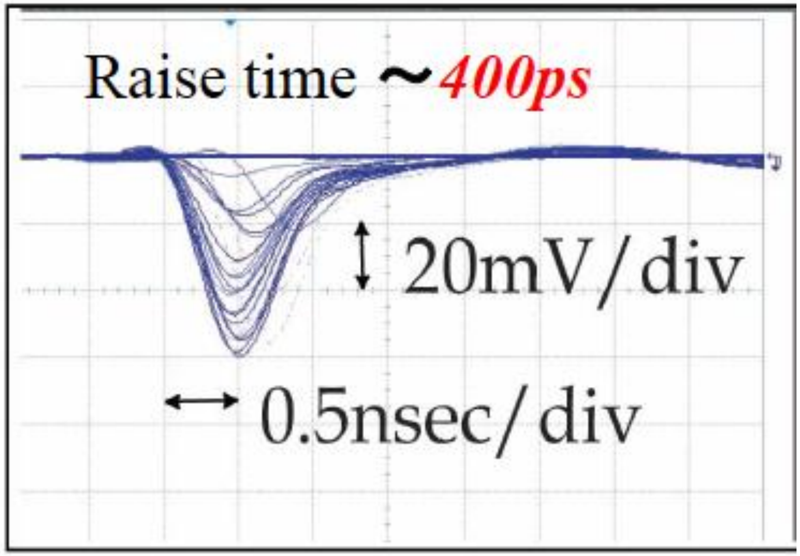

R&D with Hamamatsu photonics

- Large effective area 64%
- Position information 16ch
- Single photon detection
- Fast raise time: ~400ps
- Gain: >1x10^6 at B=1.5T
- T.T.S.(single photon): ~35ps at B=1.5T
- Position resolution: <5mm

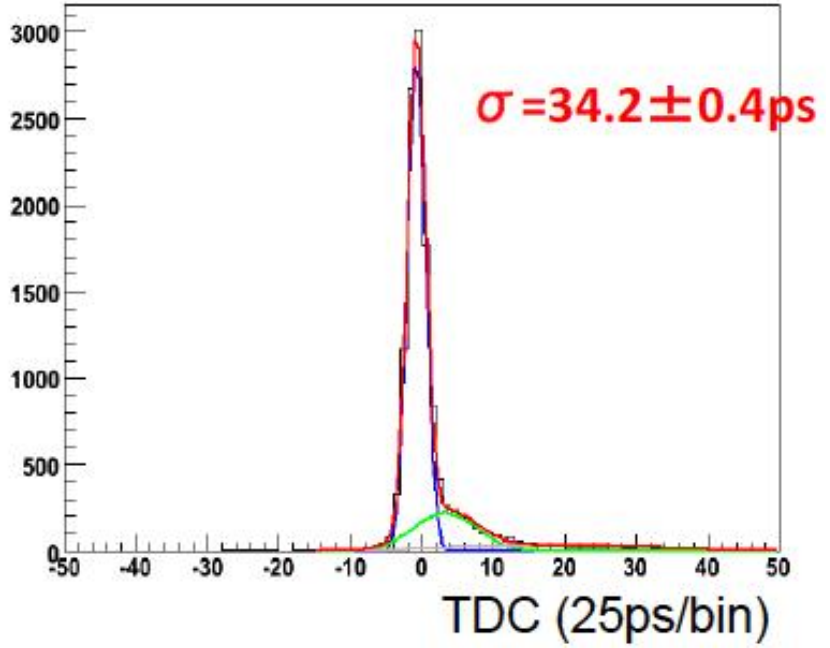

Lifetime test for square-shape MCP-PMT

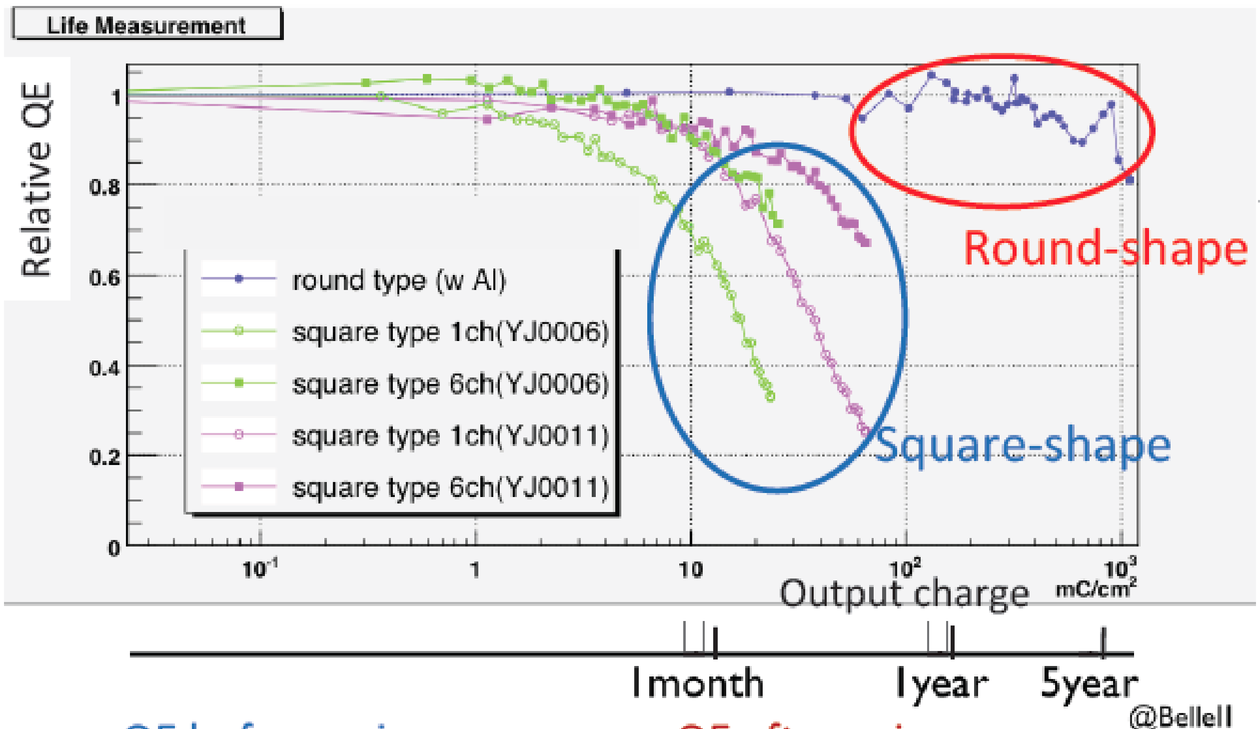

The aluminum layer is not enough!

– Ch.1 drops more rapidly than ch.6?

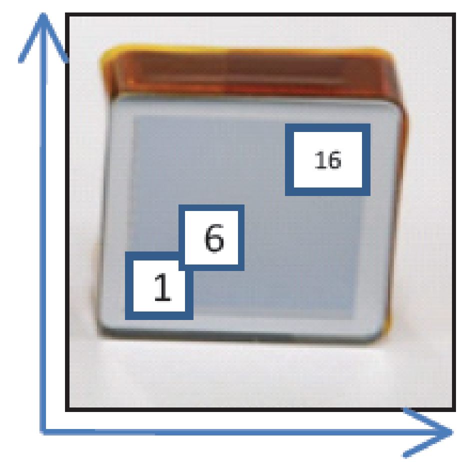

QE before aging

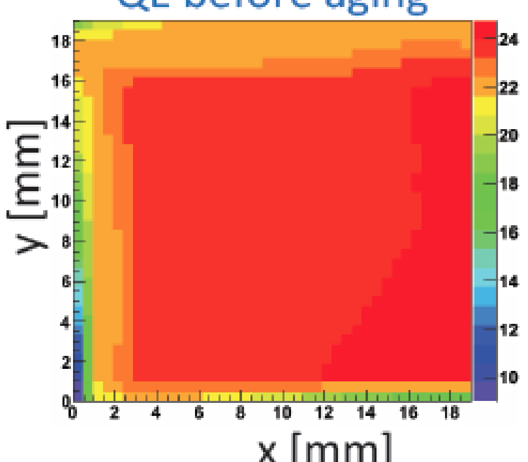

QE after aging

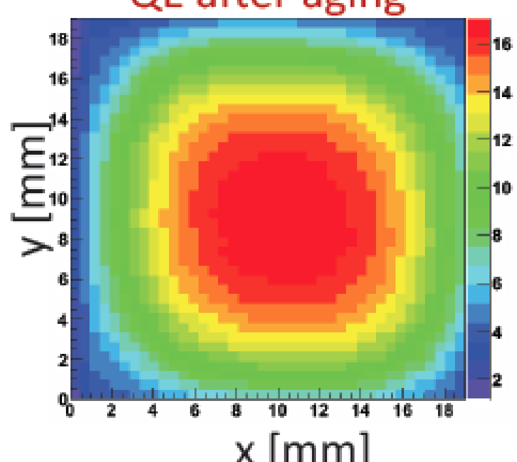

The QE drop becomes more significant toward the edges.

– Related to the structure?

K. Inami (Nagoya univ.)
on behalf of Belle-II PID group

Lifetime study

K. Inami (Nagoya univ.)
on behalf of Belle-II PID group

- Inner structure of round-shape and square-shape MCP-PMTs

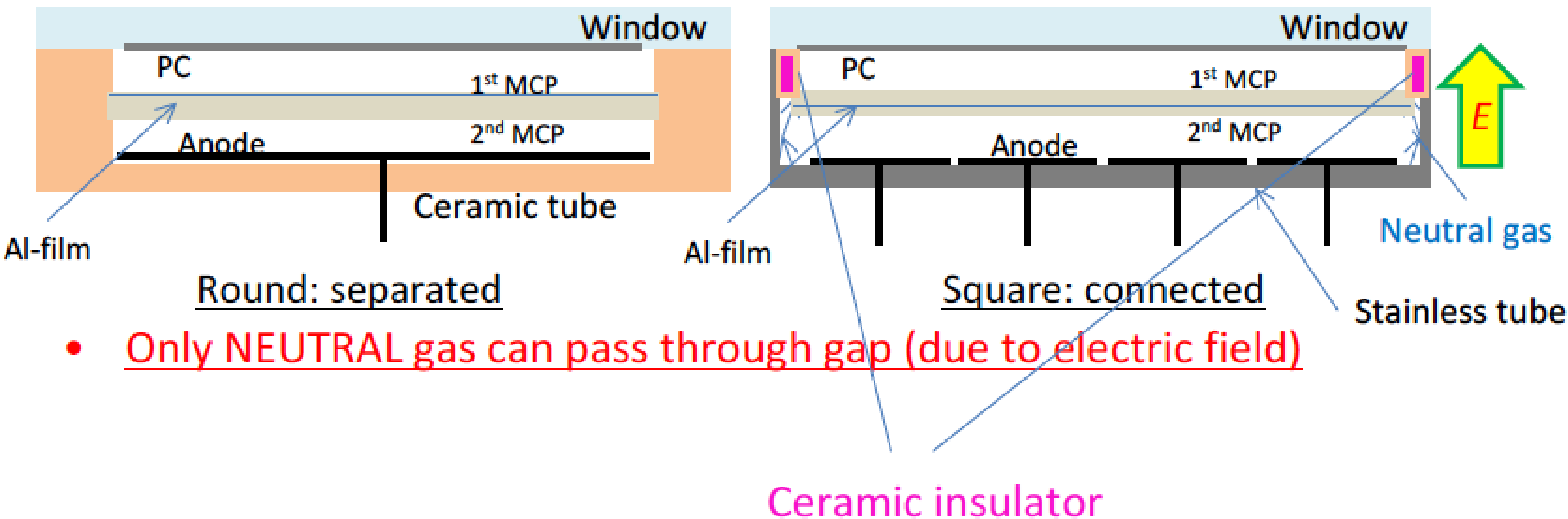

- Only NEUTRAL gas can pass through gap (due to electric field)

- Following modifications are made.
  - Blocking the path that connects the p.c. and the anode sides,
  - Adopting a low out-gassing type of MCPs.

Lifetime result

K. Inami (Nagoya univ.)
on behalf of Belle-II PID group

- Achieve >1 C/cm² even for bi-alkali p.c.

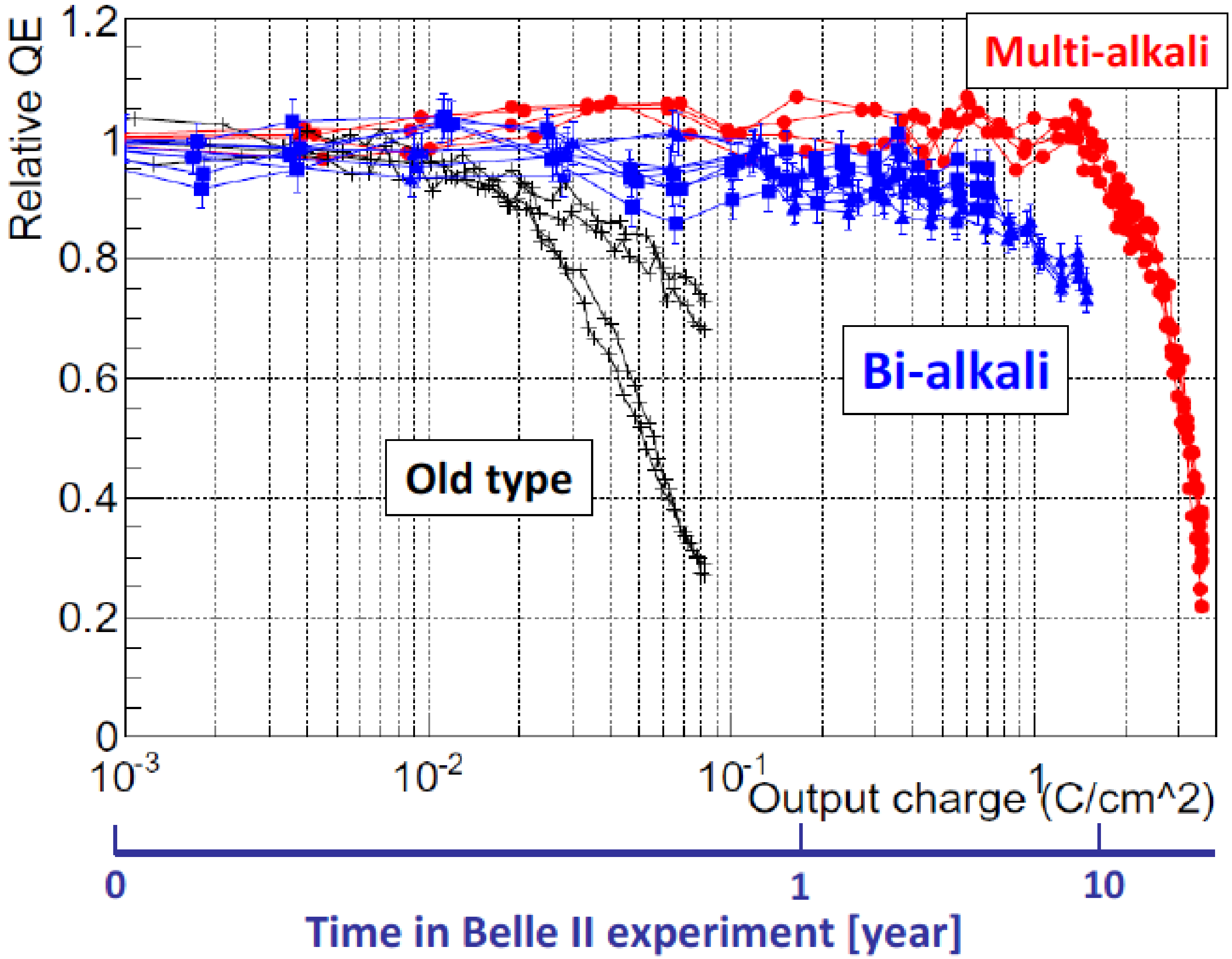

UChicago, Argonne, Fermi, +……

Large-Area Picosecond Photo-Detector (LAPPD) Project

Next-Generation MCP-PMT

Project with 4 primary goals:

1. Low-Cost LAPPD with good timing and spatial resolution (~$10/sq-in area cost)
2. Large-Area TOF particle/photon detectors with picosecond time resolution
3. Understanding photo-cathodes so that high QE cathodes can be reliably made with tailored spectral response, and new materials & geometries can be developed
4. Produce commercializable modules within 3 years & transfer technology to industry

(Chin-Tu Chen, University of Chicago)

Panel-Based DOI-Coded TOF PET

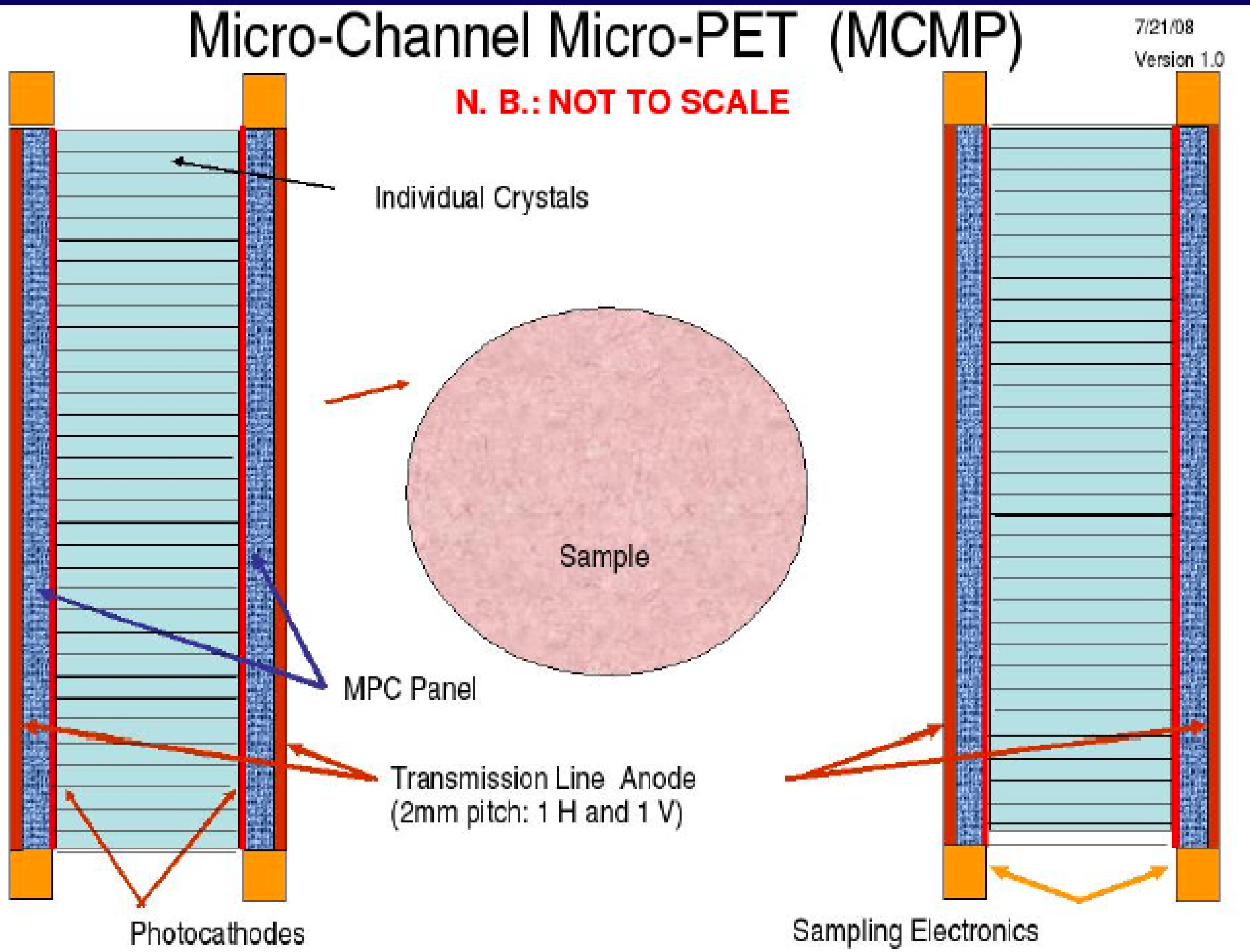

__*Potential Applications:*__

(DOI+TOF)-PET/CT

Reconfigurable, Integrative, Modular "Super-Modules"

[a] High-Resolution "Cube"

[b] High-Sensitivity "Multi-Layer"

[c] High-Throughput "Multi-Object"

[d] Whole-Body

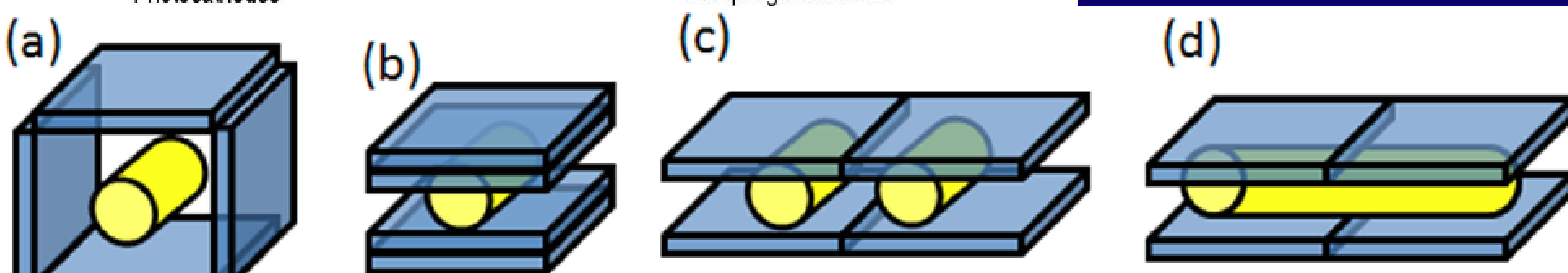

(Chin-Tu Chen, University of Chicago) **UC, ANL, FNAL, etc.**

Conclusions

Benefits of TOF are *HUGE*:

- **5x effective efficiency gain w/ 500 ps timing**
- **Greatest improvement in large patients**
- **Faster reconstruction algorithm convergence**

Rebirth of TOF PET Due To New Scintillators:

- **575 ps for LSO, 350 ps for $LaBr_3$**

Still *LOTS* To Do:

- **Electronics**
- **Module Design**
- **Reconstruction**
- **Photodetectors**
- **Scintillators**
- **Evaluation**

How Far Can TOF PET Go?

- 100 ps Timing Resolution
- 23x Effective Efficiency Increase
- *Very* Fast Reconstruction

Acquire & Reconstruct Image in <1 Minute

Avalanche Photodiode Arrays

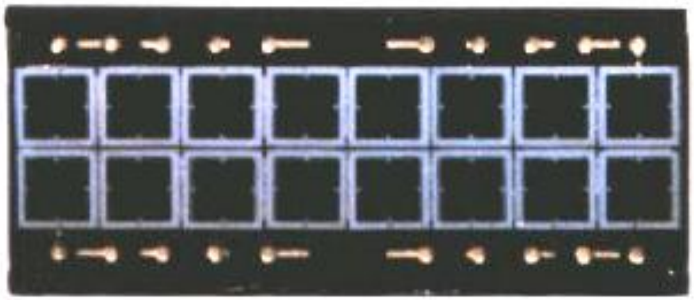

Hamamatsu Photonics

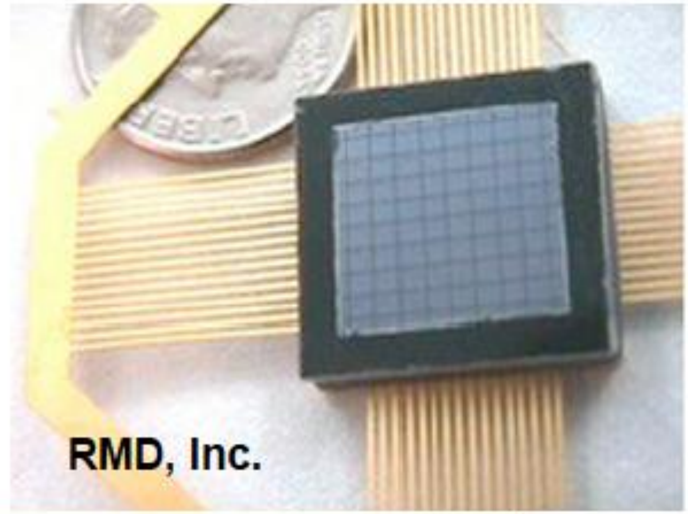

RMD, Inc.

Advantages:

- High Quantum Efficiency ⇒ Energy Resolution
- Smaller Pixels ⇒ Spatial Resolution
- Individual Coupling ⇒ Spatial Resolution

Challenges:

- Dead Area Around Perimeter
- Signal to Noise Ratio
- Reliability and Cost
- # of Electronics Channels

Steady Progress Being Made

Position-Sensitive APD (PSAPD)

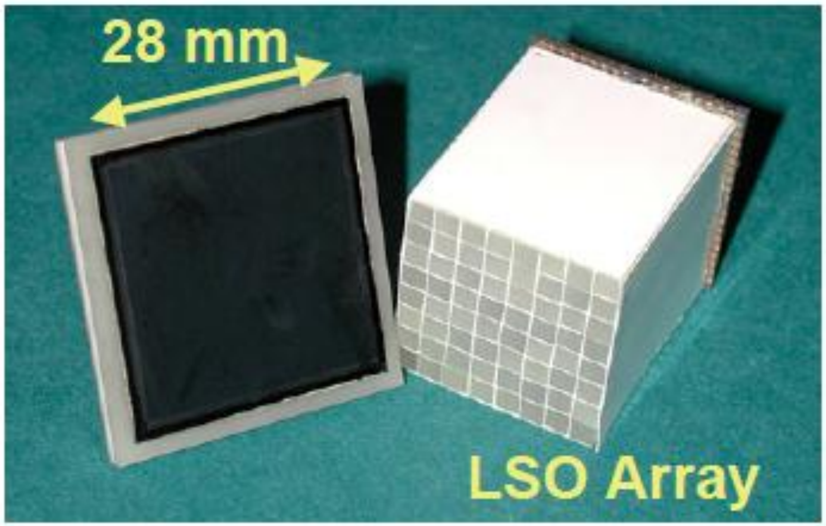

Flood Map,
–20° C

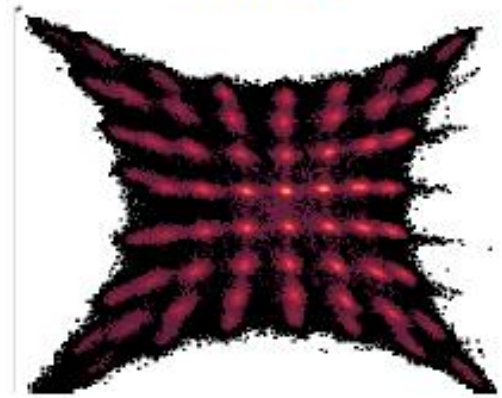

- 15% fwhm Energy Resolution
- 3 ns fwhm Timing Resolution

APD Analog of a Position-Sensitive PMT

*Data and image courtesy of K. Shah, RMD, Inc.

SiPM – Silicon Photomultiplier

Features

> High gain
> **Fast response time**
> Low bias voltage (tens of volts)
> **Insensitive** to magnetic field
> **Compact** and rugged
> Small nuclear counter effect

> Non-linearity at higher light levels
> Dark noise a problem at very low light levels
> Less mature technology

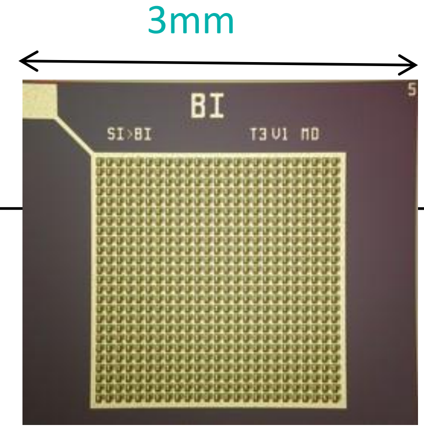

***Avalanche Photodiode** working in limited Geiger mode, courtesy by FK-irst, Italy*

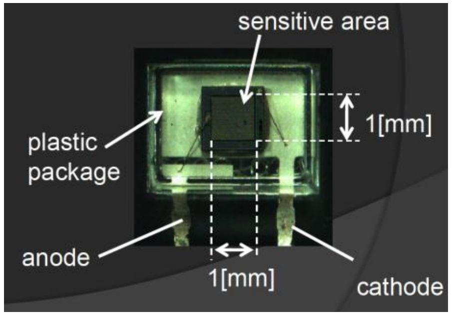

Philips Digital SiPM Module

SiPM – Development Platform in Medical Imaging

Current developments

1. Small Animal PET Scanner
2. Hybrid PET/MR preclinical/clinical scanner
3. PEM (PET for Mammography)
4. Prostate scanner

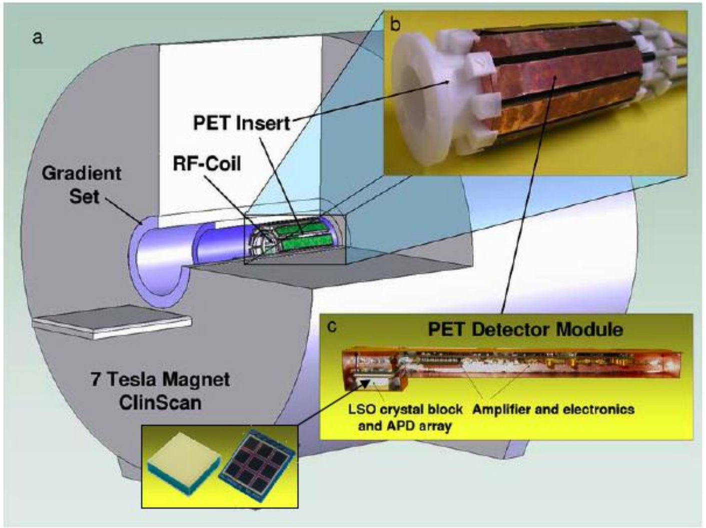

Slide Courtesy: Judenhofer

Naviscan PEM Imager

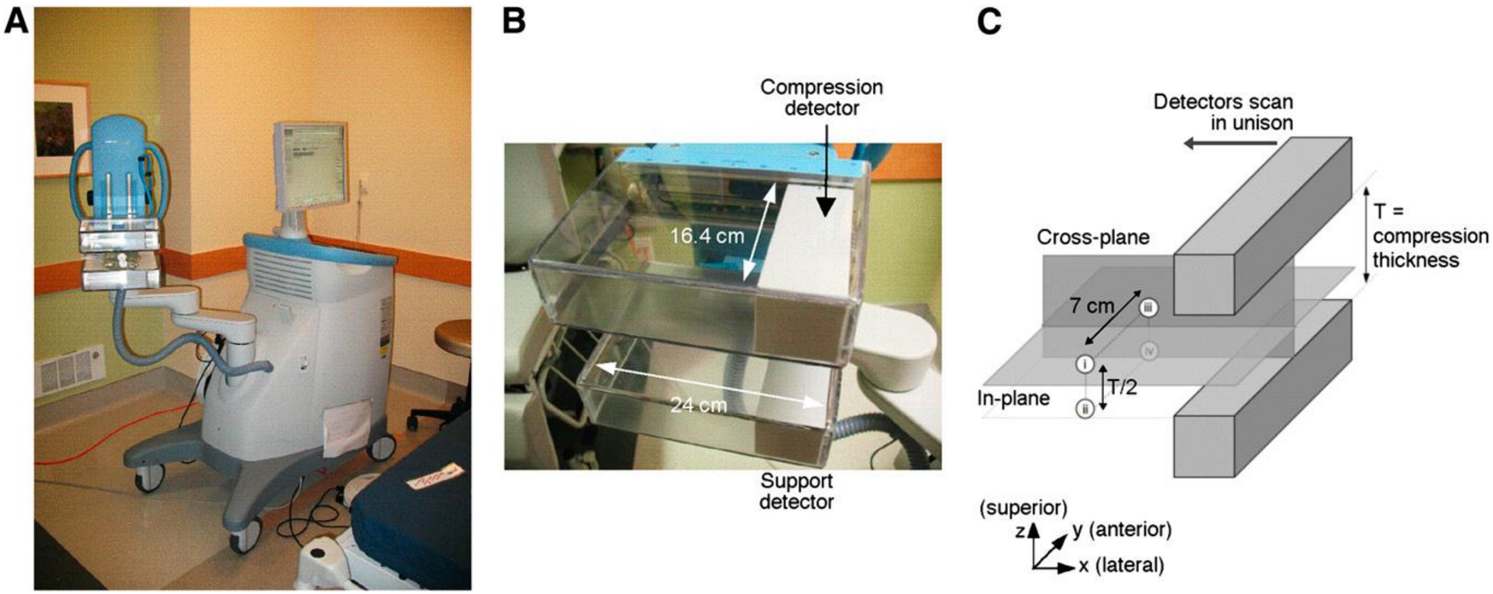

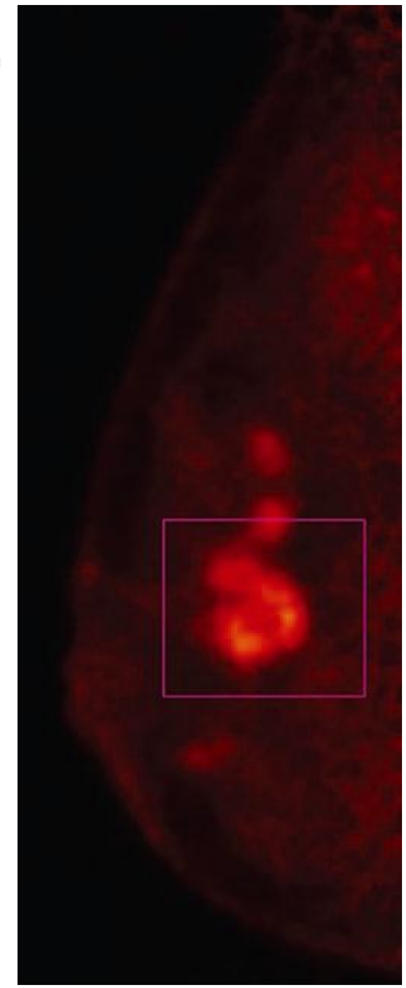

ClearPEM Concept

❑ ClearPEM design parameters:

- High detection sensitivity (5% at 10 cm plate separation)
- DoI resolution 2mm
- Spatial resolution (1.4 mm FWHM)
- Time resolution 1.3 ns r.m.s.

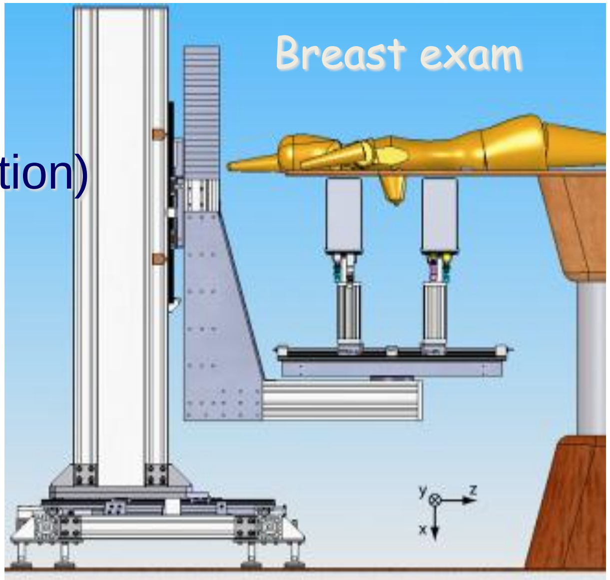

❑ Scanner concept:

- Two planar heads
- Mammary gland and axilla region exams
- Exam with the patient in prone position
- Adjustable distance between heads and rotation angle

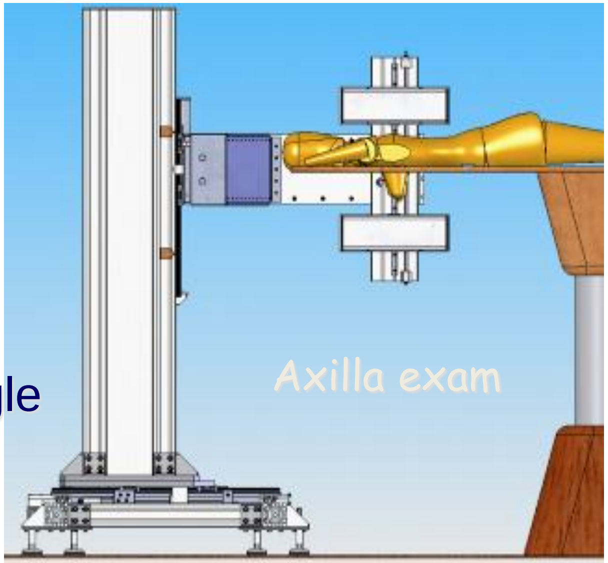

Detector Technology

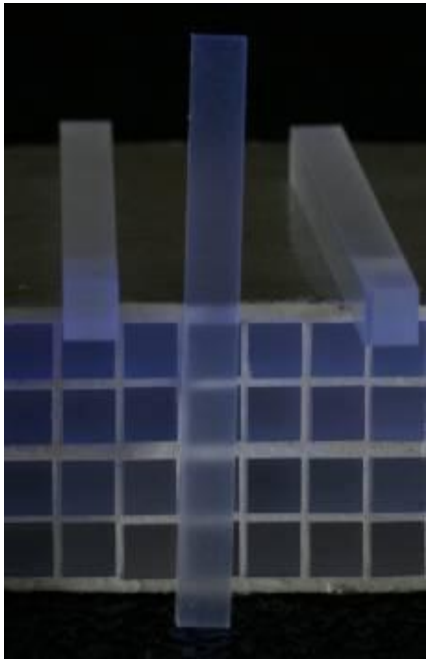

LYSO Scintillating Crystals

Density (g.cm-3)	Light Yield (photons/MeV)	Emission peak (nm)	Time constant (ns)
7.4	27000	420	40

Avalanche Photodiodes

Operating voltage V_R	**350-450 V**
Gain uniformity within a sub-array	**±15%**
Dark current I_d per APD pixel at V_R	**≤ 10 nA**
Quantum efficiency at λ=420 nm	**≥ 70 %**
Excess noise factor at V_R	**≤ 2.3 @ λ=420 nm**

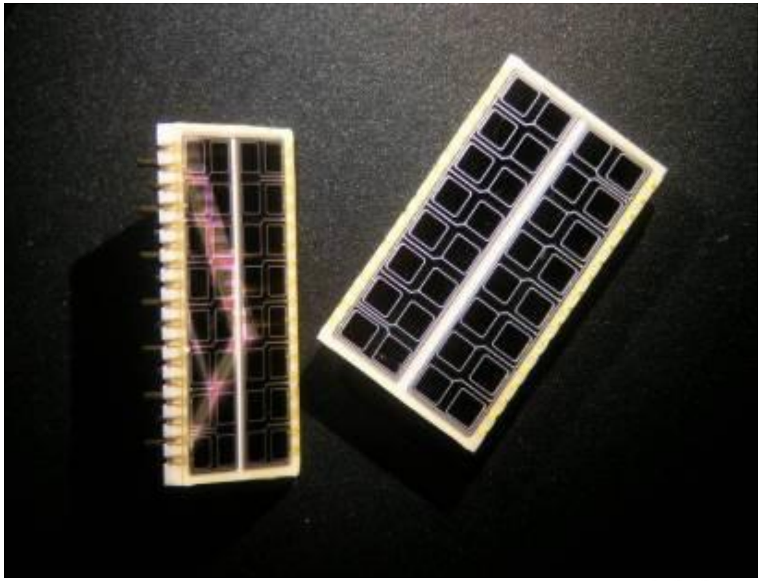

Frontend Electronics Integration

Compact system in the Detector Head:

- 6144 APD channels
- 384 HV lines
- 128 high speed (600 MHz) output lines
- High frequency clock (100 MHz)

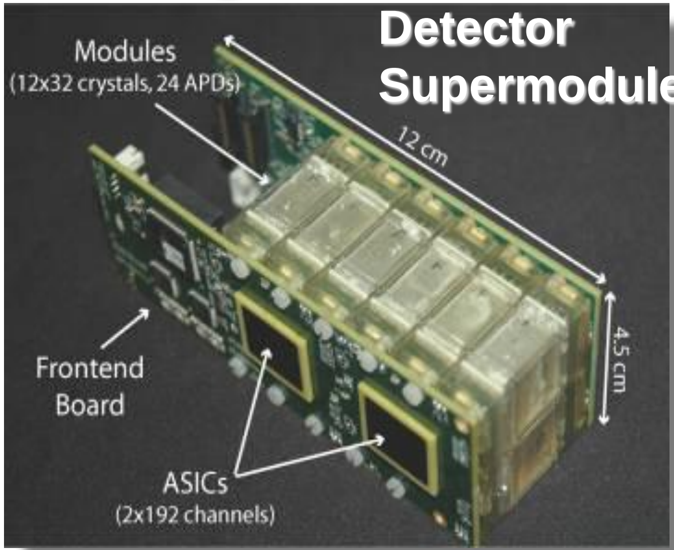

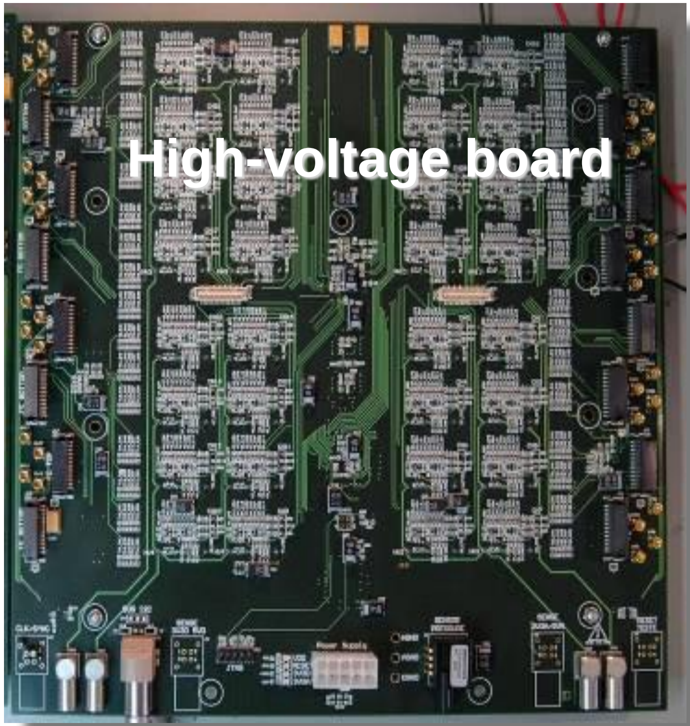

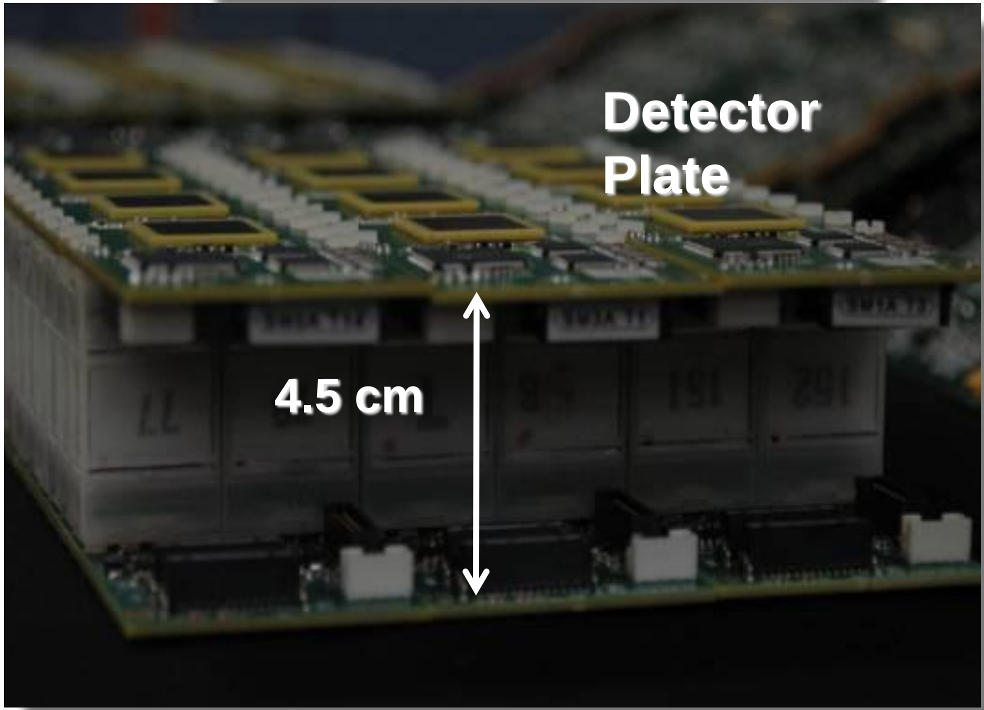

Detector Heads

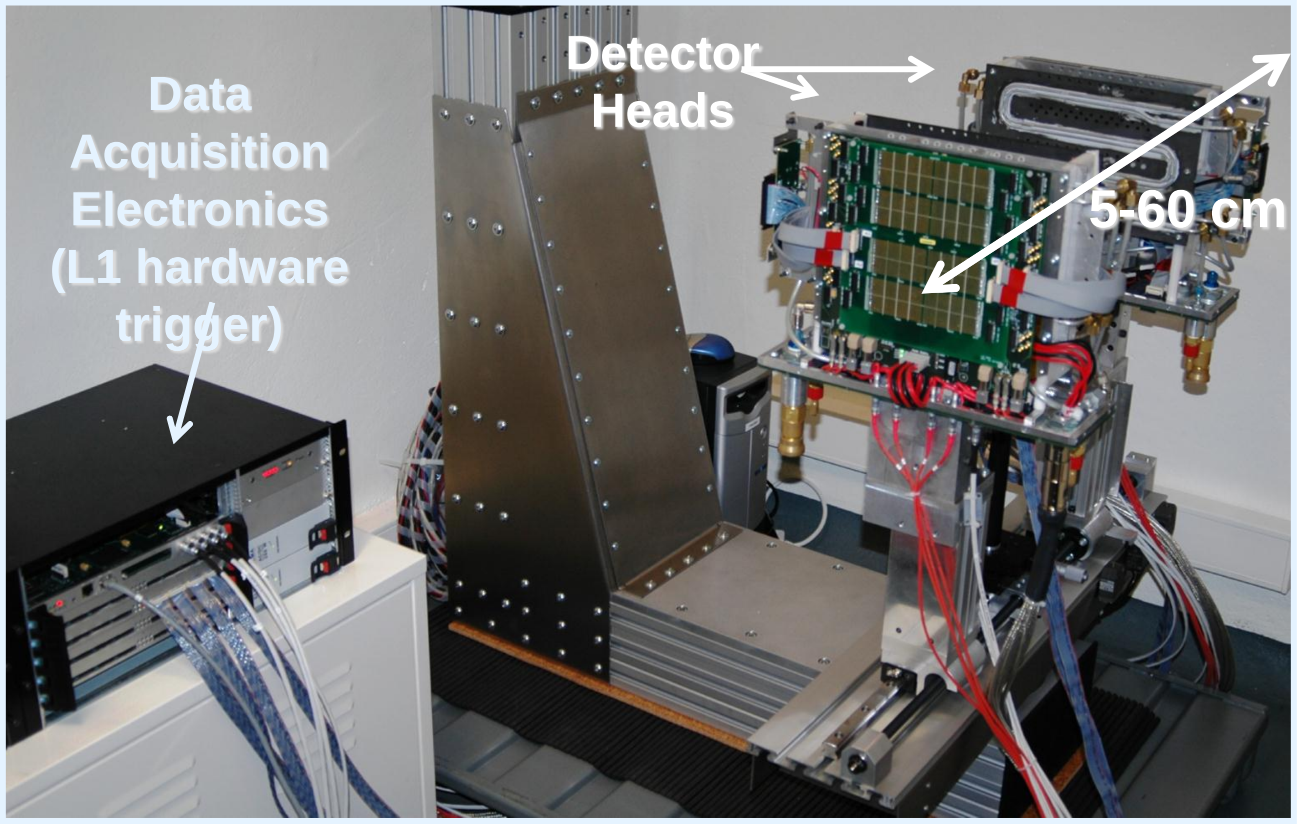

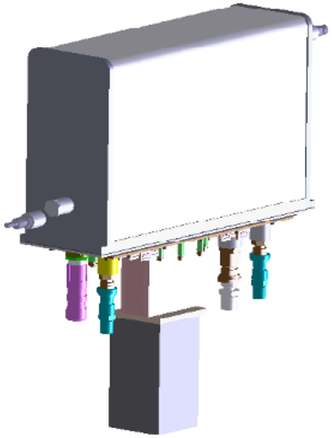

Cooling system : water cooled plates 18.0±0.1
Nitrogen atmosphere inside detector head

Data Acquisition System

L1 Trigger/DAQ system is housed in a single crate with two dedicated buses

Sophisticated coincidence trigger (36 k calibration constants)

Frontend to L1 bandwidth up to 156 Gb/s

Level 2 DAQ: high-end computer server

ClearPEM scanner

Robotized gantry: 6 movement axis

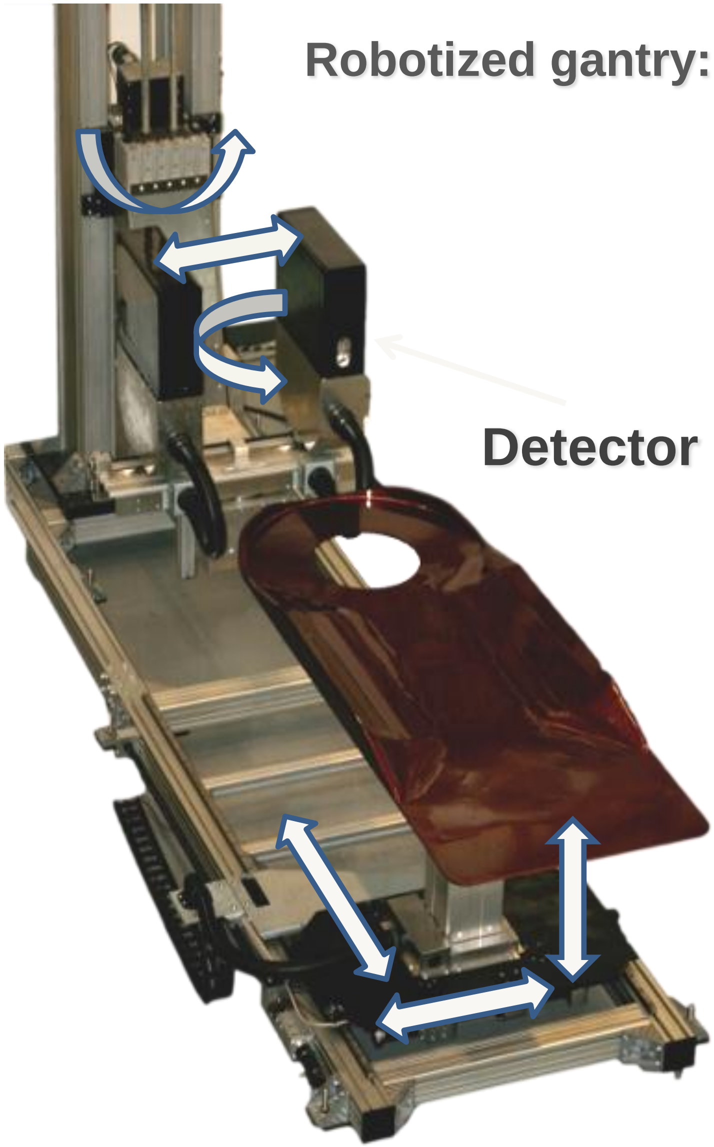

Detector Heads

Operation, Monitoring, Reconstruction and Visualization Software

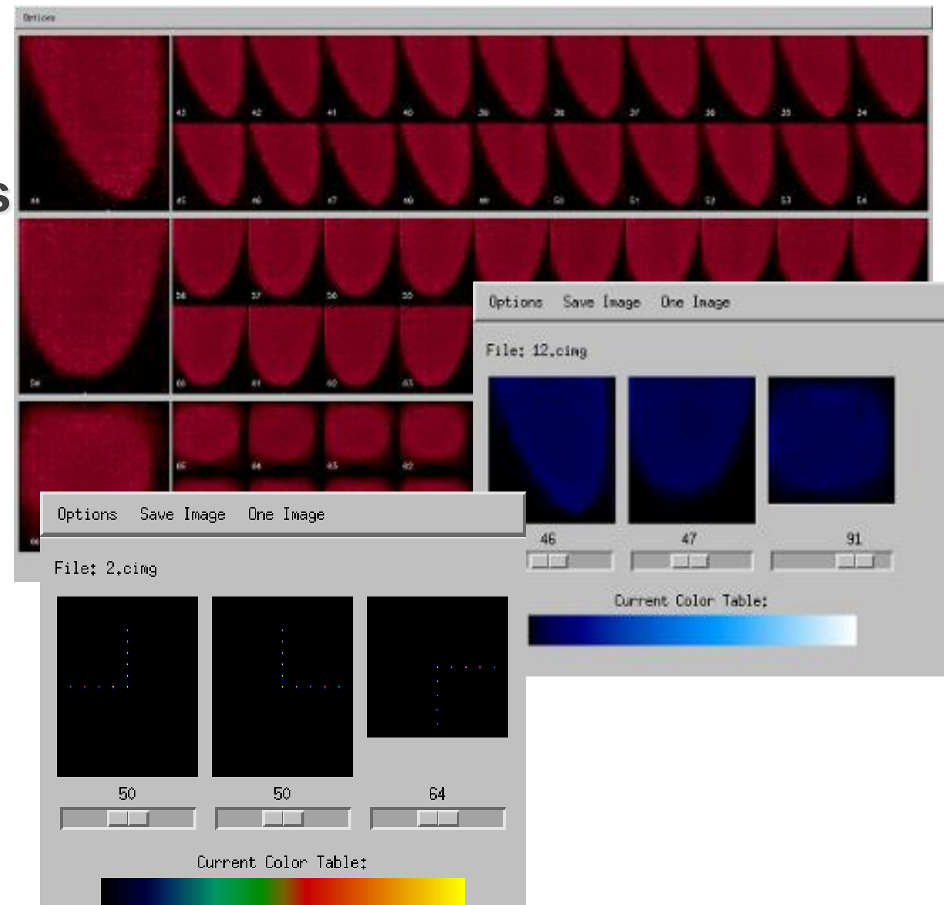

http://www.youtube.com/watch?v=90cJUHOMzVk&NR=1

ClearPEM Images

- Two acquisitions with orthogonal plate orientations for each source location (400-600 keV)
- Simultaneous reconstruction of 16 source positions

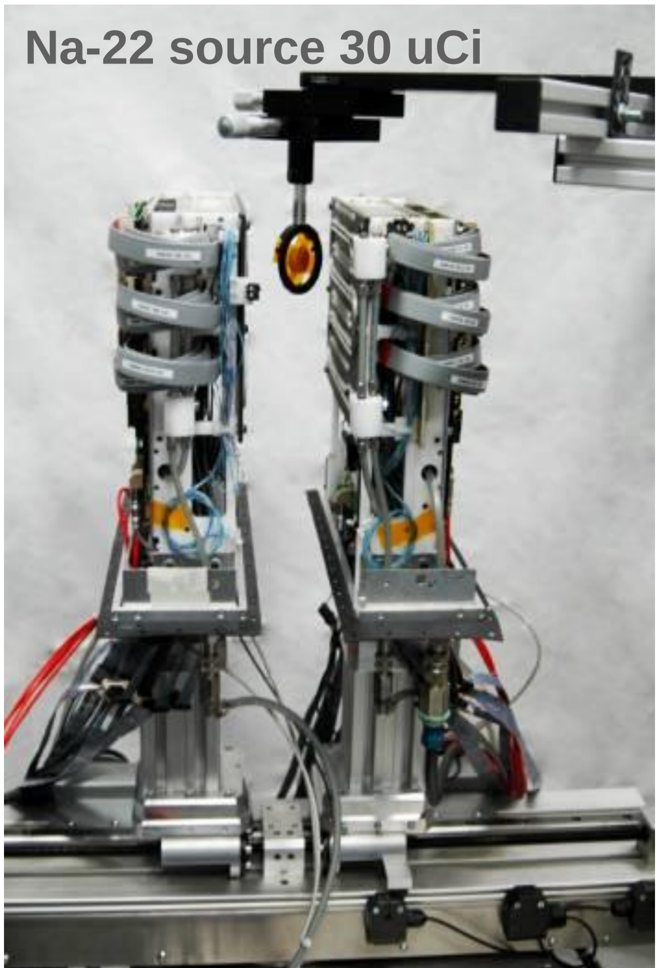

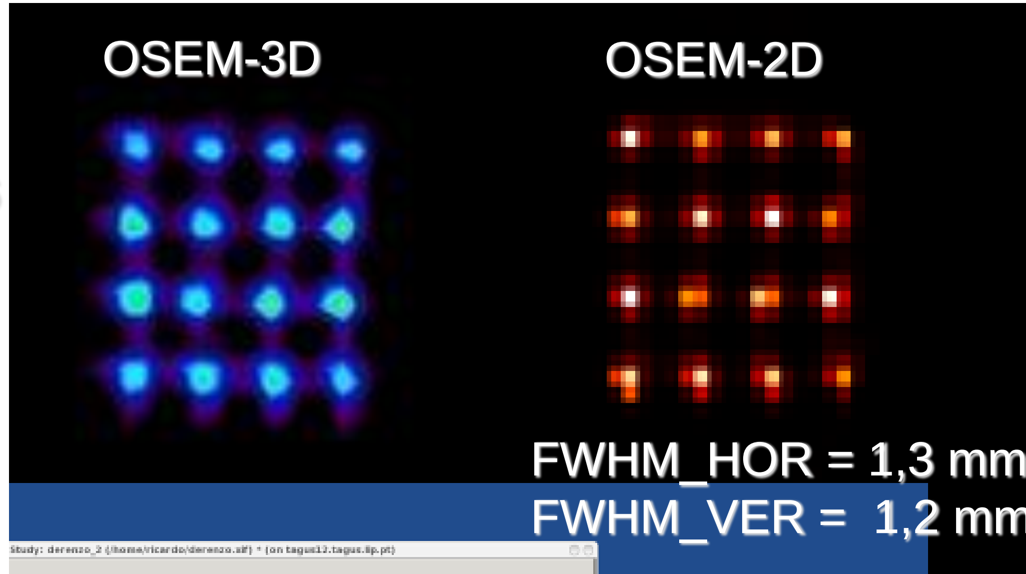

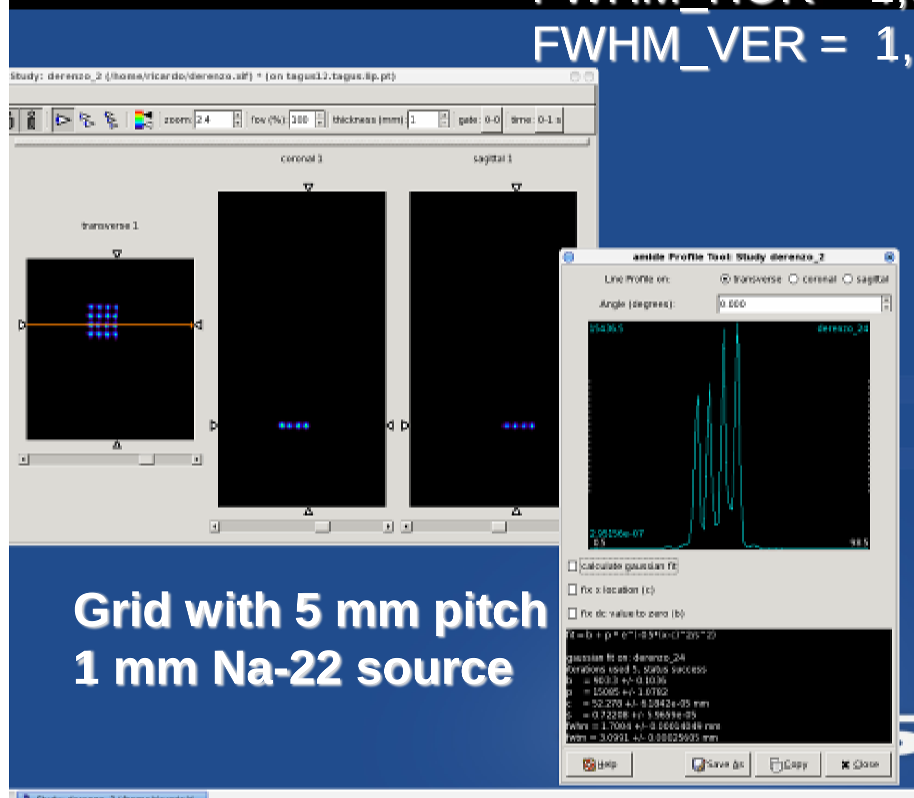

Clinical Trials

Scanner installed at IPO Hospital, Porto

First patients

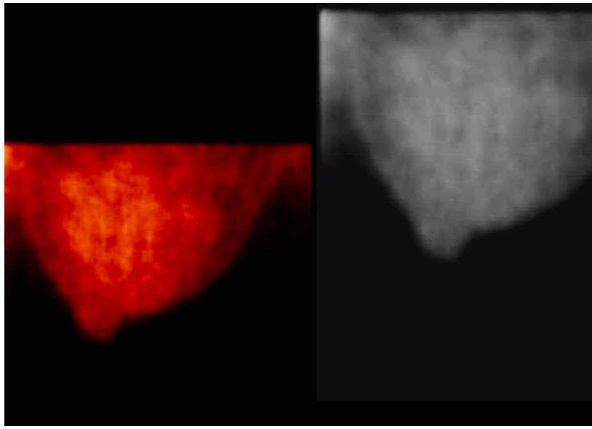

Prostate PET Imaging

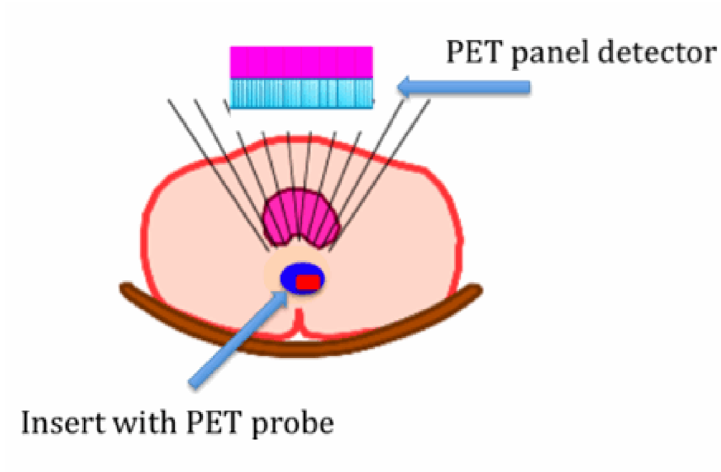

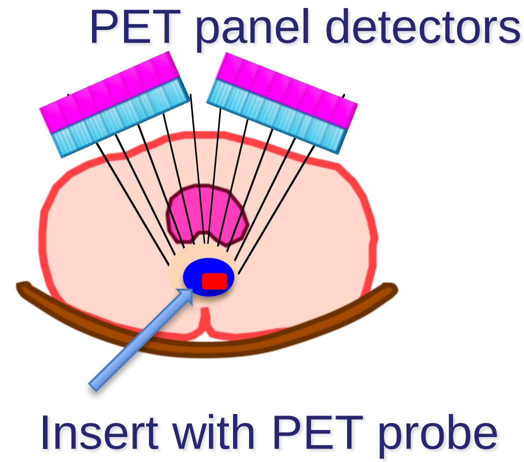

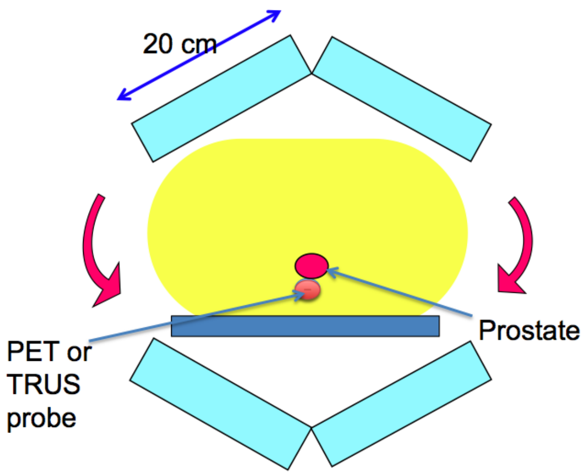

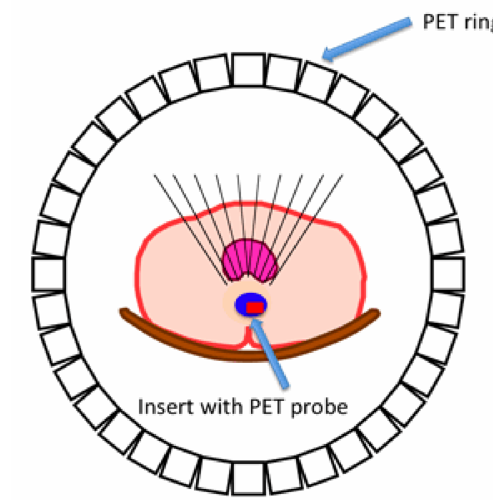

Several approaches under study for high resolution PET imaging of the prostate. Top: the PET probe with single PET panel, and probe with two panels in a stereotactic geometry. Bottom: four-panel rotating PET + probe system, and the prostate PET probe operating with the ring PET (for example from a standard PET/CT scanner).

Optimal Probe Option
Tests of the monolithic MPPC module

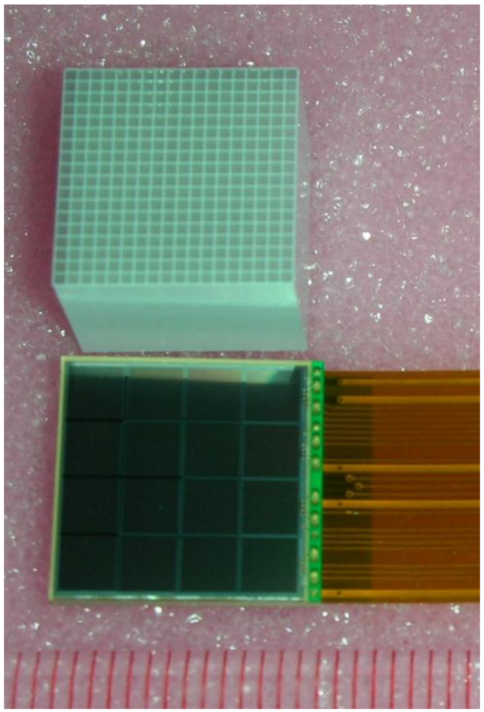

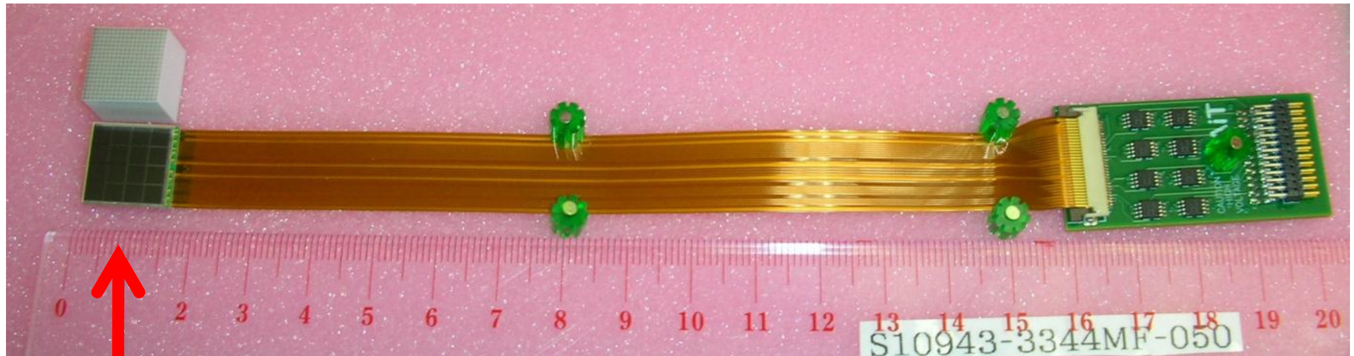

No active electronics inside the MRI coil

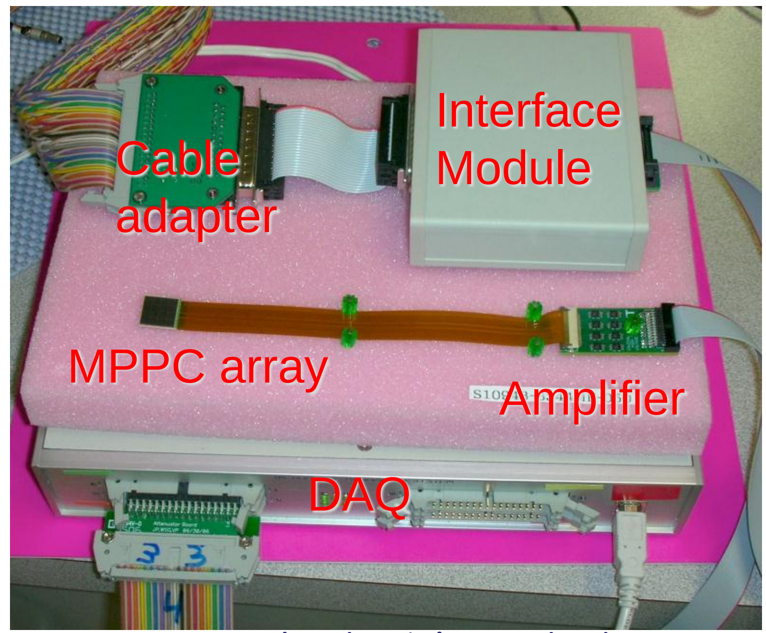

0.7mm step x 10mm thick DOI LYSO array with double sided output, from Proteus. S10943-3344MF-050 MPPC array from Hamamatsu. Amplifier board, interface module, cable adaptor, and DAQ box all from AiT Instruments.

ENDO TOFPET US

Endoscopic TOFPET & Ultrasound

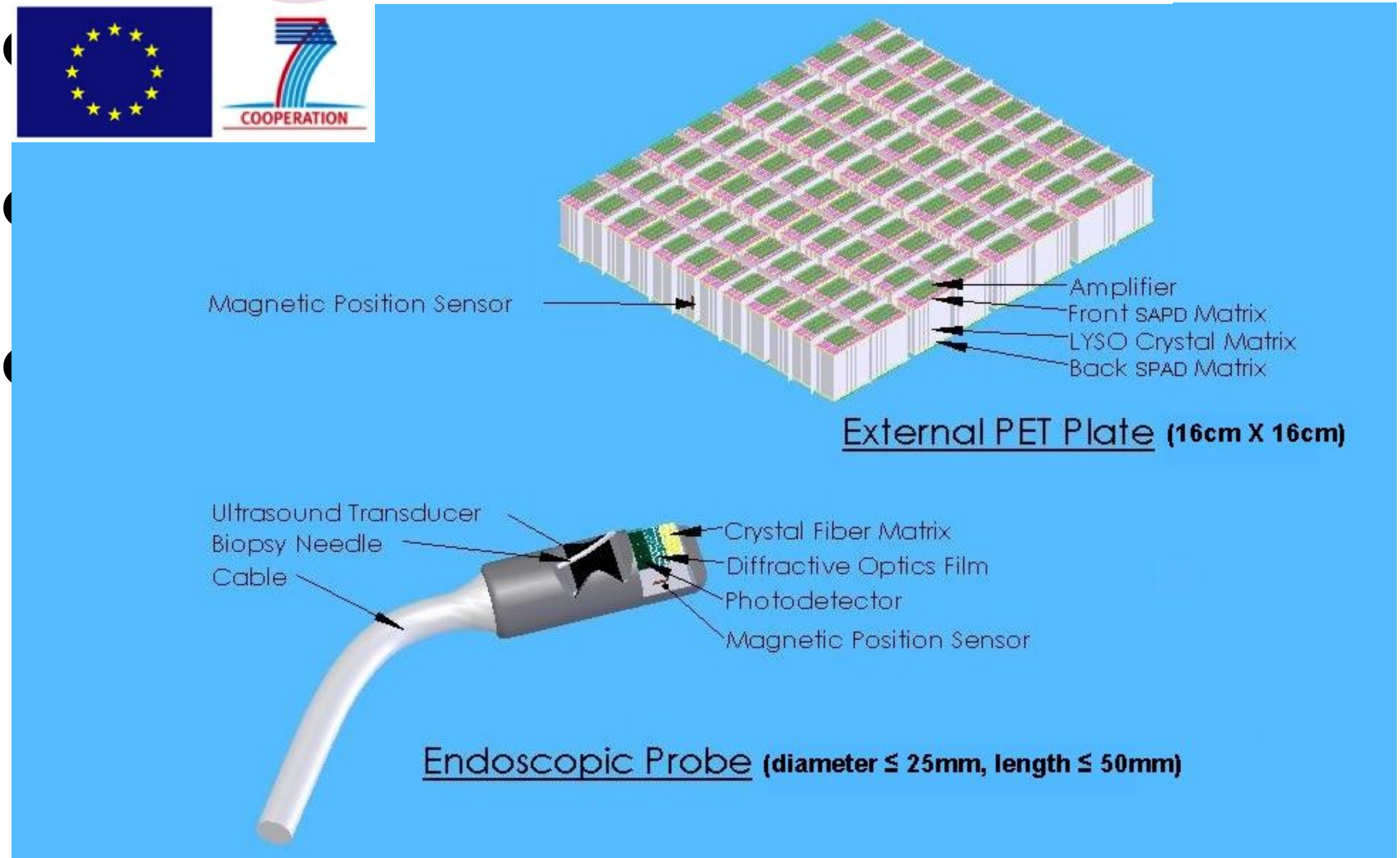

PRIOR ART – UPRIGHT PET BRAIN IMAGER

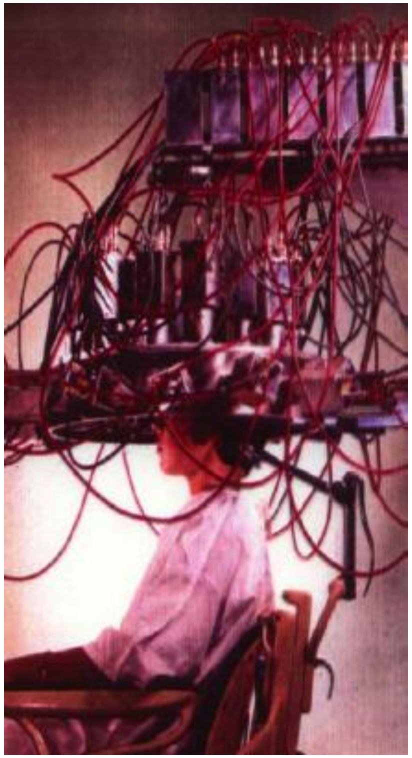

Photograph of one of the first brain PET scanners at Brookhaven National Laboratory, the " Headshrinker " (1961),

Photograph of the developed PET Hat with a subject

Photograph of a novel PET Hat ring imager, permitting imaging a 4.5 cm brain section of a sitting person. The detector modules are built on the basis of the H8500 PMTs. (Yamamoto, Kobe).

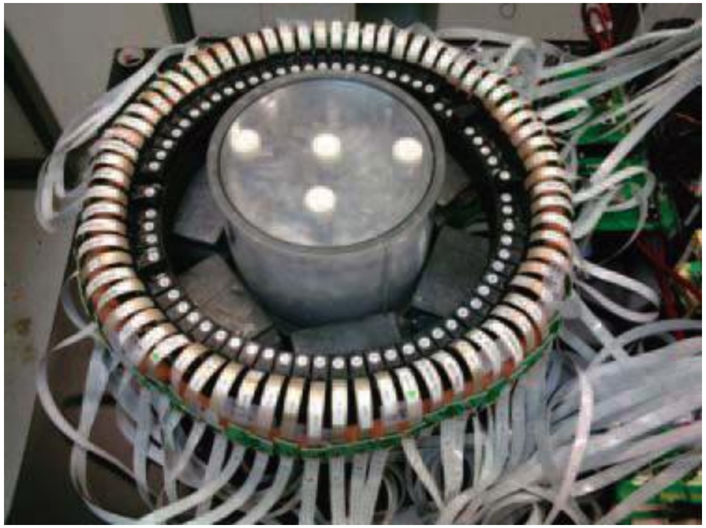

The prototype brain PET consisting of 72 compact detector modules built with SensL SiPMs. This imager covers a narrow 12mm slice of the brain but can operate in an MRI magnet (Korea).

Short History of IP for the Wearable PET Brain Imagers: From RatCap to HelmetPET

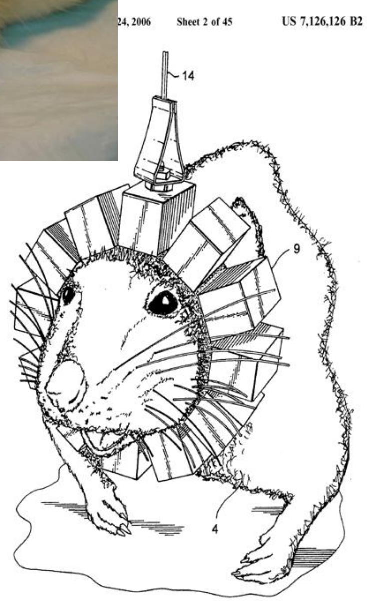

Figure 2

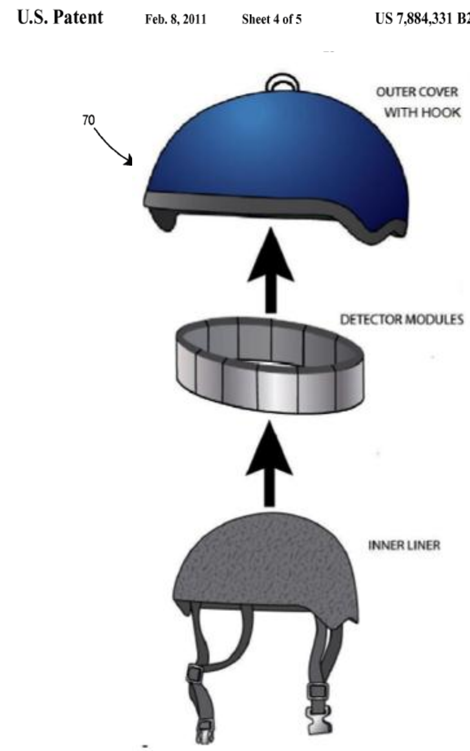

Fig. 8

Left: RatCap PET (non-compliant animal); Center: PET Hat and compliant sitting patient; Right: Helmet for a compliant standing, moving etc patient).

Awake Animal Project

DOE funded research on imaging of the awake rat

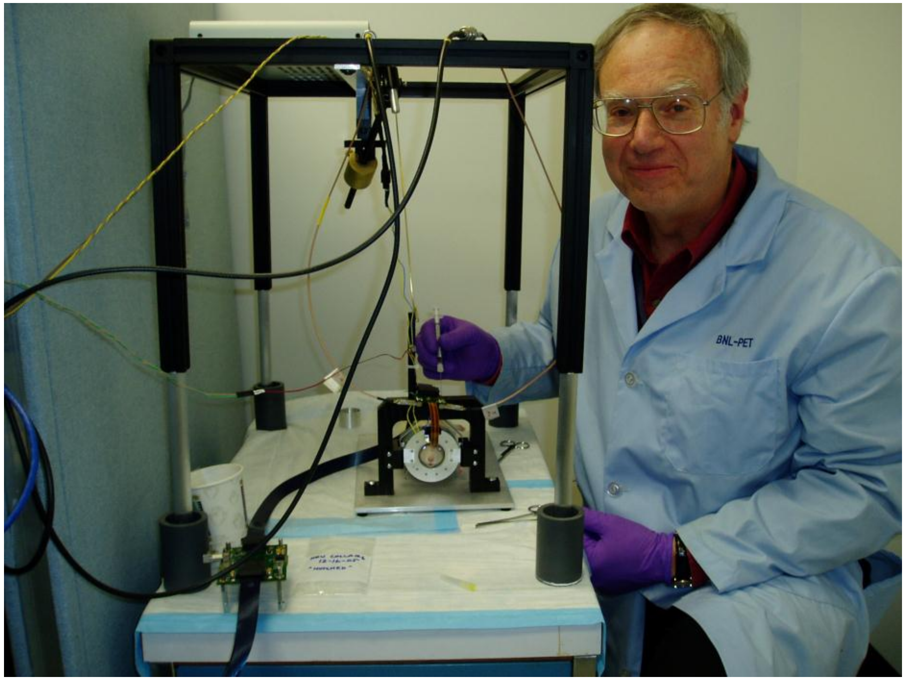

For the first time we can watch the brain in action during behavior in small animals

RatCAP Prototype Chip Development

The key to making the RatCAP possible was the development of a minaturized, novel electronics device which allows the signals from the RatCAP to be collected, amplified and analyzed

Electronics developed at BNL

Chip by itself

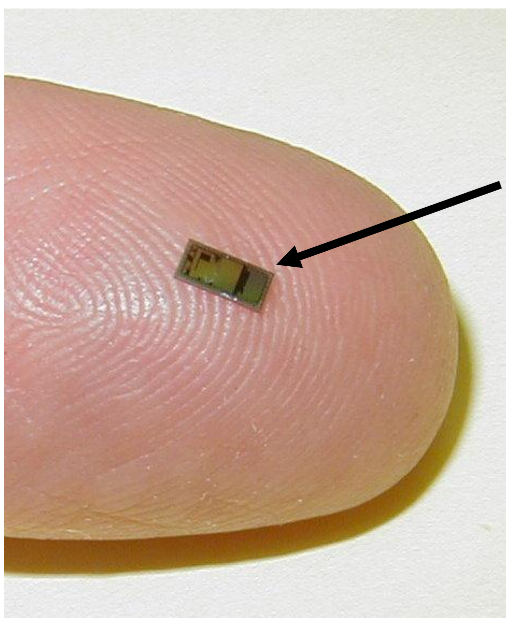

Chip packaged and ready for use

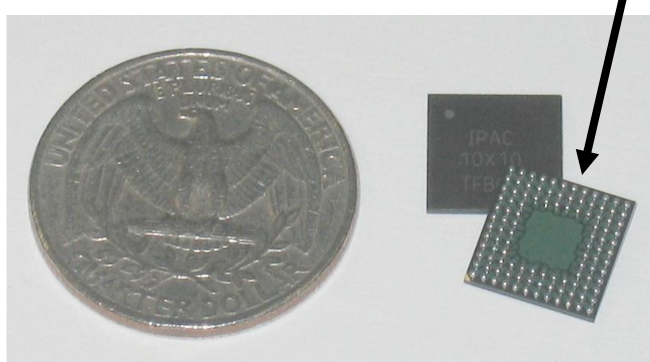

Commercial crystals and light amplifier used in the RatCAP

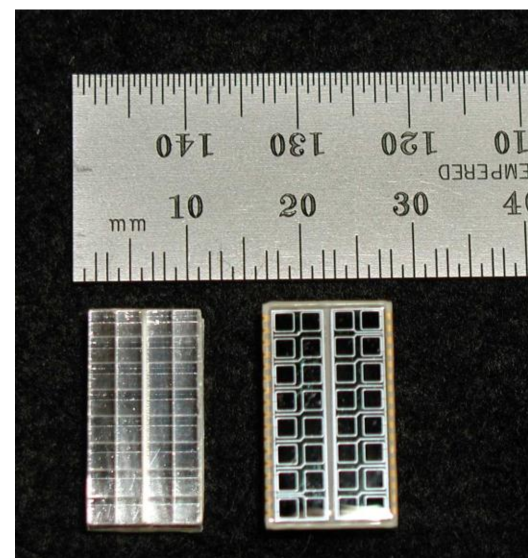

Small Animal (Rat) PET / MRI Camera

Standard Non-Magnetic Components

- LSO crystals
- Aluminum housing
- Fiberglass, kapton, plastic, silicon

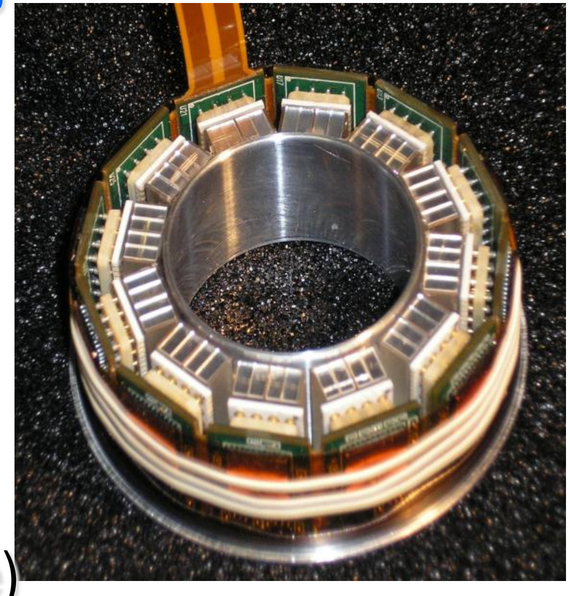

Image courtesy of Craig Woody, *Brookhaven National Laboratory*

Special Non-Magnetic Components

- APDs (special pins)
- APD sockets
- Non-magnetic flex circuit board (substrate)
- Non magnetic electronic components (solder leads)

Shielding from RF

- Aluminum housing
- Kapton cable carrying signals

- Non-Magnetic Version of RATCAP
  - Planned to Use for Neurology

Simultaneous PET/MRI Based on RatCAP in Small Animals & for Breast Imaging

BROOKHAVEN NATIONAL LABORATORY

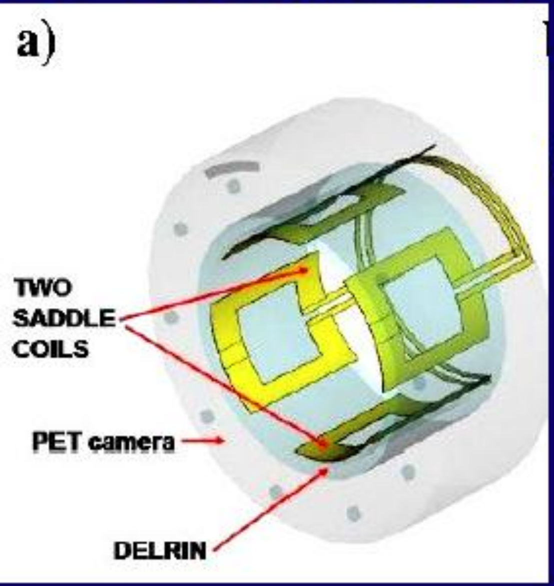

MRI Coil

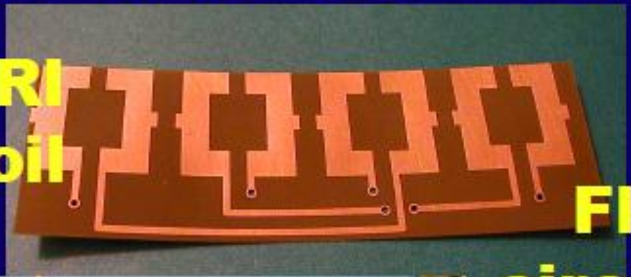

Flex circuit board

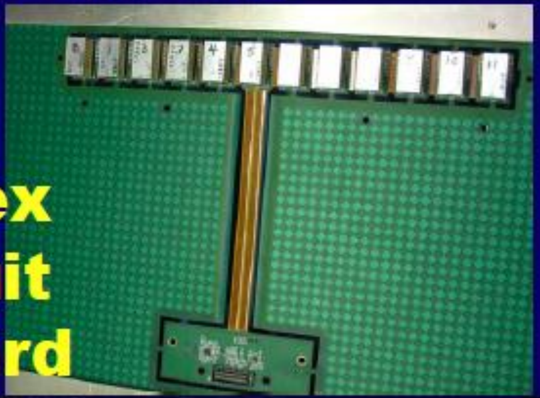

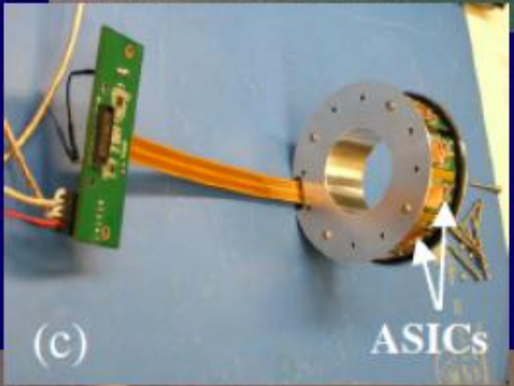

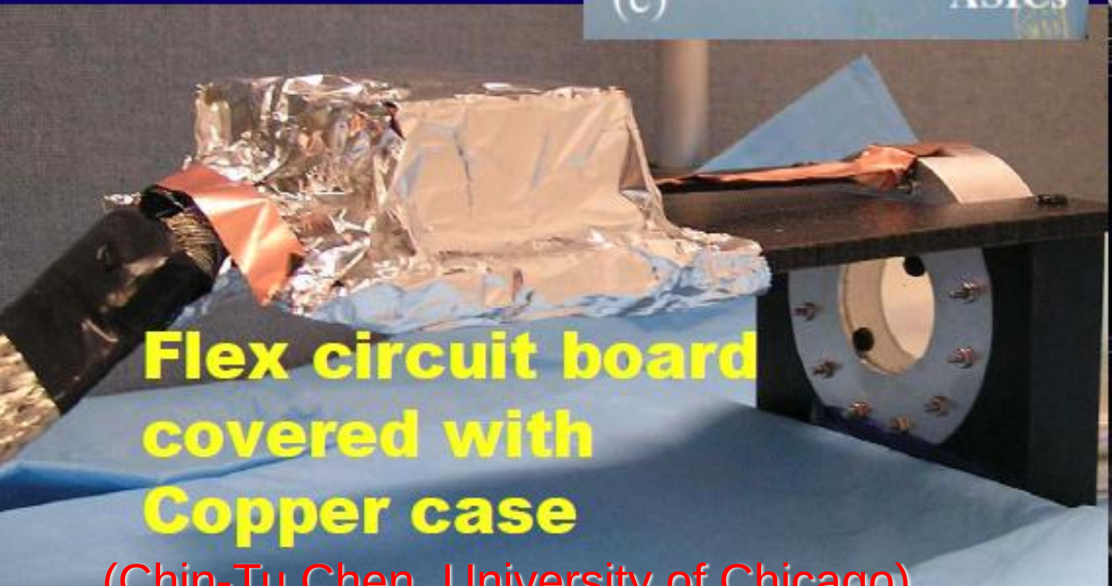

Flex circuit board covered with Copper case

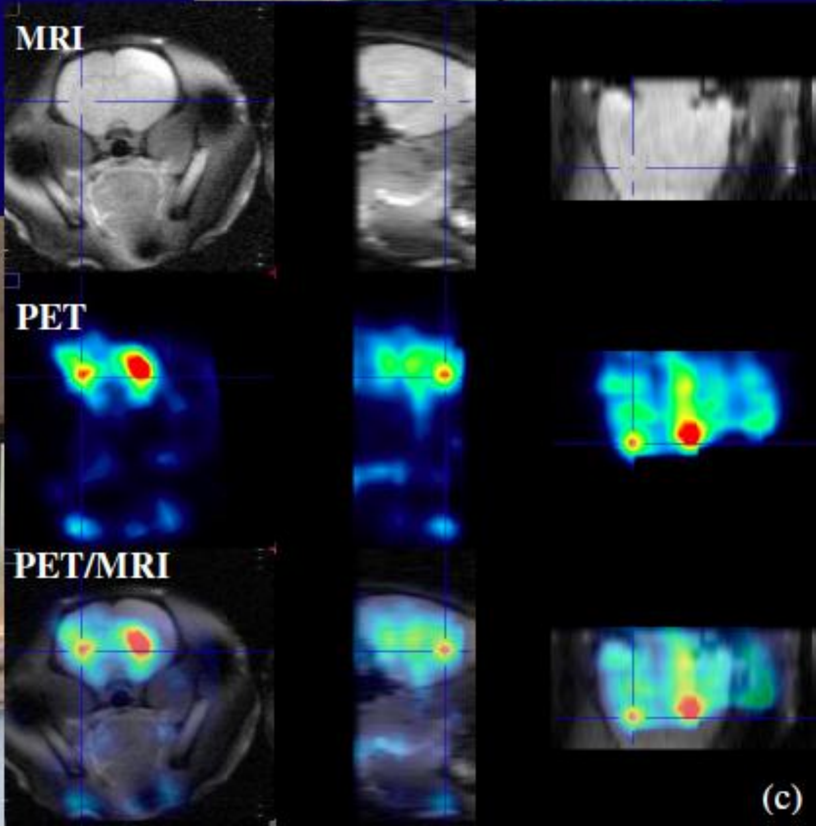

(Chin-Tu Chen, University of Chicago)

PET-MRI System for Breast Imaging

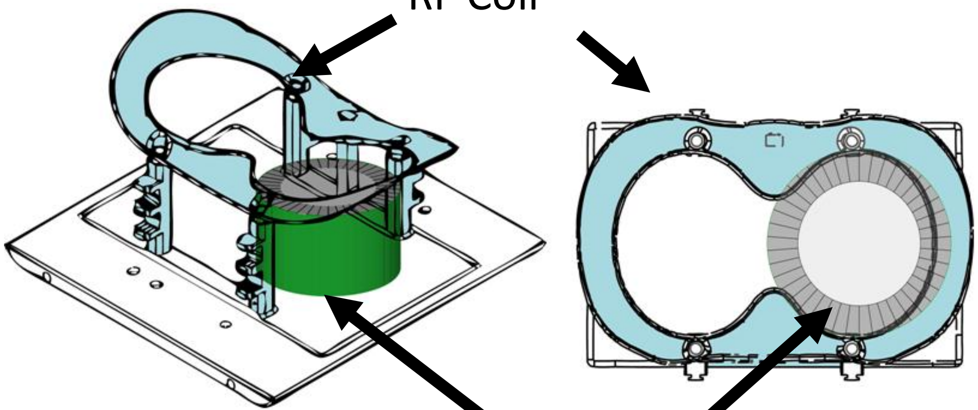

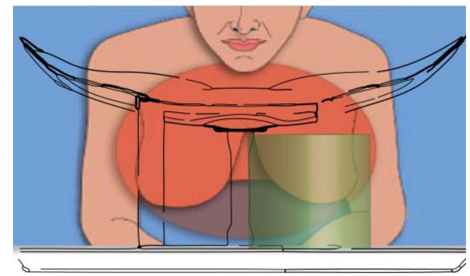

Patient positioned with Breast PET insert & Aurora Breast RF coil

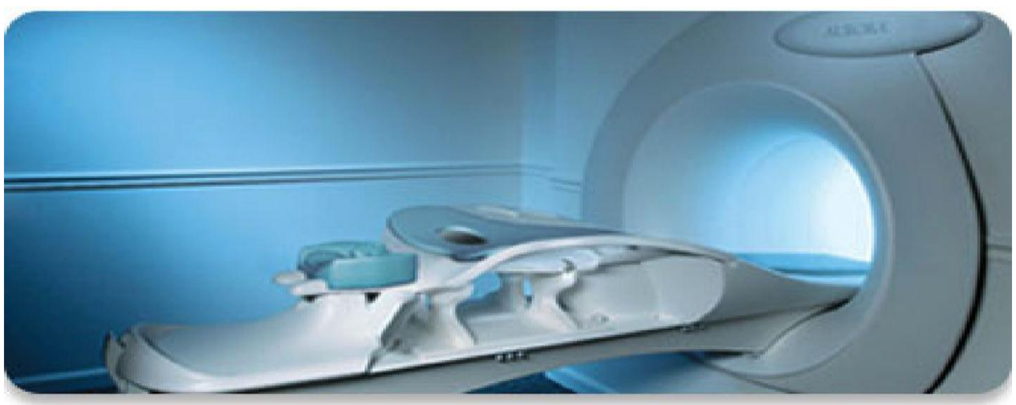

Aurora Dedicated 1.5 T Breast MRI

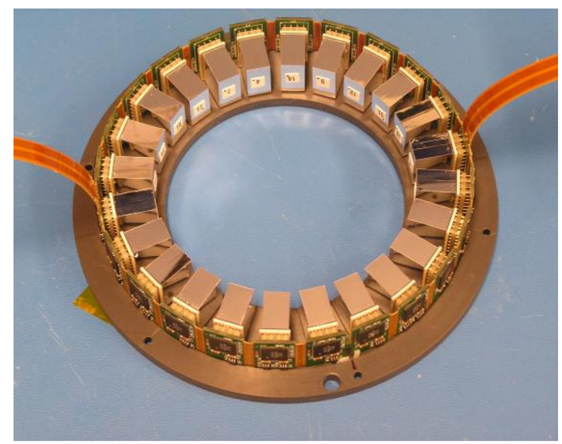

- 24 detector blocks
- 2.2 x 2.2 x 15 mm^3 LYSO

SiPM – BrainPET Scanner

- PET detector ring located inside MRI
  - PET detector: between RF and gradient coils
  - PET electronics: outside MR bore

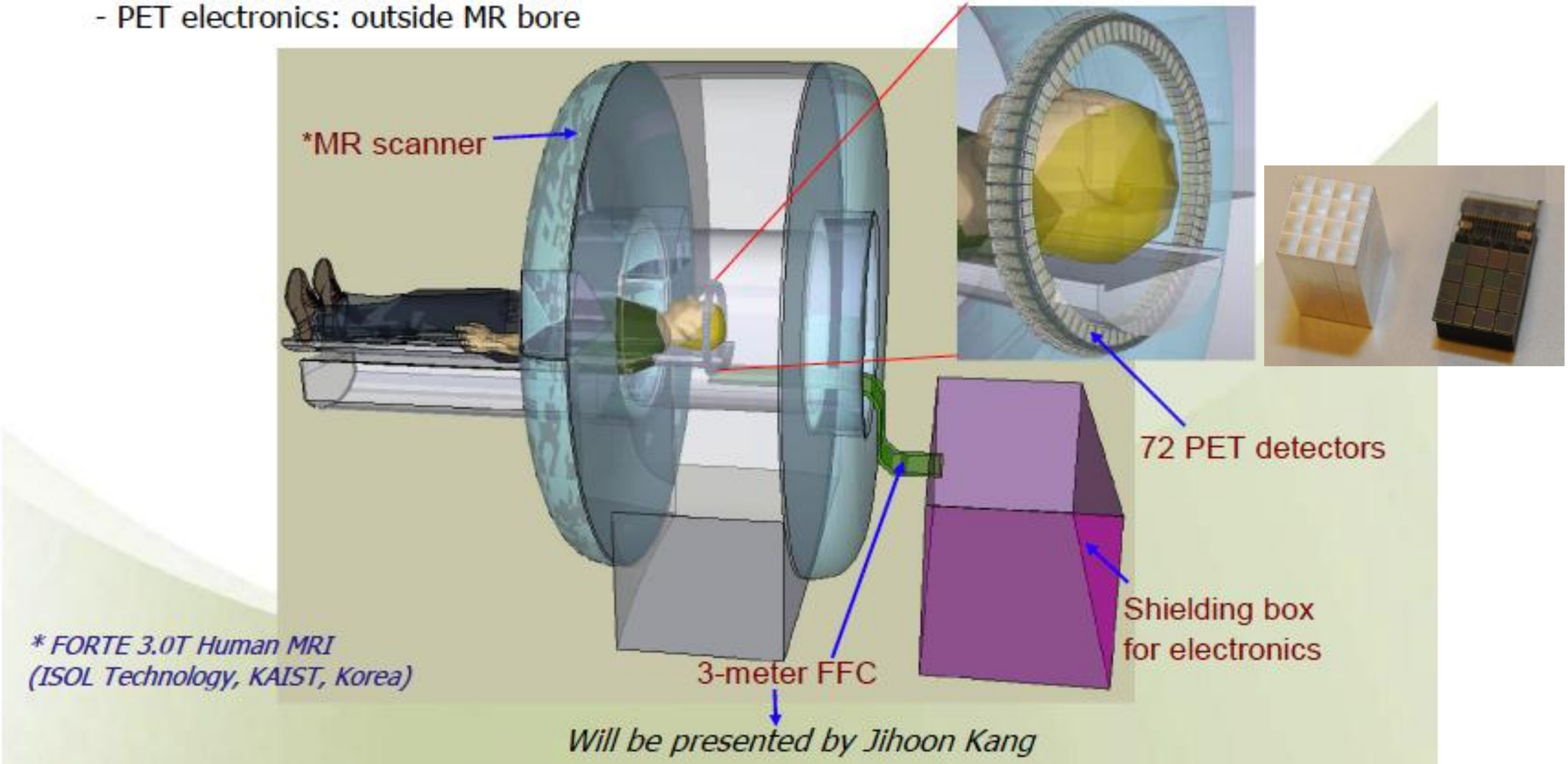

HELMET_PET BRAIN IMAGER

- Upright compatible
- High efficiency
- Low dose
- Pediatric compatible
- Screening compatible
- Mobile
- Head movement compatible (co-registered to head/brain)
- High resolution
- MRI compatible- potential (as insert)

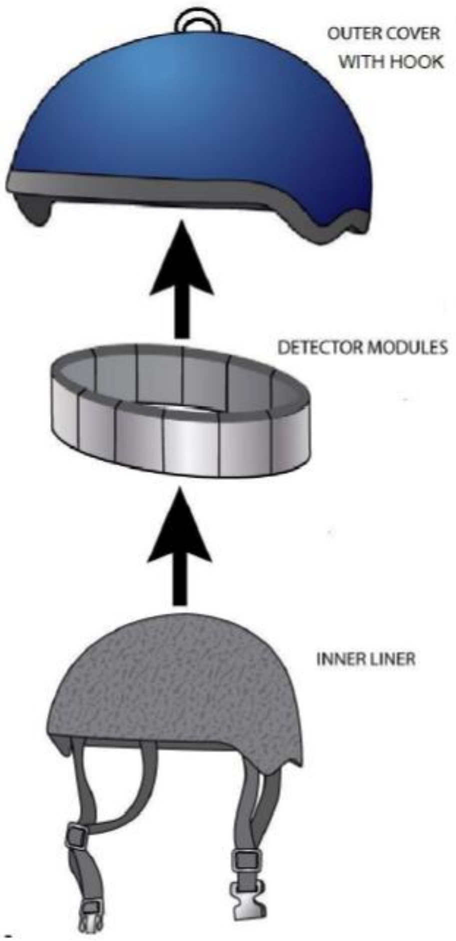

Examples of some possible situations with patients wearing the imager helmet: sitting in a chair *(left)*, exercising *(center)*, and laying down on a bed *(right)*. Another option with a (helium) balloon supporting the weight of the helmet, allowing for even more movement freedom during imaging session, is not shown here. Except for the case of a patient on a bed, the helmet is suspended by a flexible harness /suspension attached to a hook on the helmet.

PRODUCTION OF COMPACT DETECTOR MODULES FOR THE FIRST NO-DOI, NO-TOF PROTOTYPE

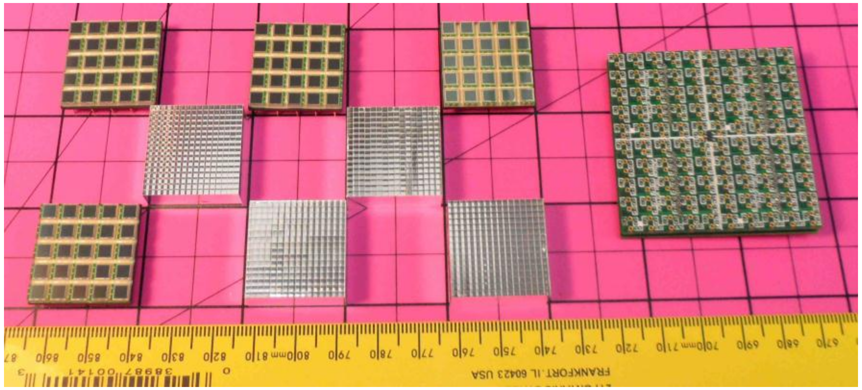

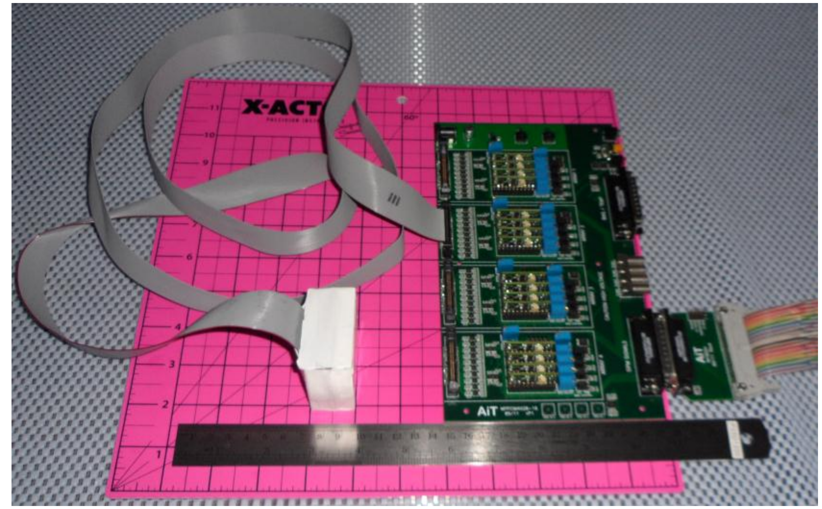

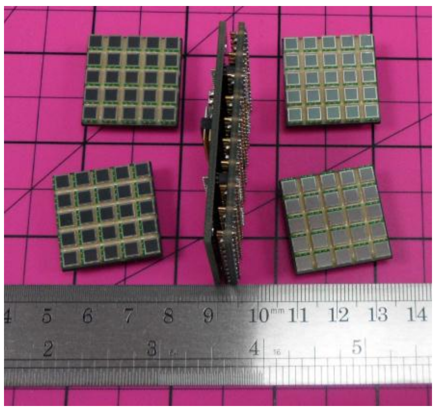

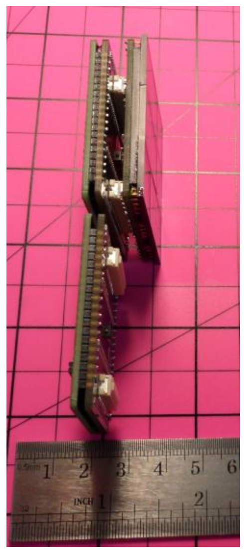

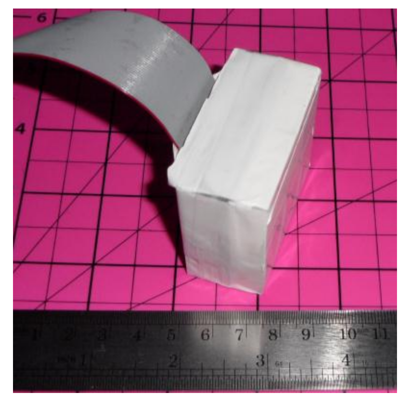

Left: Assembly of one ~5cm square compact module of the first Helmet_PET prototype. Four Hamamatsu 25 MPPC arrays assembled on one resistive readout base from AiT Instruments. Four 1.5mm step 10mm thick LYSO arrays from Proteus coupled to form one compact module. There are no amplifiers or other active components on board the detector module, but in the distant (at the other end of the 2m cable) electronics board. There are 4 output channels per module.

Dedicated Compact Imagers: New Applications and Structures

Take advantage of the additional information from TOF to overcome incomplete data problems

TOF

No-TOF

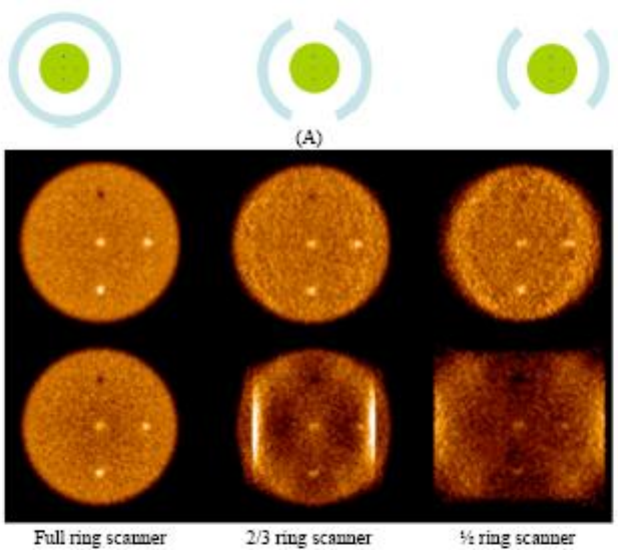

"A proposal for a TOF PET and SPECT MRI probe for diagnosis and follow up of prostate cancer".

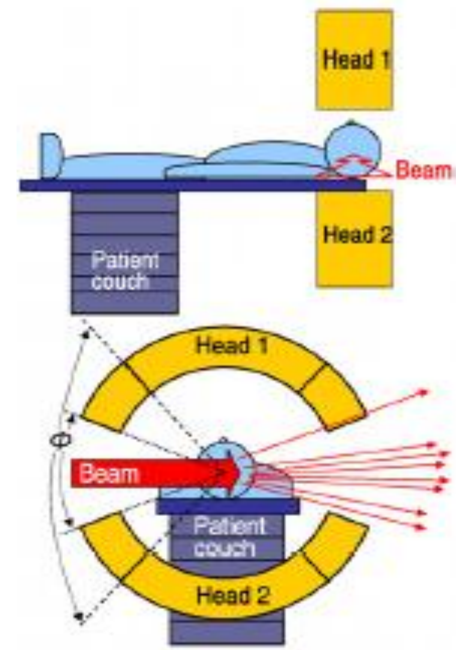

"Design considerations for a limited-angle, dedicated breast TOF PET scanner", S. Surti and J.S. Karp, MIC 2007

"Direct time-of-flight for quantitative, real-time in-beam PET: a concept and feasibility study", P. Crespo, G. Shakirin, Fine Fiedler, W. Enghardt and A. Wagner, PMB 2007

Example: SiPM Timing Results

	FWHM in coincidence **Hama. 25μ**	FWHM in coincidence **Hama. 50μ**	FWHM in coincidence **Hama. 100μ**
Fill Factor:	30.8%	61.5%	78.5%
Number of Pixels:	14400	3600	900
Best Settings:	73V Bias 150mV Th.	72.4V Bias 100mV Th.	70.3V Bias 300mV Th.
LSO with LSO $2x2x10mm^3$:	340±9ps	220±4ps	280±9ps
LFS $3x3x15mm^3$:	429±10ps	285±8ps	340±3.2ps
LuAG:Pr with LuAG:Pr $2x2x8mm^3$:	1061±40 ps	672±30 ps	826±40 ps
LuAG:Ce with LuAG:Ce $2x2x8mm^3$:	1534±50 ps	872±50 ps	1176±50ps
LYSO with LYSO $2x2x8mm^3$:			282±9ps
LYSO with LYSO $0.75x0.75x10mm^3$:	360±22ps	208±20ps	

Paul Lecoq

Conclusions

- Techniques of experimental particle/nuclear physics have played and still play a substantial role in medical imaging: detection concepts, detector materials, electronics, simulations, reconstructions,…
- "Even" gas detectors and Silicon detectors are used in medical imaging
- PET invented many years ago but only from 2001 it got full recognition for its unique clinical role after it was combined with CT (power of multi-modality)
- SPECT and PET imaging as molecular imaging is providing critical assistance with patient diagnosis and treatment, as well as with work on understanding disease origin and cures (also in small animal studies)
- SPECT and PET improvements are under way to reach the physical limits of the techniques (the role for particle physicists !)
- Rebirth of TOF PET
- New technologies: scintillators, photodetectors, solid state materials – spin-offs from particle physics
- Organ-specific PET imagers are becoming available with better performances and at a lower cost
- MRI – compatibility is becoming an important and necessary feature

Thank you !

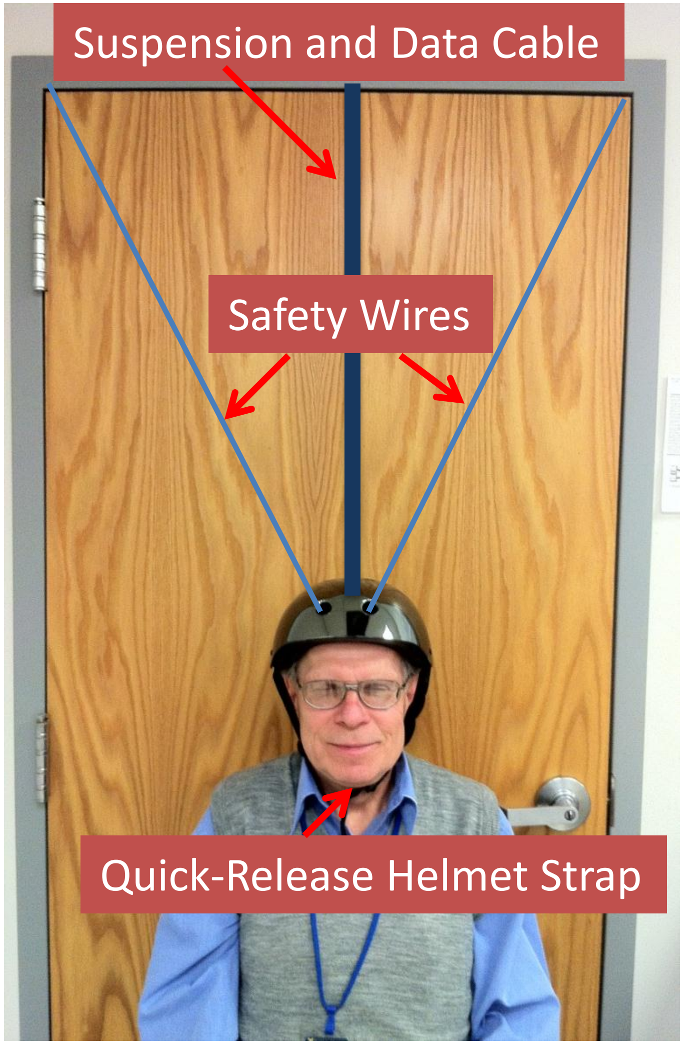
Suspension and Data Cable
Safety Wires
Quick-Release Helmet Strap